



HAL
open science

Functional analysis of the proliferation antigen, KI-67 roles in cancer

Karim Mrouj

► **To cite this version:**

Karim Mrouj. Functional analysis of the proliferation antigen, KI-67 roles in cancer. Agricultural sciences. Université Montpellier, 2018. English. NNT : 2018MONTT006 . tel-01834620

HAL Id: tel-01834620

<https://theses.hal.science/tel-01834620>

Submitted on 10 Jul 2018

HAL is a multi-disciplinary open access archive for the deposit and dissemination of scientific research documents, whether they are published or not. The documents may come from teaching and research institutions in France or abroad, or from public or private research centers.

L'archive ouverte pluridisciplinaire **HAL**, est destinée au dépôt et à la diffusion de documents scientifiques de niveau recherche, publiés ou non, émanant des établissements d'enseignement et de recherche français ou étrangers, des laboratoires publics ou privés.

THESE POUR OBTENIR LE GRADE DE DOCTEUR DE L'UNIVERSITE DE MONTPELLIER

En Biologie Santé

École doctorale

CBS2 n°168 – Sciences Chimiques et Biologiques pour la Santé

Unité de recherche Institut de Génétique Moléculaire de Montpellier CNRS-UMR 5535

Titre de la thèse

**ANALYSE FONCTIONNELLE DES ROLES DE L'ANTIGENE DE
PROLIFERATION, KI-67, DANS LES CANCERS**

**FUNCTIONAL ANALYSIS OF THE PROLIFERATION ANTIGEN KI-67'S
ROLES IN CANCER**

Présentée par
MROUJ KARIM
Le 31 Mai 2018

Sous la direction de Fisher Daniel

Devant le jury composé de

Présidente du Jury : Mme. Pannequin Julie

Mr. Fisher Daniel, IGMM, CNRS-UMR 5535, Université de Montpellier

Mr. Besson Arnaud, LBCMCP, CNRS-UMR 5088, Université Paul Sabatier

Mr. Santamaria David, IECB, INSERM U1218, Université de Bordeaux

Mme. Pannequin Julie, IGF, CNRS-UMR 5203, Université de Montpellier

Directeur de Thèse

Rapporteur

Rapporteur

Examinatrice



**UNIVERSITÉ
DE MONTPELLIER**

Abstract

The cell proliferation antigen Ki-67 is constitutively expressed in cycling mammalian cells and is widely used as a cell proliferation marker to grade tumours. Despite its use in cancer histopathology its functions are poorly understood. The aim of this project is to improve understanding of Ki-67 functions and its requirements in cancer initiation and progression. We found that Ki-67 is dispensable for cell proliferation and Ki-67 mutant mice did not exhibit any developmental abnormalities, and were fertile and aged well. Although Ki-67 was uncoupled from cell proliferation, Ki-67 was found to promote heterochromatin organization in proliferating cells. Studying Ki-67 expression control, we have found that cell cycle regulation accounts for Ki-67 variability levels in normal human cells, proliferating tissues in mice, human cancer cell lines and cancer patients.

Using our Ki-67 mutant mice, we found that Ki-67 depletion can protect mice from intestinal carcinogenesis in two different experimental models used. Moreover, analysis of the consequence of Ki-67 ablation in the mouse breast cancer cell line, 4T1 has revealed its requirements for the maintenance of the stem-like properties of these cancer cells. More importantly, Ki-67 depletion strongly affects 4T1 tumour growth and formation of lung metastases *in vivo*. Similarly, Ki-67 absence strongly impaired the development of the TNBC-derived MDA-MB-231 xenografts *in vivo*. Moreover, comparison of Ki-67 dependent alterations in gene expression in 4T1 cells by RNA sequencing revealed widespread transcriptome changes following Ki-67 depletion. Together, these results suggest a specific involvement of Ki-67 in cancer initiation and progression and may constitute a potential therapeutic target in cancer therapy.

Keywords: Ki-67, chromatin, regulation, tumorigenesis, metastases

Résumé

L'antigène de prolifération cellulaire Ki-67 est exprimé de manière constitutive dans les cellules de mammifères. Ki-67 est régulièrement utilisé en tant que marqueur de prolifération cellulaire pour classer les tumeurs. Cependant, malgré son utilisation fréquente en histopathologie, ses fonctions sont encore mal caractérisées. Mes travaux de thèse ont eu pour objectif d'améliorer la compréhension des fonctions biologiques de Ki-67 ainsi que d'étudier l'importance de son expression dans l'initiation et la progression des cancers. Nous avons montré que Ki-67 était dispensable à la prolifération cellulaire. Quant aux souris mutantes Ki-67, elles ne présentaient aucune anomalie de développement, étaient fertiles et vieillissaient normalement. Néanmoins, l'expression de Ki-67 s'est révélée être requise pour l'organisation de l'hétérochromatine dans les cellules prolifératives. En étudiant le contrôle de l'expression de Ki-67, nous avons pu mettre en évidence que les différents niveaux d'expression de Ki-67, souvent observés dans les lignées cellulaires transformées ou non, les tissus et les échantillons de tumeurs des patients, seraient expliqués par une régulation via la machinerie du cycle cellulaire.

En utilisant nos souris mutantes Ki-67, nous avons également montré que l'absence de Ki-67 permettait de protéger les souris contre la carcinogenèse intestinale dans les deux différents modèles expérimentaux utilisés. De plus, l'analyse de la conséquence de l'ablation de Ki-67 dans la lignée tumorale murine, 4T1, a révélé que Ki-67 est requis pour le maintien des propriétés souches de ces cellules cancéreuses. En outre, la déplétion de Ki-67 a fortement affecté la croissance des tumeurs et la formation de métastases pulmonaires chez les souris. De façon similaire, l'absence de Ki-67 a fortement altéré le développement des xéno greffes de la lignée MDA-MB-231 dans des souris immuno-déficientes. De plus, le séquençage de l'ARN dans les cellules 4T1 a révélé l'existence d'altérations importantes au niveau transcriptomique, suite à la déplétion de Ki-67.

L'ensemble de ces résultats suggère une implication spécifique de Ki-67 dans l'initiation et la progression tumorale et que Ki-67 serait une cible thérapeutique potentielle et intéressante dans le traitement du cancer.

Mots-clés: Ki-67, chromatine, régulation, tumorigenèse, métastase

Table of Contents

Introduction	1
<i>Chapter I: Discovery & Early studies.....</i>	<i>1</i>
<i>Chapter II: Ki-67 molecular characterization.....</i>	<i>2</i>
<i>Chapter III: Ki-67 expression and control during the cell cycle.....</i>	<i>7</i>
<i>Chapter IV: The Ki-67 localization is cell cycle-dependent.....</i>	<i>10</i>
<i>Chapter V: The biological significance of Ki-67.....</i>	<i>12</i>
<i>1. Ki-67 and cell proliferation.....</i>	<i>12</i>
<i>2. Ki-67 a potential role in chromatin compaction.....</i>	<i>13</i>
<i>3. Ki-67 is involved in the organisation of the perichromosomal layer during mitosis.....</i>	<i>20</i>
<i>Chapter VI: Ki-67 in cancer.....</i>	<i>23</i>
<i>1. Ki-67 as a proliferation marker: a useful tool in the clinic.....</i>	<i>23</i>
<i>2. Ki-67: a potential role in tumour development and metastasis formation.....</i>	<i>26</i>
<i>Chapter VII: Epigenetic mechanisms of tumorigenicity.....</i>	<i>28</i>
Materials and Methods.....	33
Results.....	38
<i>I. Ki-67 is dispensable for cell proliferation but required for heterochromatin formation.....</i>	<i>38</i>
<i>II. Cell cycle regulation accounts for variability in Ki-67 expression levels.....</i>	<i>41</i>
<i>III. Ki-67: a new important player in cancerogenesis.....</i>	<i>43</i>
<i>1. The ablation of Ki-67 affects the transforming potential of Ras in mouse cells.....</i>	<i>43</i>
<i>2. Ki-67 depletion can protect mice from intestinal carcinogenesis.....</i>	<i>44</i>

2.1. <i>Ki-67 depletion inhibits the development of colonic neoplasms in AOM-DSS treated mice</i>	44
2.2. <i>Ki-67 depletion affects the formation of intestinal neoplasms in the <i>Apcd</i>¹⁴ mouse model</i>	47
3. <i>Ki-67 depletion does not affect the chemically acute induced intestinal inflammation in mice</i>	49
4. <i>Ki-67 is required for tumour development and establishment of metastasis</i>	50
4.1. <i>Ki-67 is dispensable for 4T1 cell proliferation</i>	50
4.2. <i>Ki-67 is required for the maintenance of the stem-like properties of 4T1 cells</i>	53
4.3. <i>Ki-67 depletion strongly affects 4T1 tumour growth and formation of lung metastases in athymic nude mice</i>	55
4.4. <i>Ki-67 absence prevents 4T1 tumour immune-mediated response and affects lung metastasis formation in immuno-competent mice</i>	57
5. <i>Ki-67 ablation sensitize cells to DNA methyltransferases inhibition</i>	60
6. <i>Ki-67 absence strongly impaired the development of MDA-MB-231 tumours in vivo</i>	62
7. <i>Ki-67 depletion does not affect MDA-MB-231 migration ability in vitro</i>	65
8. <i>Ki-67 depletion generates widespread transcriptomic changes in 4T1 cancer cells</i>	66
Discussion & perspectives	69
References	83

List of Figures

Figure 1: Immuno-cytochemical detection of Ki-67-reactive nuclear antigen in cytocentrifuge slides of HL60 cells.	2
Figure 2: The human MKI67 gene and Ki-67 mRNA structures.....	4
Figure 3: Comparison of human and mouse Ki-67 structural elements.....	6
Figure 4: Signaling integration through the CDK4/6–RB Pathway.....	8
Figure 5: Cell cycle-dependent localization of the Ki-67 protein.....	11
Figure 6: Mouse pericentromeric heterochromatin.....	16
Figure 7: Comparative analysis of the distribution of Ki-67 and nucleolar DNA.....	18
Figure 8: Ki-67 and the assembly of the mitotic Chromosome Periphery.	21
Figure 9: Proposed model of Ki-67-mediated mitotic chromosomes segregation....	23
Figure 10: Variable levels of Ki-67 staining in breast cancer.	25
Figure 11: Oncogenic reprogramming induced by epigenetic alterations.	31
Figure 12: Ki-67 ablation affects the transforming capacity of oncogenic Ras.....	44
Figure 13: Ki-67 depletion inhibits the development of colonic neoplasms in AOM-DSS treated mice.	46
Figure 14: Ki-67 depletion affects the formation of intestinal neoplasms in the <i>Apc^{d14}</i> mouse model.	48
Figure 15: Ki-67 depletion does not affect the chemically acute induced intestinal inflammation in mice.	50
Figure 16: CRISPR/Cas9-mediated ablation of Ki-67 does not affect the proliferative capacity of 4T1 cells.	52
Figure 17: Ki-67 is required for the maintenance of the stem-like properties of 4T1 cells.	54
Figure 18: Ki-67 depletion strongly affects 4T1 tumour growth and formation of lung metastases in athymic nude mice.....	56
Figure 19: Ki-67 absence prevents 4T1 tumour immune-mediated response and affects lung metastasis formation in Balb/c mice.....	59
Figure 20: Ki-67 ablation sensitizes cells to DNA methyltransferases inhibition.	61
Figure 21: CRISPR/Cas9-mediated ablation of Ki-67 does not affect the proliferative capacity of the TNBC-derived cell line, MDA-MB-231.	63
Figure 22: Ki-67 absence strongly impaired the development of MDA-MB-231 tumours in vivo.	64
Figure 23: Ki-67 depletion does not affect MDA-MB-231 migration ability in vitro.	66
Figure 24: Widespread transcriptomic changes in Ki-67 depleted 4T1 cells.....	68

Abbreviations

CDKs: Cyclin-dependent kinases

RB: Retinoblastoma

FHA: Forkhead-associated

hNIFK: human nucleolar protein interacting with the FHA domain of pKi-67

Hklp2: human kinesin-like protein 2

PP1: Protein Phosphatase 1

CD: Conserved Domain

NLS: Nuclear localization signal

PKC: Protein kinase C

APC/C: anaphase promoting complex, or cyclosome

MEFs: mouse embryonic fibroblasts

FCs: fibrillar centres

DFCs: dense fibrillar components

GCs: granular components

HDACs: histone deacetylases

HMTs: histone methyltransferases

DAPI: 4',6-diamidino-2-phenylindole

HP1: heterochromatin protein 1

DNMTs: DNA methyltransferases

UHRF1: Ubiquitin-like, containing PHD and RING finger domains 1

PNC: perinucleolar compartment

NAD: nucleolus-associated DNA

rDNA: ribosomal DNA

rRNA: ribosomal RNA

OR: olfactory receptor

ZNF: zinc-finger

PCNA: proliferating cell nuclear antigen

MCM: minichromosome maintenance

IHC: immunohistochemistry

ER: estrogen receptor

PgR: progesterone receptor

RENCA: renal cell carcinoma

CSCs: cancer stem cells

PDACs: pancreatic ductal adenocarcinomas

5-aza-dC: 5-aza-2'-deoxycytidine

PcG: polycomb group

PRC1/2: Polycomb repressive complex1/2

EZH2: Enhancer of zeste homolog 2

SUZ12: Suppressor of zeste 12 protein homolog

ESCs: embryonic stem cells

EMT: epithelial–mesenchymal transition

TGF- β : transforming growth factor beta

PR: perichromosomal layer

TNBC: triple-negative breast cancer

CRC: colorectal cancer

CRISPR: clustered regularly interspaced short palindromic repeats

TALEN: transcription activator-like effector nucleases

AOM: azoxymethane

DSS: dextran sodium sulphate

Apc: adenomatous polyposis coli

gDNA: genomic DNA

ALDH1: aldehyde dehydrogenase 1

MDSCc: myeloid-derived suppressor cells

RNA-seq: RNA sequencing

GSEA: Gene Set Enrichment Analysis

RRBS: reduced representation bisulfite sequencing

DYNAMETs: dynamic sensors of DNA methylation

iPS: induced pluripotent stem

ChIP: chromatin immunoprecipitation

VEGF: vascular endothelial growth factor

Introduction

Chapter I: Discovery & Early studies

The proliferation antigen Ki-67 was originally defined by a mouse monoclonal antibody that was obtained using a hybridoma from a mouse injected with nuclei of the Hodgkin's disease derived-lymphoma cell line L428. The resulting antibody was able to recognize a nuclear antigen present only in proliferating cells (e.g. cells from gastrointestinal mucosa, undifferentiated spermatogonia...) but did not react with cells in resting stage such as lymphocytes, monocytes, or Paneth's cells of gastrointestinal mucosa ¹. To demonstrate the association between Ki-67 presence and the proliferative status of a given cell population, Gerdes et al. (1983) induced the expression of the antigen recognized by Ki-67 in peripheral blood lymphocytes, following stimulation with phytohaemagglutinin A. This same antigen was not detected anymore in acute promyelocytic leukemia (HL60) cells stimulated with phorbol-esters for differentiation into mature macrophages (**fig.1**) ¹. In order to characterize the expression pattern of Ki-67 nuclear antigen, a cell cycle analysis was conducted. It showed its presence in G1, S, G2 and mitosis, and its absence in quiescent cells ². Due to its presence in all cycle phases, immuno-labelling techniques using Ki-67 antibody would constitute a valuable tool to assess the proportion of proliferating cells in tissue sections of various human neoplasms ². Indeed, Lellé et al. (1987) used Ki-67 immunostaining to determine the growth fraction of different breast invasive carcinomas, and obtained results that were similar to those obtained with other methods previously used in clinical settings such as thymidine labelling ³. By using a bivariate flow-cytometry analysis combining the immunocytochemical staining of Ki-67 and DNA in HeLa cells. Sasaki et al. (1987) showed an increased Ki-67 expression through cell cycle progression, with a greatest level at G2-M phase. Furthermore, DNase I treatment led to the disappearance of the antigen from these cells. This suggested that Ki-67 is not bound to the nuclear matrix, but instead to DNA ⁴. Although the use of Ki-67 immuno-labelling in cancer histopathology to determine the growth fraction of human neoplasms was becoming

more frequent and well documented ⁵, the nature of the antigen recognized by Ki-67 remained unknown.

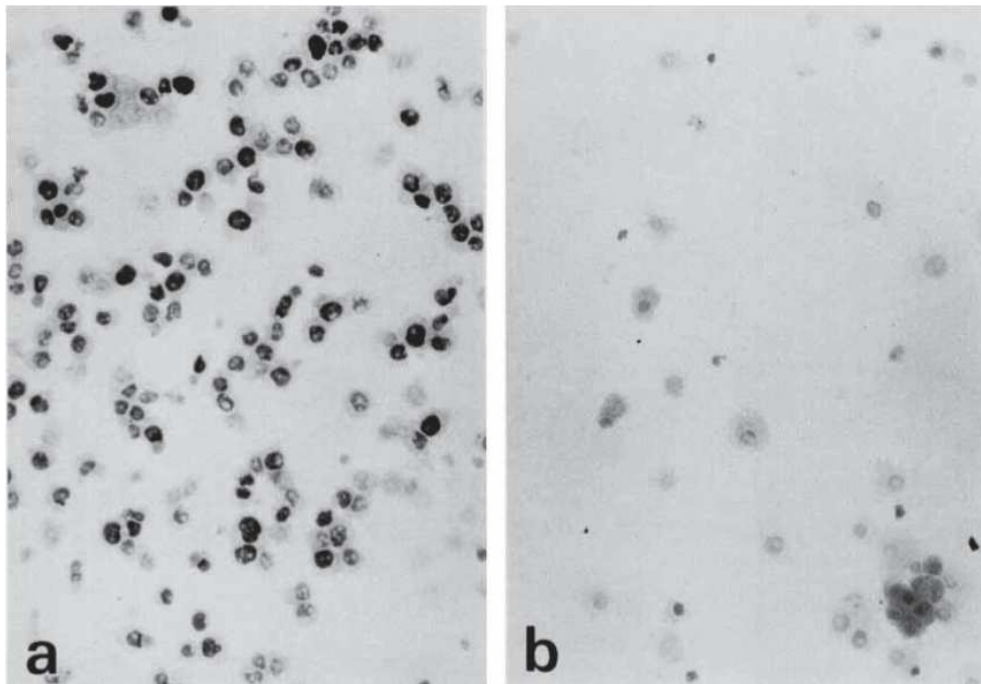


Figure 1: Immuno-cytochemical detection of Ki-67-reactive nuclear antigen in cytocentrifuge slides of HL60 cells (a) before and after (b) TPA.

Nearly 80% of cells were positively stained (black staining) with Ki-67 monoclonal antibody (a), whereas the staining almost disappeared following 84h of TPA-induced differentiation of HL60 into mature macrophages (b). X130 (adapted from ¹).

Chapter II: Ki-67 molecular characterization

By immuno-screening a cDNA library prepared from the lambda gtl 1 of IM-9 cells with Ki-67 antibody, Gerdes et al. (1991) were able to isolate and sequence a 1095-bp fragment, which was then sub-cloned and bacterially expressed for further analysis. This fragment could hybridize with a large 7.5 to 9.5 kb mRNA extracted from proliferating cells in Northern blot analysis. Moreover, immunoblotting with Ki-67 using cell lysates of continuously dividing cells has revealed the presence of two bands with molecular weights of 345 and 395 kD. Furthermore, biochemical characterization showed that Ki-67 is highly susceptible to protease treatment, and is a non-histone protein ⁵. Isotopic *in situ* hybridization was performed using this cDNA fragment as a probe, which allowed the mapping of Ki-67 gene locus on the long arm of chromosome 10; 10q25-ter ⁶.

Later on, cloning and sequencing the full length Ki-67 cDNA revealed the presence of 15 exons and 14 introns. This allowed the identification of two distinct spliced isoforms that varied in the presence or absence of exon 7 (**fig.2**). In fact, these two isoforms correspond to the two bands reported by Gerdes et al. (1991) in immunoblotting analysis using Ki-67 antibody ⁷.

The Ki-67 human gene; MKI67 consists of a sequence of 29965 bp length comprising 15 exons and 14 introns. Interestingly, exon 13 of this gene contains 16 homologous segments of 366 bp, known as Ki-67 repeats, each including a highly conserved new motif of 66 bp called the Ki-67 motif. Computational analysis of Ki-67 cDNA and its corresponding amino acid sequences did not reveal any significant homology with other known protein families in the queried protein databases ⁸. Orthologs of the MKI67 gene have been found in several vertebrates including chimpanzee, rhesus monkey, dog, cattle, mouse, rat and Xenopus.

The Ki-67 core promoter is located from -223 to +12 nucleotides relative to the transcription start site, which is in exon 2. This TATA-less and GC-rich promoter harbours several putative Sp1 binding sites that are essential to transcriptional regulation of the Ki-67 gene ^{9, 10}. Previous studies revealed that the MKI67 gene promoter contains binding sites for the E2F family of transcription factors. Among the genes targeted by E2F transcription factors are genes that encode proteins implicated in the regulation of cell-cycle machinery such as, Cyclines, Cyclin-dependent kinases and proteins from the Retinoblastoma (RB1) family ^{11, 12}.

site for the serine/threonine phosphatase, Protein Phosphatase 1 (PP1). In fact PP1 and protein phosphatase 2A are two of the major serine/threonine-specific phosphatase families that are required for mitotic exit, through their ability to counteract mitotic kinases¹⁹. The PP1 domain is located between amino acid residues 502 to 563 and a conserved domain (CD) of unknown function that includes a 22 amino acid motif²⁰.

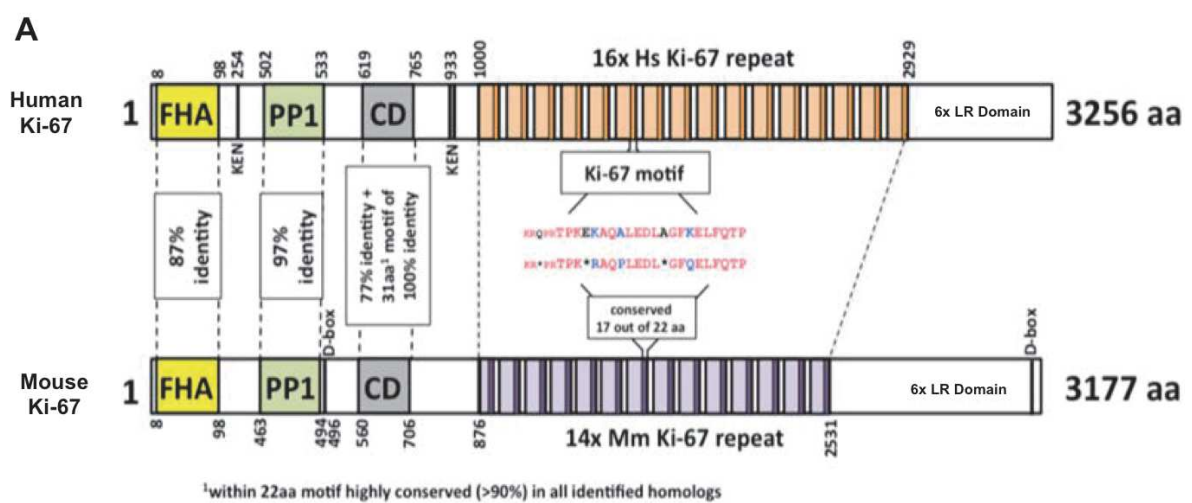
At the centre, Ki-67 protein display a unique feature: the occurrence of 16 repeated elements, known as the “Ki-67 repeats”, each consisting of 122 amino acid residues. These Ki-67 repeats share between 43 and 62% identical amino acid residues. Furthermore, these repetitive elements enclose a highly conserved region of 22 amino acids called the “Ki-67 motif”. The “Ki-67 motif” has 72 to 100% similarity to the consensus sequence and contains the epitope (F K E L), recognized by the original Ki-67 prototype antibody⁸. While in the Ki-67 murine homologue (**fig.3**) only 14 repeat units were discovered, the “Ki-67 motif” consensus sequence is strongly conserved (17 out of 22 amino acids) between the two species²¹.

The C-terminus has a conserved leucine/arginine (LR) rich domain through which Ki-67 can bind DNA^{22, 23}.

Since Ki-67 is a nuclear protein, two putative monopartite nuclear targeting sequences (502-505 & 687-690 aa) at the N-terminal part were revealed. These sequences could function as nuclear localization signals (NLS), which lead to the import of Ki-67 through the classical importin α/β nuclear import mechanism. In addition, computer analysis has shown the presence of eight bipartite nuclear targeting signals that also could mediate the nuclear localization of Ki-67^{8, 13}.

Early studies have shown a high susceptibility of this protein to protease treatment⁵. This characteristic may be explained by the presence of 10 strong and 40 weak ‘P-E-S-T’ (Pro, Glu, Ser, Thr) sites, which function as proteolytic signals that target Ki-67 for rapid degradation^{8, 24}. Following Ki-67 translation, computer analysis has predicted several post-translational modifications including 19 N-myristoylation, 3 amidation and over 200-phosphorylation site, including 143 Protein kinase C (PKC), 89 casein kinase II, 2 tyrosine kinase sites and 8 consensus sites for Cdc2 kinase⁸. However, the biological relevance of these post-translational modifications is still elusive.

Initially, two protein isoforms of Ki-67 were found at the predicted molecular weights of respectively 359 (isoform α) and 320 kDa (isoform β), resulting from the alternative splicing of exon 7⁷. Analysing Ki-67 expression in different cultured cells and tumour tissues has indicated the presence of three other isoforms: Ki-67 γ (lacking exon 3, 4, and 7), Ki-67 δ (lacking exons 3 to 12) as well as Ki-67 ϵ (lacking parts of exon 7). Although these five splice variants differ in their N-termini, they contain identical C-terminal and central (i.e. exon13) regions with the later carrying the “Ki-67 repeats”, where the epitope (F K E L) recognized by the prototype Ki-67 antibody is found²⁵.



B

Position	Peptide	Score	Cutoff	Type
Human Ki-67 isoform 1				
254-256	ELDVKSQKENVLQYCRK	17.59	8.28	KEN
933-935	ERPFETYKENIELKEND	16.09	8.28	KEN
939-941	YKENIELKENDEKMKAM	18.59	8.28	KEN
Human Ki-67 isoform 2				
573-575	ERPFETYKENIELKEND	16.09	8.28	KEN
579-581	YKENIELKENDEKMKAM	18.59	8.28	KEN
Mouse Ki-67				
496-499	RGETPTKRKSLGTHSPAV	5.88	5.16	D
3139-3142	CLRSRKTIVALDESPKPR	5.69	5.16	D

Figure 3: Comparison of human and mouse Ki-67 structural elements.

(A) Top: cartoon of human (long form) and mouse Ki-67 protein highlighting conserved elements and functional motifs. Domains are indicated by boxes (FHA, forkhead-associated domain; PP1, PP1-binding domain; CD, conserved domain; D-box: APC/C targeting destruction box motifs; KEN: APC/C-Cdh1 targeting KEN box motifs). Highly conserved regions are indicated by dotted line with percentage of identical amino acids.

(B) APC/C targeting motifs identified in human (both isoforms) and mouse Ki-67 (adapted from²⁶).

Chapter III: Ki-67 expression and control during the cell cycle

Early characterization of the antigen recognized by the Ki-67 prototype antibody indicated that Ki-67 expression is associated with cell populations known to proliferate efficiently. Conversely, upon cellular differentiation or induced proliferation arrest, Ki-67 expression was completely abrogated ¹.

Analysis of Ki-67 expression during the first G1 phase showed inconsistencies between studies, some authors were reporting that cells in the initial G1 phase were completely negative for Ki-67 ²⁷, while other authors claimed a positive staining for Ki-67 in the late G1 phase ². Although, Ki-67 expression during the initial G1 phase was a matter of discussion, all the studies that investigated Ki-67 expression upon induction of cell proliferation confirmed that G1 cells in subsequent divisions were positive for Ki-67 expression. Nonetheless, these studies did not agree on the relative Ki-67 expression during the G1 phase. In fact, two different patterns were reported: an increased expression, already starting in late G1 ²¹, or a decreased expression until the onset of DNA replication ²⁷. Some authors hypothesised that these variations may be explained by local growth conditions that might influence the proliferative potential of cells, and therefore may affect Ki-67 expression during G1 phase ²⁸. Indeed, these observations raise questions as to whether Ki-67 expression is a late marker of cell cycle entry, and whether it can still be detected in cells leaving the cell cycle.

During the S phase, Ki-67 staining increases. This increase becomes more remarkable during the G2 phase, and staining intensity is highest in metaphase. As the cells move through the end of mitosis (i.e. anaphase/telophase) the intensity of Ki-67 staining begins to decrease ²⁹. These observations raise the question of how the expression of Ki-67 in proliferating cells is promoted from the onset of S phase to metaphase, and what the mechanisms controlling its expression and degradation during cell cycle progression are.

Previous studies have demonstrated the importance of the signalling pathway that leads to the accumulation of D cyclin-CDK4/6 activity, resulting in the phosphorylation

of the RB protein family, allowing the removal of RB-mediated repression of the E2F transcription activity. In fact, several experiments have indicated the critical role of E2F proteins in the regulation of the expression of genes required for DNA replication and subsequent cell cycle progression (**fig. 4**)³⁰.

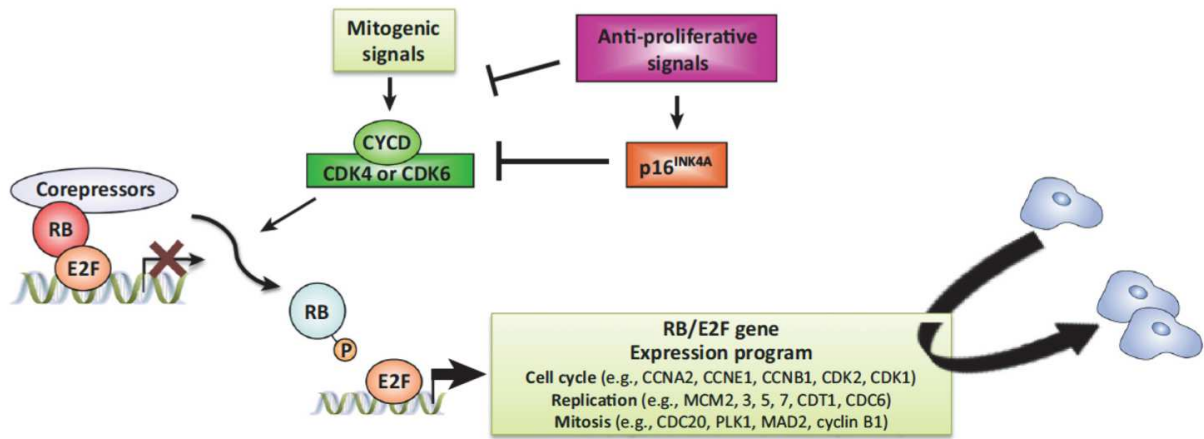


Figure 4: Signaling integration through the CDK4/6–RB Pathway.

In response to dominant mitogenic conditions, the accumulation of active cyclin D-CDK4/6 complexes can initiate the phosphorylation of RB and release of the E2F family of transcription factors. This can be counter-balanced by the activity of physiological CDK4/6 inhibitors such as p16INK4a. The E2F family coordinates a gene expression program that is needed for cell cycle progression, DNA replication and mitosis (Adapted from³¹).

Although the transcriptional control of Ki-67 is poorly understood, it has been shown that the MKI67 promoter gene contains binding sites for the canonical G1-regulatory E2F family of transcription factors, and that Ki-67 mRNA accumulates upon E2F overexpression¹¹. Furthermore, an analysis of genes targeted by E2F in human primary fibroblasts showed the binding of E2F proteins to Ki-67 promoter following cell cycle entry³². This raises the possibility that the E2F proteins might induce Ki-67 expression through the CDK4/6-RB signalling pathway. Indeed, detailed analysis would be required to determine whether Ki-67 is directly promoted by CDK4/CDK6-dependant RB phosphorylation. Moreover, it is important to determine whether the cell cycle regulation accounts for Ki-67 expression variability in non-transformed and cancer cell lines as well as in tumours and human cancers.

As mentioned above, an increase in Ki-67 staining intensity was seen from the onset of S phase until metaphase. However, since the biological half-life of the Ki-67 protein was reported to be rather short (1h), this increase cannot be simply explained by an accumulation of proteins synthesized during this cell cycle time period²⁹. This implies that the Ki-67 protein expression might be the consequence of two opposing

mechanism: an active *de novo* synthesis, probably dependent on cell cycle regulators (i.e. CDK4/6-RB), and an effective protein degradation process, likely during late mitosis and G1 phase.

As discussed above, early molecular characterization of the Ki-67 protein revealed the presence of 10 strong and 40 weak 'P-E-S-T' (Pro, Glu, Ser, Thr) sites, proteolytic signals that are characteristic of proteins displaying a short biological half-life^{8, 24}.

The anaphase promoting complex, or cyclosome (APC/C), in association with Cdc20 or Cdh1 (encoded by the *Fzr1* gene in mammals), constitutes an ubiquitin ligase complex that specifically targets cell cycle proteins for degradation in late mitosis and G1 phase. While APC/C-Cdc20 complex is active during early mitosis, APC/c-Cdh1 is preferentially active from late mitosis to G1 phase³³.

In order to target proteins for degradation, APC/C-Cdc20 or APC/c-Cdh1 are able to recognize specific amino acid sequences present in their substrates. Although the most frequent motifs found in these substrates are the destruction (D) box (RXXLXXXXN/D/E) and KEN (KENXXXN) box, other motifs such as the A box can also be recognized by these complexes³⁴. Interestingly, human Ki-67 isoforms contain two or three KEN boxes, whereas mouse Ki-67 contains two D-boxes. Mouse Ki-67 contains an additional sequence, AQRKQPSR at 2680–2687, which is highly similar to the A-box that is recognized by APC/C-Cdh1 (**fig.3**). This suggests that Ki-67 might be a target for the APC/C-Cdh1 ubiquitin complex.

To test the potential role of Cdh1 in Ki-67 protein degradation, our team has previously conducted experiments to analyse Ki-67 expression in mouse embryonic fibroblasts (MEFs) lacking the *Frz1* gene³⁵. As expected, asynchronous *Fzr1* heterozygous MEFs showed different Ki-67 levels, however, unlike these heterozygous MEFs, Ki-67 expression was upregulated and more homogeneously expressed in *Fzr1* knockout MEFs. More importantly, assessment of Ki-67 expression in *Fzr1*-knockout mice in combination with BrdU incorporation assay showed that Ki-67 was overexpressed and uncoupled from cells that incorporate BrdU in all tissues examined, indicating that Ki-67 expression is regulated by APC/C-Cdh1 in mice.

Although uncovering the precise mechanisms underlying the regulation of Ki-67 during progression of the cell cycle may help shed some light on the biological

activity of this protein, looking at its cellular localization during each stage may also provide important insights regarding the biological functions of Ki-67.

Chapter IV: The Ki-67 localization is cell cycle-dependent

While Ki-67 is active in all cell cycle phases, its cellular distribution varies throughout the stages (**fig.5A**).

In early G1 cells, Ki-67 is located at numerous foci throughout the nucleoplasm. These foci correspond to centromeric (alpha-satellite), telomeric (minisatellite) and heterochromatic blocks (satellite III). However, during G1 progression (i.e. mid/late G1) the proportion of Ki-67 localized in these heterochromatic regions declines and most of Ki-67 becomes associated with reforming nucleoli³⁶. This association with the nucleoli organelles is maintained in S and G2⁶. These organelles form at the end of mitosis and constitute the primary site of ribosome biogenesis. Within the nucleolus, three distinct sub-regions are distinguished: fibrillar centres (FCs), dense fibrillar components (DFCs) and granular components (GCs). While most of the nucleolar proteins are found in the GC region where ribosome subunit assembly is finalized, transcription of rDNA repeats and processing/modification of pre-rRNA transcripts take place in the FC and the DFC, respectively³⁷. Indeed, microscopy analysis has revealed that Ki-67 localizes to a particular region of the DFC that is deficient in nucleolin, p130 and fibrillarin, named the “fibrillarin-deficient region of the dense fibrillar component”^{38, 39}.

Moving through mitosis, Ki-67 relocates during prophase from the dissociating nucleoli to coat the surface of condensed chromosomes. This mitotic localization is accompanied by Ki-67 phosphorylation by protein kinase C and cdc2/Cyclin B⁴⁰. In metaphase, Ki-67 covers the outer surface of individual chromosomes and constitutes a component of the perichromosomal periphery (**fig.5B**). This mitotic compartment comprises different proteins and ribonucleoprotein complexes; many of them originate from nucleoli such as the nucleolar proteins fibrillarin and nucleolin^{20, 19}. This association with the perichromosomal periphery is maintained during anaphase. However, toward the end of telophase, as the chromosomes start to decondense, Ki-67 becomes dephosphorylated and disperses throughout the nucleoplasm at the sites of newly reformed nucleoli^{6, 40}. It is noteworthy that the

integration of Ki-67 to the reforming nucleoli occurs at a relatively late time point, when other nucleolar proteins such as fibrillarin, nucleolin are already present ⁶.

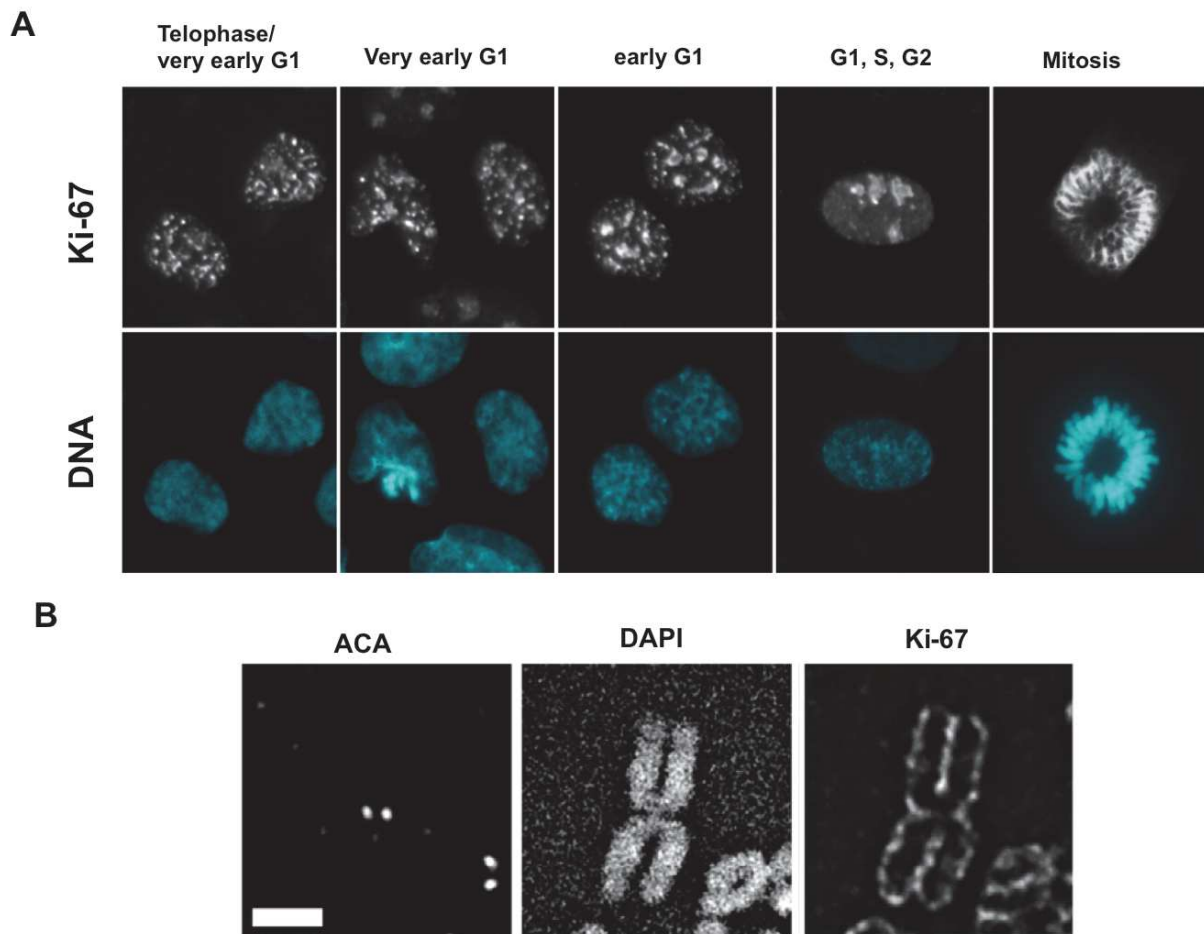


Figure 5: Cell cycle-dependent localization of the Ki-67 protein.

(A) During the early G1, Ki-67 co-localizes with telomeric and pericentromeric regions that correspond to the foci (white foci) revealed by Ki-67 staining. During the G1 phase progression, this co-localization is reduced, at the end of G1, Ki-67 integrates into the nucleoli and remains (G1, S, G2) until the onset of mitosis. At mitosis, Ki-67 covers the condensed chromosomes and become associated with the perichromosomal layer. (B) Light microscopy visualization of the perichromosomal layer on RPE metaphase chromosomes (DAPI) using anti-centromere antibody (ACA), and Ki-67 antibodies. Scale bar; 1 μ m (B). (Adapted from ^{38 & 41}).

In summary, it is clear that the Ki-67 protein is associated with cell proliferation, and that its expression and localization vary throughout the cell cycle. However, it remains unknown whether its regulation is also integrated into the regulatory protein network that drives the cell cycle progression. More importantly, it is critical to uncover the biological significance of Ki-67 presence, both in physiological circumstances and in malignancies.

Chapter V: The biological significance of Ki-67

Although considerable efforts have been made towards molecular characterization of the Ki-67 protein, its function remains elusive.

One reason for the difficulty in elucidating the functional role of Ki-67 might be the lack of apparent homology with other proteins having known functions. Other reasons might be the size and the high susceptibility of Ki-67 to protease cleavage, which makes handling this protein in biochemical assays problematic. Furthermore, Ki-67 is present only in vertebrates, thus excluding the possibility of studying its cellular functions in simple organisms such as yeast and flies.

Nevertheless, some progress has recently been made in the understanding of the biological importance of Ki-67.

1. Ki-67 and cell proliferation

Early studies that aimed to decipher the functional role of Ki-67 in proliferating cells have assumed that Ki-67 is required for cell proliferation and cell cycle progression. In fact, it was reported that DNA synthesis could be inhibited in cultured cells following their incubation with oligodeoxynucleotides complementary to the Ki-67 mRNA⁷. In line with this, the microinjection of antibodies targeting Ki-67 into nuclei of Swiss-3T3 cells has reduced the rate of cell division²¹. In proliferating cells there is an increased demand for protein synthesis that is achieved by changes in the rate of ribosome biogenesis. In fact, some reports have suggested a potential involvement of Ki-67 in rRNA synthesis in response to mitogenic signals, and speculated that Ki-67 may act as an “intensifier” of ribosome biogenesis, therefore supporting cell proliferation^{42, 43}.

These observations suggest that Ki-67 might be required for cell proliferation. However, in addition to the technical limitations (e.g. potential off-targets...) of such approaches, the authors of these studies did not use loss of function (i.e. null mutation) approaches in order to address the role of Ki-67 in cell proliferation. More importantly, it was shown that Ki-67 is expressed in the embryonic nuclei at the first mitosis during mouse development⁴⁴. Indeed, it will be important to investigate the *in vivo* requirement for Ki-67 in development (e.g. organogenesis) and tissue differentiation.

2. Ki-67 a potential role in chromatin compaction

In eukaryotes, chromatin results from the association between DNA and histone proteins. Depending on the level of chromatin compaction, two distinct structural and functional states are distinguished: gene-high content, less compacted euchromatin and gene-low content, highly condensed heterochromatin⁴⁵. While, facultative heterochromatin is enriched by H3K27me3 marks and is typically found in genes that are regulated during development. Constitutive heterochromatin typically assembles mainly at repetitive elements such as pericentromeric tandem repeats, is characterized by high levels of H3 trimethylation on lysine 9 (H3K9me3) and DNA methylation, and is found in gene-poor chromosomal regions⁴⁶.

In fact, different chromatin-modifying enzymes are involved in the formation of these heterochromatin domains. Initially recruited, the combined action of histone deacetylases (HDACs) and the SUV39 family histone H3K9 methyltransferases (HMTs) ensure hypo-acetylation of histones and hyper-methylation of H3K9 at the nucleation sites. Methylated H3K9 in turn can bind to heterochromatin HP1 proteins and therefore recruit further chromatin modifiers, which subsequently lead to the spread of heterochromatin along large chromatin domains⁴⁵.

Thanks to its staining pattern in immunofluorescence approaches, mouse pericentromeric heterochromatin (**fig.6A**) became a model for studying the organization and maintenance of constitutive heterochromatin⁴⁷. In mouse somatic cells, for example at the pericentromeric loci, H3K9me3 co-localize with 4',6-diamidino-2-phenylindole (DAPI)-dense foci that correspond to the major satellite repeats (**fig.6B**). At the pericentromeric heterochromatin the presence of H3K9me3 acts as a platform for the targeting of several HP1 isoforms (e.g. HP1 α) that in turn recruit many factors, including histone deacetylases and chromatin remodelling enzymes to ensure transcriptional silencing, DNA methylation, and chromosomal cohesion⁴⁶.

Although previous studies attributed a highly stable state to these constitutive heterochromatin domains, recent discoveries challenged this view and showed the dynamic nature of these regions. Indeed, HP1 proteins were found to be highly dynamic, fluctuating between chromatin-bound and free forms in the nucleoplasm⁴⁵.

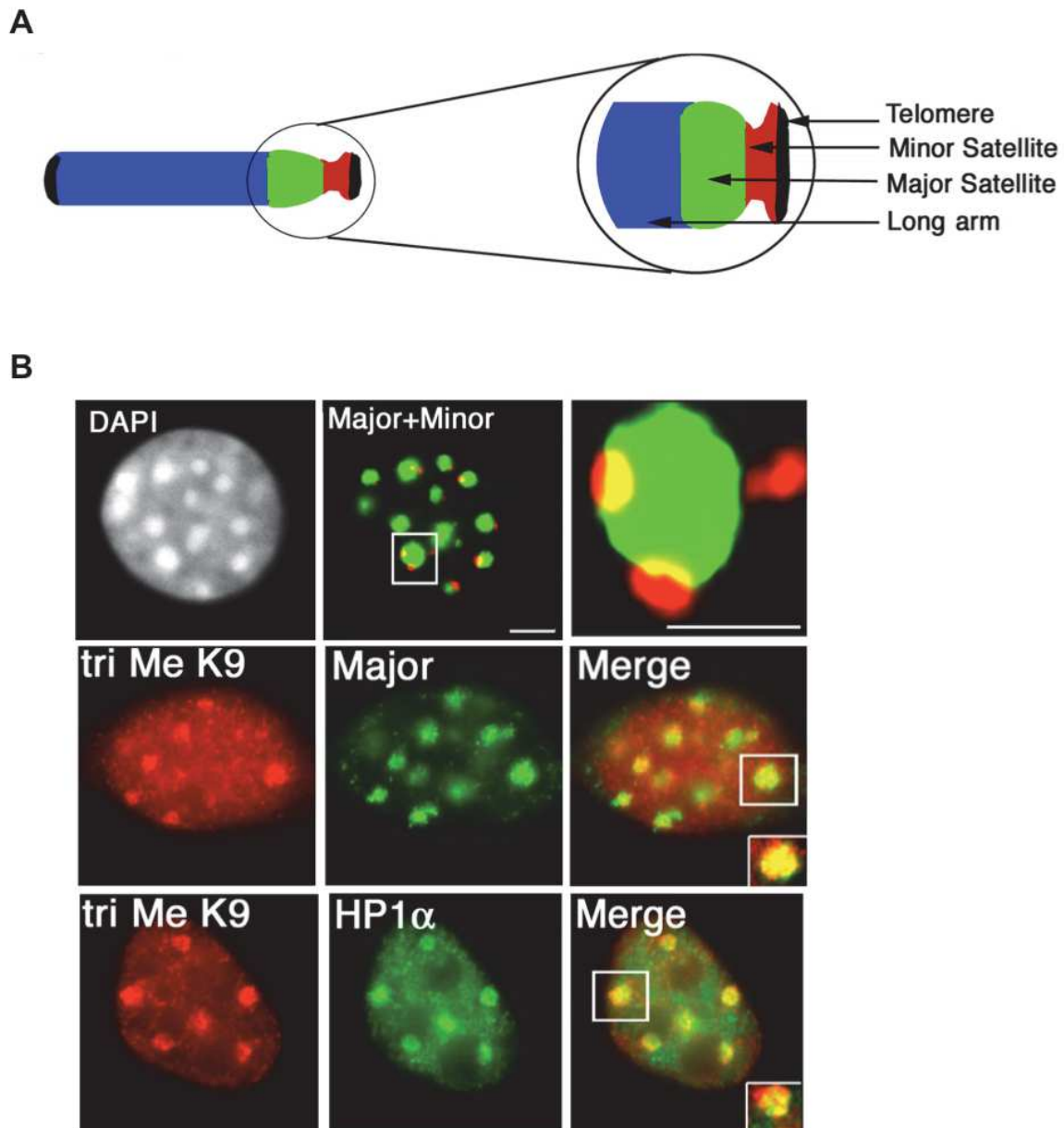


Figure 6: Mouse pericentromeric heterochromatin.

(A) An acrocentric mouse chromosome scheme with a close-up view of the centromeric region highlighting the localization of telomeres (black), major satellites (green), and the long arm of the chromosome (blue). (B) DNA sequences (major & minor satellites) and marks (H3K9me3 & HP1 α) associated with the pericentromeric heterochromatin in 3T3 cells. (B, Top) DNA fish of major (green) and minor (red) satellite DNA (DAPI) with a close view of selected foci. (B, middle) H3K9me3 (tri Me K9) staining (red) combined with Fish for major satellite. (B, bottom) H3K9me3 (tri Me K9) staining (red) combined with HP1 α staining (green). Scale bars; 5 μ m (Adapted from ⁴⁷).

Besides H3K9me3 enrichment, major satellites are specifically methylated on cytosines by DNA methyltransferases (DNMTs). While *de novo* methyltransferases DNMT3a and DNMT3b establish the DNA methylation, DNMT1 is known as the maintenance methyltransferase, and was shown to be involved with the Ubiquitin-like, containing PHD and RING finger domains 1 (UHRF1) cofactor in propagating

DNA methylation patterns after DNA replication⁴⁶. Originally, it was speculated that H3K9me3, H4K20me3 and/or H3K27me3 presence was required for subsequent DNA methylation; SUV39HA/2-mediated H3K9 dimethylation or trimethylation was shown to be a prerequisite for efficient targeting of DNMT3B at pericentromeric heterochromatin. Furthermore, UHRF1 can bind specifically both H3K9me3 and HP1 proteins, which mediate DNMT1 recruitment^{48, 49}.

In addition to H3K9me3, methylation of H4K20 and H3K27 is found in silenced heterochromatin regions and is also involved in heterochromatin formation and maintenance. As mentioned above, the H3K27me modification constitutes a characteristic hallmark of facultative heterochromatin, and is needed for maintaining transcriptional repression programs that are initiated during development in many organisms. The Polycomb Repressive Complex 2 (PRC2) that contains EZH2, EED, SUZ12, RBBP4/7 and JARID2 catalyses this methylation on H3K27. In fact, through its SET domain, the histone methyltransferase (HMT) EZH2 is able to catalyse H3K27 di-methylation and tri-methylation (H3K27me_{2/3}) but requires both EED and SUZ12 to ensure this catalytic reaction⁵⁰. Interestingly, while overexpression of EZH2 was shown to increase CpG methylation, conversely EZH2 depletion decreases H3K27 methylation and DNA methylation at specific known EZH2 target genes. Furthermore, binding of DNMTs to certain EZH2 targets promoters involved a physical interaction between EZH2 and DNMTs⁴⁸. Moreover, H3K27me₃ is recognized by the E3 ubiquitin ligases RING1B found in the canonical PRC1 and is thought to mediate H2AK119 monoubiquitylation and promote chromatin compaction which in turn result in transcriptional repression⁴⁹.

Together, these epigenetic modifications cooperate with additional factors to regulate the mammalian genome organization by modulating the chromatin dynamics and thus regulating its accessibility and compactness. Nonetheless, the patterns of these modifications are specific of a given cellular state or of a specific developmental program, participating therefore in the establishment of cellular identity⁵¹.

Early studies that aimed to understand the biochemical properties of Ki-67 suggested a possible interaction between Ki-67 and DNA⁴. The first evidence of this potential interaction came from the enhanced affinity seen of two different Ki-67 antibodies

toward the repeat regions of the Ki-67 protein when the later is in complex with DNA⁵². Additionally, an *in vitro* experiment using Ki-67 from nuclear extracts revealed the capacity of Ki-67 to interact with DNA cellulose⁴⁰. Furthermore, interphase nuclei from HeLa cells treated with micrococcal nuclease yielded chromatin fragments that carried Ki-67⁵³.

In line with these observations, analysis of Ki-67 localization has shown a co-localization between Ki-67 and centromeric proteins within the nucleolus. Moreover, disruption of nucleolar integrity using a specific drug in fibroblasts led to redistribution of Ki-67 to regions of heterochromatin as defined by DAPI staining³⁸. More detailed characterization allowed the mapping of the DNA binding domain of Ki-67 to its C-terminal 321 residues (2938-3256 aa), which contain several pairs of leucine (L) and arginine (R) residues^{23, 39}. Indeed, overexpression of the LR domain in human cells induced chromatin compaction that was accompanied by Heterochromatin Protein 1 (HP1) recruitment to chromatin³⁹. HP1 proteins were discovered within complexes involved in heterochromatin-mediated gene silencing. In human cells, three HP1 paralogs were identified: HP1 α and HP1 β are both found in heterochromatic regions such as centromeres and telomeres, and are associated with transcriptional gene silencing. Conversely, HP1 γ is localized in euchromatin regions (i.e. gene-rich regions of the genome) and is involved in transcriptional elongation and RNA processing⁵⁴.

As previously mentioned, in early G1 cells, Ki-67 was located in small nuclear foci and at the periphery of nucleoli. Immunofluorescence analysis conducted on such cells showed a co-localization between Ki-67 and both HP1 α and HP1 γ at heterochromatic regions, which were densely stained with Hoechst 33342. This co-localization was further enhanced after disruption of nucleolar integrity leading to redistribution of Ki-67 to centromeric chromatin⁵⁵. Moreover, the LR domain of Ki-67 was able to interact with all the HP1 isoforms *in vitro* and *in vivo*. Interestingly, ectopic expression of HP1 fused to GFP in HeLa cells resulted in the relocalization of endogenous Ki-67 associated with nucleoli to newly formed GFP-HP1 nucleoplasmic foci²².

Together, these results indicate that the interaction between Ki-67 and HP1 isoforms takes place in heterochromatic regions during the early G1 when Ki-67 is not

confined in nucleoli, suggesting a role of Ki-67 in the organization of chromatin compaction.

To study the functional distribution of Ki-67 during interphase, Cheutin et al. (2003) used confocal microscopy and electron tomography to examine the organization of Ki-67 in the lung carcinoma derived-cell line A549. As described by previous studies, microscopy analysis followed by 3D reconstruction confirmed that Ki-67 is absent from the fibrillar and the granular components of the nucleolus. Indeed, these observations showed that Ki-67 forms a shell around the nucleoli, and is co-localized with perinucleolar heterochromatin at the periphery of the nucleolus (**fig.7A**)⁵⁶.

In fact, the perinucleolar compartment (PNC) is a dynamic structure located at the periphery of the nucleolus (**fig.7B**). The PNC is enriched with RNA-binding proteins and a subset of newly synthesized pol III transcripts⁵⁷. This structure is present throughout interphase; it is disassembled at the beginning of mitosis, following its dissociation from nucleoli. The PNC is then reassembled in daughter cells during late telophase⁵⁷. Although the functional relevance of this structure is still elusive, studies have shown the prevalence of the PNC in several primary tumours, whereas it is almost absent in non-transformed cells. Furthermore, PNC presence was correlated with metastatic capacity in different types of solid tumours, since its prevalence increases in cell lines derived from distant metastasis⁵⁸.

More detailed characterization revealed that Ki-67 forms 250–300 nm diameter cords, which are composed of 30–50-nm-thick fibers. These analyses suggest a potential Ki-67 involvement in the organization of perinucleolar chromatin⁵⁶.

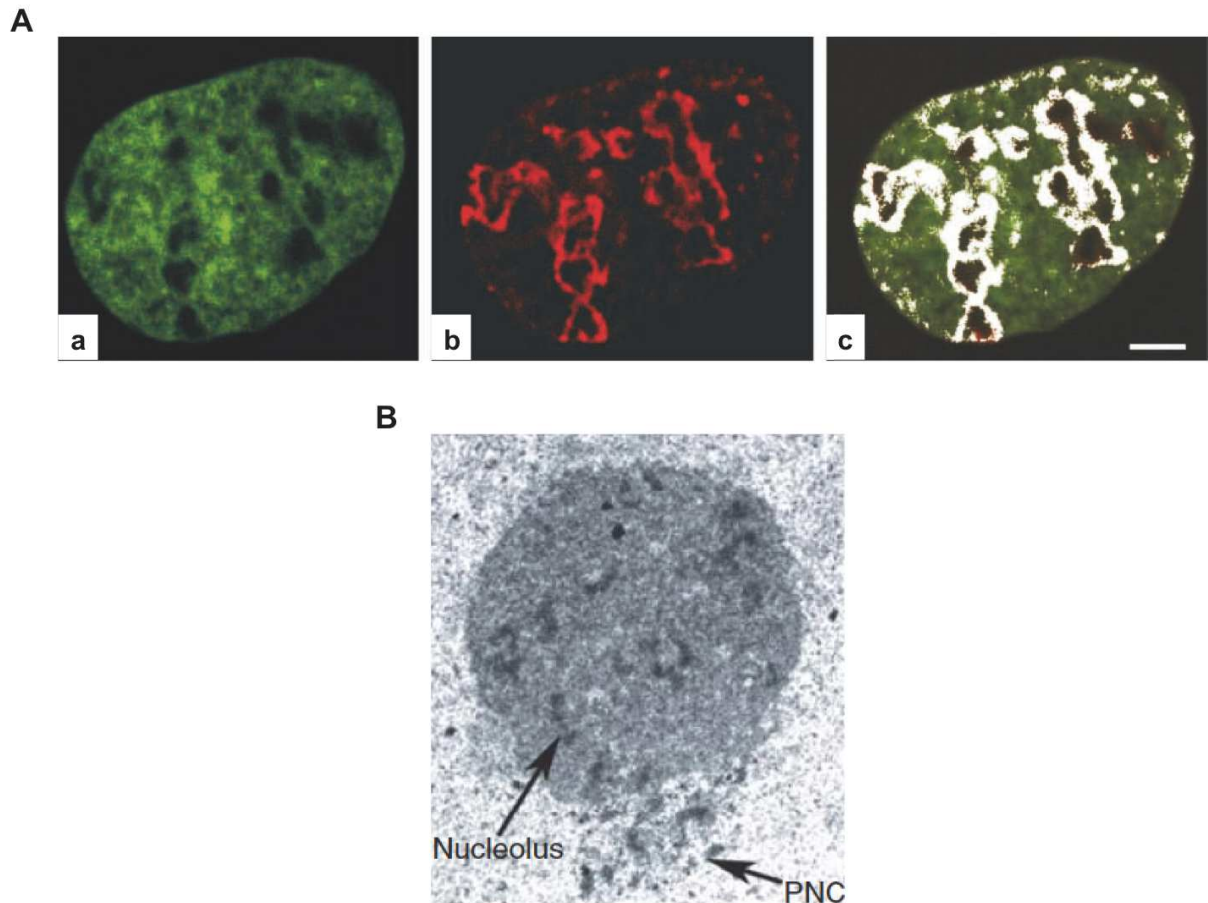


Figure 7: Comparative analysis of the distribution of Ki-67 and nucleolar DNA.

(A) Optical sections of confocal microscopy analysis of the distribution of Ki-67 (b) relative to DNA stained by chromomycin A3 (a) in A549 cells showing the almost co-localization pattern (c): 'White area' between Ki-67 and DNA at the nucleolar periphery. (B) Electron microscopy section showing the perinucleolar compartment (PNC) at the periphery of the nucleolus. Scale bar; 3 μ m. (Adapted from ^{56 & 57}).

Although the protein composition of nucleoli was well known ³⁷, the nature of chromatin enriched with the nucleolus-associated DNA (NAD) was not yet characterized. Indeed, fluorescent *in situ* hybridization (FISH) analysis conducted on human lymphocyte metaphase spreads localized the NAD to the short-arms of acrocentric chromosomes (i.e. chromosomes 13, 14, 15, 21 and 22), in which clusters of ribosomal DNA (rDNA) repeat units and centromeres of several chromosomes are found. Moreover, sequencing and mapping of the NAD in the human genome identified one thousand thirty-seven genes within the NAD. In fact, bioinformatics and statistical analyses showed enrichment in members of the zinc-finger (ZNF), olfactory receptor (OR), defensin and immunoglobulin gene families. In addition, block of certain types of satellite repeats (e.g. α -Satellite) and RNA genes were also identified in these domains ⁵⁹. More importantly, the nucleolus-associated

chromatin domains displayed specific enrichment of multiple repressive histone marks (i.e. H3K27me3, H3K9me3, and H4K20me3) compared to the active histone mark H3K4Me1, resulting in reduced global gene expression. These results suggest that NADs form large inactive chromatin domains in the interphase nucleus⁵⁹.

Interestingly, the α -Satellite DNA localization to the perinucleolar region was reduced in HeLa cells upon depletion of Ki-67, but not of nucleolin, a nucleolar protein also found at the perinucleolar region⁶⁰. Similarly, nucleolar integration of lacO array proximal to the rDNA repeats was reduced following Ki-67 depletion in HT1080 cell line²⁰. These results suggest that Ki-67 is required for efficient localization of NADs to nucleoli.

In line with these findings, previous results from our team showed that Ki-67 knockdown in both HeLa and U2OS cells caused the disruption of PNC heterochromatin as mirrored by a reduction in perinucleolar DAPI staining. Also, Ki-67 silencing in these cells decreased the nucleolar association of the centromeric histone variant CENP-A. More importantly, Ki-67 down-regulation led to altered expression of genes highly enriched in NADs, such as genes encoding zinc-finger proteins and olfactory receptors. This effect on gene expression following Ki-67 depletion might be attributed to an altered chromatin compaction, specifically in the perinucleolar heterochromatin.

To determine how Ki-67 might be mechanistically involved in chromatin compaction, our team has identified Ki-67 interacting partners. Among the proteins found are at least seventeen proteins that are involved in histone methylation complexes or interactors of methylated chromatin. These results suggest that Ki-67 might promote heterochromatin formation and maintenance by targeting these interactors to their specific genomic sites. In fact, Ki-67 down-regulation resulted in reduction of H3K9me3 and H4K20me3 recruitment at heterochromatin sites. Conversely, overexpression of Ki-67 induced formation of ectopic heterochromatin foci enriched in these histone methylated marks and HP1 isoforms.

Together, these studies suggest a potential role of Ki-67 in promoting chromatin compaction and genome organization. Although the exact molecular mechanisms underlying this function are still missing, it will be interesting to determine whether Ki-67 might be involved in chromatin remodelling processes associated with cell

proliferation, for example during tumour development.

3. Ki-67 is involved in the organisation of the perichromosomal layer during mitosis

Early characterization of Ki-67 showed a particular staining found in mitotic cells. In fact, during late prophase and in late diplotene of meiosis, Ki-67 relocates to the outer surface of chromosomes where it contributes, with other components, to the formation of the perichromosomal layer, also known as the chromosome periphery.^{2, 61} Thanks to technological advances, the molecular analysis of this chromosomal compartment revealed a complex network of proteins and RNA molecules (many derived from nucleoli) that coats the outer surface of chromosomes (**fig.8A**). In fact, analysis conducted in metaphase RPE1 cells showed that the periphery constitutes 30%-47% of the entire chromosome volume and encloses 33% of chromosomal proteins. Remarkably, Ki-67 alone represents 1.6% of the total chromosomal protein mass. These results indicate that chromosomes are not mainly composed of chromatin structures as was previously suggested⁴¹.

In addition to shedding some light on the composition of chromosome periphery, recent technologies allowed a better understanding of the organisation of this mitotic compartment. Interestingly, Ki-67 appears to play an important role in the organisation and the assembly of the chromosome periphery following its recruitment to this compartment by the p150 subunit of the human CAF-1 protein^{62, 60}. Indeed Booth et al. (2014) showed that Ki-67 depletion prevented the accumulation of NIFK, B23, nucleolin, and four novel chromosome periphery proteins at the periphery of human chromosomes (**fig.8B**). Microscopy analysis of chromosomes from Ki-67-depleted cells suggested that the entire perichromosomal compartment is almost lost²⁰. Consistent with these observations, Ki-67 depletion prevented the association of several other nucleolar proteins, but also of pre-rRNAs, to the chromosome periphery⁶³. Conversely, removal of these proteins or rRNAs did not affect the localization of Ki-67 at the chromosome periphery^{20, 63}. Furthermore, in the absence of Ki-67, many of these mislocalised proteins formed aggregates of 1-5 μm located at one end of the metaphase plate. These structures were then spread throughout the cytoplasm

toward mitotic exit ²⁰. Together these studies suggest that Ki-67 constitutes a major organiser of this compartment by acting as a scaffolding protein or an interaction platform to assemble the different components of this mitotic layer ⁶³.

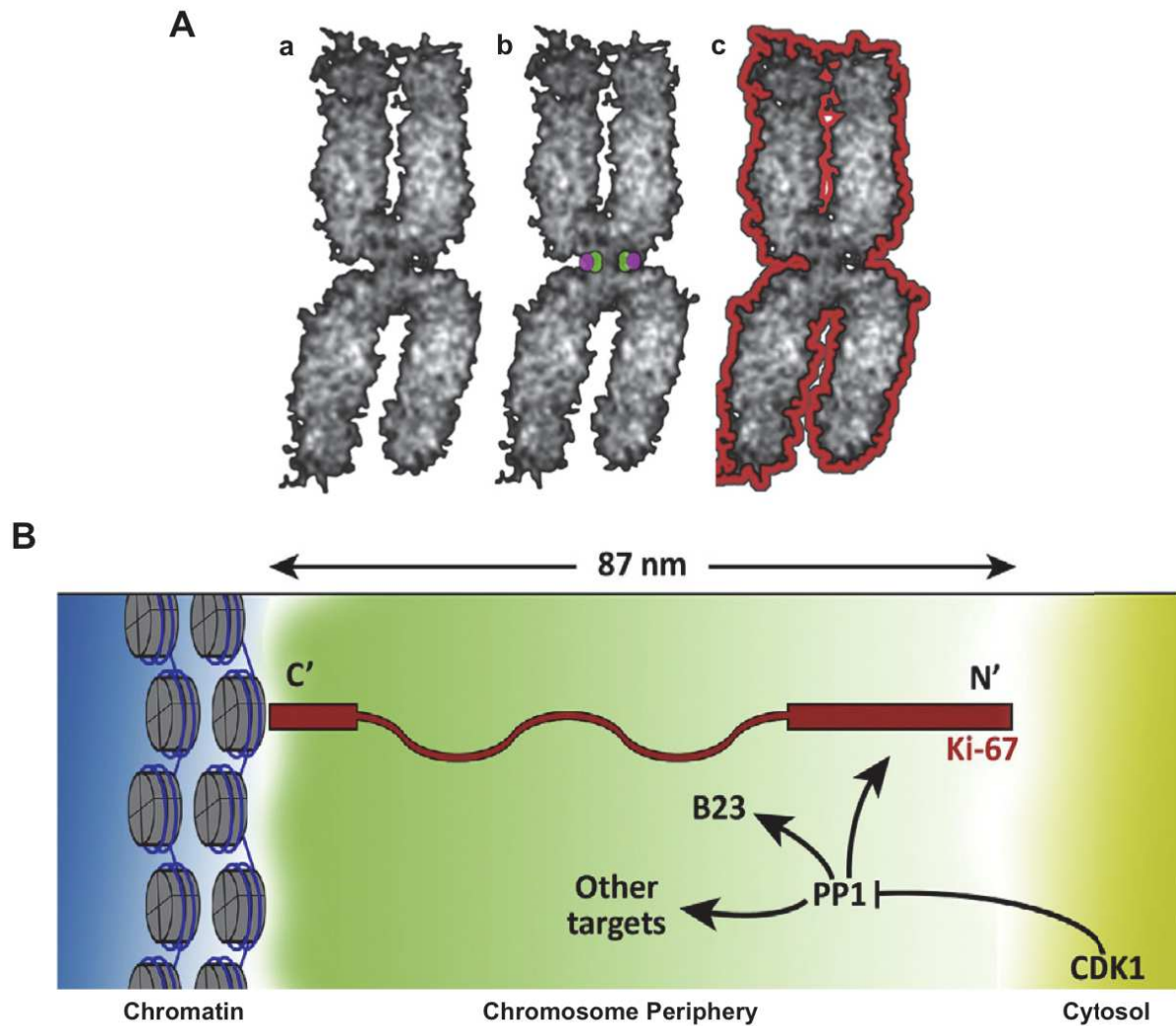


Figure 8: Ki-67 and the assembly of the mitotic Chromosome Periphery.

(A) Scheme depicting some of the core components of a mitotic Chromosome: the chromatin (a, grey) consisting of nucleosome units, the centromere (b, green) and kinetochore (b, magenta) and the Chromosome Periphery (c, red) which harbors different protein types (e.g. Nucleolar proteins) and RNAs. (B) Scheme of Ki-67 (red) at the mitotic Chromosome Periphery. Through its C-Terminus binds to chromatin (blue) while its N-Terminus comprises the binding site of the Protein Phosphatase 1 (PP1) that is negatively regulated by CDK1. Ki-67 allows the targeting of many proteins (e.g. B23) to the Chromosome Periphery promoting therefore its assembly (Adapted from ⁶²).

In addition to its role in the assembly of the perichromosomal layer, other studies aimed to decipher the functional relevance of Ki-67 enrichment in this compartment. Although Ki-67 was dispensable for the initial chromosome individualisation and condensation during prophase, Ki-67 was required to maintain the individualization of

mitotic chromosomes by preventing them from coalescing into a single chromatin mass during metaphase, which ensured normal chromosome segregation at anaphase⁶⁴. Similar to these findings, microscopic modelling and segmentation analysis of Ki-67-depleted chromosomes from RPE1 cells identified only 20 individual units, compared to the 46 seen in wild-type cells. Furthermore, while the removal of Ki-67 before mitotic entry in HCT116 cells did not affect the early mitotic chromosome assembly during prophase, it yielded to deformed mitotic chromosomes⁶⁵, thus confirming the clumping phenotype of Ki-67-depleted chromosomes reported by Cuylen et al. (2016)⁴¹. This chromosome separation function of the human Ki-67 protein was attributed to its physicochemical properties (i.e. brush-like; amphiphilic structure), which were similar to those of surface-active agents (surfactants). Thus, through a surfactant mechanism at the phase boundary between mitotic chromatin and the cytoplasm, Ki-67 coating of mitotic chromosomes prevents them from aggregating (**fig.9**)⁶⁴. It's important to note that Ki-67-depleted cells did survive the impaired chromosome individualisation, which might be explained by the initial separation of prophase chromosomes allowing access to kinetochores before coalescence⁶⁴. Moreover, the loss of the perichromosomal periphery following Ki-67 depletion did not impede the mitotic chromosome condensation or its intrinsic structure. However, notable alterations were observed in nucleolar reassembly and nuclear organisation in post-mitotic cells whose sensitivity to various stress conditions increased compared to their control counterparts^{20, 64}.

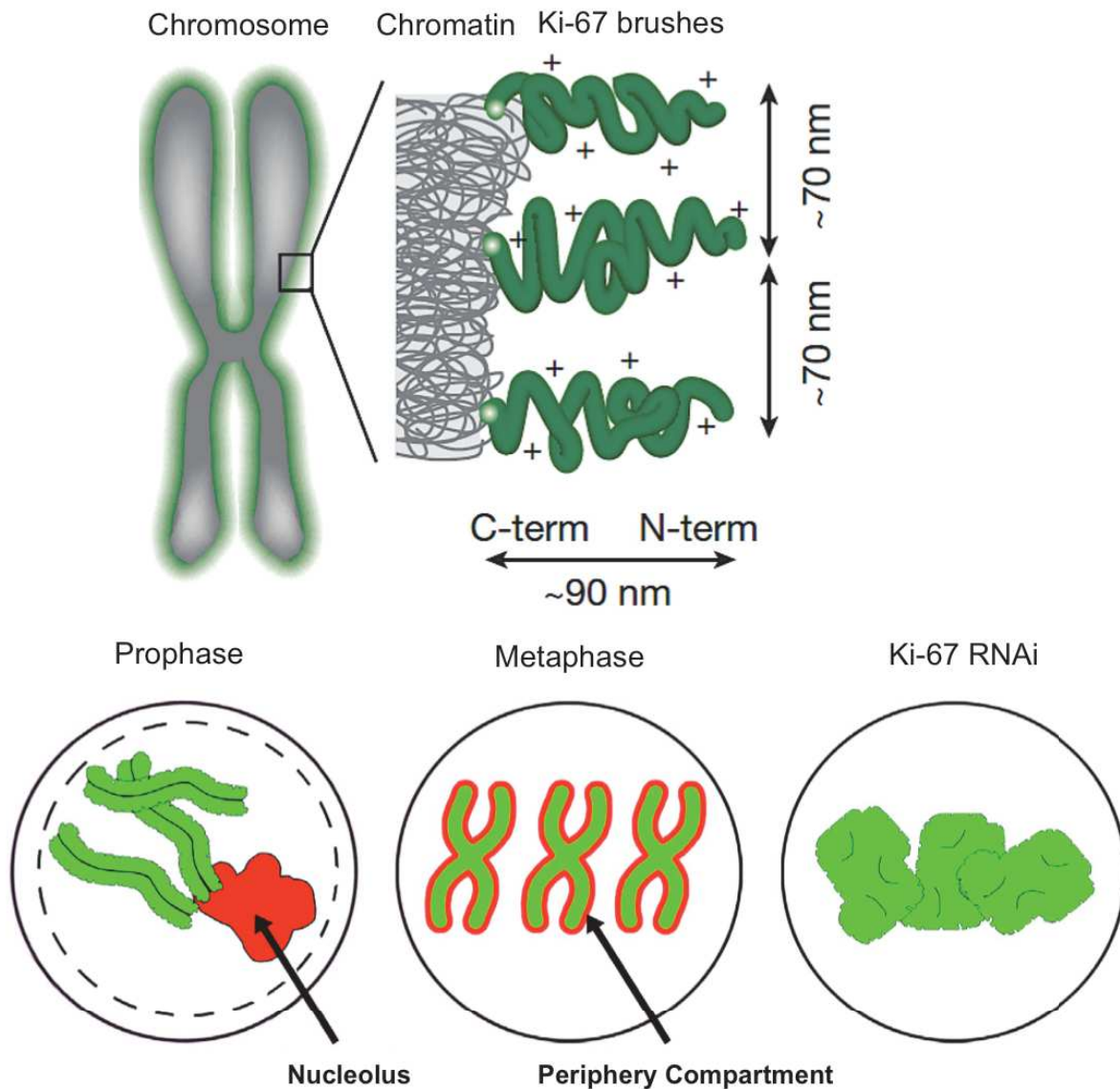


Figure 9: Proposed model of Ki-67-mediated mitotic chromosomes segregation.

Through a surfactant (brush-like structure) mechanism, Ki-67 coating of mitotic chromosomes ensures their proper individualization during metaphase and in its absence they aggregate together (Adapted from ⁶⁴ & ⁴¹).

Chapter VI: Ki-67 in cancer

1. Ki-67 as a proliferation marker: a useful tool in the clinic

Uncontrolled proliferation represents one of the key features of malignancies. Indeed, assessment of the proliferative activity of tumour samples is commonly employed to determine the growth fraction of neoplastic cell populations ⁶⁶. To assess this proliferative activity, immunohistochemistry (IHC) evaluation of specific markers of

proliferation, such as Ki-67, proliferating cell nuclear antigen (PCNA) and minichromosome maintenance (MCM) is commonly used in cancer-histopathology⁶⁶.

Following its discovery, early studies that used Ki-67 labelling to determine the growth fraction of different breast invasive carcinomas have shown results similar to other methods previously used in the clinic such as thymidine labelling³.

Thanks to its presence during all cell cycle stages and association with cell proliferation, Ki-67 has become a marker of choice for comparing proliferation across tumour samples. For example, in breast cancer, labelling of Ki-67 with the monoclonal MIB-1 antibody on paraffin sections by an IHC method is frequently used for measuring and monitoring tumour proliferation in cancer-histopathology⁶⁷. In breast cancer samples, a strong correlation was found between Ki-67 expression and histological grading since both parameters are associated with the proliferative status. Moreover, it was reported that advanced tumour stages and lymph node metastases correlate with an elevated Ki-67 expression. This suggests that Ki-67 could be used as an indicator of a tumour aggressive behaviour⁶⁸.

Previously, several studies have extensively investigated the potential use of Ki-67 as a prognostic marker in breast cancer (e.g. disease progression, disease recurrence...); however, it appears that the clinical utility of Ki-67 as a prognostic marker might be significant only within defined tumour subgroups and/or when combined with different biomarkers. This was illustrated by the creation of an IHC-based assay combining a panel of four markers (i.e. IHC4), which consists of estrogen receptor (ER), progesterone receptor (PgR), HER2, and Ki-67⁶⁹.

Despite the wide use of Ki-67 in the clinic, the substantial variability in Ki-67 scoring methodologies across laboratories in addition to the lack of defined cut-offs have hindered its potential uses for example to predict the prognosis and the efficacy of therapeutic options in breast cancer patients⁷⁰. More importantly, biological heterogeneity of Ki-67 expression is often observed across specimens (**fig.10**), which in turn may affect the interpretation of Ki-67 staining⁶⁷.

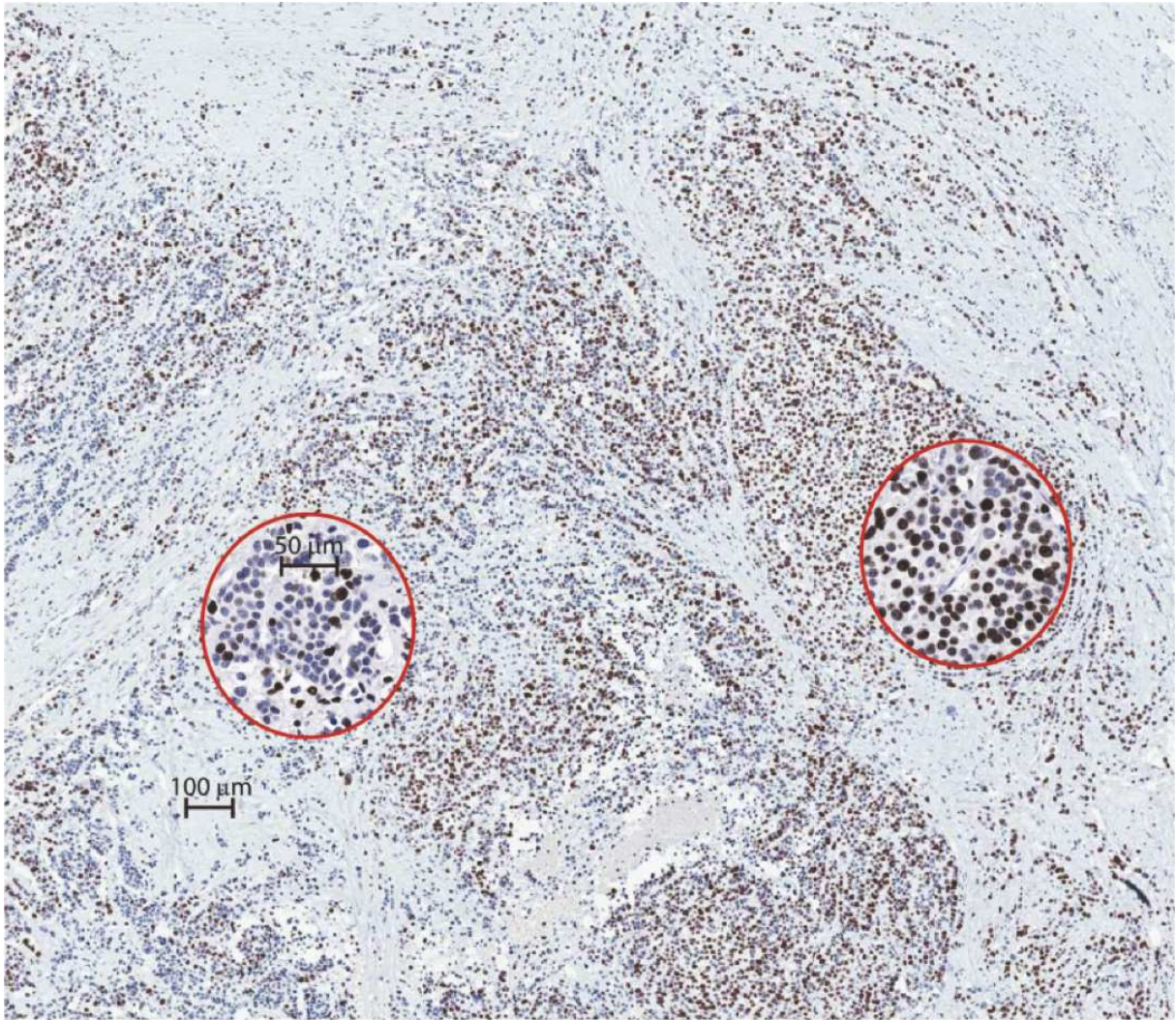


Figure 10: Variable levels of Ki-67 staining in breast cancer.

Breast tumour biopsies stained for Ki-67 with the MIB1 antibody (brown stain) and counterstained with Mayer's hematoxylin (blue stain). The two-circled areas in red (higher magnification) illustrate the different levels in Ki-67 expression that can be observed within tumour samples. Scale bars; 100um, 50um (circles areas). (Adapted from ⁶⁷).

In addition to its potential prognostic utility, many studies have assessed the predictive value of Ki-67 in breast cancer following therapy. While, no strong evidence supports the potential use of Ki-67 to predict the benefit from specific treatment for breast cancer patients ⁷¹, Ki-67 expression was used to assess the anti-tumour activity of some newly cancer therapeutic agents.

Among the therapeutic strategies used, therapies targeting the cell cycle machinery proteins such as CDKs were developed over the past years. In fact specific inhibition of CDK4/6 by PD 0332991 resulted in anti-tumour activity on human tumour xenografts ⁷². This activity was associated with a significant suppression of pRb hyperphosphorylation that results in a G1 arrest in sensitive cells ⁷².

Subsequent preclinical studies using this drug reported a growth-inhibitory in oestrogen receptor-positive and HER2-negative breast cancer, leading to its clinical approval ⁷³. However, in these studies the anti-proliferative effects of PD 0332991 were evaluated by Ki-67 expression. Yet, as discussed above, Ki-67 may be directly promoted by CDK4/CDK6-dependent RB phosphorylation. Indeed, following PD 0332991 treatment, cells may continue to proliferate without Ki-67 expression. Thus, it is critical to determine whether loss of Ki-67 after CDK4/CDK6 inhibition indeed reflects cell cycle arrest by correlating with other known independent markers of cell proliferation.

Together, these observations point toward a need for a better characterizations of Ki67 expression variability and the mechanisms underlying its regulation in order to optimally exploit this protein for the clinical management of cancer patients.

Although the utility of Ki-67 as a proliferation marker is abundantly documented, the functional relevance of Ki-67 in tumour development and metastasis colonization of distant anatomical sites is still elusive. Indeed, it is essential to determine whether Ki-67 expression might influence tumour formation and cancer cells dissemination in already established cancerogenesis models.

2. Ki-67: a potential role in tumour development and metastasis formation

Despite the wide use of Ki-67 in cancer histopathology, little is known about its involvement in the tumorigenesis process. In fact, since its discovery, only few studies have investigated the role that Ki-67 might play in promoting tumour development and establishing subsequent metastases in distant sites.

Using a murine renal cell carcinoma (RENCA) model, Kausch et al. (2004) analysed the effects of Ki-67-directed antisense oligonucleotides (ON) on the growth of orthotopically implanted syngeneic kidney tumours in immunocompetent mice. Significant tumour inhibition was shown in antisense-treated animals. Moreover, lung metastasises were also reduced in these animals compared to the control groups ⁷⁴. Interestingly, similar anti-tumoral effects were obtained following systemic

intraperitoneal administration of Ki-67-directed ON in SCID mice harbouring human renal cell carcinoma (SK-RC-35) tumours ⁷⁵.

In line with these findings, Ki-67 silencing by an oncolytic adenovirus armed with shRNA targeting Ki-67 mRNA resulted in the inhibition of human renal adenocarcinoma (786-O) growth in nude mice ⁷⁶. In another model of 3D ovarian cancer that mimics the disseminated ovarian micronodules in the human disease, inactivation of Ki-67 by a specific monoclonal antibody compromised the growth of these ovarian cells in 3D cultures compared to the non-targeting controls ⁷⁷.

Several studies have suggested that solid tumours comprise a subset of cells, referred as cancer stem cells (CSCs), that are characterized by their potential to self-renew and highest clonogenic ability to grow *in vivo* in animal tumour models ⁷⁸. Interestingly, quantification of CSCs in DLD-1 derived colon cancer cell line following Ki-67 depletion showed a reduction of this subpopulation compared to the parental cell line. This CSC reduction in DLD-1 Ki-67-depleted cells was correlated with decreased expression of known colorectal CSC markers CD133 and CD44, when assessed by flow cytometry. More importantly, DLD-1 Ki-67-depleted cells displayed reduced tumour formation when they were injected subcutaneously into athymic mice at a low density. These findings suggest that Ki-67 might be required for the maintenance of cancer stem cell niche ⁷⁹.

Ki-67, through its protein partners, could also regulate tumour progression. Indeed, a recent study has shown a significant association between Ki-67 and one of its binding partners, NIFK, in different cancer samples. In fact, detailed analysis in lung cancer revealed that NIFK promotes cancer migration and invasion *in vitro* and tumour metastasis *in vivo*. In addition, NIFK-induction of cancer proliferation was dependent on Ki-FHA binding motif, suggesting a potential requirement of NIFK-Ki-67 in lung cancer proliferation ⁸⁰.

Together these results indicate that Ki-67 might be required for tumour development and formation of metastasis, although the exact underlying mechanisms of this requirement are still missing. Indeed, detailed analysis using proper Ki-67 knockout cancer cell lines in combination with established cancer mouse models will help clarify the role that Ki-67 might play in tumour development and metastasis formation.

Moreover, it will be interesting to test whether this potential requirement of Ki-67 in tumourigenesis involves its emerging biological functions, especially those related to its ability to influence the epigenetic states that regulate chromatin compaction.

Chapter VII: Epigenetic mechanisms of tumorigenicity

Traditionally, cancer was regarded as a genetic disease, although the genetic changes in carcinogenesis were abundantly documented previously and commonly observed in several tumour types; recent evidence has highlighted the importance of the acquired epigenetic abnormalities in cancer initiation and progression. In fact, many studies have reported the aberrant reprogramming of different component of the epigenetic machinery, such as DNA methylation, histone modifications and chromatin-modifying enzymes^{51, 81}.

Alterations in DNA methylation were among the first observed in cancer cells and were associated with cancer initiation and progression. While the underlying mechanisms that trigger these changes are not fully understood, two main alteration types were reported, aberrant hypermethylation of CpG islands (gene promoter regions) and overall global hypomethylation pattern⁵¹.

Global DNA hypomethylation is observed at different genomic regions, including CpG poor promoters, repeat elements and retrotransposons. These DNA hypomethylation patterns are often linked to activation of proto-oncogenes and growth factors, which provide growth advantages to cancer cells⁸¹.

Furthermore, hypomethylation of repeat elements such as pericentromeric satellites associated with decondensation and demethylation of pericentromeric DNA result in their aberrant overexpression which leads to increase genome instability⁴⁹. For instance, aberrant satellite overexpression was reported in many aggressive epithelial cancers such as cancer of the pancreas, lung and colon. In fact analysis of both mouse and human pancreatic ductal adenocarcinomas (PDACs) primary tumours revealed a massive overexpression of pericentromeric satellite transcripts compared to healthy reference tissues. Since transcribed satellite repeats were associated with gene silencing and maintenance of chromosomal integrity, the overexpression of satellite transcripts may mirror global alterations in heterochromatin silencing⁸².

Similar to DNA hypomethylation, hypermethylation also contributes to tumorigenesis by modulating the expression of several master regulator genes. Although the mechanisms behind the gene targeting of tumour-specific CpG islands for aberrant DNA methylation are not completely understood, studies have reported that DNA hypermethylation is commonly associated with the silencing of key genes, including tumour repressor genes, transcription factors and DNA repair genes. For example, promoters of the tumour suppressor retinoblastoma (RB), CDKN2A (cell cycle regulator) and BRCA1 (DNA repair gene) undergo specific-tumour hypermethylation that lead to their inactivation⁸¹.

An emerging evidence has suggested that *de novo* methylation modification may contribute to the aberrant gene inhibition phenotype that is required for efficient tumorigenesis. Indeed, *in vitro* treatment with the demethylating agent 5-aza-2'-deoxycytidine (5-aza-dC) showed a reactivation of different aberrantly silenced genes, which was accompanied as well by a H3K9 methylation reduction in breast, bladder and colorectal cancer cell lines⁸³. In line with these observations, using the mouse model *Apc*^{Min} for intestinal tumorigenesis, Laird et al. (1995) showed that weekly administration of low doses of 5-aza-dC from birth almost completely suppressed the formation of intestinal adenomas in 3 to 5-month old mice⁸⁴. Furthermore, ablation of both *Dnmt1* and *Dnmt3b* in colon cancer cells resulted in changes in H3K9 methylation at heterochromatin and certain tumour suppressor loci⁴⁸. In fact, in human colon cancer, approximately 47% of DNMT3B-regulated genes were associated with PRC1 or PRC2. Furthermore, depletion of DNMT3B resulted in loss of the repressive histone modification Ub-H2A that is enriched at PRC1 target promoters⁸⁵.

Moreover, studies that investigated the cross talk between DNA methylation and polycomb group (PcG) proteins have suggested that genes with specific *de novo* methylation were highly enriched by H3K27 methylation. Indeed, Using chromatin immunoprecipitation analysis in colon cancer cells, Schlesinger et al. (2007) demonstrated that genes that were targeted for *de novo* tumour-specific hypermethylation were more likely to be previously marked by H3K27me3 in normal tissues rather than those lacking this specific histone modification⁸⁶. Interestingly, among the aberrantly methylated genes found in this analysis, many are known to

function as cell proliferation inhibitors through their ability to promote cell adhesion or by acting as antagonists of the WNT pathway that plays an important role in colorectal cancer development⁸⁶.

In embryonic stem cells (ESCs) PcG proteins are also needed for reversible repression of genes encoding transcription factors involved in cellular differentiation. In fact, a study has revealed that PcG targets in ESCc were 12-fold more likely to harbour a tumour-specific promoter DNA hypermethylation, suggesting that the newly acquired DNA methylation at these repressed genes may enforce their stem cell phenotypes (i.e. permanent self-renewal abilities), which in turn can predispose these cells to malignant transformation⁸⁷. These findings have important implication because PcG targets are more likely to be targeted for aberrant methylation compared to non-targets with age, which constitutes an important demographic risk factor for cancer⁴⁸. Moreover, these targeted genes in normal stem cells or early progenitor cells can be responsible for the acquisition of the cancer stem cell (CSC) phenotype during tumorigenesis^{86, 87}. Indeed, recent studies have highlighted the essential role of epigenetic dysregulation in the acquisition of uncontrolled self-renewal and the formation of CSCs⁸⁸. For instance, using a human embryonic stem cell system to model diffuse intrinsic pediatric gliomas, an aggressive brain tumour characterized by a high prevalence of CSCs, Funato et al. (2014) revealed that a K27M amino acid substitution in the tail of histone H3.3 caused genome-wide reduction in the repressive H3K27me3 mark at several master regulator genes and the re-establishment of an earlier developmental program in neural precursor cells. This resulted in the acquisition of oncogenic self-renewal ability⁸⁹. Together, these findings suggest that epigenetic changes (e.g. DNA methylation), which affect the cellular states represent the earliest events in cancer initiation (**fig. 11**).

Moreover, during tumour development these epigenetic regulators participate in the maintenance CSC state. In fact many chromatin-related enzymes and DNA-methylating enzymes (e.g. EZH2) are needed to preserve CSC self-renewal in order to avoid differentiation and sustain their malignant features⁸⁸.

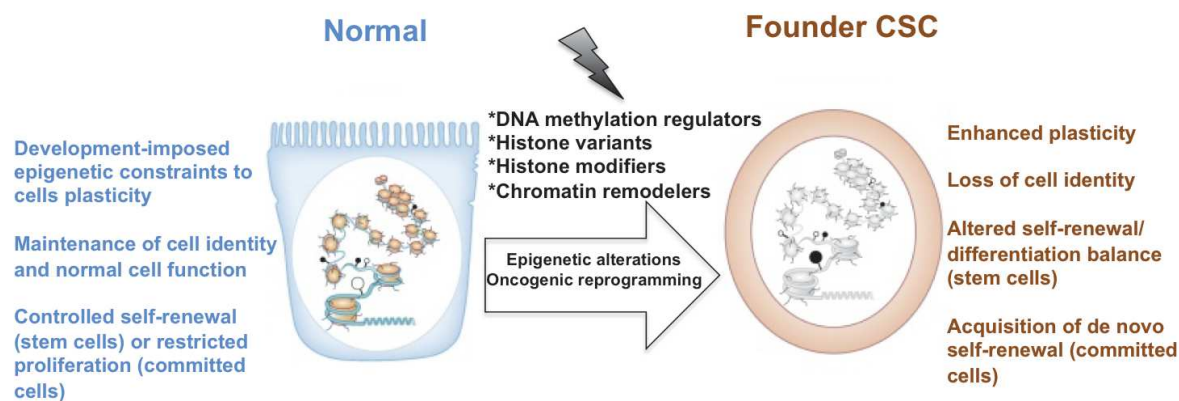


Figure 11: Oncogenic reprogramming induced by epigenetic alterations.

Alterations in chromatin-related proteins and changes in DNA methylation patterns can lead to the disruption of epigenetic regulation in either adult stem cells or committed cells, and favor neoplastic transformation. The normal function of epigenetic mechanisms (left, blue) and the consequence off epigenetic alterations (right, brown) are indicated. Normal or altered chromatin in the cell nucleus is represented in color or in grey, respectively. Empty and black circles indicate unmethylated and methylated CpGs, respectively. CSC: cancer stem cells (Adapted from ⁸⁸).

Many types of carcinomas (breast, colon...) display cell invasion and metastatic capacities. In fact, several studies have documented the contribution of the epithelial-to-mesenchymal transition (EMT) program in promoting cancer cell dissemination and metastasis.

Through the induction of EMT program, carcinoma cells are able to suppress their epithelial features and gain more mesenchymal traits that in turn promote an invasive and metastatic phenotype ⁹⁰. In fact, the replacement of E-cadherin by N-cadherin represents a hallmark of EMT that results in weaker cell-cell adhesion between adjacent cells, which in turn facilitates the dissemination of carcinoma cells from the primary tumour. Moreover, recent studies have linked the activation of EMT with the acquisition of stem-like properties, indicating that EMT can act as a mechanism for generating CSCs ⁹¹. In order to orchestrate this program, carcinoma cells rely on the activation of different combinations of EMT transcription factors (EMT-TFs) such as Slug, Snail, Twist and Zeb1 in response to various inducing signals (e.g. Wnt, TGF- β , Notch, EGF, HIF1- α , TNF α ...) emanating from the tumour microenvironment ⁹⁰. In fact, these master EMT-TFs rely on different epigenetic regulatory mechanisms in order to modulate or alter the chromatin configuration to promote the widespread changes in gene expression (e.g. silencing of epithelial genes) that occur during EMT. Indeed, previous studies have revealed that the silencing of E-cadherin expression involved a number of chromatin-modifying enzymes that cooperate with

the EMT-TFs to allow various degree of repression of the E-cadherin promoter ⁹¹. This was illustrated for example by cooperation between Snail and these chromatin-modifying enzymes to enrich the E-cadherin promoter with tri-methylated H3K9 repressive marks, promoting therefore the recruitment of DNMTs, which in turn causes CpG methylation of the promoter. Moreover, in pancreatic and colon adenocarcinoma cells, SNAIL was shown to be associated with the E-cadherin promoter and to physically interact with two polycomb repressive complex 2 (PRC2) subunits, SUZ12 and EZH2, to catalyse the trimethylation of H3K27 leading to the silencing of the E-cadherin encoding gene CDH1 ⁹². In addition to these polycomb subunits, aberrant recruitment of HDACc (e.g. HDAC2) and corresponding repressor complexes by Snail to the Cdh1 promoter was shown to have a critical role in tumour invasion and metastasis ⁹².

Together, these findings indicate the important role played by epigenetic regulators in the gene expression reprogramming that is required for the execution of the EMT process and cancer cell dissemination in general.

Aim of the project

The cell proliferation antigen Ki-67 is constitutively expressed in cycling mammalian cells and is widely used as a cell proliferation marker to grade tumours. Despite its use in cancer histo-pathology its functions are poorly understood. The aim of this project is to improve understanding of Ki-67 functions and the mechanisms underlying its expression, and more importantly its requirements in cancer initiation and progression.

Materials and Methods

Cell and mouse lines

4T1 cells were provided by Robert Hipskind (IGMM, Montpellier), the TNBC-derived cell line, MDA-MB-231 was obtained from the SIRIC of Montpellier. 3T3, 4T1 and MDA-MB-231 cells were grown in Dulbecco modified Eagle medium (DMEM - high glucose, pyruvate, GlutaMAX – Gibco® Life Technologies) supplemented with 10% foetal bovine serum (SIGMA or DUTSCHER). Cells were grown under standard conditions at 37°C in a humidified incubator containing 5% CO₂.

Athymic nude (Foxn1nu/Foxn1+) and Balb/c mice were purchased from Envigo. An adult C57BL/6 Apcd14 mutant mouse originally generated by Colnot et al. (2004) was kindly provided by the team of Philippe Jay (IGF, Montpellier).

Ethics

All animal experiments were performed in accordance with international ethics standards and were subjected to approval by the Animal Experimentation Ethics Committee of Languedoc Roussillon.

Vectors and antibodies

Antibodies: Ki-67: clone SP6 (Abcam), cyclin A: 6E6 (Novocastra), PCNA: ab18197 (Abcam), beta-catenin: BD610154 (BD-Bioscience), Ras (G12V Mutant Specific): D2H12 #14412 (CST), Actin: A2066 (Sigma).

Lentiviral Vectors used for lentiviruses construction: LentiCRISPRv2 (Addgene plasmid #52961), pMD2.G (Addgene plasmid #12259), psPAX2 (Addgene plasmid #12260),

Retroviral vectors used for retroviruses construction: pBabe-puro (Addgene plasmid #1764), pBabe-puro Ras V12 (Addgene plasmid #1768), gag/pol (retroviruses packaging) and Maloney (envelope) were a gift from Leatitia Linares (IRCM, Montpellier).

CRISPR/Cas9-mediated genome editing

The sgRNAs targeting a sequence found in exon 3 (murine Mki67) or exon 6 (human MKI67) in addition to the non-targeting control sequences were initially designed by Shalem, Sanjana et al., (2014)⁹³. Cloning of the target sequence into the LentiCRISPRV2 lentiviral vector was conducted as previously described by Sanjana, Shalem, et al. (2014)⁹⁴. Following the cloning, lentiviruses encoding the sgRNA targeting sequences were engineered to transduce cells (4T1 and MDA-MB-231). Following cell transduction, the CRISPR/Cas9 activity was selected using puromycin. Resistant cells were then isolated and were seeded as a single cell clones in 96 well-plate for further investigation.

AOM-DSS induced colon carcinogenesis

Mice were divided into 3 groups: Mki67^{+/+}; Mki67^{+/-}2ntΔ & Mki67^{2ntΔ/2ntΔ} and were given a single intraperitoneal injection of AOM (A5486, Sigma Aldrich, 10 mg/kg body weight in 0.9% saline) at first week following adaptation. One week later, the animals were given 2% Dextran Sodium Sulfate (DSS) (MP Biomedicals) added to the drinking water for 7 consecutive days. After this, DSS-containing water was removed and changed by regular drinking water, then mice were sacrificed at week 16-post AOM-DSS treatment and colon tissues were removed.

Colons were flushed and fixed over-night in neutral buffered formalin (10%) before paraffin embedding. Briefly, 4-μm-thick sections were dewaxed in xylene and rehydrated in graded alcohol baths. Slides were incubated with 3% H₂O₂ for 20 min and washed in PBS to quench endogenous peroxidase activity before antigen retrieval. Antigen retrieval was performed by boiling slides for 20 min in 10 mM sodium citrate buffer, pH 6.0. Nonspecific binding sites were blocked in blocking buffer (TBS, pH 7.4, 5% dried milk, and 0.5% Triton X-100) for 60 min at RT. Sections were then incubated with an anti beta-catenin (BD610154, BD-Bioscience) diluted in blocking buffer overnight at 4°C. Envision+ (Dako) was used as a secondary reagent. Signals were developed with DAB (Sigma-Aldrich). After dehydration, sections were mounted in Pertex (Histolab). Sections were imaged using the Nanozoomer-XR Digital slide Scanner C12000-01 (Hamamatsu).

DNA replication assay_EdU labelling

Analysis of DNA replication progress in cells was achieved by treatment with 10 μM 5-ethynyl-2'-deoxyuridine (EdU)(LifeTechnologies) for the desired pulse time.

Cells were harvested, washed once with cold PBS, then, resuspended in 300μL cold PBS and fixed with 700μL chilled 100% ethanol. Replicating cells were analysed by flow-cytometry (BD FACSCanto II Becton Dickinson) according to the protocol from 'Click-iT™ Plus EdU Alexa Fluor™ 647 Flow Cytometry Assay Kit' (Invitrogen) in order to separate proliferating cells that have incorporated EdU and non-proliferating cells that have not. Results were then analysed using the 'FlowJo®' software. Percentage of EdU+ population in each condition was plotted according to the corresponding pulse time.

Mammosphere assay

The mammosphere formation assay was performed under culturing conditions similar to those previously described by Shaw et al. (2012). Briefly, 500 cells were plated per well in low-adherence 96 well-plate covered with poly-2-hydroxyethyl-methacrylate (poly-Hema). After 7 days in culture (37°C & 5% CO₂), images of formed mammospheres were acquired and counted using an automated high-content microscopy analysis (Cellomics Thermo).

Aldehyde Dehydrogenase 1 (ALDH1) activity

ALDH1+ enzymatic activity was determined using the 'ALDEFLUOR' kit (Stem Cell Technologies) following the manufacturer instructions. For each sample, half of cell/substrate mixture was treated with diethylaminobenzaldehyde (DEAB); an inhibitor of ALDH activity. ALDEFLUOR/DEAB treated cells were used to define negative gates. FACS was conducted with $\geq 1.10^5$ cells.

In vivo tumour transplantation

Animals were housed in the ZEFI animal facility of IGMM and were maintained in a specific pathogen-free environment and fed ad libitum. For each experimental group, 8 mice were included. 6-8 weeks-old female athymic nude (Foxn1nu/Foxn1+) and Balb/c mice (Envigo) were used.

To generate primary tumours, 1.10^6 cells (4T1) or 3.10^6 cells (MDA-MB-231) of log-phase viable 'mouse pathogen-free' (test IMPACT1, Iddex) were implanted into the fourth inguinal mammary gland (in 50ul PBS (4T1) or 200ul PBS (MDA-MB-231)).

Primary tumour volume was measured every week by electronic calliper using the formula " $\pi/6 * S^2$ (Smaller radius)*L (Larger radius)".

At the end of the experiment, following animal sacrifice, primary tumours were excised and fixed over-night in neutral buffered formalin (10%) before paraffin embedding (see above). IHC analysis of Ki-67 expression of the different tumour tissue sections was conducted as described earlier.

Analysis of lung metastatic burden

Dissected lungs were stained with 15% India Ink (diluted in distilled water). Stained lungs were washed with 5ml of Fekete's solution (40 ml glacial acid acetic, 80 ml formalin, 580 ml ethanol 100%, 200 ml water) to remove the excess of Ink. A magnifying microscope connected to a digital camera was used to visualise metastatic nodules and enumerate the number of surface nodules.

siRNA transfection

The SMARTpool: ON-TARGETplus siRNAs were purchased from GE Dharmacon (Lafayette, CO, USA). Cells were transfected with SMARTpool: ON-TARGETplus siRNA non-targeting (D-001810-10) or MKI-67 (L-003280-00) and at 10 nM using INTERFERin®-mediated delivery according to the manufacturer instructions (Polyplus transfection®).

Cell extracts and Western-blotting

Frozen pellets (harvested by trypsinization, washed with cold PBS) were lysed directly in Laemmli buffer at 95°C. Protein concentrations were determined by BCA protein assay (Pierce Biotechnology). Equivalently loaded proteins were separated by SDS-polyacrylamide gel electrophoresis (SDS-PAGE) (7.5% and 12.5% gels). The proteins were then transferred to Immobilon membranes (Milipore) at 1.15 mA/cm² for 120 min with a semidry blotting apparatus. Membranes were blocked in TBST pH

7.6 (20 mM Tris, 140 mM NaCl, 0.1% Tween-20) containing non-fat dry milk (5%), incubated with the primary antibody for 2 hours at RT or over-night at 4°C, washed several times with TBST for a total of 45 minutes, incubated with secondary antibody at 1/5000 dilution for 1 hour at RT and washed several times in TBST. The detection system used was Western Lightning Plus-ECL (PerkinElmer) and Amersham Hyperfilm™ (GE Healthcare).

qRT-PCR

For reverse transcription reaction (cDNA synthesis), 500 ng of purified RNA in total volume of 10 μ L, extracted by RNeasy Mini Kit (Qiagen), were mixed with 1 μ L of 10 mM dNTPs mix (LifeTechnologies) and 1 μ L of 50 μ M random hexaprimers (NEB). Samples were incubated at 65°C for 5 minutes, then immediately transferred on ice. Next, into samples were added 5 μ L of 5xFirst Strand Buffer, 2 μ L 100 mM DTT and 1 μ L RNasin RNase Inhibitor (Promega). Samples were incubated at 25°C for 10 minutes and at 42°C for 2 minutes. 1 μ L of SuperScript® III Reverse Transcriptase (LifeTechnologies) was added to each sample, prior to incubation at 50°C for 60 minutes, 70°C for 15 minutes.

qPCR was performed using LightCycler® 480 SYBR Green I Master (Roche) and LightCycler® 480 qPCR machine. The reaction contained 5 ng of cDNA, 2 μ L of 1 μ M qPCR primer pair, 5 μ L 2x Master Mix, and final volume made up to 10 μ L with DNase free water. Primers used for both mouse (Mki67) and human (MKI67) Ki-67 in addition to the housekeeping genes are similar to those used by Sobecki et al., 2016. qPCR was conducted at 95°C for 10 min, and then 40 cycles of 95°C for 20 s, 58°C for 20 s and 72°C for 20 s. The specificity of the reaction was verified by melt curve analysis.

Wound closure assay

Cells transfected with control (siCTRL) or Ki-67 siRNA (siKi-67) were seeded 48h post-siRNA transfection in each well of Culture-Inserts® (Ibidi, Bonn, Germany) at 3.2.10⁵ cells/ml. After incubation for 24h, each insert was detached and the progression of cell migration (wound closure) was subsequently monitored over time using time-lapse microscopy. The wound area (μ m²) closed by cells was evaluated every 2h over a period of 14h. The rate of cell migration (μ m²/h) was then calculated using the slope.

Focus Formation assay

3T3 Wild-type (WT) and two Ki-67 TALEN-mutant clones were transduced with either empty control retroviruses or H-Ras-G12V expressing retroviruses. After verification of Ras-G12V expression, cells were seeded at 1.10⁵ cells/well (6 well-plate) in triplicate and were allow to grow for 2-weeks (media was changed every 2 days). Cells were then fixed (4% formaldehyde) and stained with 0.5% (w/v) crystal violet to visualize the foci formed.

RNA sequencing library preparation

Total RNA was extracted using Trizol (Life Technologies) following manufacturer's instructions from wild type and two separate clones of 4T1 K-67 knockout cell lines to avoid clonal bias. The RNA samples were run on Agilent 2100 bioanalyzer to measure RNA integrity. For library preparation, cDNA synthesis was performed on rRNA-depleted samples using the TruSeq Stranded Total RNA Library Preparation (RS-122-2301). All sequencing libraries were prepared with two biological replicates. Indexed cDNA libraries were sequenced by MGX (Montpellier) on an Illumina HiSeq2000 with a single 51 bp read and a 10 bp index read.

Sequencing of cDNA library and data processing

Sequencing reads were quality assessed and trimmed for any remaining sequencing adaptor using Trimmomatic (v0.22). Reads were subsequently aligned to mouse genome buildmm9 using Tophat (v2) and the corresponding transcript gtf file. Reads aligning to transcripts were counted and quantified by RPKM using htseq count. Differential gene expression analysis was conducted using read counts with the Bioconductor deseq package.

Statistical analysis

Significant differences between the different experimental groups were tested using an unpaired two-tailed Student t test or ANOVA in Prism 5 (GraphPad). For all analyses, P values < 0,05 (*), P values < 0,01 (**), P values < 0,001 (***) and P values < 0,0001 (****) were considered to indicate a statistically significant result.

Results

I. Ki-67 is dispensable for cell proliferation but required for heterochromatin formation

Although it has been more than 30 years since its initial discovery, the biological functions of Ki-67 remain largely elusive. In fact, the association of Ki-67 with a proliferative state has led to the assumption that Ki-67 might be required for cell proliferation.

Before this project, previous work conducted by our team allowed us to successfully generate Ki-67 mutant mice using the TALEN genome editing approach. Mice that had mutations disrupting the coding sequence were obtained. In order to investigate the potential biological consequences of Mki67 disruption, two Ki-67 mutant lines were selected for further analysis, one with a 2-nucleotide deletion (Mki67^{2ntΔ/2ntΔ}) and the other one with a 21-nucleotide deletion (Mki67^{21ntΔ/21ntΔ}).

These mutant lines did not exhibit any developmental abnormalities, and both were fertile and aged well. As discussed above, Ki-67 is highly expressed in proliferating cells such as those found in the crypts of the lining of the mouse intestine. The progeny of these cells migrate to the surface of the villi, where they become fully differentiated (e.g. Goblet cells). Indeed, an assessment of Ki-67 in the crypts of the small intestine using IHC/IF and immunoblotting analysis showed a strong reduction (>90%) of Ki-67 expression in these mutant mice. In addition, the cell proliferation rate at the crypts was not affected in Mki67^{21ntΔ/21ntΔ} mice when monitored by BrdU incorporation. Furthermore, in the intestinal epithelium, analysis of Wnt signalling and differentiation of goblet and tuft cells showed no differences between WT and Mki67^{21ntΔ/21ntΔ} mice. These results suggest that a full-length functional Ki-67 is not required for mouse development and tissue differentiation.

To study the physiological consequences of Ki-67 depletion, we next isolated and cultured embryonic fibroblasts (MEFs) from day-13 mouse embryos. Homozygous Mki67^{2ntΔ/2ntΔ} MEFs showed at least a 90% reduction of Ki-67 expression compared to Mki67^{+/+} and Mki67^{+/2ntΔ} MEFs, as assayed by immunoblotting analysis. More

importantly, the proliferation of these Ki-67-depleted MEFs was not affected, as assessed by active DNA synthesis via the EdU incorporation assay, demonstrating that Ki-67 is dispensable for cell proliferation.

As mentioned above, the TALEN-mediated Mki67 disruption did not result in a complete Ki-67 gene ablation. A Ki-67 null 3T3 cell line was previously generated using two TALEN-pairs, one upstream of the initiation ATG and one downstream of the stop codon. Ki-67 expression was completely eliminated in these cell lines, as determined by qRT-PCR, immunofluorescence and western blotting analysis. As observed in Ki-67-mutant MEFs, these 3T3 Ki-67 null cells proliferated normally and could enter and exit the cell cycle with kinetics similar to those of wild-type cells. This confirmed that Ki-67 is not required for cell proliferation.

Although Ki-67 was uncoupled from cell proliferation, Ki-67 was found to promote heterochromatin organization in proliferating cells. Ki-67 was required for the maintenance of a high level of compaction typical of heterochromatin, and mediated long-range interactions between different regions of the genome that are packaged into heterochromatin. In fact, proteomic analysis of Ki-67 interactors revealed that Ki-67 interacting partners are involved in histone methylation complexes or are interactors of methylated chromatin required for heterochromatin maintenance. This suggested that Ki-67 might help target these proteins to their genomic sites in order to promote chromatin compaction. In line with this hypothesis, upon Ki-67 depletion, heterochromatin-associated marks H3K9me3 and H3K20me3 were reorganised within the nucleus and were strongly reduced at pericentromeric heterochromatin as mirrored by specific FISH analysis of major satellite repeats. Furthermore, Ki-67 overexpression induced the formation of ectopic heterochromatic foci highly enriched in these heterochromatin-associated marks in addition to HP1 proteins.

As discussed above, several studies uncovered the essential role played by Ki-67 in the organization of the mitotic perichromosomal layer (PR) and therefore the faithful partitioning of nucleolar proteins between daughter cells. In accordance with these studies, Ki-67 was identified as one of the first trans-acting factors involved in PR formation and subsequent distribution of nucleolar components in daughter cells, which is necessary for a proper nucleologenesis.

Together, these findings point toward an important role of Ki-67 in heterochromatin

organization. The results describing these findings were published in a paper entitled: “The cell proliferation antigen Ki-67 organises heterochromatin” in the journal *eLife* in 2016 ²⁶.

The cell proliferation antigen Ki-67 organises heterochromatin

Michal Sobecki^{1,2†}, Karim Mrouj^{1,2}, Alain Camasses^{1,2}, Nikolaos Parisis^{1,2}, Emilien Nicolas³, David Llères^{1,2}, François Gerbe^{2,4,5}, Susana Prieto^{1,2}, Liliana Krasinska^{1,2}, Alexandre David^{2,4,5}, Manuel Eguren⁶, Marie-Christine Birling⁷, Serge Urbach^{2,4,5,8}, Sonia Hem⁹, Jérôme Déjardin^{2,10}, Marcos Malumbres⁶, Philippe Jay^{2,4,5}, Vjekoslav Dulic^{1,2}, Denis LJ Lafontaine³, Robert Feil^{1,2}, Daniel Fisher^{1,2*}

¹Montpellier Institute of Molecular Genetics (IGMM) CNRS UMR 5535, Centre National de la Recherche Scientifique (CNRS), Montpellier, France; ²Faculty of Sciences, University of Montpellier, Montpellier, France; ³RNA Molecular Biology, Center for Microscopy and Molecular Imaging, Fonds de la Recherche Nationale, Université Libre de Bruxelles, Charleroi-Gosselies, Belgium; ⁴Institute of Functional Genomics (IGF), CNRS UMR 5203, Centre National de la Recherche Scientifique (CNRS), Montpellier, France; ⁵U1191, Inserm, Montpellier, France; ⁶Spanish National Cancer Research Centre, Madrid, Spain; ⁷ICS, Mouse Clinical Institute, Illkirch-Graffenstaden, France; ⁸Functional Proteomics Platform, Institute of Functional Genomics, Montpellier, France; ⁹Mass Spectrometry Platform MSPP, SupAgro, Montpellier, France; ¹⁰Institute of Human Genetics (IGH) CNRS UPR 1142, Centre National de la Recherche Scientifique, Montpellier, France

*For correspondence: daniel.fisher@igmm.cnrs.fr

Present address: [†]Department of Genome Biology, Institute for Integrative Biology of the Cell, Université Paris Sud, Gif-sur-Yvette, France

Competing interests: The authors declare that no competing interests exist.

Funding: See page 30

Received: 21 December 2015

Accepted: 06 March 2016

Published: 07 March 2016

Reviewing editor: Fiona M Watt, King's College London, United Kingdom

© Copyright Sobecki et al. This article is distributed under the terms of the [Creative Commons Attribution License](#), which permits unrestricted use and redistribution provided that the original author and source are credited.

Abstract Antigen Ki-67 is a nuclear protein expressed in proliferating mammalian cells. It is widely used in cancer histopathology but its functions remain unclear. Here, we show that Ki-67 controls heterochromatin organisation. Altering Ki-67 expression levels did not significantly affect cell proliferation in vivo. Ki-67 mutant mice developed normally and cells lacking Ki-67 proliferated efficiently. Conversely, upregulation of Ki-67 expression in differentiated tissues did not prevent cell cycle arrest. Ki-67 interactors included proteins involved in nucleolar processes and chromatin regulators. Ki-67 depletion disrupted nucleologenesis but did not inhibit pre-rRNA processing. In contrast, it altered gene expression. Ki-67 silencing also had wide-ranging effects on chromatin organisation, disrupting heterochromatin compaction and long-range genomic interactions. Trimethylation of histone H3K9 and H4K20 was relocalised within the nucleus. Finally, overexpression of human or *Xenopus* Ki-67 induced ectopic heterochromatin formation. Altogether, our results suggest that Ki-67 expression in proliferating cells spatially organises heterochromatin, thereby controlling gene expression.

DOI: [10.7554/eLife.13722.001](https://doi.org/10.7554/eLife.13722.001)

Introduction

The cell proliferation antigen Ki-67 (Ki-67 or Ki67) is constitutively expressed in cycling mammalian cells (*Gerdes et al., 1983*). It is therefore widely used as a cell proliferation marker to grade tumours. Ki-67 is a nuclear DNA-binding protein (*MacCallum and Hall, 2000*) with two human isoforms that have predicted molecular weights of 320kDa and 359kDa (*Gerdes et al., 1991*). The domain structure of Ki-67 is represented in *Figure 1*. All homologues contain an N-terminal Forkhead-associated (FHA) domain, which can bind both to DNA and to phosphorylated epitopes. The

eLife digest Living cells divide in two to produce new cells. In mammals, cell division is strictly controlled so that only certain groups of cells in the body are actively dividing at any time. However, some cells may escape these controls so that they divide rapidly and form tumors.

A protein called Ki-67 is only produced in actively dividing cells, where it is located in the nucleus – the structure that contains most of the cell's DNA. Researchers often use Ki-67 as a marker to identify which cells are actively dividing in tissue samples from cancer patients, and previous studies indicated that Ki-67 is needed for cells to divide. However, the exact role of this protein was not clear. Before cells can divide they need to make large amounts of new proteins using molecular machines called ribosomes and it has been suggested that Ki-67 helps to produce ribosomes.

Now, Sobecki et al. used genetic techniques to study the role of Ki-67 in mice. The experiments show that Ki-67 is not required for cells to divide in the laboratory or to make ribosomes. Instead, Ki-67 alters the way that DNA is packaged in the nucleus. Loss of Ki-67 from mice cells resulted in DNA becoming less compact, which in turn altered the activity of genes in those cells.

Sobecki et al. also identified many other proteins that interact with Ki-67, so the next step following on from this research is to understand how Ki-67 alters DNA packaging at the molecular level. Another future challenge will be to find out if inhibiting the activity of Ki-67 can hinder the growth of cancer cells.

DOI: [10.7554/eLife.13722.002](https://doi.org/10.7554/eLife.13722.002)

most characteristic feature of Ki-67 is the presence of multiple tandem repeats (14 in mice, 16 in human) containing a conserved motif of unknown function, the 'Ki-67 domain'. Two other conserved motifs include a Protein Phosphatase 1 (PP1)-binding motif ([Booth et al., 2014](#)) and a 31 amino acid conserved domain (CD) of unknown function, 100% identical between human and mouse, that includes a 22 amino acid motif conserved in all homologues. Ki-67 homologues also have a weakly conserved leucine/arginine rich C-terminus which can bind to DNA and, when overexpressed, promotes chromatin compaction ([Scholzen et al., 2002](#); [Takagi et al., 1999](#)).

Ki-67 protein levels and localisation vary through the cell cycle. Its maximum expression is found in G2 phase or during mitosis ([Endl and Gerdes, 2000b](#)). In interphase, Ki-67 forms fibre-like structures in fibrillarin-deficient regions surrounding nucleoli ([Verheijen et al., 1989b](#); [Kill, 1996](#); [Cheutin et al., 2003](#)). Ki-67 also colocalises with satellite DNA ([Bridger et al., 1998](#)) and is found in protein complexes that bind to satellite DNA ([Saksouk et al., 2014](#)). It remains associated with nucleolar organiser regions of acrocentric chromosomes throughout interphase ([Bridger et al., 1998](#)). Ki-67 is a direct substrate of the cyclin-dependent kinase CDK1 ([Blethrow et al., 2008](#)) and is hyperphosphorylated in mitosis. This may regulate its expression and / or localisation ([Endl and Gerdes, 2000a](#)). In HeLa cells, Ki-67 binds tightly to chromatin in interphase, whereas this binding is weakened in mitosis ([Saiwaki et al., 2005](#)) when it associates with condensed chromosomes before relocating to the chromosome periphery ([Verheijen et al., 1989a](#)).

Ki-67 is generally assumed to be required for cell proliferation. An early study found that injection of antisense oligonucleotides that block Ki-67 expression inhibited cell proliferation ([Schluter et al., 1993](#)). Subsequent studies have shown that unperturbed Ki-67 expression levels are required for normal proliferation rates in various cell lines ([Kausch et al., 2003](#); [Rahmanzadeh et al., 2007](#); [Zheng et al., 2006](#); [2009](#)). However, no complete Ki-67 loss of function studies have been reported. Therefore, it remains unclear what its functions are and whether it is essential for cell proliferation.

The dynamic localisation of Ki-67 has led to suggestions that it could coordinate nucleolar disassembly and reassembly at either side of mitosis ([Schmidt et al., 2003](#)). Indeed, Ki-67 is required to localise nucleolar granular components to mitotic chromosomes, thereby potentially playing a role in nucleolar segregation between daughter cells ([Booth et al., 2014](#)). It has also been reported that Ki-67 has roles in ribosome biogenesis ([Rahmanzadeh et al., 2007](#)), consistent with its nucleolar localisation and apparent role in cell proliferation.

In this work, we characterise the cellular roles of Ki-67 using knockdown and genetic approaches. We find that mutant mice with disrupted Ki-67 expression are viable and fertile. Preventing Ki-67 downregulation upon cell cycle exit in vivo does not impede differentiation. Thus, Ki-67 expression

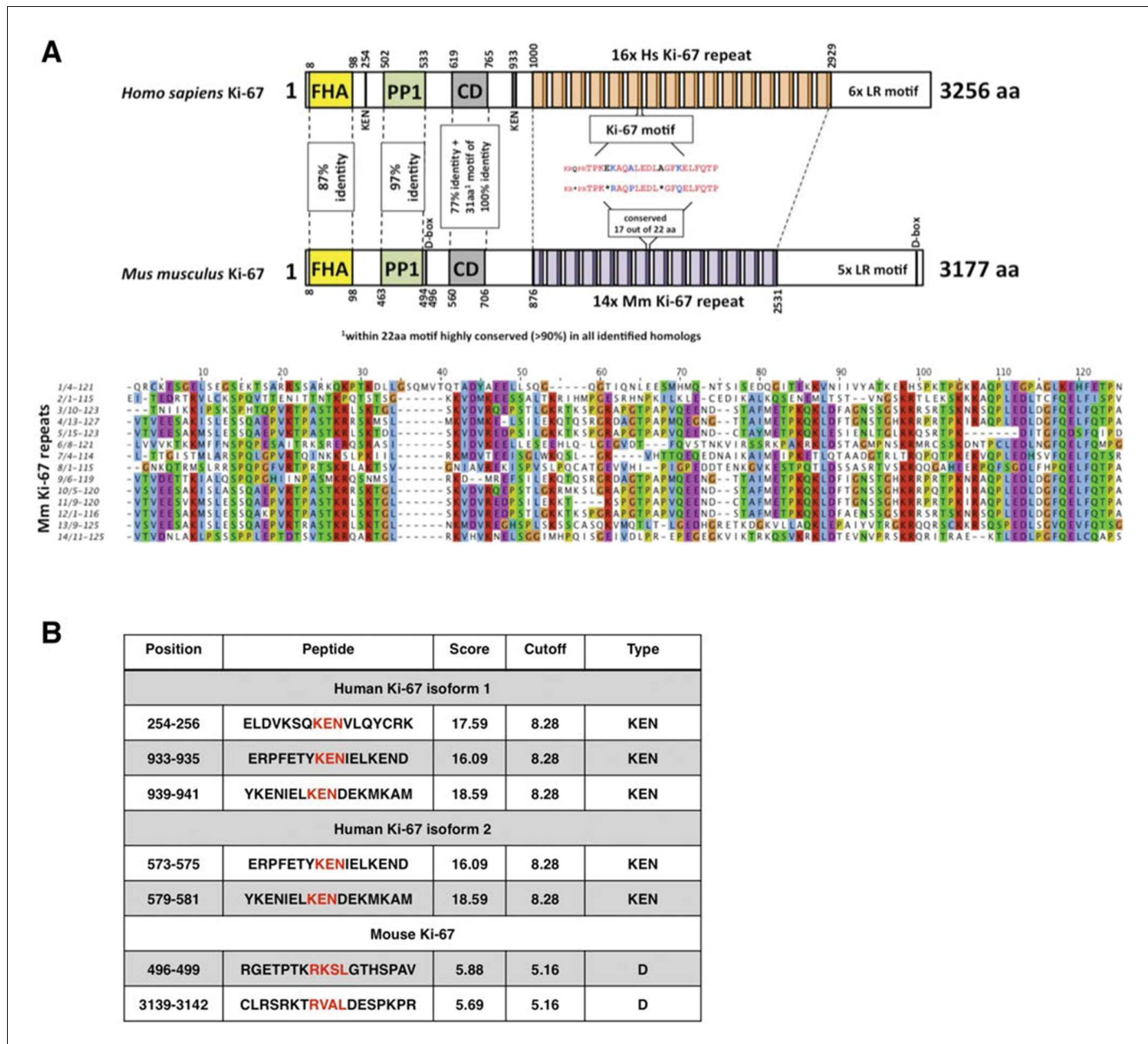


Figure 1. Comparison of human and mouse Ki-67 structural elements. (A) Top: cartoon of human (long form) and mouse Ki-67 protein highlighting conserved elements and functional motifs. Domains are indicated by boxes (FHA, forhead-associated domain; PP1, PP1-binding domain; CD, conserved domain; D-box: APC/C targeting destruction box motifs; KEN: APC/C-Cdh1 targeting KEN box motifs). Highly conserved regions are indicated by dotted line with percent of identical amino acids. Bottom: alignment of mouse Ki-67 repeats. (B) APC/C targeting motifs identified in human (both isoforms) and mouse Ki-67.

DOI: 10.7554/eLife.13722.003

can be uncoupled from cell proliferation. Instead, we show that Ki-67 is an essential mediator of heterochromatin organisation and long-range chromatin interactions, controlling gene expression. As it is expressed at high levels only in proliferating cells, our results suggest that Ki-67 links heterochromatin organisation to cell proliferation.

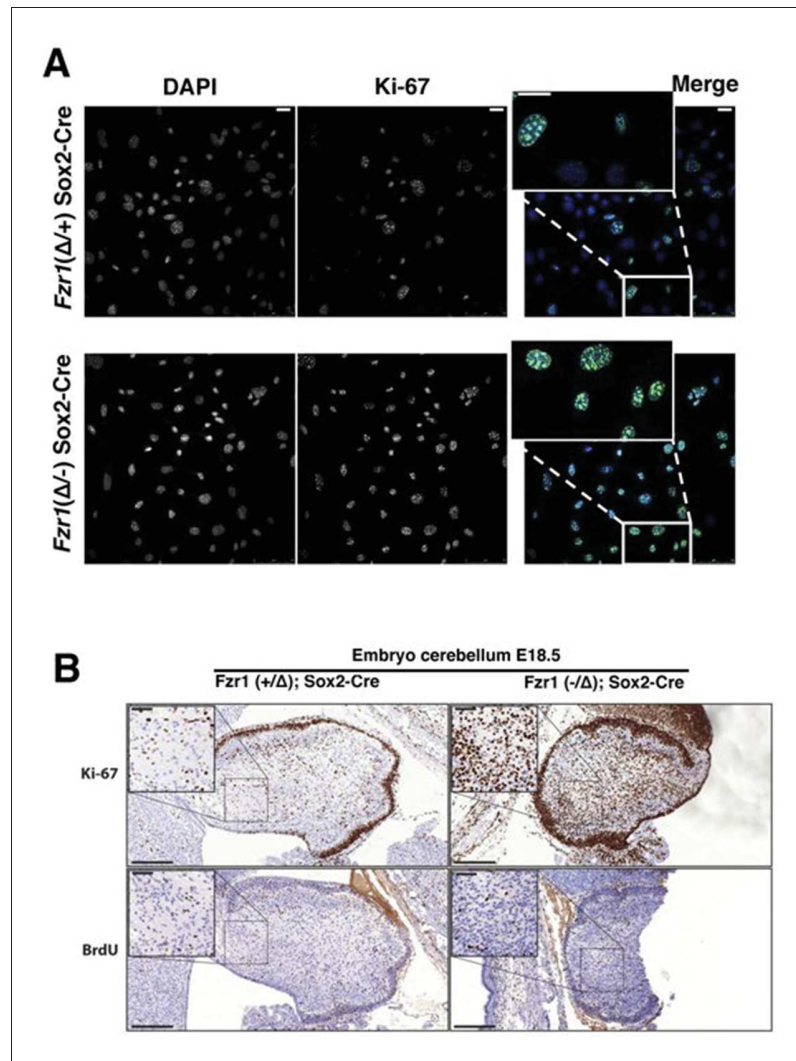


Figure 2. Maintenance of Ki-67 expression in quiescent cells in vivo by Cdh1 mutation. (A) Immunofluorescence analysis of Ki-67 in MEF cells isolated from embryo (E13.5) of *Fzr1(+/-);Sox2-Cre* and *Fzr1(-/-);Sox2-Cre* mice. Scale bar, 25 μm . (B) IHC staining of Ki-67 and BrdU in sagittal sections of embryo cerebellum (E18.5) of *Fzr1 (+/-); Sox2-Cre* and *Fzr1 (-/-);Sox2-Cre* mice. Bars, 200 μm . Bars in zoom, 50 μm .

DOI: [10.7554/eLife.13722.004](https://doi.org/10.7554/eLife.13722.004)

The following figure supplement is available for figure 2:

Figure supplement 1. Ki-67 expression is restricted to proliferating cells by APC/C-Cdh1.

DOI: [10.7554/eLife.13722.005](https://doi.org/10.7554/eLife.13722.005)

Results

Mouse development is not affected by genetic up- and downregulation of Ki-67 expression

Given the tight correlation between Ki-67 expression and cell proliferation, it is often assumed that Ki-67 is required for cell proliferation and that its downregulation might promote cell cycle exit. We tested these hypotheses genetically. Ki-67 protein expression is regulated during the cell cycle, and we speculated that it might be a target for the APC/C-Cdh1 ubiquitin ligase complex. This complex is active in late mitosis and G1, and triggers degradation of substrates containing D-boxes and KEN boxes. Human Ki-67 isoforms contain two or three KEN boxes, whereas mouse Ki-67 contains two D-boxes (**Figure 1A,B**). Mouse Ki-67 contains an additional sequence, AQRKQPSR at 2680–2687,

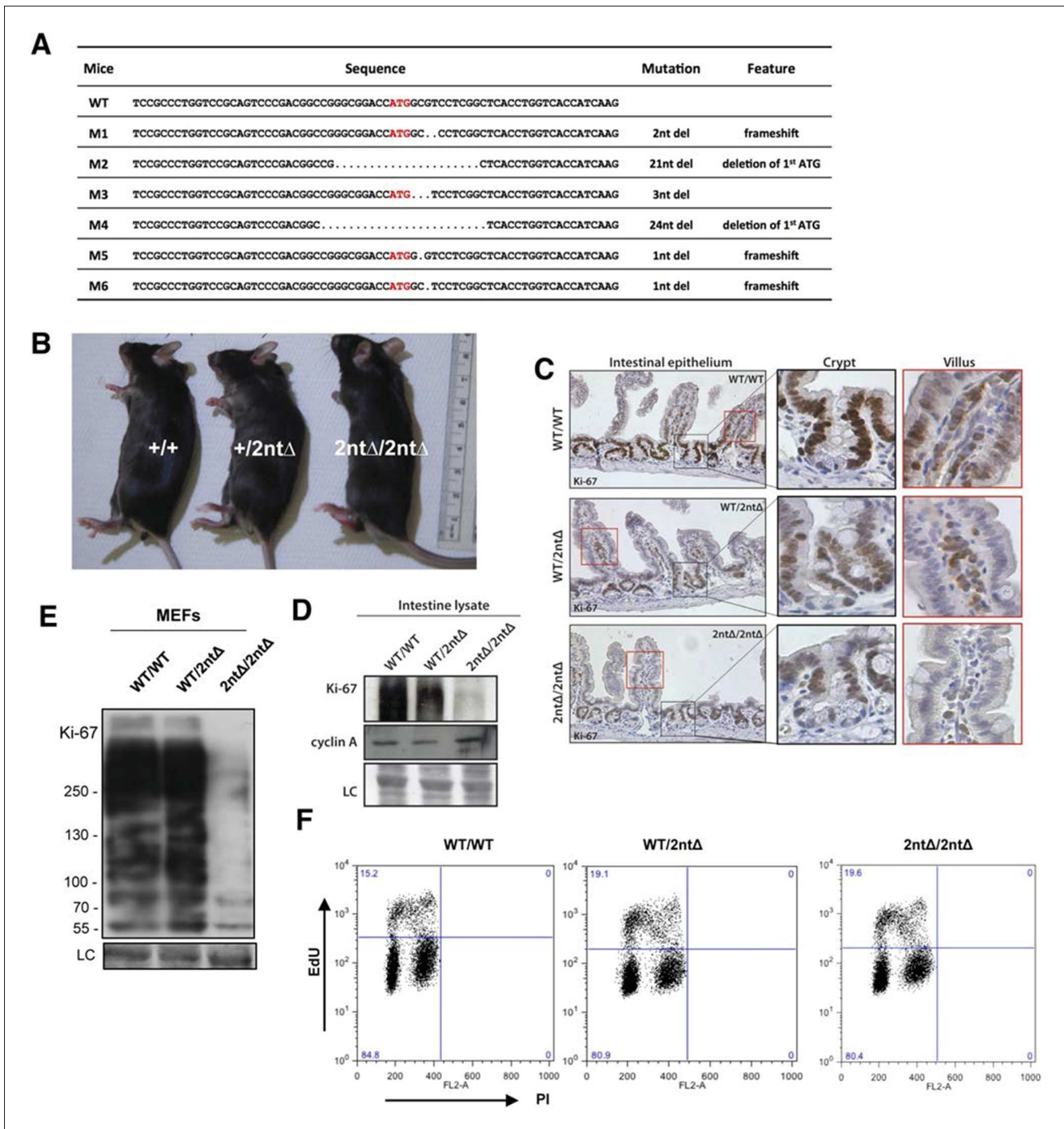


Figure 3. Mouse development with a mutated Ki-67 gene. (A) Table describing Ki-67 mutant mouse lines resulting from germline transmission of mutations generated by cytoplasmic injection of TALEN-encoding mRNA into zygotes. (B) Macroscopic appearance of littermate female mice at 10 weeks of age. Genotypes are specified. (C) IHC staining of Ki-67 in sagittal section of intestine from *Mki67*^{WT/WT}, *Mki67*^{WT/2ntΔ} and *Mki67*^{2ntΔ/2ntΔ} mice. (D) Western blots of Ki-67 and cyclin A expression from intestine isolated from *Mki67*^{WT/WT}, *Mki67*^{WT/2ntΔ} and *Mki67*^{2ntΔ/2ntΔ} mice. LC, loading control. (E) Western blot of Ki-67 in MEFs from WT, *Mki67*^{WT/2ntΔ} and *Mki67*^{2ntΔ/2ntΔ} mice. LC, loading control. (F) Flow cytometry profiles in WT, *Mki67*^{WT/2ntΔ} and *Mki67*^{2ntΔ/2ntΔ} MEFs showing EdU incorporation upon a 1 hr pulse and DNA content.

DOI: [10.7554/eLife.13722.006](https://doi.org/10.7554/eLife.13722.006)

The following source data and figure supplements are available for figure 3:

Figure supplement 1. Ki-67 mutant mice develop normally.

DOI: [10.7554/eLife.13722.007](https://doi.org/10.7554/eLife.13722.007)

Figure 3 continued on next page

Figure 3 continued

Figure supplement 2. Ki-67 mutant mice develop normally.

DOI: [10.7554/eLife.13722.008](https://doi.org/10.7554/eLife.13722.008)

Figure supplement 3. Background Ki-67 levels in Ki-67 mutant mice.

DOI: [10.7554/eLife.13722.009](https://doi.org/10.7554/eLife.13722.009)

Figure supplement 4. Background Ki-67 levels in Ki-67 mutant mice.

DOI: [10.7554/eLife.13722.010](https://doi.org/10.7554/eLife.13722.010)

Figure supplement 5. Ki-67 mRNA levels are not reduced in Ki-67 mutant mice.

DOI: [10.7554/eLife.13722.011](https://doi.org/10.7554/eLife.13722.011)

Figure supplement 6. Normal proliferation and differentiation in Ki-67 mutant mice.

DOI: [10.7554/eLife.13722.012](https://doi.org/10.7554/eLife.13722.012)

Figure supplement 7. Ki-67 mRNA levels are not reduced in MEFs from Ki-67 mutant mice.

DOI: [10.7554/eLife.13722.013](https://doi.org/10.7554/eLife.13722.013)

Figure supplement 8. Generation of Ki-67-mutant NIH-3T3 cells.

DOI: [10.7554/eLife.13722.014](https://doi.org/10.7554/eLife.13722.014)

Figure supplement 9. Ki-67-mutant NIH-3T3 cells proliferate normally.

DOI: [10.7554/eLife.13722.015](https://doi.org/10.7554/eLife.13722.015)

Figure supplement 10. Basal translation of Ki-67 with a mutated ATG.

DOI: [10.7554/eLife.13722.016](https://doi.org/10.7554/eLife.13722.016)

Figure supplement 11. SILAC proteomics analysis of Ki-67 expression with a mutated ATG.

DOI: [10.7554/eLife.13722.017](https://doi.org/10.7554/eLife.13722.017)

Figure supplement 11—source data 1. SILAC quantitation of Ki-67 peptides from WT and Mki67-mutant NIH-3T3 cells.

DOI: [10.7554/eLife.13722.018](https://doi.org/10.7554/eLife.13722.018)

which is highly similar to the A-box, a third APC/C-Cdh1 recognition motif (Littlepage and Ruderman, 2002). To see whether Cdh1 regulates Ki-67, we analysed mouse embryo fibroblasts (MEFs) lacking the *Fzr1* gene that encodes Cdh1 (Garcia-Higuera et al., 2008). Asynchronous *Fzr1* heterozygous MEFs, that are at different stages of the cell cycle, had variable Ki-67 levels, whereas in the *Fzr1* knockout MEFs Ki-67 was upregulated and more homogeneously expressed (Figure 2A). To see whether sustained Ki-67 expression in quiescent cells would have a negative impact on cell cycle arrest in vivo, we analysed *Fzr1*-knockout mice. Here, Ki-67 was overexpressed and uncoupled from cells that incorporate BrdU in all tissues examined (Figure 2B, Figure 2—figure supplement 1). Thus, Ki-67 expression is regulated by APC/C-Cdh1 in mice and its downregulation is not a prerequisite for cell cycle exit.

We next investigated the functional consequences of Ki-67 downregulation for normal tissue development and homeostasis. To disrupt the gene encoding Ki-67, *Mki67*, in the mouse germline, we used a TALEN pair targeting the unique ATG start codon. This is predicted to generate null alleles (Figure 3—figure supplement 1A). After cytoplasmic injection of these TALEN-encoding mRNAs into zygotes, 10 out of 54 mice had mutations disrupting the coding sequence. We crossed founder mutant mice, and four gave germline transmission of the mutation. Due to mosaicism, this resulted in six lines: two lines with mutations eliminating the initiation codon and four lines with deletions which cause frameshifts immediately downstream of the ATG (Figure 3A). From these, we selected a 2-nucleotide deletion (2ntΔ) mutant that retains the ATG initiation codon but has a frameshift in the next codon (Figure 3—figure supplement 1B), and a 21-nucleotide deletion (21ntΔ) that eliminates the ATG (Figure 3—figure supplement 1C). We crossed these mice and, unexpectedly, obtained homozygous mutants at the expected Mendelian frequency that were indistinguishable from heterozygous or wild-type (WT) littermates (Figure 3B, Figure 3—figure supplement 1D). Both deletion mutant lines showed normal growth and were fertile. Sagittal sections from *Mki67*^{2ntΔ/2ntΔ} mice did not reveal any obvious defects in tissue morphology (Figure 3—figure supplement 2). Since the intestinal epithelium is the most highly proliferative adult mouse tissue, we compared its morphology between WT and mutant mice. In WT animals, the proliferative crypt compartment was strongly stained for Ki-67 by immunohistochemistry (IHC), while only minimal levels of Ki-67 were observed in the differentiated cells on the villus (Figure 3C, top), as expected. In contrast, in the mutants, proliferating crypt cells showed only residual levels of Ki-67 staining by IHC (Figure 3C, bottom) or immunofluorescence (Figure 3—figure supplement 3). Immunoblotting of intestinal

epithelium preparations could detect a weak band of similar size to WT Ki-67 (**Figure 3D**; **Figure 3—figure supplement 4**). The signal was, however, reduced by at least 90% in both mutants compared to WT tissue. Three different Ki-67 antibodies gave similar results. These are all extremely sensitive as they recognise the highly repeated Ki-67 domain. They should also detect N-terminally truncated Ki-67 that would result from translation from the ATG at position 433. qRT-PCR analysis showed that Ki-67 mRNA level was, unexpectedly, increased rather than reduced in the intestinal tissue (**Figure 3—figure supplement 5**). In the intestinal epithelium, analysis of Wnt signalling and differentiation of goblet and tuft cells showed no differences between WT and *Mki67*^{21ntΔ/21ntΔ} mice (**Figure 3—figure supplement 6**). These results show that high Ki-67 levels and an intact Ki-67 gene are not required for development or differentiation in vivo.

To see if cells from Ki-67 mutant mice had normal proliferation capacity we isolated embryonic fibroblasts (MEFs) from day-13 embryos. Homozygous *Mki67*^{2ntΔ/2ntΔ} MEFs had at least 90% lower Ki-67 levels (**Figure 3E**). We could not confirm by immunoblotting whether or not the protein was full-length or truncated since SDS-PAGE cannot resolve 15kDa differences between proteins of nearly 400 kDa, and no antibodies are available against the N-terminus of Ki-67. As with intestinal tissue, the loss of Ki-67 expression was not due to mRNA degradation, as shown by qRT-PCR (**Figure 3—figure supplement 7**). Indeed, in the homozygous mutant, the Ki-67 mRNA level was increased to a level comparable with that of proliferating NIH-3T3 cells. Mutant MEF proliferated comparably to controls, and flow cytometric assessment of EdU incorporation after a 1 hr EdU pulse showed similar numbers of replicating cells in Ki-67 WT and mutant cells (**Figure 3F**).

The low level residual Ki-67 expression in homozygous Ki-67 mutants suggests that TALEN or the conceptually-related CRISPR approaches may not lead to complete loss of expression, even when the translation initiation codon has been mutated. To further investigate whether Ki-67 translation can occur with a mutated initiation codon, we used the same TALEN pair to generate monoclonal Ki-67 mutant mouse NIH-3T3 cell lines, allowing analyses of translation that are technically impossible using animal tissues. We also performed the same procedure in the absence of TALENs to isolate wild-type clones. We obtained nine mutants with very low Ki-67 expression. Cloning and sequencing showed that five had biallelic mutations around the ATG codon (**Figure 3—figure supplement 8**). As in mice, even though Ki-67 was visible by immunofluorescence, Ki-67 was barely detectable by Western blot in all clones analysed (**Figure 3—figure supplement 9A**). All clones proliferated efficiently (**Figure 3—figure supplement 9B**). qRT-PCR showed that mutants did not have decreased Ki-67 mRNA levels compared to WT NIH-3T3 cells; indeed, like mutant MEFs, clone 14 had a higher level (**Figure 3—figure supplement 9C**). We selected two clones for further analysis of Ki-67 translation. Clone 14 had lost the ATG codon in one allele, but had acquired an insertion of 4 nucleotides after the ATG in the second allele, generating the same shifted reading frame as the *Mki67*^{2ntΔ/2ntΔ} mice. Clone 21 had lost the ATG codon in both alleles, thus mimicking the situation with *Mki67*^{21ntΔ/21ntΔ} mice. qRT-PCR quantification of Ki-67 mRNA from ribosome purifications shows that in clones 14 and 21 there was no decrease in ribosome association with Ki-67 mRNA; indeed, in clone 14 it increased, probably due to the higher Ki-67 mRNA level (**Figure 3—figure supplement 10**). To definitively determine levels of Ki-67 translation in the mutants, we performed SILAC quantitative mass spectrometry from exponentially growing WT or mutant NIH-3T3 cells cultured in light (L) (WT) or heavy-labelled (H) medium (clones 14 and 21). Chromatin was purified and run on SDS-PAGE. Peptides were purified from two gel slices, one around the predicted size of full length Ki-67 (>250 kDa; band 1) and one at a smaller size (130k Da-250 kDa, band 2). Ki-67 could not be positively identified in clones 14 and 21 (**Figure 3—figure supplement 11**). In peptides from WT cells (L), 44 peptides derived from Ki-67 were identified by MS/MS. In contrast, in peptides from mutant cell lines (H), no MS/MS spectra for Ki-67 could be identified in either band. Selecting the 're-quantify' option in MaxQuant (that forces quantitation of identified light peaks against any peaks that have the expected difference in m/z ratio), the ratios H/L observed for putative Ki-67 peaks were in the range of most typical contaminants that are only found unlabelled in a SILAC experiment. In band 1, the median normalised H/L intensity ratio of the 5 corresponding m/z peaks in clone 14 was 0.095 (mean, 0.100, SD, 0.02), and in clone 21 (7 peptides) was 0.191 (mean 0.203, SD 0.05). In band 2, which would result from truncated or degraded Ki-67, there were only 3 corresponding peaks, with median H/L ratios for clones 14 and 21 of 0.358 (mean, 0.402, SD, 0.30) and 0.500 (mean, 0.454, SD 0.33) respectively. Taken together, these results show that if Ki67 is translated in the mutant cell lines, it is at trace levels that are not positively identifiable by state-of-the-art mass

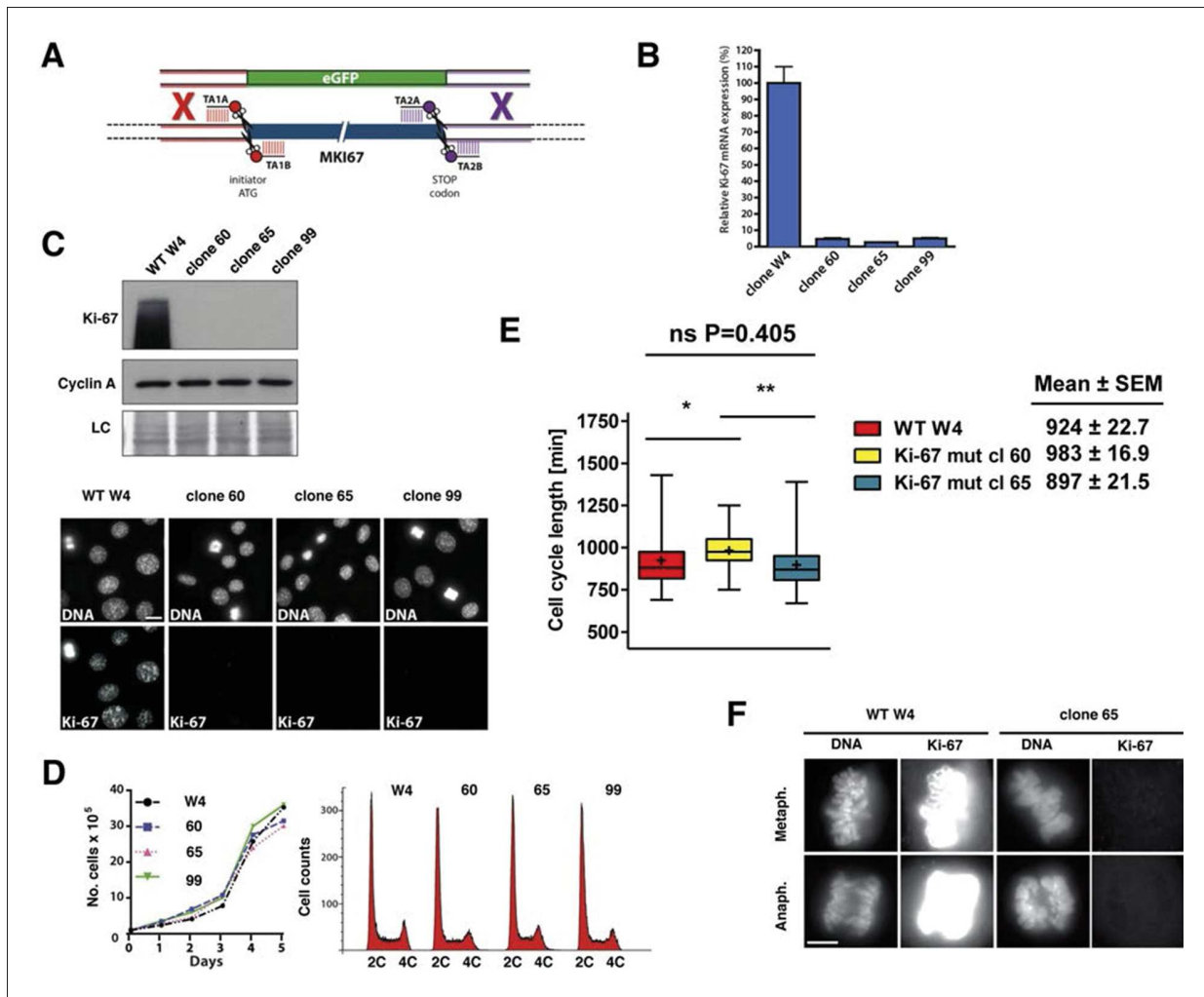


Figure 4. Cell proliferation without Ki-67. (A) Schematic representation of strategy for TALEN-mediated generation of *Mki67* null allele. (B) qRT-PCR analysis of Ki-67 mRNA levels in NIH-3T3 WT clone W4 and Ki-67-negative 60, 65, 99 clones. (C) Top: Western blot of Ki-67 and Cyclin A in NIH-3T3 WT clone W4 and Ki-67-negative mutant clones 60, 65, 99; LC, loading control; below, Ki-67 immunofluorescence; bar, 10 μ m. (D) Left, growth curves of WT and Ki-67 null cell lines 60, 65 and 99; right, cell cycle distribution analysed by flow cytometry. (E) Cell cycle length of WT clone W4 and Ki-67 null clones 60 and 65 as determined by time-lapse videomicroscopy. (F) Cells of clone 65 show altered chromosomal periphery in mitosis. The Ki-67 staining is deliberately overexposed to demonstrate absence of detectable Ki-67 in clone 65, even in metaphase. Bar, 5 μ m.

DOI: 10.7554/eLife.13722.019

The following figure supplement is available for figure 4:

Figure supplement 1. Generation of NIH-3T3 cells lacking Ki-67.

DOI: 10.7554/eLife.13722.020

spectrometry. At best, translation can occur from the mutated Ki-67 gene with an estimated 10% efficiency. The product is most likely an N-terminally truncated protein lacking the conserved FHA-domain, arising from a downstream in-frame ATG.

Cells lacking Ki-67 proliferate efficiently

Given the above results, it remained possible that very low levels of Ki-67 remain after *Mki67* gene mutation and that they might suffice to sustain cell proliferation. To rule out this possibility we devised a 'double TALEN' strategy to completely eliminate Ki-67 expression. We designed and synthesised an additional TALEN pair targeting a sequence downstream of the translation stop codon. We co-transfected the ATG TALEN pair and the Stop TALEN pair with a GFP knock-in construct containing homology arms (Figure 4A). We thus isolated several monoclonal cell lines in which Ki-67

mRNA was essentially eliminated (**Figure 4B**), indicating efficient nonsense-mediated decay (NMD). These cell lines had no residual Ki-67 protein expression (**Figure 4C**), confirming that the basal immunostaining seen in clones 14 and 21 indeed reflected trace level Ki-67 expression. We used Southern blotting of genomic DNA to characterise these alleles. The 3' end of the *Mki67* gene remained intact in all clones, while the 5' end of mutants showed a rearrangement consistent with a tandem insertion of multiple copies of the knockin construct upstream of the *Mki67* ORF (**Figure 4—figure supplement 1**). Thus, the *Mki67* gene was severely disrupted but not deleted. These Ki-67-negative cells proliferated normally. Growth curves and DNA content profiles were indistinguishable from controls (**Figure 4D**). Time-lapse videomicroscopy showed that although individual clones had slightly different cell cycle lengths, cell division time was not significantly different between WT and mutant clones (**Figure 4E**). We noticed that mitotic cells of one of the clones lacking Ki-67 had an altered chromosomal periphery (**Figure 4F**). Such a phenotype has previously been reported in Ki-67 knockdown HeLa cells (**Booth et al., 2014**). Nevertheless, these cells could divide efficiently.

Next, we tested whether *Mki67* mutant clones had altered kinetics of cell cycle exit or entry. To do this, we quantified cells that could replicate by measuring 5-ethynyl-2-deoxyuridine (EdU) incorporation into DNA. We found that 42% of WT *Mki67* cells could still incorporate some level of EdU even after 72 hr with 0.1% serum, but only 13% or 28% of mutant clones 60 or 65, respectively, could do so (**Figure 5A**). This suggested that *Mki67* disruption rendered cells slightly more sensitive to serum starvation. Upon addition of serum to quiescent cells, WT and *Mki67* mutants entered the cell cycle with similar kinetics (**Figure 5A**). Ki-67 remained completely undetectable in mutants (**Figure 5B**).

As Ki-67 is frequently used to assess proliferation in human cancer cells, we tested whether human cells lacking Ki-67 can proliferate. We generated stable human cell lines with inducible or constitutive expression of shRNA that silenced Ki-67 or a non-silencing control (**Figure 5—figure supplement 1A, 2A**). We used the non-transformed human fibroblast cell line BJ-hTERT, and two commonly used cancer cell lines, HeLa and U2OS, which are of epithelial and mesenchymal origin, respectively. In BJ-hTERT, inducing shRNA expression largely prevented Ki-67 expression but had no detectable effect on the kinetics of entry into the cell cycle, as judged by expression of cell cycle regulators and EdU incorporation (**Figure 5—figure supplement 1B**). Further reducing residual Ki-67 levels with siRNA also did not affect cell proliferation (**Figure 5—figure supplement 1C**). Similarly, constitutive knockdown of Ki-67 in stable shRNA-expressing HeLa or U2OS cells had no effect on cell cycle distribution nor on the expression of cell cycle regulators (**Figure 5—figure supplement 2B**). Analysing single cells by immunofluorescence showed that knockdown U2OS cells with undetectable Ki-67 expression incorporated EdU in a similar manner to control cells, demonstrating efficient DNA synthesis (**Figure 5—figure supplement 2C**).

Taken together, these results show that although Ki-67 elimination might have minor effects on cell cycle exit and mitosis, mammalian cells can nevertheless proliferate efficiently in the absence of detectable Ki-67.

Ki-67 interacts with proteins involved in nucleolar processes and chromatin regulation

To investigate possible molecular functions of Ki-67, we identified interacting proteins. To do this, we expressed FLAG-tagged versions of full-length human Ki-67 or an unrelated protein (TRIM39) in U2OS cells, and pulled down proteins from nuclear extracts with anti-FLAG antibody (**Figure 6—figure supplement 1**). These were analysed by label-free mass spectrometry. This approach identified 406 proteins specific to the Ki-67 pulldown (**Figure 6—figure supplement 2**). These included known Ki-67 partners: CDK1, an established Ki-67 kinase (**Blethrow et al., 2008**), nucleolar protein NIFK (**Takagi et al., 2001**), protein phosphatase 1 (**Booth et al., 2014**), and five subunits (HCFC1, HSPA8, MATRIN3, RBBP5 and WDR5) of a histone methylase complex that interacts with the nuclear receptor coregulator NRC (also known as NCOA6; **Garapaty et al., 2009**). Gene ontology and STRING analysis classified the Ki-67 interactors as being enriched in two general processes: chromatin regulation and ribosomal biogenesis (**Figure 6, Figure 6—figure supplement 2**). Specifically, interactors could be subdivided into groups involved in chromatin modification and transcription, ribosomal subunit biogenesis, pre-rRNA processing, protein translation, and splicing. These interactions suggested that Ki-67 might be involved not only in ribosomal biogenesis, as previously suggested (**Rahmanzadeh et al., 2007**), but also in regulating chromatin. Among chromatin regulators

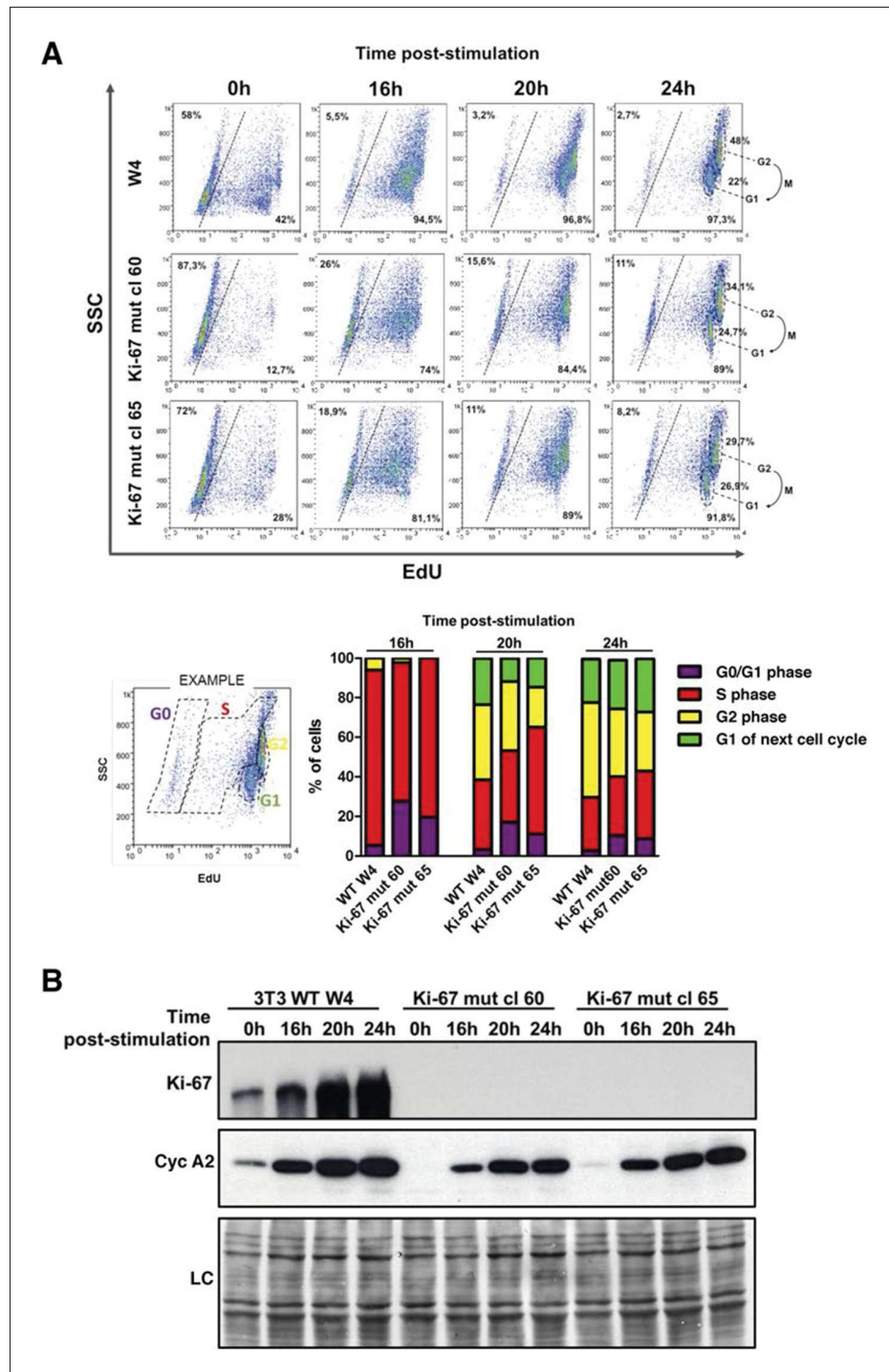


Figure 5. Cells lacking Ki-67 enter the cell cycle efficiently. (A) Top, re-entry of cell cycle in NIH-3T3 WT clone W4 and Ki-67-negative mutant clones 60 and 65 after serum starvation-induced cell cycle arrest. Progression of cell cycle entry analysed by FACS using EdU staining. Bottom, quantification of cell cycle phases in this experiment. (B) Western blot analysis of Ki-67 (upper panel) and cyclin A2 (lower panel) upon cell cycle entry. LC, loading control. DOI: [10.7554/eLife.13722.021](https://doi.org/10.7554/eLife.13722.021)

The following figure supplements are available for figure 5:

Figure supplement 1. Cells lacking Ki-67 proliferate efficiently. DOI: [10.7554/eLife.13722.022](https://doi.org/10.7554/eLife.13722.022)

Figure 5 continued on next page

Figure 5 continued

Figure supplement 2. Cells lacking Ki-67 proliferate efficiently.

DOI: [10.7554/eLife.13722.023](https://doi.org/10.7554/eLife.13722.023)

interacting with Ki-67, we found the NRC-interacting methylase complex; KMT2D, ASH2L and SUZ12 proteins which are components of MLL and PRC2/EED-EZH1 complexes which regulate histone H3 methylation (Patel et al., 2009; Pasini et al., 2004); SETD1A, HCFC1, HDAC2, YY1 and RCOR1, which are components of H3K4 demethylase complexes and co-repressors; and UHRF1, which binds to H3K9me3-modified chromatin and is involved in both maintaining DNA methylation and heterochromatin formation (Bostick et al., 2007; Guetg et al., 2010; Rottach et al., 2010). Ki-67 also interacts with TIP5, the major component of the nucleolar remodelling complex (NoRC) which is required to establish and maintain perinucleolar heterochromatic rDNA, as well as NoRC-interacting proteins TTF1 and DNM3.

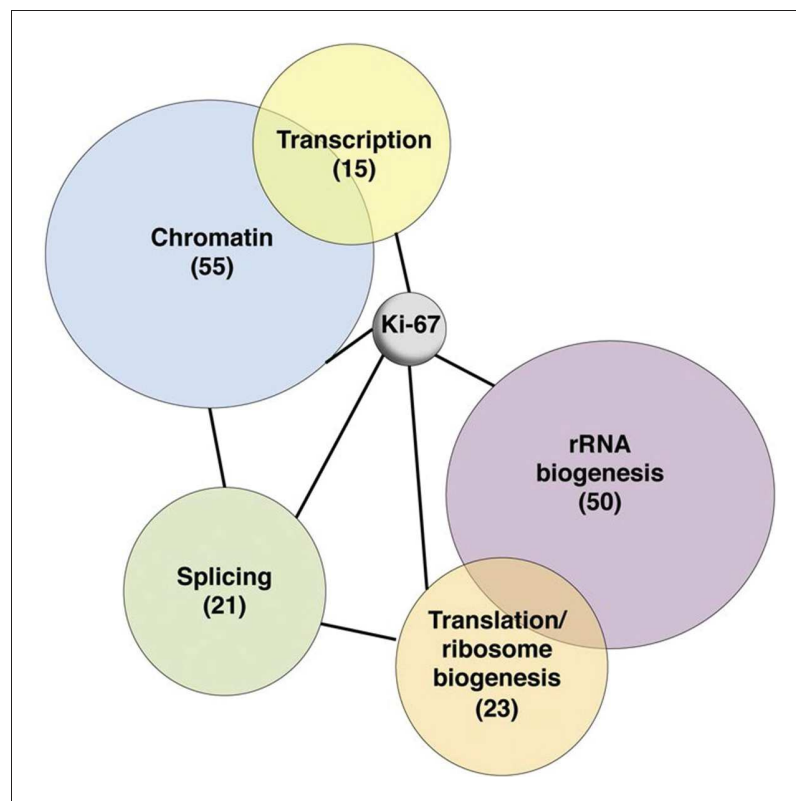


Figure 6. Ki-67 interacts with proteins involved in nucleolar processes and chromatin. Simplified STRING analysis reveals network interactions between proteins associating with Ki-67. The full network is shown in **Figure 6—figure supplement 2**; data is provided in **Figure 6—source data 1**.

DOI: [10.7554/eLife.13722.024](https://doi.org/10.7554/eLife.13722.024)

The following source data and figure supplements are available for figure 6:

Source data 1. Ki-67 interacting proteome.

DOI: [10.7554/eLife.13722.025](https://doi.org/10.7554/eLife.13722.025)

Figure supplement 1. The Ki-67 interactome.

DOI: [10.7554/eLife.13722.026](https://doi.org/10.7554/eLife.13722.026)

Figure supplement 2. Ki-67 interacts with proteins involved in nucleolar processes and chromatin.

DOI: [10.7554/eLife.13722.027](https://doi.org/10.7554/eLife.13722.027)

Ki-67 is required for perichromosomal region formation during nucleologenesis

We first focused on a possible role of Ki-67 in ribosome biogenesis, a process linked to nucleolar assembly and structure, and which is required for cell proliferation (*Hernandez-Verdun et al., 2010*). One of the candidate Ki-67 interactors involved in rRNA biogenesis was the Pescadillo homologue PES1, which participates in pre-rRNA processing and is localised in the nucleolar granular components (GC) (*Rohrmoser et al., 2007; Tafforeau et al., 2013*). During interphase, we found that Ki-67 localised at the cortical periphery of the GC, visualised using PES1. Ki-67 formed a boundary between the perinucleolar heterochromatin (clearly visible as a 'ring' in the DAPI staining) and the GC (*Figure 7A, Figure 7—figure supplement 1*). Whereas nucleolar disruption using Actinomycin D or the CDK inhibitors DRB or Roscovitine caused nuclear relocalisation of Ki-67 and GC proteins (*Figure 7—figure supplement 2*), depletion of Ki-67 did not affect the gross structure of the nucleolus, as determined by PES1 staining (*Figure 7A, Figure 7—figure supplement 3*).

During mitosis, the nucleolus undergoes a dramatic cycle of disassembly and reassembly (*Hernandez-Verdun et al., 2010*). Briefly, soon after the onset of mitosis, when transcription is shut down, the nucleolus is rapidly disassembled; it then slowly reforms through the formation of intermediary organelles that undergo consecutive transformations, identifying three distinct organelle stages, and the process is complete by telophase. The first of these three intermediary organelles is a sheath of nucleolar proteins that forms around the surface of the mitotic chromosomes, the so-called 'perichromosomal region' or PR. To date, not much is known about the *trans*-acting factors involved in PR formation. Remarkably, we found that Ki-67 depletion totally disrupted PR formation and PES1 no longer associated with the chromosome surface (*Figure 7B*). A similar finding, using other nucleolar proteins than PES1 as PR markers, was recently reported (*Booth et al., 2014*).

Having established that Ki-67 controls nucleolar assembly during mitosis, we wondered whether Ki-67 is required for pre-rRNA processing. We found that Ki-67 knocked down U2OS cells, that have essentially undetectable Ki-67, could still incorporate normal levels of 5-ethynyl uridine (EU) in nucleolar RNA. This suggests that rRNA transcription is not altered (*Figure 8—figure supplement 1*). We next looked at pre-rRNA processing pathways by Northern blotting of precursor rRNAs or intermediates (*Figure 8—figure supplement 2*). This showed that silencing Ki-67 expression by shRNA or siRNA had no significant effect on pre-rRNA processing in four different cancer cell lines (*Figure 8A*). We did, however, notice a marginal but reproducible increase in the level of the 47S precursor rRNA, indicating a mild delay in the early nucleolar pre-rRNA cleavage steps (*Figure 8B*). The tumour suppressor TP53 (p53) is a sensor of nucleolar stress resulting from defective ribosome biogenesis, and it represses ribosomal gene transcription (*Bursac et al., 2014*). Impairment of early pre-rRNA cleavage steps upon depletion of Ki-67 was independent of p53 (*Figure 8B*). Taken together, these results demonstrate that while Ki-67 is dispensable for efficient pre-rRNA processing, it is essential for the formation of the perichromosomal layer during nucleologenesis.

Depletion of Ki-67 affects gene transcription

These results showed that in spite of its role in early steps of nucleologenesis, Ki-67 is not essential for expression of rRNA genes. We next asked whether it is involved in control of mRNA expression. We performed genome-wide transcriptome analysis from U2OS and HeLa cells expressing non-silencing control or Ki-67 shRNA, using Agilent gene-microarrays. Ki-67 knockdown led to downregulation (corrected p value <0.02, Fold-change >1.5) of over 200 genes (*Figure 8C*). Expression of cell cycle regulatory genes was not affected. Additionally, Ki-67 silencing caused upregulation (corrected p value <0.02, Fold-change >1.5) of a wide variety of genes involved in neural, testis and cardiovascular system development and differentiation (*Figure 8C*). These were strikingly enriched in genes encoding zinc-finger proteins and olfactory receptors, two gene families that are highly enriched in nucleolar associated-domains (NADs) of perinucleolar heterochromatin (PNHC) (*Németh et al., 2010*). This suggested that effects of Ki-67 downregulation on gene expression might be due to an altered chromatin state, in particular of PNHC.

Ki-67 promotes heterochromatin organisation

In support of a potential role for Ki-67 in heterochromatin organisation, we found that Ki-67 knockdown in HeLa and U2OS cells caused a marked reduction in perinucleolar DAPI staining (*Figure 7A,*

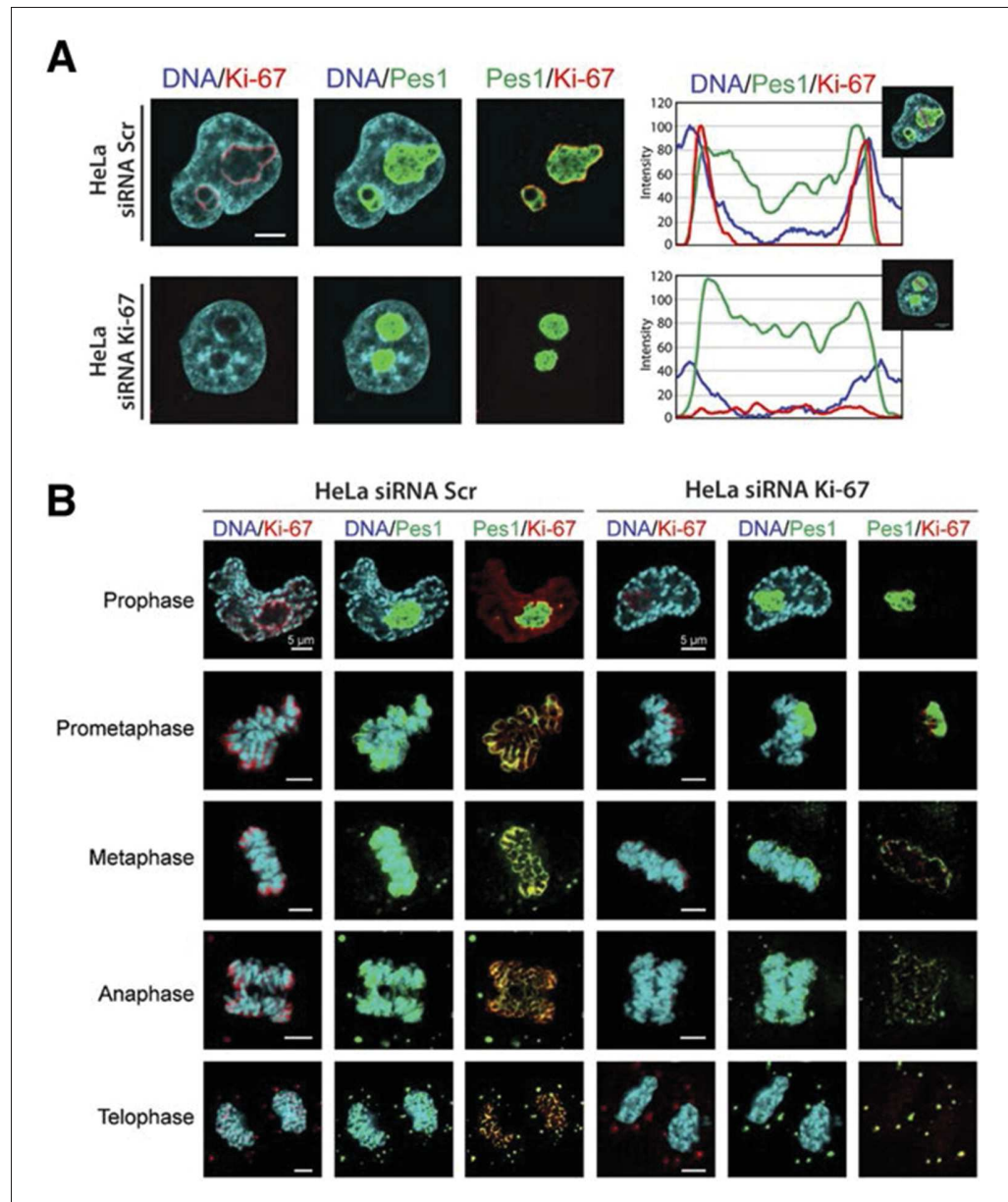


Figure 7. Ki-67 localises PES1 to mitotic chromosomes. (A) Analysis of the interphase localisation of PES1 and Ki-67 proteins by immunofluorescence in HeLa cells 72 hr after transfection with control siRNA (scramble; Scr) or Ki-67 RNAi. Right, line scans showing the distribution of fluorescence signals within indicated nucleoli (dashed line). Images were captured in confocal mode with a spinning-disk microscope. Bar, 5 μ m. (B) Analysis of the mitotic localisation of PES1 and Ki-67 proteins by immunofluorescence in HeLa cells 72 hr after transfection with control siRNA (scramble; Scr) or Ki-67 RNAi. Bar, 5 μ m.

DOI: [10.7554/eLife.13722.028](https://doi.org/10.7554/eLife.13722.028)

The following figure supplements are available for figure 7:

Figure supplement 1. Ki-67 is a nucleolar protein localizing in the cortical side of the GC.

DOI: [10.7554/eLife.13722.029](https://doi.org/10.7554/eLife.13722.029)

Figure supplement 2. Ki-67 follows GC components upon drug-induced nucleolar disruption.

DOI: [10.7554/eLife.13722.030](https://doi.org/10.7554/eLife.13722.030)

Figure supplement 3. Depletion of Ki-67 does not affect overall nucleolar structure.

DOI: [10.7554/eLife.13722.031](https://doi.org/10.7554/eLife.13722.031)

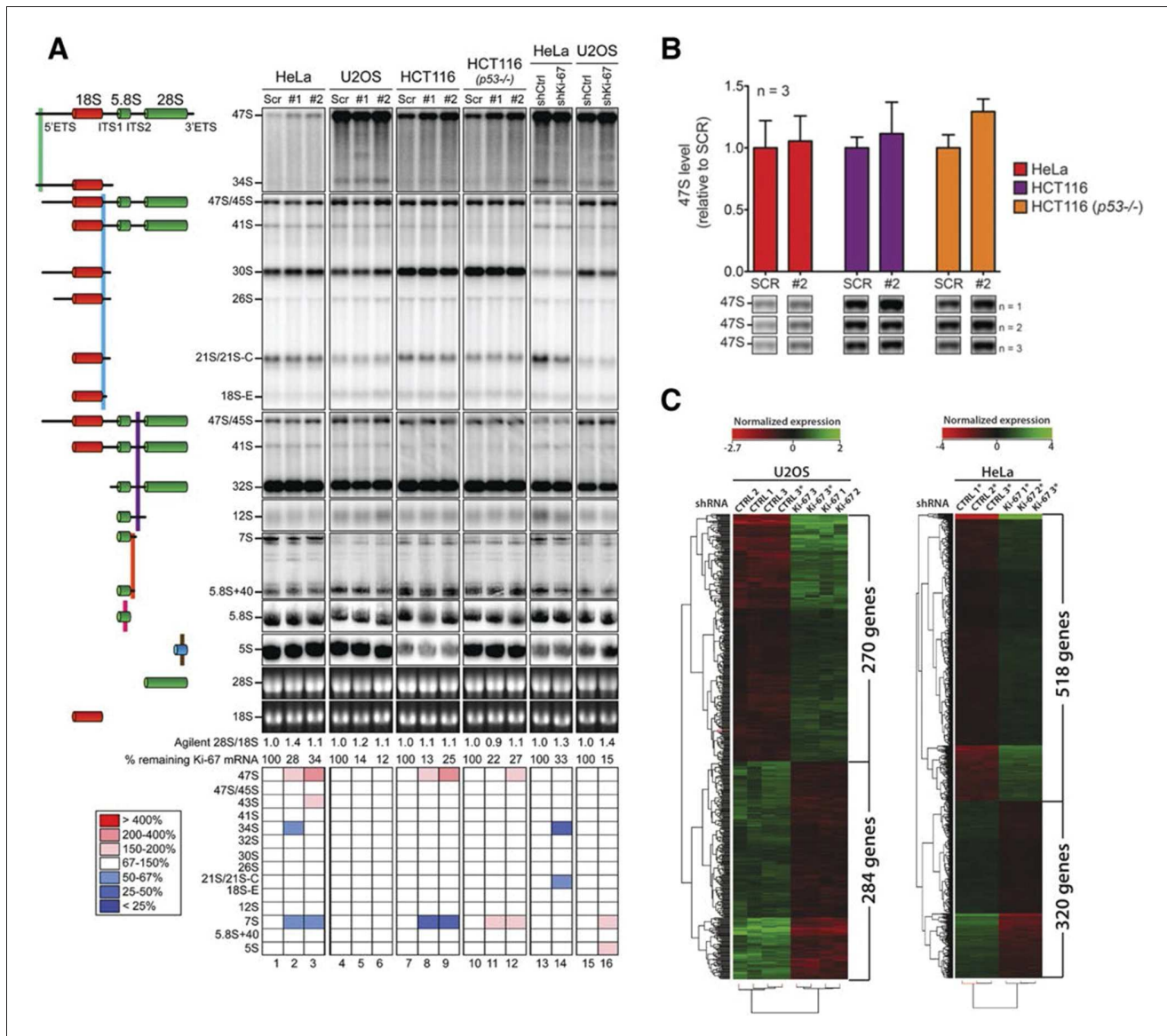


Figure 8. Ki-67 is not required for rRNA biogenesis but controls gene transcription. (A) Northern-blot analysis of total RNA extracted from HeLa and U2OS cells constitutively expressing shRNA against Ki-67; and HeLa, U2OS, HCT-116 and HCT-116 TP53 (-/-) depleted of Ki-67 by siRNA for 72 hr in two biological replicates (#1 and #2) or with scrambled siRNA control (Scr). Pre-rRNA intermediates were analysed by probing with different primers located in the different spacers of the 47S sequence (5'ETS-green; ITS1-blue; ITS2-purple). (B) Quantification of 47S rRNA precursor in HeLa, HCT-116 and HCT-116 TP53 (-/-) depleted of Ki-67 by siRNA for 72 hr in three biological replicates (n=1–3). (C) U2OS cells (left) or HeLa cells (right) show transcriptome profile differences (fold change >1.5; corrected p-value <0.02) between asynchronous cells constitutively expressing control (CTRL) or Ki-67 shRNA. Heat-maps present the expression levels of differentially expressed genes between biological replicates (1,2,3) and technical replicates (3, 3*). Data is provided in **Figure 8—source data 1 and 2**.

DOI: [10.7554/eLife.13722.032](https://doi.org/10.7554/eLife.13722.032)

The following source data and figure supplements are available for figure 8:

Source data 1. Ki-67-dependent transcriptome in U2OS cells.

DOI: [10.7554/eLife.13722.033](https://doi.org/10.7554/eLife.13722.033)

Source data 2. Ki-67-dependent transcriptome in HeLa cells.

DOI: [10.7554/eLife.13722.034](https://doi.org/10.7554/eLife.13722.034)

Figure supplement 1. Ki-67 depletion does not hinder rRNA transcription.

DOI: [10.7554/eLife.13722.035](https://doi.org/10.7554/eLife.13722.035)

Figure supplement 2. Human pre-rRNA processing pathway involves two major pathways.

DOI: [10.7554/eLife.13722.036](https://doi.org/10.7554/eLife.13722.036)

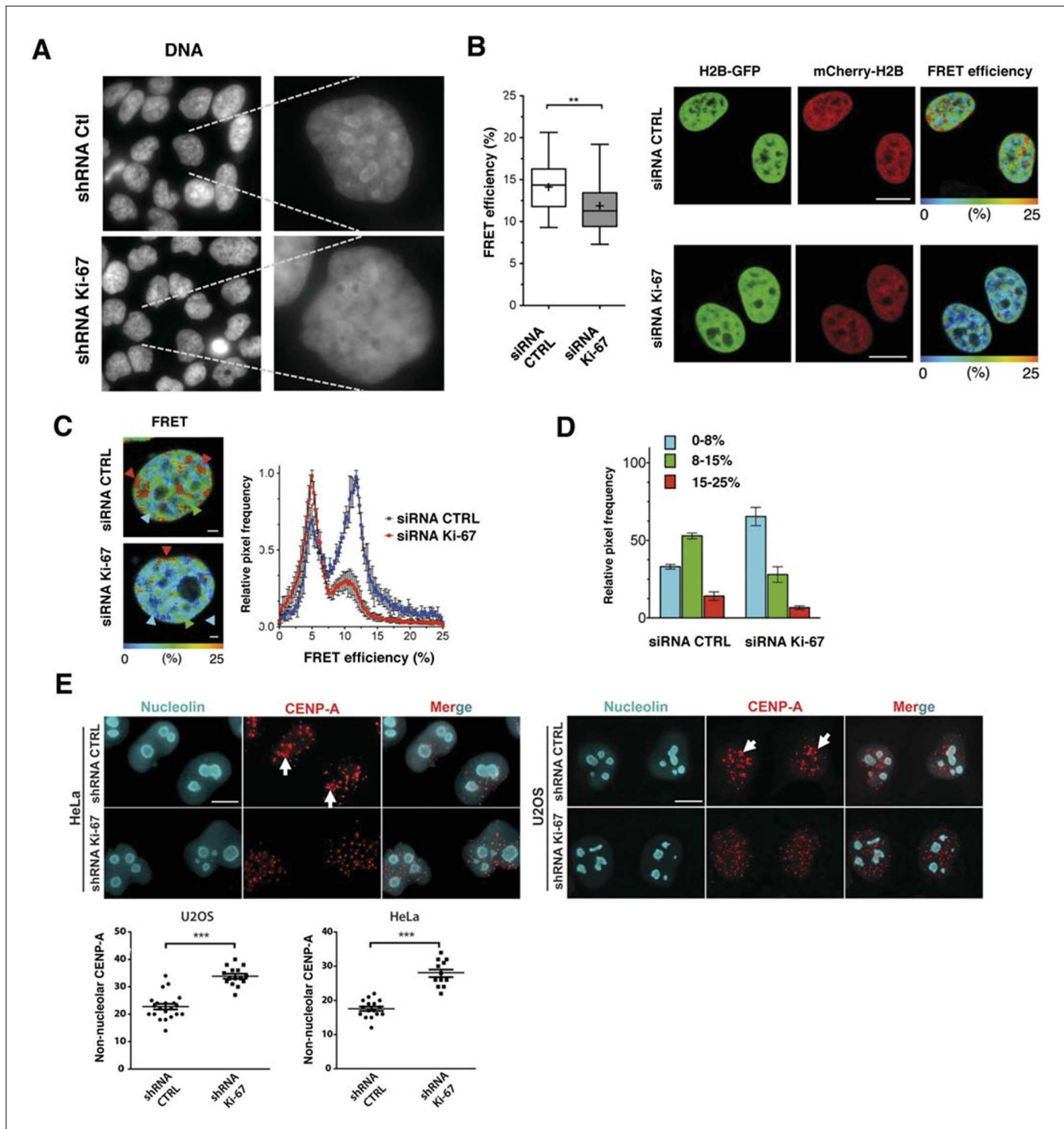


Figure 9. Ki-67 promotes heterochromatin interactions. (A) DAPI staining in control and stable Ki-67-knockdown U2OS cells. (B) HeLa cells stably expressing GFP-H2B and mCherry-H2B, depleted using Ki-67 or non-targeting (CTRL) siRNA. Left, FRET efficiency (cross shows mean value) ** Different, $p < 0.01$. FRET efficiency and spatial distribution shown by a pseudocolour scale of FRET (%) values from 0 to 25%. Bars, 10 μm . (C) Left, representative HeLa^{H2B-2FP} nuclei showing spatial distribution of FRET efficiency. Arrowheads show different chromatin compaction states (high FRET, red; intermediate, green; low, blue), Bars, 2 μm . Right, mean FRET distribution curves from siRNA control (blue curve, $n=8$) and siRNA Ki-67 (red curve, $n=11$) nuclei. (D) Relative fraction of the three FRET efficiency populations (blue (low), FRET efficiency $\leq 8\%$; green (medium), 8–15%; and red (high), 15–25%) in siRNA control and siRNA Ki-67 nuclei. Error bars indicate SD. (E) Immunofluorescence of CENP-A localisation in control and stable Ki-67 knockdown HeLa (left) and U2OS (right) cells. Nucleolar localisation (white arrows). Nucleolin was used as nucleolar marker. Bar, 10 μm . Below: quantification in different cells of numbers of CENP-A spots not associated with the nucleolus.

DOI: [10.7554/eLife.13722.037](https://doi.org/10.7554/eLife.13722.037)

Figure 9 continued on next page

Figure 9 continued

The following figure supplement is available for figure 9:

Figure supplement 1. Knockdown of Ki-67 in H2B FRET cell line.

DOI: [10.7554/eLife.13722.038](https://doi.org/10.7554/eLife.13722.038)

9A). We thus hypothesised that Ki-67 might be required for heterochromatin compaction. To directly assess chromatin compaction in living cells, we used a Förster Resonance Energy Transfer-Fluorescence Lifetime Imaging Microscopy (FRET-FLIM)-based assay. In this system, HeLa cells stably co-express versions of histone H2B labelled with eGFP and mCherry. Inter-nucleosomal interactions between H2B-eGFP and H2B-mCherry generates FRET, whose efficiency depends on the distance between nucleosomes (Llères *et al.*, 2009). We depleted Ki-67 by siRNA and studied the effects on FRET efficiency in interphase cells (Figure 9—figure supplement 1). As expected (Llères *et al.*, 2009), a heterogeneous FRET efficiency map was observed throughout control siRNA nuclei, reflecting different chromatin compaction states (Figure 9B). Upon Ki-67 depletion, the mean FRET percentage decreased, reflecting a reduction in total chromatin compaction (Figure 9B). The highest FRET populations, including heterochromatin regions at the nuclear periphery and around nucleoli, were largely eliminated upon Ki-67 depletion, with a few remaining condensed foci predominantly located at the nuclear periphery (Figure 9C,D). In contrast, a population of less compact chromatin increased.

Reduced compaction of heterochromatin implies disruption of short-range interactions of chromatin. To determine whether Ki-67 knockdown also affects long range interactions, we assessed interactions between perinucleolar and pericentromeric heterochromatin. We stained for the centromeric histone variant CENP-A to determine the localisation of centromeric DNA. In HeLa and U2OS cells, CENP-A showed a non-random nuclear localisation and clustered around nucleoli (Figure 9E, arrowheads), confirming that CENP-A can be used as a surrogate marker for adjacent pericentromeric DNA. Consistent with our hypothesis, this interaction was disrupted upon Ki-67 knockdown, and the CENP-A signal was no longer grouped around nucleoli but dispersed throughout the nucleus (Figure 9E). These results imply that Ki-67 mediates interaction between different regions in the genome that are normally packaged into heterochromatin, and could potentially maintain silencing of genes by recruiting them to constitutive heterochromatin.

Constitutive heterochromatin, including PNHC, is characterised by histone post-translational modifications H3K9me3 and H4K20me3. We asked whether they were affected by downregulation of Ki-67. Stable shRNA-mediated Ki-67 knockdown in HeLa, U2OS and inducible knockdown in BJ-hTERT fibroblasts caused a visible reduction in nucleolar staining of H3K9me3 and H4K20me3 (Figure 10—figure supplements 1–3). This mark was relocalised either to foci in proximity to the nucleolus or a punctate pattern dispersed throughout the nucleus. In mouse cells, where pericentromeric heterochromatin is prominent, H3K9me3 staining colocalised with DAPI-dense chromocentres, but TALEN-ablation of *Mki67* resulted in general nuclear punctate H3K9me3 that was excluded from nucleoli (Figure 10A,B). Western blotting revealed that Ki-67 depletion did not affect the overall levels of these chromatin modifications (Figure 10—figure supplement 4). We also analysed the localisation of heterochromatin protein 1 (HP1), which binds to chromatin containing H3K9me3. Immunofluorescence showed that, surprisingly, despite the loss of the intense H3K9me3 staining regions in the *Mki67* mutant cells, all three HP1 isoforms maintained their localisation at DAPI-dense regions (Figure 10—figure supplement 5). Next, we determined whether heterochromatic histone marks were reduced on specific DNA sequences, or whether they were retained but the sequences themselves were delocalised. To do this we examined co-localisation of H3K9me3 with mouse major satellite DNA, by combining immunofluorescence with fluorescent in situ hybridisation (FISH). In control cells, major satellite DNA, DAPI-dense regions and H3K9me3 largely colocalised (Figure 10C). In cells lacking Ki-67, major satellite DNA was still present at regions of compacted DNA, despite the loss of H3K9me3 at these regions (Figure 10C). Taken together, these results suggest that Ki-67 is required for maintaining heterochromatic histone marks at genomic regions that are organised into heterochromatin.

These results suggest that Ki-67 is required for heterochromatin organisation. To see whether Ki-67 is sufficient to promote heterochromatin formation, we cloned a full-length cDNA encoding human Ki-67, that we fused to the eGFP gene, and transfected it into U2OS cells. There was a strong

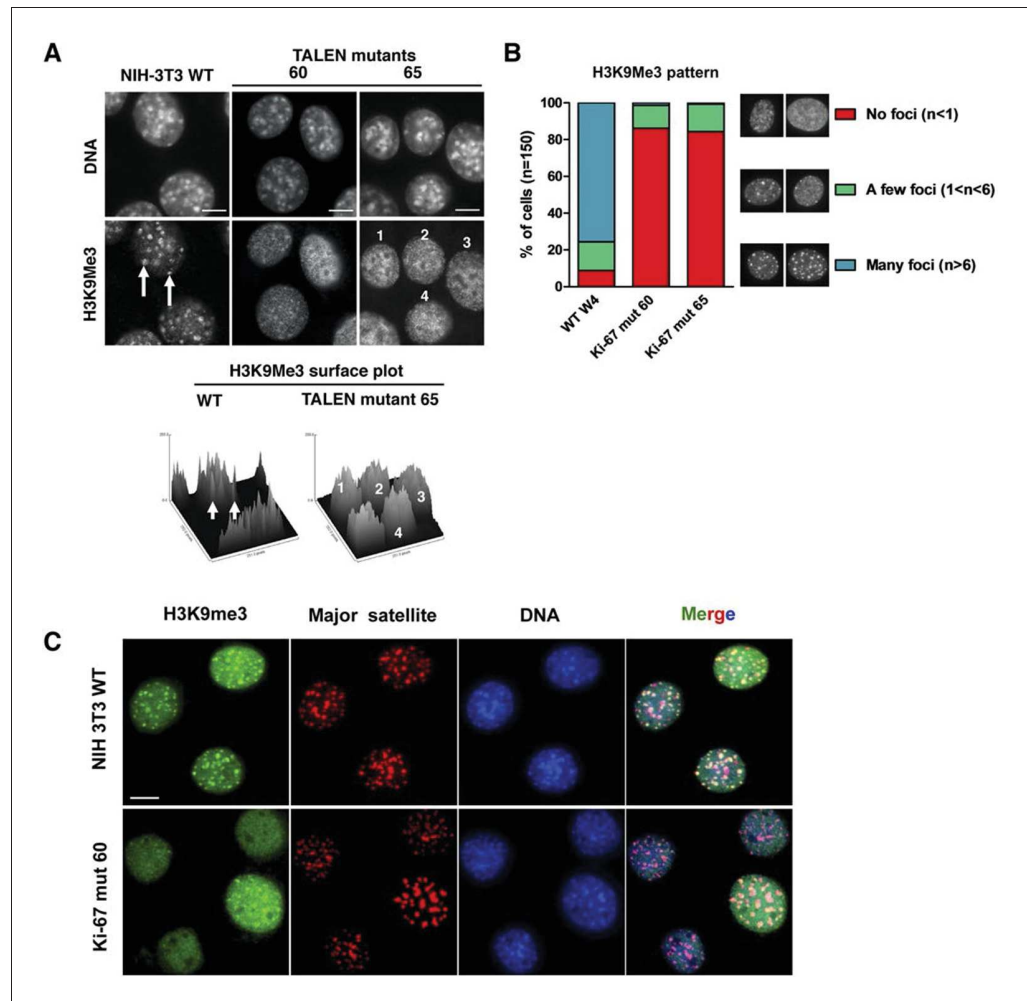


Figure 10. Ki-67 controls heterochromatin organisation. (A) Top, immunofluorescence analysis of H3K9me3 in mouse NIH-3T3 WT and *Mki67* TALEN mutant clones 60 and 65. Bars, 5 μ m. Below: graphs showing quantification of pixel intensity scans for H3K9me3. (B) Quantification of H3K9me3 patterns in WT and Ki-67 mutant clones. (C) Immunofluorescence of H3K9me3, FISH of major satellite DNA and DAPI staining in WT W4 and Ki-67 mutant clone 60. Bar, 10 μ m.

DOI: [10.7554/eLife.13722.039](https://doi.org/10.7554/eLife.13722.039)

The following figure supplements are available for figure 10:

Figure supplement 1. Heterochromatic histone mark localisation requires Ki-67.

DOI: [10.7554/eLife.13722.040](https://doi.org/10.7554/eLife.13722.040)

Figure supplement 2. Heterochromatic histone mark localisation requires Ki-67.

DOI: [10.7554/eLife.13722.041](https://doi.org/10.7554/eLife.13722.041)

Figure supplement 3. Heterochromatic histone mark localisation requires Ki-67.

DOI: [10.7554/eLife.13722.042](https://doi.org/10.7554/eLife.13722.042)

Figure supplement 4. Overall heterochromatic histone mark levels do not change upon Ki-67 knockdown.

DOI: [10.7554/eLife.13722.043](https://doi.org/10.7554/eLife.13722.043)

Figure supplement 5. HP1 localises normally to chromocentres in Ki-67 mutant cells.

DOI: [10.7554/eLife.13722.044](https://doi.org/10.7554/eLife.13722.044)

correlation between cells with higher levels of exogenous Ki-67 and appearance of DAPI-dense foci resembling ectopic heterochromatin, marked by H3K9me3 and HP1 (Figure 11A). Cells showing this phenotype were negative for cyclin A staining, suggesting that they were unable to enter S-phase, whereas lower expression did not prevent cyclin A accumulation (Figure 11B). They were also negative for histone H3 Ser-10 phosphorylation, a mitotic marker (Figure 11—figure supplement 1). If

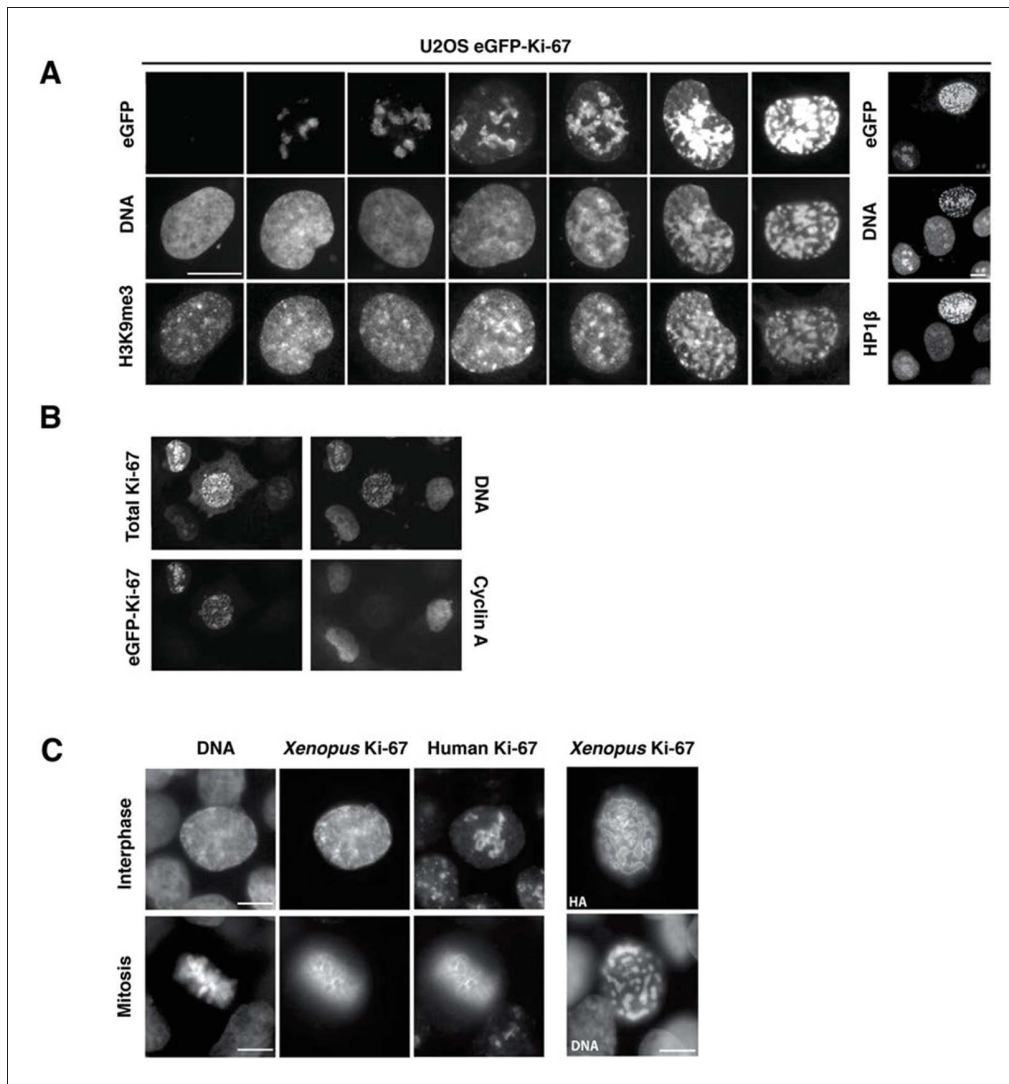


Figure 11. Overexpression of Ki-67 induces ectopic heterochromatin. (A) Overexpression of full length Ki-67 N-terminal fusion with eGFP in U2OS cells induces ectopic heterochromatin, as visualised by DAPI staining (middle) and immunofluorescence of H3K9Me3 (left) or HP1 β (right). Eight representative cells that have different levels of Ki-67 expression, as determined by eGFP fluorescence intensity, are shown. Bar, 10 μ m. (B) U2OS cells expressing high levels of exogenous eGFP-Ki-67 and showing ectopic chromatin condensation are negative for cyclin A staining by immunofluorescence. (C) Left: Immunofluorescence analysis of the localisation of endogenous human and ectopically expressed *Xenopus* Ki-67 in U2OS cells, showing colocalisation in metaphase at the perichromosomal region. Right: DNA condensation caused by high overexpression of *Xenopus* Ki-67 in U2OS cells. Bars, 10 μ m.

DOI: [10.7554/eLife.13722.045](https://doi.org/10.7554/eLife.13722.045)

The following figure supplements are available for figure 11:

Figure supplement 1. Overexpression of Ki-67 induces ectopic heterochromatin.

DOI: [10.7554/eLife.13722.046](https://doi.org/10.7554/eLife.13722.046)

Figure supplement 2. A *Xenopus* Ki-67 homologue (A) Chromatin proteomics in replicating *Xenopus* egg extracts.

DOI: [10.7554/eLife.13722.047](https://doi.org/10.7554/eLife.13722.047)

controlling heterochromatin organisation is a major function of Ki-67, it is likely to be conserved in more distantly related Ki-67 homologues. In a proteomics-based screen for proteins associated with replicating chromatin in egg extracts, we identified a putative *Xenopus* Ki-67 homologue (**Figure 11—figure supplement 2**). To assess whether *Xenopus* and human Ki-67 are functionally conserved, we cloned and HA-tagged full-length *Xenopus* Ki-67 and expressed it in U2OS cells. Whereas in interphase, exogenous *Xenopus* Ki-67 is present ubiquitously on chromatin, it colocalises

with endogenous Ki-67 in mitosis at the perichromosomal region (**Figure 11C**). Overexpression of *Xenopus* Ki-67, like human Ki-67, caused extreme chromatin compaction (**Figure 11C**). We conclude that controlling heterochromatin is a conserved essential function of Ki-67.

Discussion

Ki-67 has long been assumed to be essential for cell proliferation (*Schluter et al., 1993; Kausch et al., 2003; Starborg et al., 1996; Rahmzadeh et al., 2007; Zheng et al., 2006; 2009*). Using various genetic and knockdown approaches, we found no evidence for this in any cell type we tested: HeLa, U2OS, BJ-hTERT and NIH-3T3 fibroblasts. Our data show that Ki-67 expression can be uncoupled from cell proliferation in both directions. Indeed, not only can cells lacking Ki-67 proliferate efficiently, conversely, interfering with Ki-67 downregulation by disrupting the *Cdh1* gene did not prevent cell cycle exit in vivo. It remains possible that certain cell lines are more sensitive to inhibition of Ki-67 expression, eg cancer cell lines of bladder (*Kausch et al., 2003*) or renal (*Zheng et al., 2006; 2009*) origins. Alternatively, off-target effects of previous antisense or RNAi approaches might have contributed to the cell proliferation defects observed in previous studies, as none of them employed restoration controls using silencing-insensitive constructs. Such rescue experiments are virtually unfeasible given the large size of Ki-67, the targeting of silencing oligonucleotides to the repeated domains, and the fact that Ki-67 overexpression induces ectopic heterochromatin. Several other studies used different approaches. In one, microinjection of an anti-Ki-67 antibody in 3T3 cells did not cause an abolition of cell division (*Starborg et al., 1996*). Instead, there was a modest reduction, from 80% to 64%, of dividing cells over a 36-hr period. Another study used chromophore-mediated light inactivation of Ki-67 after injecting chromophore-labelled Ki-67 antibodies, and found an inhibition of ribosomal RNA synthesis (*Rahmzadeh et al., 2007*). However, such an approach might cause non-specific collateral damage to nucleolar processes where Ki-67 is localised.

We found that rather than promoting cell proliferation, the role of Ki-67 is to organise heterochromatin. We showed that Ki-67 is required for the maintenance of a high level of compaction typical of heterochromatin, and mediates long-range interactions between different regions of the genome that are packaged into heterochromatin. We speculate that heterochromatin compaction relies on local interactions that depend on Ki-67. Cells lacking Ki-67 show altered gene expression profiles upon long-term Ki-67 silencing, with a striking correlation between upregulation of genes that normally are physically associated with perinucleolar heterochromatin (*Németh et al., 2010*). To determine possible mechanisms of action of Ki-67, we comprehensively identified its interacting partners. We thus found at least seventeen proteins that are involved in histone methylation complexes or are interactors of methylated chromatin required for heterochromatin maintenance. This suggests that Ki67 might target these proteins to their genomic sites to promote heterochromatin formation. Consistent with this hypothesis, Ki-67 downregulation led to reduction of H3K9me3 and H4K20me3 at heterochromatin, while Ki-67 overexpression caused appearance of ectopic heterochromatic foci enriched in these methylation marks. Unexpectedly, Ki-67 downregulation did not prevent association of HP1 isoforms with heterochromatin. Possibly, low levels of H3K9me3 or H4K20me3 persist and are sufficient for recruitment of HP1, or alternative mechanisms exist to localise HP1 to chromatin. The former hypothesis would be consistent with the observation that loss of the Suv39H methyltransferases that are responsible for H3K9me3 and H4K20me3 abrogates HP1 recruitment to heterochromatin in mice, whose late embryonic growth and survival is impaired (*Peters et al., 2001*). Nevertheless, evidence for the latter possibility has been provided by a study in *C.elegans*, in which genome-wide distribution of HP1 binding, as assessed by ChIP-seq, was conserved in animals lacking H3K9 di- and trimethylation (*Garrigues et al., 2015*).

Given the requirement for Ki-67 expression in organising heterochromatin, it is perhaps surprising that mouse development is not affected by Ki-67 downregulation. This once again highlights the robustness of biological systems. However, to determine whether mouse development can occur normally in the complete absence of Ki-67 will require a gene deletion rather than a gene disruption mediated by genome-editing, as we found that even deletion of the translation initiation ATG using TALENs did not completely abolish Ki-67 expression. The eight subsequent ATG codons are out of frame, and the next in-frame ATG is 433 bp downstream. Translation from any frameshifted ATG will lead to a premature stop codon within 65 nucleotides. Although NMD of the mRNA did not occur,

translation was strongly reduced. This is probably due to the presence of many out-of-frame ATG codons before the next in-frame ATG codon, as well as the distance from the 5' end of the mRNA. It is likely that the residual Ki-67 in proliferating cells occurred from the next in-frame ATG, thus eliminating the most highly conserved domain of Ki-67, the Forkhead-associated (FHA) domain. However, the unexpected translation in the mutants suggests that care should be taken to examine possible low level expression of proteins after mutating start sites using genome editing approaches.

Since Ki-67 is degraded upon cell cycle exit, we speculate that this may alter chromatin structure. For example, Ki-67 degradation might be involved in heterochromatin rearrangements observed during senescence onset. Facultative heterochromatic foci, that characterise some senescent cells (Narita *et al.*, 2003; 2006) are not a consistent feature of senescence in all cell types. In contrast, large-scale satellite heterochromatin decondensation is an early step in senescence in all cells studied and it precedes loss of H3K9me3 (Swanson *et al.*, 2013). As Ki-67 is required for heterochromatin compaction, its degradation may be involved in the heterochromatin decompaction occurring upon senescence onset. Heterochromatin reorganisation caused by Ki-67 downregulation does not interfere with cell cycle progression or cell proliferation, but likely contributes to remodelling of gene expression. Heterochromatin is also less compact in highly proliferative pluripotent stem cells, suggesting that heterochromatin organisation is critical for determining transcriptional responses (Fussner *et al.*, 2011). Ki-67 overexpression, which led to pronounced chromatin condensation, appeared to arrest the cell cycle in G1, implying that controlled Ki-67 degradation is required to allow unperturbed progression through the cell cycle.

The nucleolus is a potent cancer biomarker (Derenzini *et al.*, 2009), and a recently demonstrated target in cancer therapy. Inhibitors of nucleolar functions have indeed been shown to selectively kill cancer cells, leaving non-cancerous cells intact (Bywater *et al.*, 2012; Peltonen *et al.*, 2014). It is therefore critical to understand how the nucleolus forms during mitosis. An important step in nucleolar assembly is the formation of a sheath of nucleolar proteins around the chromosome surface on the metaphase plate. This so-called perichromosomal layer has been suggested to play roles in chromosome protection, in the faithful partitioning of nucleolar proteins between daughter cells, and in the segregation of opportunistic passenger proteins. Whether the PR performs any of these functions or has other, unidentified, roles will be a promising field for future studies. In this study, we have identified Ki-67 as one of the first *trans*-acting factors involved in PR formation during nucleologenesis, corroborating a recent report (Booth *et al.*, 2014).

In conclusion, our data reveal a novel concept whereby heterochromatin organisation is linked to cell proliferation by Ki-67. As heterochromatin organisation is often compromised in cancer cells (Carone and Lawrence, 2013) and Ki-67 expression is widely used in clinical assessments in cancer, these data provide a rationale for further investigation of the functional consequences of Ki-67 expression in tumour samples. Importantly, our data suggest that Ki-67 is likely to modulate transcription in cancer cells.

Materials and methods

Ethics

All animal experiments were performed in accordance with international ethics standards and were subjected to approval by the Animal Experimentation Ethics Committee of Languedoc Roussillon.

Cell lines

Normal human diploid foreskin fibroblasts (HDF) were provided by Jacques Piette (CRBM, Montpellier), the *hTERT*-immortalized foreskin fibroblast cell line (BJ hTERT) was provided by Jean Marc Lemaitre (IRB, Montpellier). U2OS, HeLa, NIH3T3 mouse fibroblasts were obtained from the American Type Culture Collection. They were not authenticated but were mycoplasma-free (tested weekly). U2OS, HeLa and NIH 3T3 were grown in Dulbecco modified Eagle medium (DMEM - high glucose, pyruvate, GlutaMAX – LifeTechnologies, ThermoFisher Scientific, Paris, France) supplemented with 10% foetal bovine serum (Sigma-Aldrich, Lyon, France or HyClone, GE Healthcare, Paris, France). BJ hTERT were grown in DMEM supplemented with 10% foetal calf serum (Sigma-Aldrich) and 2 mM L-glutamine. Apart from murine embryo fibroblasts (MEFs), cells were grown under standard conditions at 37°C in a humidified incubator containing 5% CO₂. MEFs were grown

in DMEM supplemented with 10% fetal bovine serum and 1% Penicillin/Streptomycin at 37°C in an incubator containing 3% O₂ and 5% CO₂.

Cell synchronisation

G0 block

HDF, BJ hTERT and NIH-3T3 cell lines at 20% confluency were washed once with PBS and incubated with medium supplemented with 0.1% FBS for 72 hr. Cells were stimulated to enter the cell cycle by adding fresh medium with 10% FBS. Onset of S phase was observed at 16 hr after restimulation by EdU incorporation assay.

Lentiviral infection

The lentiviral constitutive and inducible knockdown systems were packaged into non-replicating lentivirus HIV-1 using II generation packaging system – psPAX by PVM platform (IGF, Montpellier). Immortalized BJ-hTERT and U2OS cells were infected at MOI 10 with lentivirus armed pTRIPZ GAPDH positive CTRL and Ki-67 inducible shRNA, and immortalized BJ hTERT, U2OS and HeLa were infected at MOI 10 with lentivirus armed pGIPZ shRNA non-silencing and Ki-67 constitutive system. Lentiviral transduction was performed according to the manufacturer's protocol (Thermo Scientific). 2 days after infection cells were selected with 10 µg/ml puromycin for 4 days. Cells were treated with progressively increased puromycin concentrations up to 60 µg/ml, to select the most highly transduced population.

shRNAs

The lentiviral constitutive knockdown vectors containing shRNAs were purchased from ThermoFisher Scientific.

1. pGIPZ shRNAmir Ki-67 (clone ID: V2LHS-151787)

AGGCTACAAACTCGTAAGGAAATAGTGAAGCCACAGATGTATTCCTTACGAGTTTGTAGCCG

2. pGIPZ shRNAmir CTRL non-targeting (RHS4346)

ACCTCCACCCTCACTCTGCCATTAGTGAAGCCACAGATGTAATGGCAGAGTGAGGG

TGGAGGG

The lentiviral doxycycline-inducible knockdown positive control vector containing shRNA GAPDH was purchased from Thermo Scientific.

3. pTRIPZ shRNAmir GAPDH

CCCTCATTTCCTGGTATGACAATAGTGAAGCCACAGATGTATTGTCATACCAGGAAATGAGGT

pTRIPZ shRNAmir Ki-67 vector was obtained by sub-cloning to replace the shRNAmir GAPDH in pTripZ with the shRNAmir sequence from pGIPZ shRNAmir Ki-67.

Induction of shRNA expression in cells transduced with inducible pTripZ shRNA

To induce expression of shRNA, cells were treated with 2 µg/ml doxycycline hyclate (Sigma-Aldrich) for minimum 24 hr and then during the period of designed experiments. Downregulation of mRNA of shRNA target genes was analysed 24 hr post induction.

siRNA transfection

The SMARTpool: ON-TARGETplus siRNAs were purchased from GE Dharmacon (Lafayette, CO, USA). Cells were transfected with SMARTpool: ON-TARGETplus siRNA non-targeting (D-001810-10), MKI67 (L-003280-00) and FZR1 (L-015377-00) at 100 nM by Calcium Phosphate transfection method.

Calcium phosphate transfection

Materials

2.5 M CaCl₂, 2x HBSS buffer (50 mM HEPES, 280 mM NaCl, 1.5 mM Na₂HPO₄, 10 mM KCl; pH 7,04), sterile H₂O.

Cells were plated at density of 1.5x10⁴/cm² in the afternoon the day before transfection. 30 min before transfection, growing medium with antibiotics were exchanged for 2 ml of growing medium without antibiotics, if cells were plated on 21 cm². Calcium phosphate–DNA coprecipitate were

prepared by pipetting 112.5 μL sterile H_2O , 12.5 μL of 2.5 M CaCl_2 and 2 μL of 100 μM siRNA (final concentration - 100 nM in medium above cells), without vortexing. CaCl_2 -siRNA solution were combined with equal volume of 2xHBSS buffer. Coprecipitates were incubated at room temperature for 5 min, mixed by pipetting, added drop by drop into medium above cells and distributed by moving back and forward.

Cell extracts and western-blotting

Frozen pellets (harvested by trypsinization, washed with cold PBS) were lysed directly in Laemmli buffer at 95°C (without β -mercaptoethanol and bromophenol blue) and sonicated in a chilled bath for 10 min in 30 s/30 s ON/OFF intervals. Protein concentrations were determined by BCA protein assay (ThermoFisher). Equivalently loaded proteins were separated by SDS-polyacrylamide gel electrophoresis (SDS-PAGE) (usually on 12 cm x 14.5 cm 7.5% and 12.5% gels) at 35 mA in TGS buffer (25 mM Tris, 200 mM glycine, 0.1% SDS). The proteins were then transferred to Immobilon membranes (Milipore) at 1.15 mA/cm² for 120 min with a semidry blotting apparatus containing transfer buffer (25 mM Tris, 200 mM Glycine, 0.2% SDS, 20% EtOH). Membranes were blocked in TBST pH 7.6 (20 mM Tris, 140 mM NaCl, 0.1% Tween-20) containing non-fat dry milk (5%), incubated with antibody for 2 hr at RT with agitation in TBST containing non-fat dry milk (1.25%), washed several times with TBST for a total of 45 min, incubated with secondary antibody at 1/5000 dilution in TBST containing non-fat dry milk (1.25%) for 1 hr at RT with agitation and washed several times for 1 hr in TBST. Secondary antibodies were either goat antibodies to mouse IgG-HRP (immunoglobulin G – horseradish peroxidase) (DACO) or donkey antibodies to rabbit IgG-HRP (immunoglobulin G – horseradish peroxidase) (GE Healthcare). The detection system used was Western Lightning Plus-ECL (PerkinElmer, Paris, France) and Amersham Hyperfilm (GE Healthcare).

FLIM-FRET measurements

FLIM-FRET experiments were carried out on a HeLa^{H2B-2FPs} cell line stably expressing GFP and mCherry tagged histone H2B as previously described (Lières *et al.*, 2009). Fluorescence Lifetime Imaging Microscopy (FLIM) was performed using an inverted laser scanning multiphoton microscope LSM780 (Zeiss) equipped with temperature-controlled environmental black walls chamber. Measurements were acquired at 37°C, with a 63 \times oil immersion lens NA 1.4 Plan-Apochromat objective from Zeiss. Two-photon excitation was achieved using a Chameleon Ultra II tunable (680–1080 nm) laser (Coherent) to pump a mode-locked frequency-doubled Ti:Sapphire laser that provided sub-150-femtosecond pulses at a 80-Mhz repetition rate with an output power of 3.3 W at the peak of the tuning curve (800 nm). Enhanced detection of the emitted photons was afforded by the use of the HPM-100 module (Hamamatsu R10467-40 GaAsP hybrid PMT tube). The fluorescence lifetime imaging capability was provided by TCSPC electronics (SPC- 830; Becker & Hickl GmbH). TCSPC measures the time elapsed between laser pulses and the fluorescence photons. EGFP and mCherry fluorophores were used as a FRET pair. The optimal two-photon excitation wavelength to excite the donor (EGFP) was determined to be 890 nm (Lières *et al.*, 2007). Laser power was adjusted to give a mean photon count rate of the order 4.10⁴–10⁵ photons/s. For imaging live cells by FLIM, the standard growth medium was replaced with phenol red-free DMEM supplemented with 10% FBS. Fluorescence lifetime measurements were acquired over 90 s and fluorescence lifetimes were calculated for all pixels in the field of view (256 \times 256 pixels) and then a particular region of interest (e.g., nucleus) was selected using SPCImage software (Becker & Hickl, GmbH).

Analysis of the fluorescence lifetime measurements for FRET experiments

The analysis of the FLIM measurements was performed by using SPCImage software. Because FRET interactions cause a decrease in the fluorescence lifetime of the donor molecules (EGFP), the FRET efficiency can be calculated by comparing the FLIM values obtained for the EGFP donor fluorophores in the presence and absence of the mCherry acceptor fluorophores. Mean FRET efficiency images were calculated such as the FRET efficiency, $E_{\text{FRET}} = 1 - (\tau_{\text{DA}}/\tau_{\text{D}})$, where τ_{DA} is the mean fluorescence lifetime of the donor (H2B-EGFP) in the presence of the acceptor (mCherry-H2B) expressed in the HeLa^{H2B-2FPs} and τ_{D} is the mean fluorescence lifetime of the donor (H2B-EGFP) expressed in HeLa^{H2B-GFP} in the absence of acceptor. In the non-FRET conditions, the mean

fluorescence lifetime value of the donor in the absence of the acceptor was calculated from a mean of the τ_D by applying an exponential decay model to fit the fluorescence lifetime decays.

In the FRET conditions, we applied a biexponential fluorescence decay model to fit the experimental decay curves $f(t) = a e^{-t/\tau_{DA}} + b e^{-t/\tau_D}$. By fixing the noninteracting proteins lifetime t_D using data from control experiments (in the absence of FRET), the value of t_{DA} was estimated. Then, the FRET efficiency (E_{FRET}) was derived by applying the following equation: $E_{\text{FRET}} = 1 - (\tau_{DA}/\tau_D)$ at each pixel in a selected ROI using SPCLImage software. The FRET distribution curves from these ROIs were displayed from the extracted associated matrix using SPCLImage and then normalized and graphically represented using Excel and GraphPad Prism software.

Immunofluorescence

Cells were seeded on 12 mm diameter coverslips #1.5 coated with 1% gelatine. Before fixation coverslips were washed once with PBS. Then, cells were fixed either in 3.7% formaldehyde for 15 min at RT or in cold 100% MeOH (10 min, -20°C). Formaldehyde fixed cells were immediately washed twice with PBS and permeabilized in 0.2% TRITON X-100 for 15 min at RT, while MeOH fixed cells on coverslips were transferred on tissue paper and kept at RT to dry. Next, cells were blocked in blocking solution (5% FBS; 0.1% Tween-20 in PBS) for 30 min at RT, incubated overnight with primary antibodies diluted in blocking solution at 4°C , washed 3 times 5 min with PBS-Tween (0.1% Tween-20 in PBS), incubated with secondary antibody at RT for 1 hr, and washed 4 times 5 min with PBS-Tween. Secondary antibodies were diluted 1:1000 for fluorophores Alexa488; 555; 568 and 1:500 for fluorophore Alexa647. Coverslips were washed in distilled water prior mounting on slide with ProLong Gold Antifade Reagent with DAPI.

Nucleolar imaging

HeLa or U2OS cell lines were cultured in 96-well plates. For siRNA-mediated Ki-67 depletion, a transfection reagent (mix of 0.125 μl of Interferin and 20 μl of Optimem) was added to each well of the plate and left for 10 min at RT°. SiRNA (10 μl of 100 nM) were added and left for another 30 min at RT°. Cells (70 μl of 300,000 cells/ml dilution) were then added to each well and the plates were incubated for 3 days at 37°C with 5% CO₂. Nucleolar structure disruption was performed by treatment of the cells with 0.2 $\mu\text{g/ml}$ of Actinomycin D, 40 μM roscovitine or 60 μM DRB for 90 min.

For immunofluorescence, cells were fixed in 2% formaldehyde, washed in PBS and blocked in PBS supplemented with 5% BSA and 0.3% Triton X-100 during 1 hr at RT°. Anti-Pes 1 antibody (1:1,000; courtesy from E. Kremmer), anti-Ki-67 antibody (1:500, Cell Signaling) and/or anti-Fibrillarin antibody (1:250, antibodies online) were diluted in PBS supplemented with 1% BSA, 0.3% Triton X-100 and incubated with the cells O/N at 4°C . Cells were washed in PBS and incubated with the secondary antibody coupled to AlexaFluor 488 or 594 (1:1,000; Invitrogen) in PBS, 1% BSA, 0.3% Triton X-100 for 1 hr at RT°. Cells were washed in PBS and treated with DAPI.

Microscopy was performed on a Zeiss Axio Observer.Z1 microscope driven by MetaMorph (MDS Analytical Technologies, Canada). Images were captured in the confocal mode using a Yokogawa spindisk head and the HQ2 camera with a laser illuminator from Roper (405 nm 100 mW Vortran, 491 nm 50 mW Cobolt Calypso, and 561 nm 50 mW Cobolt Jive) and 40x or 100x objectives (Zeiss). Line scans and images were constructed using Image J. The CellProfiler software was used to quantify the DAPI intensity at the peri-nucleolar region of about 100 individual cells and classical statistical t-test was applied to the data to compare the intensity distributions.

Immunohistochemistry

Freshly dissected small intestines were flushed and fixed for 4 hr in neutral buffered formalin before paraffin embedding. Briefly, 5- μm -thick sections were dewaxed in xylene and rehydrated in graded alcohol baths. Antigen retrieval was performed by boiling slides for 20 min in 10 mM sodium citrate buffer, pH 6.0. Nonspecific binding sites were blocked in blocking buffer (TBS, pH 7.4, 5% dried milk, and 0.5% Triton X-100) for 60 min at RT. Sections were then incubated with primary antibodies diluted in blocking buffer overnight at 4°C . Primary antibodies used were as follows: anti Ki-67 (Ab16667) and anti DCLK1 (Ab31704) were from Abcam, Cambridge, UK. Anti beta-catenin (BD610154) was from BD-Bioscience, Oxford, UK. Anti BrdU (G3G4) was from the Developmental Studies Hybridoma Bank. Slides were then washed two times with 0.1% PBS-Tween (Sigma-Aldrich)

before incubation with fluorescent secondary antibodies conjugated with either Alexa 488, Cyanin-3, or Cyanin-5 (Jackson ImmunoResearch Laboratories, Inc.) and Hoechst at 2 $\mu\text{g}/\text{ml}$ (Sigma-Aldrich) in PBS–Triton X-100 0.1% (Sigma-Aldrich). Stained slides were then washed two extra times in PBS before mounting with Fluoromount (Sigma-Aldrich). Methods used for bright-field immunohistochemistry were identical, except that slides were incubated with 1.5% H_2O_2 in methanol for 20 min and washed in PBS to quench endogenous peroxidase activity before antigen retrieval. Envision+ (Dako) was used as a secondary reagent. Signals were developed with DAB (Sigma-Aldrich) and a hematoxylin counterstain (DiaPath) was used. After dehydration, sections were mounted in Pertex (Histolab). Goblet cells staining was achieved with a periodic acid/Schiff's reaction (Sigma-Aldrich)."

FISH

FISH of major satellite DNA in combination with immunofluorescence was performed in formaldehyde fixed cells, as in (Saksouk *et al.*, 2014).

Table of antibodies used in western blotting and immunofluorescence

Protein	Clone	WB dilution	IF dilution	Company	Reference
human Ki-67	SP6	1/300	1/300	Abcam	ab16667
human Ki-67	35/Ki-67	1/200	1/200	BD Transduction Laboratories	610968
mouse Ki-67	SolA15	1/300	1/300	Ebioscience	14-5698-80
human pRB	G3-245	1/300	x	BD Pharmingen	554136
human cyclin A	6E6	1/250	1/100	Novocastra	NCL-CYCLIN A
cyclin A	H-432	1/500	1/300	Santa Cruz Biotechnology	sc-751
phospho-Histone H3 (Ser 10)		1/500		Cell signaling	9701
trimethyl-Histone H3 (Lys 9)		x	1/500	Milipore	07-442
trimethyl-Histone H4 (Lys 20)		x	1/500	Abcam	ab9053
HP1 α	15.19s2	x	1/500	Milipore	05-689
HP1 β		x	1/200	Abcam	ab10478
HP1 γ	2MOD-1G6			Active motif	39981
nucleolin	4E2	x	1/500	Abcam	ab13541
CENP-A		x	1/400	Cell signaling	2186
Pes1		1/1000		Gift from E. Kremmer	
Fibrillarin		1/250		Antibodies online	

Nuclear extract preparation

Materials

Buffer A (10 mM HEPES pH 7.9; 10 mM KCl; 0.1 mM EDTA; 0.1 mM EGTA + freshly added 0.2 mM Na_3VO_4 ; 20 μM MG132; 1 mM DTT; Complete-Protease inhibitor cocktail); IGEPAL CA-630 (Sigma-Aldrich); Buffer C (20 mM HEPES pH 7.9; 1 mM EDTA; 1 mM EGTA; 400 mM NaCl; 25% glycerol + freshly added 0.2 mM Na_3VO_4 ; 20 μM MG132; 1 mM DTT; Complete-Protease inhibitor cocktail).

10^7 cells were harvested by trypsinization, washed once with cold PBS, pelleted by centrifugation and resuspended in 200 μL chilled buffer A. Then, cells were incubated on ice for 5 min. 10% IGEPAL CA-630 was added to each lysate (to a final concentration of 0.2%) and the samples were vortexed for 15 s prior to incubation on ice for 15 min. The lysates were pelleted by centrifugation at 13,000 x

g for 30 s at 4°C, supernatants were kept as a cytoplasmic fraction. Residual pellets were resuspended in 300 µL of ice-cold buffer C prior to incubation for 1 hr at 4°C with rotation. Next, the lysates were vortexed for 30 s and centrifuged for 10 min at high speed at 4°C. Supernatant were collected as a nuclear extract and stored at -80°C. Protein concentration were determined by Bradford assay (Sigma-Aldrich).

Ki-67 mRNA engagement in polysome fractions

Cells were pre-treated 5 min with 20 µg/mL of emetine, before being collected, washed and resuspended in ice cold homogenization buffer (50 mM Tris-HCl pH7.5, 5 mM MgCl₂, 25 mM KCl, 0.2M Sucrose, 0.5% NP-40, EDTA-free protease inhibitors (Roche), 10 U/ML RNAse Out (Invitrogen), DEPC water). We then lysed cells using Lysing Matrix D beads and FastPrep sample preparation system (MP Bio). The cleared lysate was layered on 15–50% sucrose gradient in the same buffer (homogenization buffer minus NP-40). Following centrifugation at 35,000 rpm (Beckman, SW41.Ti) for 2.5 hr at 4°C, gradients were fractionated (density gradient fractionator, Teledyne Isco) with absorbance measured continuously at 254 nm. We isolated RNA from fractions with TRIzol (Thermo Fisher Scientific) following the manufacturer's instructions. We then reverse transcribed purified RNA into cDNA following RT-PCR method. We analysed Ki-67 mRNA level in polysome fractions using two *Mki67* primer pairs (5'-AATCCAACCTCAAGTAAACGGGG-3', 5'-TTGGCTTGCTCCATCCTCA-3' and 5'-CATCAGCCCATGATTTTGCAAC-3', 5'-CTGCGAAGAGAGCATCCATC-3') normalizing to housekeeping genes (*Gapdh*: 5'-AAATGGTGAAGGTGGTGTG-3', 5'-AATCTCCACTTTGCCAC TGC-3'; *B2m*: 5'-GGTCTTTCTGGTGCTTGTCT-3', 5'-GCAGTTCAGTATGTTCCGGCTT-3'; *Actb*: 5'-TCCTGGCCTCACTGTCCAC-3', 5'-GTCCGCCTAGAAGCACTTGC-3'; *Hprt*: 5'-AAGCCTAAGA TGAGCGCAAG-3', 5'-TTACTAGGCAGATGGCCACA-3').

Cloning of cDNA of full-length Ki-67 tagged with GFP and 3xFLAG

Materials

SuperScript II Reverse Transcriptase (ThermoFisher), Pfu DNA Polymerase (Promega, Lyon, France), pGEM-T Easy Vector (Promega), Gateway pENTR Vector (LifeTechnologies), KpnI (NEB), AlflI (NEB), Ligase T4 (Promega).

Table of primers

Name	Sequence
BamHI-AF	AAGGATCCGCCGCCACCATGTGGCCACGAGACGCCTG
AR	GGCCACGTGCCGTGTCTTTCA
BF	AAGGAGCAACCGCAGTT
BR	TGTGTCCATAGCTTCCCTAC
CF	GATAAAGGCATCAACGTGTTC
CR	GGAGTTTATGAAGCCGATTC

Total RNA purified from exponentially growing HeLa cells was used as a template in reverse transcription reaction using SuperScript II Reverse Transcriptase (ThermoFisher) with primers AR, BR and CR to synthesize cDNA template. Full length Ki-67 cDNA was obtained by cloning into pGEM-T vector of three overlapping parts amplified using Pfu DNA Polymerase and primers pairs BamHI-AF/AR, BF/BR and CF/CR. Three parts of full length cDNA were joined together by digestion and ligation reactions. Parts B and C were digested with KpnI enzyme and ligated together. Parts A and BC were digested with AlflI and ligated together. Full length cDNA were cloned into Gateway pENTR Vector containing KOZAK sequence by digesting with BamHI introduced site in 5' site and with SacII in 3' site. Next, KOZAK-Ki-67 cDNA were transferred into Gateway pDEST vector (pcDNA5/GFP/3xFLAG/FRT) to tagged Ki-67 construct with GFP and 3xFLAG sequence at 5' site.

Immunoprecipitation of 3xFLAG Ki-67

1.5×10^7 U2OS cells were transfected with pcDNA5 plasmid expressing 3xFLAG-Ki-67.

As a control, an equal number of cells were transfected with pcDNA3 plasmid expressing 3xFLAG-TRIM39 or 3xFLAG. 24 hr after transfection, cells were harvested and the nuclear extracts prepared. 100 μ g of nuclear protein extract were combined with 40 μ l anti-FLAG M2- agarose beads (Sigma-Aldrich), and incubated for 1 hr at 4°C with rotation. Beads were washed 5 times for 5 min at 4°C with rotation with washing buffer (20 mM HEPES pH 7.9; 1 mM EDTA; 1 mM EGTA; 150 mM NaCl; 25% glycerol + freshly added 0.2 mM Na_3VO_4 ; Complete-Protease inhibitor cocktail) and the precipitates were eluted by 50 μ L of SDS denaturation buffer, and heating at 95°C for 5 min.

Mass spectrometry analysis

Eluted proteins were reduced, alkylated, analysed in a 4–20% gradient gel (BioRad) and entire lanes were sliced. Tryptic peptides were prepared for mass spectrometry, essentially as described, and then concentrated with a pre-column (Thermo Scientific, C18 PepMap100, 300 μ m \times 5 mm, 5 μ m, 100 A) at a flow rate of 20 μ L/min using 0.1% formic acid. Samples were separated with a C18 reversed-phase capillary column (Thermo Scientific, C18 PepMap100, 75 μ m \times 250 mm, 3 μ m, 100 A) at a flow rate of 0.3 μ L/min using the following gradient: 8–28% acetonitrile in 40 min and then from 28–42% in 10 min. The HPLC system was coupled online to a Q-TOF Maxis Impact (Bruker Daltonik GmbH, Bremen, Germany) mass spectrometer. Up to 30 data-dependent MS/MS spectra were acquired in positive ion mode. MS/MS raw data were analysed using Data Analysis software (Bruker Daltonik GmbH, Bremen, Germany) to generate the peak lists. The Homo sapiens Complete Proteome database (downloaded on Uniprotkb 20131108, contains 88,266 sequences) was queried locally using the Mascot search engine v.2.2.07 (Matrix Science, <http://www.matrixscience.com>) and with the following parameters: 2 missed cleavages, carbamidomethylation of Cysteine as fixed modification and oxidation of Methionine, phosphorylation of Threonine and Serine as variable modifications. MS tolerance was set to 20ppm for parent ions and 0.05 Da for fragment ions.

For SILAC, samples were prepared as described (*Skorupa et al., 2013*). Peptides were analysed online by nano-flow HPLC–nanoelectrospray ionization using an Q Exactive mass spectrometer (Thermo Fisher Scientific) coupled to an Ultimate 3000 RSLC (Dionex, Thermo Fisher Scientific). Desalting and pre-concentration of samples were performed on-line on a Pepmap pre-column (0.3 mm \times 10 mm, Dionex). A gradient consisting of 0–40% B in A for 60 min, followed by 80% B/20% A for 15 min (A = 0.1% formic acid, 2% acetonitrile in water; B = 0.1% formic acid in acetonitrile) at 300 nL/min was used to elute peptides from the capillary reverse-phase column (0.075 mm \times 150 mm, Pepmap, Dionex).

Raw data analysis was performed using the MaxQuant software (v. 1.5.0.0) (*Cox and Mann, 2008*) using standard parameters except Requantity option set as TRUE or FALSE. Peak lists were searched against the UniProt Mouse database (release 2015_11; <http://www.uniprot.org>), 255 frequently observed contaminants as well as reversed sequences of all entries.

Graphical representations were generated using perseus (1.5.3.2).

RT-PCR

Materials

10 mM dNTPs (LifeTechnologies), 50 μ M random hexaprimers (NEB, Evry, France), SuperScript II Reverse Transcriptase (ThermoFisher), RNasin Plus RNase Inhibitor (Promega).

1000 ng of purified RNA in total volume of 10 μ L, extracted by RNeasy Mini Kit (Qiagen, Paris, France), were mixed with 1 μ L of 10 mM dNTPs (2.5 mM of each) and 1 μ L of 50 μ M random hexaprimers (New England Biolabs). Samples were incubated at 65°C for 5 min, then immediately transferred on ice. Next, into samples were added 5 μ L of 5xFirst Strand Buffer, 2 μ L 100 mM DTT and 1 μ L RNasin RNase Inhibitor. Samples were incubated at 25°C for 10 min and at 42°C for 2 min. 1 μ L of SuperScript II Reverse Transcriptase was added to each sample, prior to incubation at 42°C for 60 min, 70°C for 15 min.

qPCR

qPCR was performed using LightCycler 480 SYBR Green I Master (Roche, Grenoble, France) and LightCycler 480 qPCR machine. The reaction contained 5 ng of cDNA, 2 μ L of 1 μ M qPCR primer

pair (final concentration of each primer was 200 nM in reaction mixture), 5 μ L 2x Master Mix, and final volume made up to 10 μ L with DNase free water. qPCR was conducted at 95°C for 10 min, and then 40 cycles of 95°C for 20 s, 58°C for 20 s and 72°C for 20 s. The specificity of the reaction was verified by melt curve analysis. Each sample was performed in three replicates.

Table of qPCR primers (Tm - 60°C)

Target	Forward	Reverse
human <i>MKI67</i> Qiagen	Qiagen QuantiTect Hs_MKI67_1_SG	
human <i>MKI67</i>	TGACCCTGATGAGAAAGCTCAA	CCCTGAGCAACACTGTCTTTT
human <i>CCNA2</i>	AGGAAAATTCAGCTTGTGGG	CACAACTCTGCTACTTCTGGG
human <i>CCNE1</i>	CCGGTATATGGCGACACAAG	ACATACGCAAACCTGGTGCAA
human <i>CCNB1</i>	TGTGTCAGGCTTTCTCTGATG	TTGGTCTGACTGCTTGTCTCT
human <i>CDC6</i>	TTGCTCAGGAGATTTGTCAGG	GCTGTCCAGTTGATCCATCTC
human <i>FZR1</i>	TCTCAGTGAAGGGGACTCA	CAACATGGACAGCTTCTTCCC
human <i>B2M</i> (norm)	GCGCTACTCTCTCTTTCTGG	AGAAAGACCAGTCCCTTGCTGA
human <i>RPL19</i> (norm)	ATGCCGGAAAAACACCTTGG	GTGACCTTCTCTGGCATTCCG
mouse <i>Mki67</i>	AATCCAACCTCAAGTAAACGGGG	TTGGCTTGTCTCCATCCTCA
mouse <i>B2M</i> (norm.)	GGTCTTTCTGGTCTTGTCT	GCAGTTCAGTATGTTCCGGCTT

RNA electrophoresis

For analysis of high-molecular-weight species, 5 μ g of total RNA were resolved on agarose denaturing gels (6% formaldehyde/1.2% agarose in HEPES-EDTA buffer). For the analysis of the low-molecular-weight RNA species 5 μ g of total RNA were separated on denaturing acrylamide gels (8% acrylamide-bisacrylamide 19:1/8 M urea in Tris-borate-EDTA buffer [TBE]) for 4 hr at 350 V.

Northern blotting

Agarose gels were transferred by capillarity overnight in 10 \times saline sodium citrate (SSC) and acrylamide gels by electrotransfer in 0.5 \times TBE on nylon membranes (GE Healthcare). Membranes were prehybridized for 1 hr at 65°C in 50% formamide, 5 \times SSPE, 5 \times Denhardt's solution, 1% w/v SDS, 200 μ g/ml fish sperm DNA solution (Roche). The 32P-labeled oligonucleotide probe was added and incubated for 1 hr at 65°C and then overnight at 37°C.

Sequences of the probes

Oligo probe name	Sequence
LD1827 (ITS1)	CCTCGCCCTCCGGGCTCCGGGCTCCGTTAATGATC
LD1828 (ITS2)	CTGCGAGGGAACCCCCAGCCGCGCA
LD1829	GCGCGACGGCGGACGACACCGCGGCGTC
LD1844 (5'-ETS)	CGGAGGCCCAACCTCTCCGACGACAGGTCGCCAGAGGACAGCGTGTGACG
LD2079 (5'-ITS2)	GGGGCGATTGATCGGCAAGCGACGCTC
LD2132 (5.8S mat)	CAATGTGTCTGCAATTCAC
LD2133 (7SL)	GCTCCGTTTCCGACCTGGGCC
LD2655	GGAGCGGAGTCCGCGGTG

TALEN-mediated Ki-67 mutant mice

Plasmids encoding two TALEN pairs were purchased from Collectis (Paris, France). They were designed to bind the following sequence of *Mki67* gene: 5' TCCCGACGGCCGGGCGG ACCATGGCGTCCTC GGCTCACCTGGTCACCA 3'. Underlined sequences are recognised by the left or the right TALEN, respectively. Plasmids were linearized by *PacI* digestion and used as a template for *in vitro* transcription to produce TALEN-encoding mRNAs using T7 RiboMAX Express System (Promega). Transcripts were purified using MEGAclear Transcription Clean-Up Kit (Ambion, Thermo-Fisher). Quality and quantity of transcribed mRNAs were verified by BioAnalyzer (Agilent, Paris, France). Next, 32 ng or 8 ng of each TALEN-encoding mRNAs were injected into zygotes and implanted into 36 or 18 mice, respectively. 7 chimeric mutant mice were obtained with deletions ranging between 1nt and 38 nt by injection of 32 ng of each mRNAs (22% NHEJ) and 1 chimeric mouse with deletion of 24 nt by injection of 8 ng of each mRNAs. Founder mice were crossed and we obtained four mice for germline transmission (1nt, 2nt, 3nt, 24nt deletion).

Genotyping of TALEN-mediated Ki-67 mutant mice

Genomic DNA was purified from mouse-tail piece using KAPA Express Extract Kit (Kapa Biosystems, London, UK). PCR was conducted using the primers 5'GGCCAGAGCTAACTTGCGCTGACTG 3' and 5'AAACAGGCAGGAGCTGAGGCTCAGC 3' and Pfu DNA Polymerase (Promega). Product size 203 bp. Then, PCR product was cleaned up using ExoSAP-IT (Affymetrix, High Wycombe, UK) and sequenced using 5'GGCCAGAGCTAACTTGCGCTGACTG 3' primer.

Histology of TALEN-mediated Ki-67 mutant mice

Genotyped mice pups were fixed in 4% paraformaldehyde for 48 hr and formol 10% 3 days prior to after longitudinal section in 2 parts. Embryos were decalcified in EDTA 10% - Formol 2,5% before paraffin embedding. Tissue was dehydrated through a series of graded ethanol baths and then infiltrated with wax. Infiltrated tissues were then embedded into wax blocks. From these blocks, 5- μ m-thick sections were cut and then stained with hematoxylin.

MEF isolation

MEF were isolated from E13.5 embryos of the corresponding genotype. The female was killed by cervical dislocation. The uterine horns were dissected and placed into a petri dish containing PBS. Each embryo was separated from its placenta and surrounding membranes. The brain, all dark red organs and the intestine were cut away and blood was removed as much as possible. The remaining parts of the embryo were transferred into a dish containing 1 ml of 1x Trypsin-EDTA 0.25%. They were finely minced with a razor blade and incubated at 37°C for 1 hr in a 5% CO₂ incubator. Trypsin was inactivated with 4 ml of DMEM supplemented with 10% fetal bovine serum and 1% Penicillin/Streptomycin and the carcass was homogenized by several passages up and down using a pipet. Finally, 6 ml of DMEM media were added and cells were incubated at 37°C in an incubator containing 3% O₂ and 5% CO₂.

Immunohistochemistry

Mouse intestinal epithelium was processed for immunohistochemistry as described (*Gerbe et al., 2011*). *Cdh1* knockout mice were analysed by immunohistochemistry as described (*Eguren et al., 2013*).

Single TALEN-mediated Ki-67 KO in NIH-3T3 mouse fibroblasts

NIH-3T3 cells were plated at a density of 3x10⁴/cm² in the afternoon the day before transfection. Cells were transfected with plasmids encoding: TALEN pair targeted to initial ATG described in section TALEN-mediated Ki-67 KO mouse and pEGFP, or pEGFP by itself. Next day, eGFP positive cells were sorted by FACS (BD FACSAria) and around 240 cells from each condition were plated in five 96-well plates (480 wells). Two weeks later, we obtained around 50 clones from each condition. Then, TALEN-mediated mutants were screened for Ki-67 expression by immunofluorescence. Nine selected clones were then screened by PCR and sequencing.

Sequencing and PCR analysis of single TALEN Ki-67 mutant NIH-3T3 cell lines

Genomic DNA were purified from harvested cells using KAPA Express Extract Kit (Kapa Biosystems). PCR product was amplified using the primers 5' AGAGCTAACTTGCGCTGACT 3' and 5' TCGCGTC TACCGAGTGTA AAA 3' and Pfu DNA Polymerase (Promega). Product size 364 bp. For sequencing one additional amplification cycle was performed using Taq Polymerase to add a 3' dA overhang on the end of PCR fragment. Next, PCR product was ligated with pGEM-T Easy Vector (Promega). Competent bacteria were transformed with ligation reaction and plated on agar plates with ampicillin, IPTG and X-Gal. Next day ten white colonies were selected from each individual ligation reaction to perform plasmid preparation. Purified plasmids were sequenced using T7 and SP6 RNA Polymerase transcription initiation site primers.

Generation of TALEN pair targeted to site of STOP codon of the mouse *MKI67* gene

TALENs were designed using TAL Effector Nucleotide Targeter 2.0 (Cornell University) software to bind following sequence of *Mki67* gene: 5' TACCAGAAAAGTGAAACTATGTAGCAAAGACATTTAAGAAGGAAAAGT 3' and assembled using The Golden Gate TALEN kit (AddGene). Underlined sequences are recognised by the left TALEN or the right TALEN, respectively.

Double TALEN-mediated eGFP transgenic Ki-67 mutant

NIH-3T3 cells were plated at density of 3×10^4 /cm² in the afternoon the day before transfection. Cells were transfected with plasmids encoding: TALEN pair targeted to initial ATG described in section TALEN-mediated Ki-67 KO mouse; TALEN pair targeted to site of STOP codon *MKI67* gene; reporter system (Kim et al., 2013) containing STOP codon area as a target sequence; linearized construct containing *Mki67* locus replaced by eGFP gene. Two days after transfection, hygromycin selection was performed by culturing the cells in the presence of 2 mg/ml of hygromycin B for two days at 37°C. For clonal analysis, around 500 hygromycin-selected cells were plated in ten 96-well plates (960 wells). Two weeks after, around 100 clones (10%) were screened by immunofluorescence for Ki-67 expression.

DNA replication assay

Analysis of DNA replication progress in cells was achieved by treatment with 10 μM 5-ethynyl-2'-deoxyuridine (EdU) (ThermoFisher) before fixation. Replicating cells were visualized following the protocol from Click-iT EdU Alexa Fluor 488 Imaging Kit (ThermoFisher).

RNA synthesis assay

Analysis of newly synthesised RNA in cells was achieved by treatment with 2 mM 5-ethynyl uridine (EU) (ThermoFisher) for 20 min before fixation. Replicating cells were visualized following the protocol from Click-iT EU Alexa Fluor 488 Imaging Kit (ThermoFisher).

Flow cytometry

Cell cycle analysis

Cells were harvested, washed once with cold PBS, then, resuspended in 300 μL cold PBS and fixed with 700 μL chilled 100% methanol. Cells were kept at -20°C up to one day of analysis, but at least overnight. On the day of analysis, cells were pelleted by centrifugation at 6000 rpm for 5 min. After washing once with 1% BSA in PBS, cells were stained with Propidium Iodide staining solution (10 μg/ml Propidium Iodide, 1% BSA, 200 μg/ml RNase A in PBS) for 15 min at room temperature and subjected to cell cycle analysis using BD FACS Calibur (BD Biosciences, SanJose, CA).

DNA replication assay - EdU labelling

Cells were harvested, washed once with cold PBS, then, resuspended in 300 μL cold PBS and fixed with 700 μL chilled 100% methanol. Cells were kept at -20°C up to the day of analysis, but at least overnight. On the day of analysis, cells were pelleted by centrifugation at 6000 rpm for 5 min. After washing once with 1% BSA in PBS cells were stained with Click-iT EdU Alexa Fluor 488 Flow

Cytometry Assay Kit (ThermoFisher). The Click-iT™ EdU Flow Cytometry Assay system (Invitrogen) was used following the manufacturer's instructions.

Microarray analysis - transcriptome

RNA was prepared using RNeasy Mini Kit (Qiagen) following the manufacturer's instructions from U2OS shRNA non-targeting CTRL, U2OS shRNA Ki-67, HeLa shRNA non-targeting control CTRL, HeLa shRNA Ki-67 grown 3 months after initial infection with lentivirus armed pGIPZ shRNA. RNA was purified from three shRNA CTRL tumour xenografts or three shRNA Ki-67 tumour xenografts isolated from mouse C1-SM (33 days after injection), C1-OD (41 days after injection) and C2-2OR (46 days after injection) using TRIzol reagent (Life Technologies) following the manufacturer's instructions. Cy3-labelled cRNA was amplified and hybridized on the Agilent SurePrint G3 Human GE 8x60k Microarray according to the procedures by Imaxio company (Lyon, France). Raw data were preprocessed using GeneSpring GX software (Agilent Technologies) to define differently expressing genes and present data by clustered heat-maps.

Statistical analysis of transcriptome

Significant differences between experimental groups were determined using an unpaired two-tailed Student t test in Prism 5 (GraphPad). For all analyses, p values <0,05 (*), p values < 0,01 (**) and p values <0,001 (***) were considered statistically significant. Transcripts that (i) demonstrated at least a 1,5-fold change in expression, (ii) had a greater-than-background signal intensity value and were determined to be 'Present' by Affymetrix algorithms, and (iii) had a value that was significant by Student's t test and FDR (Benjamini Hochberg) correction ($p < 0.02$ (U2OS, HeLa); $p < 0.2$ (Xenografts)) were considered differentially expressed.

Acknowledgements

Many thanks to all members of the Fisher lab for helpful discussions and criticism of the paper, and all technical staff of MRI imaging facility, RHEM histology facility and IGMM mouse facility. Thanks to Daniel Gerlich, Thierry Forné, Chris Lord for helpful discussions and for reading the manuscript.

Additional information

Funding

Funder	Grant reference number	Author
Agence Nationale de la Recherche	ANR-09-BLAN-0252	Nikolaos Parris Daniel Fisher
Ligue Contre le Cancer	EL2013.LNCC/DF	Daniel Fisher
Ligue Contre le Cancer	Graduate student fellowship	Michal Sobecki
Fondation pour la Recherche Médicale	Graduate student fellowship	Michal Sobecki
GEFLUC Languedoc Roussillon	Subvention	Daniel Fisher

The funders had no role in study design, data collection and interpretation, or the decision to submit the work for publication.

Author contributions

MS, NP, Conception and design, Acquisition of data, Analysis and interpretation of data, Drafting or revising the article; KM, SU, Acquisition of data, Analysis and interpretation of data, Drafting or revising the article; AC, EN, DL, FG, AD, Conception and design, Acquisition of data, Analysis and interpretation of data; SP, LK, Acquisition of data, Drafting or revising the article; ME, Acquisition of data, Contributed unpublished essential data or reagents; M-CB, Conception and design, Acquisition of data, Contributed unpublished essential data or reagents; SH, Acquisition of data, Analysis and interpretation of data; JD, PJ, DLJL, DF, Conception and design, Analysis and interpretation of data, Drafting or revising the article; MM, Drafting or revising the article, Contributed unpublished

essential data or reagents; VD, Analysis and interpretation of data, Drafting or revising the article; RF, Conception and design, Drafting or revising the article

Author ORCIDs

Nikolaos Parisi, <http://orcid.org/0000-0002-5706-0122>

Manuel Eguren, <http://orcid.org/0000-0003-0850-939X>

Marcos Malumbres, <http://orcid.org/0000-0002-0829-6315>

Robert Feil, <http://orcid.org/0000-0002-5671-5860>

Daniel Fisher, <http://orcid.org/0000-0002-0822-3482>

Ethics

Animal experimentation: All animal experiments were performed in accordance with international ethics standards and were subjected to approval by the Animal Experimentation Ethics Committee of Languedoc Roussillon and the Ministry for Higher Education and Research

References

- Blethrow JD**, Glavy JS, Morgan DO, Shokat KM. 2008. Covalent capture of kinase-specific phosphopeptides reveals Cdk1-cyclin B substrates. *Proceedings of the National Academy of Sciences of the United States of America* **105**:1442–1447. doi: [10.1073/pnas.0708966105](https://doi.org/10.1073/pnas.0708966105)
- Booth DG**, Takagi M, Sanchez-Pulido L, Petfalski E, Vargiu G, Samejima K, Imamoto N, Ponting CP, Tollervey D, Earnshaw WC, Vagnarelli P. 2014. Ki-67 is a PP1-interacting protein that organises the mitotic chromosome periphery. *eLife* **3**:e01641. doi: [10.7554/eLife.01641](https://doi.org/10.7554/eLife.01641)
- Bostick M**, Kim JK, Estève PO, Clark A, Pradhan S, Jacobsen SE. 2007. UHRF1 plays a role in maintaining DNA methylation in mammalian cells. *Science* **317**:1760–1764. doi: [10.1126/science.1147939](https://doi.org/10.1126/science.1147939)
- Bridger JM**, Kill IR, Lichter P. 1998. Association of pKi-67 with satellite DNA of the human genome in early G1 cells. *Chromosome Research* **6**:13–24. doi: [10.1023/A:1009210206855](https://doi.org/10.1023/A:1009210206855)
- Bursac S**, Brdovcak MC, Donati G, Volarevic S. 2014. Activation of the tumor suppressor p53 upon impairment of ribosome biogenesis. *Biochimica Et Biophysica Acta* **1842**:817–830. doi: [10.1016/j.bbadis.2013.08.014](https://doi.org/10.1016/j.bbadis.2013.08.014)
- Bywater MJ**, Poortinga G, Sanij E, Hein N, Peck A, Cullinane C, Wall M, Cluse L, Drygin D, Anderes K, Huser N, Proffitt C, Bliesath J, Haddach M, Schwaebe MK, Ryckman DM, Rice WG, Schmitt C, Lowe SW, Johnstone RW, et al. 2012. Inhibition of RNA polymerase I as a therapeutic strategy to promote cancer-specific activation of p53. *Cancer Cell* **22**:51–65. doi: [10.1016/j.ccr.2012.05.019](https://doi.org/10.1016/j.ccr.2012.05.019)
- Carone DM**, Lawrence JB. 2013. Heterochromatin instability in cancer: from the Barr body to satellites and the nuclear periphery. *Seminars in Cancer Biology* **23**:99–108. doi: [10.1016/j.semcancer.2012.06.008](https://doi.org/10.1016/j.semcancer.2012.06.008)
- Cheutin T**, O'Donohue M-F, Beorchia A, Klein C, Kaplan H, Ploton D. 2003. Three-dimensional Organization of pKi-67: A Comparative Fluorescence and Electron Tomography Study Using Fluoronanogold. *Journal of Histochemistry & Cytochemistry* **51**:1411–1423. doi: [10.1177/002215540305101102](https://doi.org/10.1177/002215540305101102)
- Cox J**, Mann M. 2008. MaxQuant enables high peptide identification rates, individualized p.p.b.-range mass accuracies and proteome-wide protein quantification. *Nature Biotechnology* **26**:1367–1372. doi: [10.1038/nbt.1511](https://doi.org/10.1038/nbt.1511)
- Derenzini M**, Montanaro L, Treré D. 2009. What the nucleolus says to a tumour pathologist. *Histopathology* **54**:753–762. doi: [10.1111/j.1365-2559.2008.03168.x](https://doi.org/10.1111/j.1365-2559.2008.03168.x)
- Eguren M**, Porlan E, Machado E, García-Higuera I, Cañamero M, Fariñas I, Malumbres M. 2013. The APC/C cofactor Cdh1 prevents replicative stress and p53-dependent cell death in neural progenitors. *Nature Communications* **4**:2880. doi: [10.1038/ncomms3880](https://doi.org/10.1038/ncomms3880)
- Endl E**, Gerdes J. 2000a. Posttranslational modifications of the Ki-67 protein coincide with two major checkpoints during mitosis. *Journal of Cellular Physiology* **182**:371–380. doi: [10.1002/\(SICI\)1097-4652\(200003\)182:3<371::AID-JCP8>3.0.CO;2-J](https://doi.org/10.1002/(SICI)1097-4652(200003)182:3<371::AID-JCP8>3.0.CO;2-J)
- Endl E**, Gerdes J. 2000b. The Ki-67 Protein: Fascinating Forms and an Unknown Function. *Experimental Cell Research* **257**:231–237. doi: [10.1006/excr.2000.4888](https://doi.org/10.1006/excr.2000.4888)
- Fussner E**, Djuric U, Strauss M, Hotta A, Perez-Iratxeta C, Lanner F, Dilworth FJ, Ellis J, Bazett-Jones DP. 2011. Constitutive heterochromatin reorganization during somatic cell reprogramming. *The EMBO Journal* **30**:1778–1789. doi: [10.1038/emboj.2011.96](https://doi.org/10.1038/emboj.2011.96)
- Garapaty S**, Xu CF, Trojer P, Mahajan MA, Neubert TA, Samuels HH. 2009. Identification and characterization of a novel nuclear protein complex involved in nuclear hormone receptor-mediated gene regulation. *The Journal of Biological Chemistry* **284**:7542–7552. doi: [10.1074/jbc.M805872200](https://doi.org/10.1074/jbc.M805872200)
- García-Higuera I**, Machado E, Dubus P, Cañamero M, Méndez J, Moreno S, Malumbres M. 2008. Genomic stability and tumour suppression by the APC/C cofactor Cdh1. *Nature Cell Biology* **10**:802–811. doi: [10.1038/ncb1742](https://doi.org/10.1038/ncb1742)

- Garrigues JM**, Sidoli S, Garcia BA, Strome S. 2015. Defining heterochromatin in *C. elegans* through genome-wide analysis of the heterochromatin protein 1 homolog HPL-2. *Genome Research* **25**:76–88. doi: [10.1101/gr.180489.114](https://doi.org/10.1101/gr.180489.114)
- Gerbe F**, van Es JH, Makrini L, Brulin B, Mellitzer G, Robine S, Romagnolo B, Shroyer NF, Bourgaux JF, Pignodel C, Clevers H, Jay P. 2011. Distinct ATOH1 and Neurog3 requirements define tuft cells as a new secretory cell type in the intestinal epithelium. *The Journal of Cell Biology* **192**:767–780. doi: [10.1083/jcb.201010127](https://doi.org/10.1083/jcb.201010127)
- Gerdes J**, Schwab U, Lemke H, Stein H. 1983. Production of a mouse monoclonal antibody reactive with a human nuclear antigen associated with cell proliferation. *International Journal of Cancer* **31**:13–20.
- Gerdes J**, Li L, Schlueter C, Duchrow M, Wohlenberg C, Gerlach C, Stahmer I, Kloth S, Brandt E, Flad HD. 1991. Immunobiochemical and molecular biologic characterization of the cell proliferation-associated nuclear antigen that is defined by monoclonal antibody Ki-67. *The American Journal of Pathology* **138**:867–873.
- Guettg C**, Lienemann P, Sirri V, Grummt I, Hernandez-Verdun D, Hottiger MO, Fussenegger M, Santoro R. 2010. The NoRC complex mediates the heterochromatin formation and stability of silent rRNA genes and centromeric repeats. *The EMBO Journal* **29**:2135–2146. doi: [10.1038/emboj.2010.17](https://doi.org/10.1038/emboj.2010.17)
- Hernandez-Verdun D**, Roussel P, Thiry M, Sirri V, Lafontaine DL. 2010. The nucleolus: structure/function relationship in RNA metabolism. *Wiley Interdisciplinary Reviews. RNA* **1**:415–431. doi: [10.1002/wrna.39](https://doi.org/10.1002/wrna.39)
- Kausch I**, Lingnau A, Endl E, Sellmann K, Deinert I, Ratliff TL, Jocham D, Sczakiel G, Gerdes J, Böhle A. 2003. Antisense treatment against Ki-67 mRNA inhibits proliferation and tumor growth in vitro and in vivo. *International Journal of Cancer* **105**:710–716. doi: [10.1002/ijc.11111](https://doi.org/10.1002/ijc.11111)
- Kill IR**. 1996. Localisation of the Ki-67 antigen within the nucleolus. Evidence for a fibrillar-deficient region of the dense fibrillar component. *Journal of Cell Science* **109**:1253–1263.
- Kim H**, Kim MS, Wee G, Lee CI, Kim H, Kim JS. 2013. Magnetic separation and antibiotics selection enable enrichment of cells with ZFN/TALEN-induced mutations. *PLoS One* **8**:e56476. doi: [10.1371/journal.pone.0056476](https://doi.org/10.1371/journal.pone.0056476)
- Littlepage LE**, Ruderman JV. 2002. Identification of a new APC/C recognition domain, the a box, which is required for the Cdh1-dependent destruction of the kinase Aurora-a during mitotic exit. *Genes & Development* **16**:2274–2285. doi: [10.1101/gad.1007302](https://doi.org/10.1101/gad.1007302)
- Llères D**, Swift S, Lamond AI. 2007. Detecting protein-protein interactions in vivo with FRET using multiphoton fluorescence lifetime imaging microscopy (FLIM). *Current Protocols in Cytometry / Editorial Board, J. Paul Robinson, Managing Editor ... [Et Al.]*. doi: [10.1002/0471142956.cy1210s42](https://doi.org/10.1002/0471142956.cy1210s42)
- Llères D**, James J, Swift S, Norman DG, Lamond AI. 2009. Quantitative analysis of chromatin compaction in living cells using FLIM-FRET. *The Journal of Cell Biology* **187**:481–496. doi: [10.1083/jcb.200907029](https://doi.org/10.1083/jcb.200907029)
- MacCallum DE**, Hall PA. 2000. The biochemical characterization of the DNA binding activity of pKi67. *The Journal of Pathology* **191**:286–298. doi: [10.1002/1096-9896\(2000\)9999:9999::AID-PATH628>3.0.CO;2-J](https://doi.org/10.1002/1096-9896(2000)9999:9999::AID-PATH628>3.0.CO;2-J)
- Narita M**, Nuñez S, Heard E, Narita M, Lin AW, Hearn SA, Spector DL, Hannon GJ, Lowe SW. 2003. Rb-Mediated Heterochromatin Formation and Silencing of E2F Target Genes during Cellular Senescence. *Cell* **113**:703–716. doi: [10.1016/S0092-8674\(03\)00401-X](https://doi.org/10.1016/S0092-8674(03)00401-X)
- Narita M**, Narita M, Krizhanovsky V, Nuñez S, Chicas A, Hearn SA, Myers MP, Lowe SW. 2006. A novel role for high-mobility group proteins in cellular senescence and heterochromatin formation. *Cell* **126**:503–514. doi: [10.1016/j.cell.2006.05.052](https://doi.org/10.1016/j.cell.2006.05.052)
- Németh A**, Conesa A, Santoyo-Lopez J, Medina I, Montaner D, Péterfia B, Solovei I, Cremer T, Dopazo J, Längst G. 2010. Initial genomics of the human nucleolus. *PLoS Genetics* **6**:e1000889. doi: [10.1371/journal.pgen.1000889](https://doi.org/10.1371/journal.pgen.1000889)
- Pasini D**, Bracken AP, Jensen MR, Lazzerini Denchi E, Helin K. 2004. Suz12 is essential for mouse development and for EZH2 histone methyltransferase activity. *The EMBO Journal* **23**:4061–4071. doi: [10.1038/sj.emboj.7600402](https://doi.org/10.1038/sj.emboj.7600402)
- Patel A**, Dharmarajan V, Vought VE, Cosgrove MS. 2009. On the mechanism of multiple lysine methylation by the human mixed lineage leukemia protein-1 (MLL1) core complex. *The Journal of Biological Chemistry* **284**:24242–24256. doi: [10.1074/jbc.M109.014498](https://doi.org/10.1074/jbc.M109.014498)
- Peltonen K**, Colis L, Liu H, Trivedi R, Moubarek MS, Moore HM, Bai B, Rudek MA, Bieberich CJ, Laiho M. 2014. A targeting modality for destruction of RNA polymerase I that possesses anticancer activity. *Cancer Cell* **25**:77–90. doi: [10.1016/j.ccr.2013.12.009](https://doi.org/10.1016/j.ccr.2013.12.009)
- Peters AH**, O'Carroll D, Scherthan H, Mechtler K, Sauer S, Schöfer C, Weipoltshammer K, Pagani M, Lachner M, Kohlmaier A, Opravil S, Doyle M, Sibilia M, Jenuwein T. 2001. Loss of the Suv39h histone methyltransferases impairs mammalian heterochromatin and genome stability. *Cell* **107**:323–337. doi: [10.1016/S0092-8674\(01\)00542-6](https://doi.org/10.1016/S0092-8674(01)00542-6)
- Rahmanzadeh R**, Hüttmann G, Gerdes J, Scholzen T. 2007. Chromophore-assisted light inactivation of pKi-67 leads to inhibition of ribosomal RNA synthesis. *Cell Proliferation* **40**:422–430. doi: [10.1111/j.1365-2184.2007.00433.x](https://doi.org/10.1111/j.1365-2184.2007.00433.x)
- Rohrmoser M**, Hölzel M, Grimm T, Malamoussi A, Harasim T, Orban M, Pfisterer I, Gruber-Eber A, Kremmer E, Eick D. 2007. Interdependence of Pes1, Bop1, and WDR12 controls nucleolar localization and assembly of the PeBoW complex required for maturation of the 60S ribosomal subunit. *Molecular and Cellular Biology* **27**:3682–3694. doi: [10.1128/MCB.00172-07](https://doi.org/10.1128/MCB.00172-07)
- Rottach A**, Frauer C, Pichler G, Bonapace IM, Spada F, Leonhardt H. 2010. The multi-domain protein Np95 connects DNA methylation and histone modification. *Nucleic Acids Research* **38**:1796–1804. doi: [10.1093/nar/gkp1152](https://doi.org/10.1093/nar/gkp1152)

- Saiwaki T**, Kotera I, Sasaki M, Takagi M, Yoneda Y. 2005. In vivo dynamics and kinetics of pKi-67: transition from a mobile to an immobile form at the onset of anaphase. *Experimental Cell Research* **308**:123–134. doi: [10.1016/j.yexcr.2005.04.010](https://doi.org/10.1016/j.yexcr.2005.04.010)
- Saksouk N**, Barth TK, Ziegler-Birling C, Olova N, Nowak A, Rey E, Mateos-Langerak J, Urbach S, Reik W, Torres-Padilla ME, Imhof A, Déjardin J, Simboeck E. 2014. Redundant mechanisms to form silent chromatin at pericentromeric regions rely on BEND3 and DNA methylation. *Molecular Cell* **56**:580–594. doi: [10.1016/j.molcel.2014.10.001](https://doi.org/10.1016/j.molcel.2014.10.001)
- Schindelin J**, Arganda-Carreras I, Frise E, Kaynig V, Longair M, Pietzsch T, Preibisch S, Rueden C, Saalfeld S, Schmid B, Tinevez JY, White DJ, Hartenstein V, Eliceiri K, Tomancak P, Cardona A. 2012. Fiji: an open-source platform for biological-image analysis. *Nature Methods* **9**:676–682. doi: [10.1038/nmeth.2019](https://doi.org/10.1038/nmeth.2019)
- Schlüter C**, Duchrow M, Wohlenberg C, Becker MH, Key G, Flad HD, Gerdes J. 1993. The cell proliferation-associated antigen of antibody Ki-67: a very large, ubiquitous nuclear protein with numerous repeated elements, representing a new kind of cell cycle-maintaining proteins. *The Journal of Cell Biology* **123**:513–522. doi: [10.1083/jcb.123.3.513](https://doi.org/10.1083/jcb.123.3.513)
- Schmidt MH**, Broll R, Bruch HP, Böglér O, Duchrow M. 2003. The proliferation marker pKi-67 organizes the nucleolus during the cell cycle depending on Ran and cyclin B. *The Journal of Pathology* **199**:18–27. doi: [10.1002/path.1221](https://doi.org/10.1002/path.1221)
- Scholzen T**, Endl E, Wohlenberg C, van der Sar S, Cowell IG, Gerdes J, Singh PB. 2002. The Ki-67 protein interacts with members of the heterochromatin protein 1 (HP1) family: a potential role in the regulation of higher-order chromatin structure. *The Journal of Pathology* **196**:135–144. doi: [10.1002/path.1016](https://doi.org/10.1002/path.1016)
- Skorupa A**, Urbach S, Vigy O, King MA, Chaumont-Dubel S, Prehn JH, Marin P. 2013. Angiogenin induces modifications in the astrocyte secretome: relevance to amyotrophic lateral sclerosis. *Journal of Proteomics* **91**:274–285. doi: [10.1016/j.jprot.2013.07.028](https://doi.org/10.1016/j.jprot.2013.07.028)
- Starborg M**, Gell K, Brundell E, Höög C. 1996. The murine Ki-67 cell proliferation antigen accumulates in the nucleolar and heterochromatic regions of interphase cells and at the periphery of the mitotic chromosomes in a process essential for cell cycle progression. *Journal of Cell Science* **109**:143–153.
- Swanson EC**, Manning B, Zhang H, Lawrence JB. 2013. Higher-order unfolding of satellite heterochromatin is a consistent and early event in cell senescence. *The Journal of Cell Biology* **203**:929–942. doi: [10.1083/jcb.201306073](https://doi.org/10.1083/jcb.201306073)
- Tafforeau L**, Zorbas C, Langhendries JL, Mullineux ST, Stamatopoulou V, Mullier R, Wacheul L, Lafontaine DL. 2013. The complexity of human ribosome biogenesis revealed by systematic nucleolar screening of Pre-rRNA processing factors. *Molecular Cell* **51**:539–551. doi: [10.1016/j.molcel.2013.08.011](https://doi.org/10.1016/j.molcel.2013.08.011)
- Takagi M**, Matsuoka Y, Kurihara T, Yoneda Y. 1999. Chmadrin: a novel Ki-67 antigen-related perichromosomal protein possibly implicated in higher order chromatin structure. *Journal of Cell Science* **112**:2463–2472.
- Takagi M**, Sueishi M, Saiwaki T, Kametaka A, Yoneda Y. 2001. A novel nucleolar protein, NIFK, interacts with the forkhead associated domain of Ki-67 antigen in mitosis. *The Journal of Biological Chemistry* **276**:25386–25391. doi: [10.1074/jbc.M102227200](https://doi.org/10.1074/jbc.M102227200)
- Verheijen R**, Kuijpers HJ, van Driel R, Beck JL, van Dierendonck JH, Brakenhoff GJ, Ramaekers FC. 1989a. Ki-67 detects a nuclear matrix-associated proliferation-related antigen. II. Localization in mitotic cells and association with chromosomes. *Journal of Cell Science* **92**:531–540.
- Verheijen R**, Kuijpers HJ, Schlingemann RO, Boehmer AL, van Driel R, Brakenhoff GJ, Ramaekers FC. 1989b. Ki-67 detects a nuclear matrix-associated proliferation-related antigen. I. Intracellular localization during interphase. *Journal of Cell Science* **92**:123–130.
- Zheng JN**, Ma TX, Cao JY, Sun XQ, Chen JC, Li W, Wen RM, Sun YF, Pei DS. 2006. Knockdown of Ki-67 by small interfering RNA leads to inhibition of proliferation and induction of apoptosis in human renal carcinoma cells. *Life Sciences* **78**:724–729. doi: [10.1016/j.lfs.2005.05.064](https://doi.org/10.1016/j.lfs.2005.05.064)
- Zheng JN**, Pei DS, Mao LJ, Liu XY, Mei DD, Zhang BF, Shi Z, Wen RM, Sun XQ. 2009. Inhibition of renal cancer cell growth in vitro and in vivo with oncolytic adenovirus armed short hairpin RNA targeting Ki-67 encoding mRNA. *Cancer Gene Therapy* **16**:20–32. doi: [10.1038/cgt.2008.61](https://doi.org/10.1038/cgt.2008.61)

II. Cell cycle regulation accounts for variability in Ki-67 expression levels

Uncontrolled proliferation represents one of the main characteristics of malignancies. In breast cancer for example, immunohistochemical analysis of the percentage of cancer cells staining for Ki-67 is the most widely used method to measure and monitor tumour proliferation. Although Ki-67 constitutes a valuable tool in tumour diagnostic, substantial heterogeneity and variability in Ki-67 scoring is often observed in cancer samples across laboratories. Indeed, this variability in Ki-67 levels is a clinical problem: inconsistencies in assessments of Ki-67 labelling index hinder its use to stratify patients for therapy. This variability might contribute to inconsistencies regarding the prognostic value of Ki-67 labelling index in a given cancer type, for example triple-negative breast cancer (TNBC). Defining what constitutes Ki-67-positive expression and underlies its regulation is thus critical to understand the clinical significance of different Ki-67 levels.

Previous work by our team suggested that Ki-67 is cell cycle-regulated in both human non-transformed and cancer cells. We sought to investigate whether this regulation might account for all of the apparent variability in Ki-67 expression. We found that, similar to that of the DNA replication protein PCNA, Ki-67 expression is variable in wild-type intestine and intestinal adenomas according to the cell cycle stage as visualised by BrdU incorporation. These results indicated that Ki-67 levels are linked to the cell cycle in mice. To find out whether the same is true in humans, we investigated coregulated gene expression in human cancers, in collaboration with a bio-informatician, Dr. Jacques Colinge. We assessed the proportion of cell cycle genes among genes whose expression correlates with that of Ki-67 in a large colorectal cancer dataset. At a very high correlation coefficient (>0.6), around 80% of genes have a cell cycle annotation. Furthermore, Ki-67 interactome, obtained by combining STRING database interactions and our own Ki-67 protein physical interactions for all genes with correlation >0.5 as mentioned above, revealed that many proteins encoded by these Ki-67 co-regulated genes functionally interact in a cell cycle network. Moreover, correlations with cell cycle genes were maintained across colorectal cancer subtypes, and also in TCGA breast cancer data.

Since Ki-67 was found to be non-essential for cell proliferation (see above), this raised the possibility that Ki-67 could be down-regulated by inhibiting CDK4/6 (which was previously determined by our team to be required for Ki-67 expression) without affecting cell proliferation. We then experimentally tested whether the coupling of Ki-67 expression with cell proliferation would be maintained upon drug treatments, *in vivo*. If, upon CDK4/6 inhibition, Ki-67 continues to identify proliferating cells, then it would be a useful biomarker for palbociclib (PD 0332991) treatment. This would additionally answer the question of whether cell proliferation is abolished upon inhibiting CDK4/6 *in vivo* with palbociclib, a CDK inhibitor recently approved for treatment of certain breast cancers. To do this, we treated mice with palbociclib or vehicle after first engrafting one of two triple-negative breast cancer cell lines, MDA-MB-231, which we determined to be palbociclib sensitive *in vitro*, and MDA-MB-468, which is palbociclib-resistant.

The results showed that CDK4/CDK6 inhibition *in vivo* caused G1 cell cycle arrest and eliminated the expression of Ki-67, Cyclin A and PCNA in RB1-positive tumours (i.e. MDA-MB-231) but had no effect in RB1-negative tumours (i.e. MDA-MB-468), which continued to proliferate and express Ki-67. This revealed that Ki-67 perfectly correlates with cell proliferation responses in all samples. In addition, this cell-cycle regulation of Ki-67 expression was also found in other situations analyzed, including non-transformed human cells and human cancer cell lines with or without drug treatments.

We conclude that cell cycle regulation accounts for Ki-67 variability and that Ki-67 is a good biomarker for palbociclib response in human breast cancer cells *in vivo*, and therefore probably for any drug.

The results describing these findings were published in a paper entitled: “Cell cycle regulation accounts for variability in Ki-67 expression levels” in the journal *Cancer Research* in 2017⁹⁵.

Cell-Cycle Regulation Accounts for Variability in Ki-67 Expression Levels

Michal Sobecki¹, Karim Mrouj¹, Jacques Colinge², François Gerbe³, Philippe Jay³, Liliana Krasinska¹, Vjekoslav Dulic¹, and Daniel Fisher¹



Abstract

The cell proliferation antigen Ki-67 is widely used in cancer histopathology, but estimations of Ki-67 expression levels are inconsistent and understanding of its regulation is limited. Here we show that cell-cycle regulation underlies variable Ki-67 expression in all situations analyzed, including nontransformed human cells, normal mouse intestinal epithelia and adenomas, human cancer cell lines with or without drug treatments, and human breast and colon cancers. In normal cells, Ki-67 was a late marker of cell-cycle entry; Ki-67 mRNA oscillated with highest levels in G₂ while protein levels increased throughout the cell cycle, peaking in mitosis. Inhi-

tion of CDK4/CDK6 revealed proteasome-mediated Ki-67 degradation in G₁. After cell-cycle exit, low-level Ki-67 expression persisted but was undetectable in fully quiescent differentiated cells or senescent cells. CDK4/CDK6 inhibition *in vitro* and in tumors in mice caused G₁ cell-cycle arrest and eliminated Ki-67 mRNA in RB1-positive cells but had no effect in RB1-negative cells, which continued to proliferate and express Ki-67. Thus, Ki-67 expression varies due to cell-cycle regulation, but it remains a reliable readout for effects of CDK4/CDK6 inhibitors on cell proliferation. *Cancer Res*; 77(10): 2722–34. ©2017 AACR.

Introduction

Ki-67 is a nuclear protein expressed in all proliferating vertebrate cells, and it is a widely used biomarker to estimate the proportion of dividing cells to grade tumors. Ki-67 expression might have prognostic value, such as in the IHC4+C score in breast cancer (1). However, inconsistency in assessments of Ki-67 labeling index hinders its use to stratify patients for therapy (2). This variability might contribute to inconsistency regarding the prognostic value of Ki-67 labeling index in a given cancer type, for example, triple-negative breast cancer (TNBC; refs. 3, 4). Therefore, it is critical to define what constitutes Ki-67-positive expression and what the clinical significance of different Ki-67 levels is. This requires a better understanding of the control and functional significance of Ki-67 expression.

In cultured cells, Ki-67 levels are highest in G₂ phase and mitosis (5). In HL60 cells, Ki-67 protein was reported highly

unstable throughout the cell cycle (6), but this has not been confirmed in other cell lines. Furthermore, Ki-67 transcriptional control is poorly understood. The *MKI67* promoter of the gene encoding Ki-67 is GC-rich, contains Sp1-binding sites, but lacks a TATA box (7, 8). In primary fibroblasts, it is bound by E2F proteins (9), and Ki-67 mRNA accumulates upon E2F overexpression (10). E2F-dependent transcription, which is required for S-phase onset, is repressed by RB family proteins, whose phosphorylation by cyclin-dependent kinases (CDK) promotes cell-cycle progression. Although RB expression is lost in many cancers, it is not clear whether this leads to upregulation of Ki-67. It is also not known whether Ki-67 is frequently over- or underexpressed in cancers, for example, due to copy number variation, translational regulation, or mutation of sites affecting protein stability or promoter activity.

We, and others, recently showed that Ki-67 is not required for proliferation of mammalian cells in culture (11–13). Furthermore, mice with a disrupted *Mki67* gene were healthy and fertile, despite minimal Ki-67 expression (11). Conversely, mice lacking the *Fzr1* gene maintained Ki-67 in differentiated, nonproliferating tissues (11). Thus, Ki-67 expression can be uncoupled from, and is not required for, cell proliferation. This raises the possibility that Ki-67 staining in cancers might not always reflect cell proliferation.

Like Ki-67, CDK4 and CDK6, which trigger RB phosphorylation, are not essential for cell proliferation in most cell types in mice (14). Nevertheless, CDK4 and D-type cyclins are required for certain cancers, including breast cancers (15). CDK4/CDK6 inhibition with PD0332991 (palbociclib) has shown major benefits in breast cancer clinical trials, leading to its approval in certain clinical settings (16), and it is currently in trials for a variety of other cancers. Preclinical models using tumor explants suggest that RB-positivity can predict responses to palbociclib (17). However, in these

¹IGMM, CNRS Univ. Montpellier, Montpellier, France. ²IRCM, INSERM ICM, Univ. Montpellier, Montpellier, France. ³IGF, CNRS, INSERM, Univ. Montpellier, Montpellier, France.

Note: Supplementary data for this article are available at Cancer Research Online (<http://cancerres.aacrjournals.org/>).

M. Sobecki and K. Mrouj contributed equally to this article.

Current address for M. Sobecki: Department of Genome Biology, Institute for Integrative Biology of the Cell (I2BC), UMR 9198, CEA/CNRS/Université Paris Sud, Gif-sur-Yvette, Paris 91190, France.

Corresponding Author: Daniel Fisher, Institute of Molecular Genetics of Montpellier, CNRS, 1919 Route de Mende, Montpellier 34293, France. Phone/Fax: 334-3435-9694; E-mail: daniel.fisher@igmm.cnrs.fr

doi: 10.1158/0008-5472.CAN-16-0707

©2017 American Association for Cancer Research.

experiments, palbociclib effects were determined by Ki-67 expression itself. Yet Ki-67 expression may be directly promoted by CDK4/CDK6-dependent RB phosphorylation. Thus, upon CDK4/CDK6 inhibition, it remains possible that cells might continue to proliferate without Ki-67 expression. It is therefore essential to determine whether loss of Ki-67 after CDK4/CDK6 inhibition indeed reflects cell-cycle arrest by correlating with independent markers of cell proliferation.

In this study, we show that variability of Ki-67 levels is due to cell-cycle regulation of Ki-67 mRNA and protein in normal human cells, proliferating tissues in mice and human cancers. Furthermore, in cells that have recently exited the cell cycle, low-level Ki-67 persists. Ki-67 protein is degraded from mitosis to G₁, and G₁ arrest by CDK4/CDK6 inhibition causes loss of Ki-67 mRNA. Effects of palbociclib on Ki-67 expression always correlated with its effects on cell proliferation, including *in vivo*. These results have important implications for interpreting Ki-67 staining in cancer histopathology and for its use as a diagnostic marker.

Materials and Methods

Ethics

All animal experiments were performed in accordance with international ethics standards and were subjected to approval by the Animal Experimentation Ethics Committee of Languedoc Roussillon.

Mouse lines

The *Apc^{lox}* (*Apc^{tm2.1Cip}*) line (18) was provided by C. Perret (Cochin Institute, Paris, France). The *Villin-Cre^{ERT2}* line (19) was provided by S. Robine (Curie Institute, Paris, France).

Cell lines

Cell lines were not authenticated but were mycoplasma-free (tested weekly using Mycoalert kit). Normal human diploid foreskin fibroblasts (HDF) were from frozen stocks provided by J. Piette (CRBM, Montpellier, France) in 2001. IMR-90, U2OS, HeLa, HCT-116, MCF7, MDA-MB-231, MDA-MB-468, CAL51, HBL100, and IMR90 were originally obtained from the ATCC from 2000 to 2010. IMR-90 fibroblasts expressing HPV-16 E7 oncogene were described previously (20). U2OS, HeLa HCT-116, MCF7, MDA-MB-231, CAL51, and HBL100 were grown in DMEM with 10% FBS. HDFs were grown in DMEM supplemented with 10% FCS and 2 mmol/L L-glutamine. Cells were grown under standard conditions at 37°C in a humidified incubator containing 5% CO₂. IMR-90 WT and E7 were grown in 3% oxygen in DMEM/F12 medium supplemented with 10% FBS and 4 mmol/L L-glutamine.

Cell drug treatments

Primary cells (HDF, BJ hTERT, IMR90) were treated with 1 μmol/L PD0332991 (Tocris), 100 μg/mL cycloheximide, 20 μmol/L MG132 (Tocris), 10 μg/mL bleomycin (Sigma-Aldrich), or 2 μg/mL ICRF-193 (Sigma-Aldrich).

Cell synchronization

G₀ block. HDF at 20% confluency were washed with PBS and incubated with medium supplemented with 0.1% FBS for 72 hours. Cell-cycle entry was stimulated by adding fresh medium

with 10% FBS. Onset of S-phase was observed 16 hours later by EdU incorporation.

G₁-S block. HDF at 25% confluency were incubated with medium supplemented with 2 mmol/L thymidine or 2 mmol/L hydroxyurea for 24 hours. Cells were released from G₁-S block by washing twice with fresh medium for 5 minutes.

G₂ block. Seven hours after release from G₁-S block, HDFs were incubated with 9 μmol/L RO3306 (Tocris) for 14 hours. Cells were released from G₂ block by washing twice with fresh medium for 5 minutes. Mitosis was observed around 1 hour after release.

Cell extracts and gel electrophoresis

Frozen washed cell pellets were lysed directly in Laemmli buffer at 95°C (without β-mercaptoethanol and bromophenol blue) and sonicated on ice for 10 minutes in 30 seconds/30 seconds ON/OFF intervals. Protein concentrations were determined by BCA assay. Proteins were separated by SDS-PAGE (7.5% and 12.5% gels) at 35 mA in TGS buffer and transferred to Immobilon membranes with a semidry blotting apparatus.

Dot blot

Ten micrograms of total cell lysate in 5 μL was spotted onto nitrocellulose, blocked, and probed using standard immunoblotting procedures. Signals were quantified using PXi4 Imaging System (Syngene) and GeneTools analysis software.

Antibodies

Antibodies were: Ki-67: clone SP6 (Abcam), 35 (BD Biosciences), SolA15 (eBioscience); RB1 (BD Biosciences); cyclin A: 6E6 (Novocastra), H-432 (Santa Cruz Technology); cyclin E1: HE12 (Santa Cruz Biotechnology); cyclin D1: DSC6 (Cell Signaling Technology), EP272Y (Millipore); cyclin B1: GNS1 (Santa Cruz Biotechnology); CNDKN1A: C-19 (Santa Cruz Biotechnology); phospho-histone H3S10: 9701 (Cell Signaling Technology).

qRT-PCR

Purified RNA (1,000 ng) extracted by RNeasy Mini Kit (Qiagen) was reverse-transcribed using SuperScript II Reverse Transcriptase (Life Technologies) according to the manufacturer's instructions. qPCR was performed using LightCycler 480 SYBR Green I Master (Roche) and LightCycler 480 qPCR machine with conditions: 95°C 10 minutes, 40 cycles of 95°C 20 seconds, 58°C 20 seconds, and 72°C 20 seconds. Reaction specificity was verified by melt curve analysis. Each sample was performed in three replicates. qPCR primers used were:

MKI67 (F: TGACCCTGATGAGAAAGCTCAA, R: CCCTGAGC-AACACTGCTTTTT);

CCNA2 (F: AGGAAACTTCAGCTTGTGGG, R: CACAACTC-TGCTACTCTGGG);

CCNE1 (F: CCGGTATATGGCGACACAAG, R: ACATACGCAA-ACTGGTGCAA);

PCNA (F: CCTGCTGGGATATTAGCTCCA, R: CAGCGGTAGG-TGTCGAAGC);

CCNB1 (F: TGTGTCAGGCTTCTCTGATG, R: TTGGTCTGA-CTGCITGCTCT);

Sobecki et al.

CCND1, (F: GCTGCGAAGTGGAAACCATC, R: CCTCCTTCTG-CACACATTTGAA);

B2M (F: GCGCTACTCTCTCTTTCTGG, R: AGAAAGACCAG-TCCCTTGCTGA);

RPL19 (F: ATGCCGGAAAAACACCTTGG, R: GTGACCTTCT-CCTGGCATTGC).

Proliferation and senescence assays

Analysis of DNA replication in cells was achieved by treatment with 2 mmol/L 5-ethynyl-2'-deoxyuridine (EdU; Life Technologies) before fixation. Replicating cells were visualized following the protocol from Click-iT EdU AlexaFluor-488 Imaging Kit (Life Technologies). Beta-galactosidase staining was conducted using Senescence Detection Kit (ab65351) following the manufacturer's instructions.

Xenografts

Three million log-phase viable mouse pathogen-free (IMPACT1, Iddex) MDA-MB-231 and MDA-MB-468 cells in 0.2 mL, 50% v/v Matrigel (BD Biosciences) were injected subcutaneously into 6-week-old female athymic nu/nu mice (Envigo). Tumors were grown to an average volume of 150–200 mm³ measured by caliper using the formula " $\pi/6 \times S^2$ (smaller radius) \times L (larger radius)" before initiation of treatment. Mice were then randomized into treatment groups for each cell line: vehicle control or 150 mg/kg/day PD 0332991. PD 0332991 was orally administered (gavage) as a solution in 50 mmol/L sodium lactate, pH 4 for 5 consecutive days. Following this treatment, mice were euthanized by cervical dislocation, and tumors were excised by dissection. For each tumor sample, one part was fixed in 10% formalin overnight before transfer into 70% ethanol and another snap frozen in liquid nitrogen.

IHC

Mouse intestinal epithelium and tumors were processed for IHC as described previously (21).

Bioinformatics

We retrieved 585 transcriptomes of colorectal cancers (22) and used data as originally normalized. Spearman correlation was computed between *MKI67* Affymetrix chip probes and all other gene probes over all samples simultaneously or for each sample cluster (cancer subtypes as defined in the original publication) separately. When multiple probes were available, the pair giving the highest absolute correlation (sum of absolute values over all clusters when computed for each cluster separately) was retained. Correlation *P* values were obtained with a Student *t* distribution with *n*-2 degrees of freedom (*n* = number of samples), and corrected for multiple hypotheses (Benjamini-Hochberg; ref. 23). Correlations with FDR < 0.05 were considered. Breast tumor transcriptomes (1098 samples) were obtained from the Broad GDAC interface (<http://gdac.broadinstitute.org/>) to The Cancer Genome Atlas (TCGA) data. We used normalized RNA-seq data as provided and generated clustering of tumors with the Firehose online tool, which found 7 sample classes (Supplementary Fig. S1). Correlation computations were performed as above.

Ki-67 proteomics data (11) were filtered to obtain a Ki-67 interactome by retaining all bait proteins with Mascot identification score ratios in the top 5% with respect to negative controls (empty vectors or unrelated protein, TRIM39). We further

removed all proteins present in more than 5% of the CRAPome (24). A total of 181 proteins passed this selection (Supplementary Table S1).

Interaction networks of Ki-67 highly correlated genes were obtained using pairwise interactions found in STRING database v10 (25), considering only top 10% STRING scores.

Results

Variable Ki-67 levels correlate with cell-cycle gene expression

We first investigated whether Ki-67 expression *in vivo* varies in a cell-cycle-dependent manner by assessing Ki-67 staining on mouse intestinal epithelium. Cells in S-phase or G₂ were identified by injecting BrdUrd 2 hours prior to sacrifice. As expected, Ki-67 was absent in nonproliferating Paneth and goblet cells, whereas Ki-67 stained both BrdUrd-positive and negative nondifferentiated cells in the crypt (Fig. 1A). Ki-67 expression was higher in BrdUrd-positive cells (S-phase and G₂), and lowest in BrdUrd-negative cells, that are mostly G₁. Highest staining was observed in mitotic cells (Fig. 1A, yellow arrowheads).

We next asked whether Ki-67 expression was upregulated in tumors. We deleted exon 14 of one *Apc* allele in all intestinal epithelial cells using *Villin-Cre^{ERT2}*-mediated recombination. Adenoma formation then initiates through clonal growth from discrete epithelial cells that have lost the remaining *Apc* allele. Fig. 1B shows that Ki-67 levels were variable in both healthy tissue and in adenomas, similarly to proliferating cell nuclear antigen (PCNA; Fig. 1C), whose expression oscillates throughout the cell cycle. These results suggest that Ki-67 expression varies through the cell cycle in both normal tissues and in tumors.

We next looked at cell cycle exit *in vivo*. In the intestinal epithelium, actively proliferating crypt cells migrate upwards, exit the cell cycle, and differentiate before reaching villi. We compared Ki-67 IHC staining using different development times in serial sections of mouse intestinal epithelium. Using short exposures, Ki-67-positive staining can be seen only in cells within the proliferating crypt compartment, but longer exposures revealed low levels of Ki-67 in cells that have recently exited this compartment and started populating the adjacent villus base, where differentiating nonproliferating cells reside (Fig. 1D). Cells that have migrated up the villi have decreasing Ki-67 levels. Therefore, low Ki-67 levels reflect exit from the cell-cycle and terminal differentiation, but their assessment can be influenced by the staining protocol.

These results indicated that *MKI67* levels are linked to the cell cycle in mice. To see whether the same is true in humans, we investigated coregulated gene expression using COXPRESdb (26). Gene ontology (GO) analysis (27) revealed that mechanisms involved in mitosis and the G₂-M transition constituted the 16 most enriched biological processes of the 100 most correlated genes (Supplementary Fig. S2A; Supplementary Table S2).

To investigate genes coregulated with *MKI67* in human cancers, we first analyzed data from colorectal cancers, which have been extensively characterized at the molecular level (22). We assessed the proportion of cell-cycle genes among genes whose expression correlates with that of *MKI67*. Figure 2A shows that at a very high correlation coefficient (>0.6), around 80% of genes have a cell-cycle annotation. We next exploited STRING (25) to identify functional interactions. We superimposed high-confidence interactions determined from our

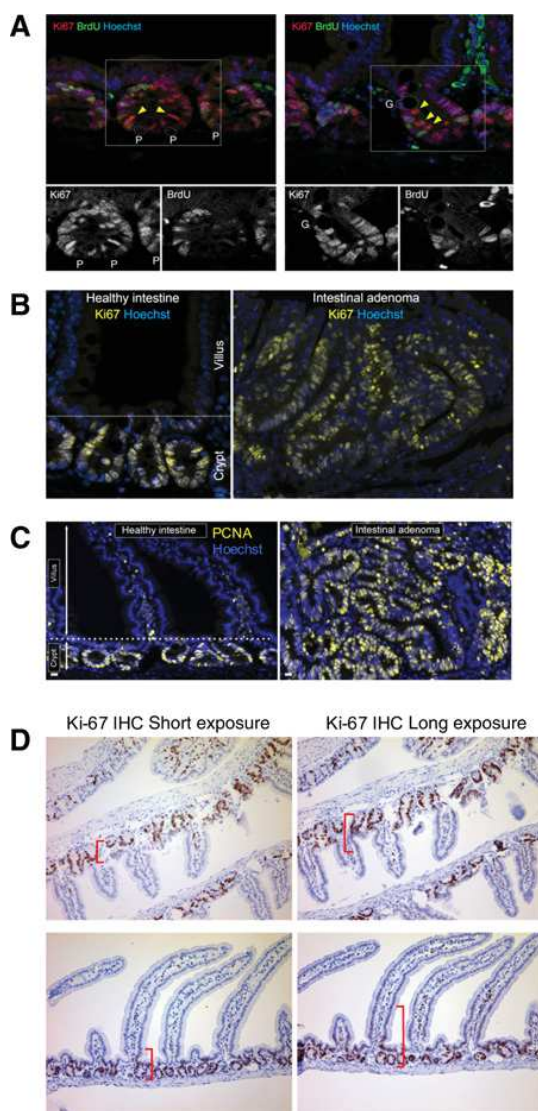


Figure 1. Cyclic expression of Ki-67 in primary cells, cancer cells, and tumors. **A**, Cyclic Ki-67 in the mouse intestinal epithelium, as shown by immunofluorescence of Ki-67 and BrdUrd (BrdU) on paraffin-stained tissue sections from wild-type mice fixed 2 hours after BrdUrd injection. P and G, Paneth and Goblet cells, respectively. Yellow arrowheads, columnar crypt stem cells. **B**, Immunofluorescence of Ki-67 in healthy intestine and adenomas from *Apc*^{-/-} mice showing variable levels of Ki-67 in cycling cells in the crypt and in tumors. **C**, Similar to **B**, stained for PCNA. **D**, Ki-67 IHC in serial sections of wild-type C57/BL6 mouse intestinal epithelium. Left, IHC short exposure; right, IHC saturating exposure in an adjacent section. Two examples are shown (top and bottom panels). Red brackets, visible Ki-67 labeling. Cells were counterstained by hematoxylin and eosin.

own, high-confidence Ki-67 physical interaction data (11). Figure 2B shows that many proteins encoded by these *MKI67* coregulated genes functionally interact in a cell-cycle network. Ki-67 interacts with both the mitotic and S-phase subnetworks.

The remaining nodes also interact with the cell-cycle network and many have a metabolism annotation (which includes transcriptional regulation). Correlations with cell-cycle genes were maintained across colorectal cancer subtypes (Supplementary Fig. S2B). To see whether these results can be generalized to other cancers, we next interrogated TCGA with Ki-67 and searched for correlated expression across all breast cancer subtypes (28). Again, cell-cycle genes were predominant among the genes most correlated with *MKI67* (Supplementary Fig. S2C and S2D), with the top hits being cyclins (*CCNA2*, *CCNB1*, *CCNB2*), *CDK1*, *FOXM1* (a mitotic gene transcription factor; ref. 29), *BUB1B* and *DLGAP5* (which controls mitotic spindle microtubule dynamics; Fig. 2C; ref. 30).

These results indicate that the main predictor of Ki-67 mRNA levels is the cell-cycle phase, with *MKI67* most correlating with expression of genes involved in mitosis. We next experimentally analyzed Ki-67 and cyclin A2 mRNA and protein levels in a panel of human cancer cell lines: nontransformed human dermal fibroblasts (HDF) and their counterparts transformed with HPV-16 E7 oncogene, and cancer cells of different tissue origins and varying aggressiveness (U2OS, HeLa, HCT-116, MCF-7, HBL-100, CAL-51, and MDA-MB-231). As different human cancer cells express multiple smaller isoforms of Ki-67 (31), we quantified the total level of all Ki-67 species by dot-blotting. As controls, we used U2OS cells expressing nontargeting shRNA or Ki-67 shRNA (11), and HDF treated with the CDK4/CDK6 inhibitor PD0332991 (PD), which can induce senescence (32). As expected, Ki-67 shRNA or PD caused loss of both Ki-67 protein and mRNA. Ki-67 expression directly correlated with cyclin A2 expression at both protein (Fig. 2D) and mRNA (Fig. 2E) levels in all cell lines, including HDF treated with PD. Thus, Ki-67 levels are similar between cell types but depend on cell-cycle regulation.

Cell-cycle regulation of Ki-67 expression

To better understand cell-cycle variability of Ki-67 expression, we followed Ki-67 protein and mRNA levels in HDF cells synchronized throughout two cell cycles after release from quiescence. We used sequential block and release from CDK1 inhibition with RO-3306, which arrests cells at the G₂-M transition (33), and thymidine, which arrests cells in S-phase (Fig. 3A and B). Both Ki-67 and cyclin A2 mRNA levels oscillated, peaking at G₂ before decreasing in M-phase, as identified by phospho-histone H3 staining, dropping further in G₁ and rising again in the next cell cycle (Fig. 3C). Protein levels were also cyclic, peaking in mitosis (Fig. 3D). However, unlike mitotic cyclins, Ki-67 was not completely degraded during mitosis. We confirmed and extended these results to other cell lines by quantifying Ki-67 expression in asynchronous single HDF, HCT-116 or U2OS cells by immunofluorescence using markers of different cell-cycle stages (Supplementary Fig. S3A and S3B). Similar cell-cycle variation in Ki-67 expression level was found in a genome-scale proteomics and transcriptome analysis of a minimally perturbed cell cycle in human leukemic NB4 cells (34).

Next, we asked whether Ki-67 mRNA is sensitive to serum withdrawal after the restriction point, in cells released from a hydroxyurea-mediated S-phase block. Whereas D-type cyclin expression rapidly declined between S-phase and mitosis upon serum withdrawal, Ki-67 mRNA was stable, recapitulating cyclin A2 (Fig. 4A). Arresting cells in G₁ by CDK4/CDK6 inhibition with PD for 24 hours caused disappearance of Ki-67

Sobecki et al.

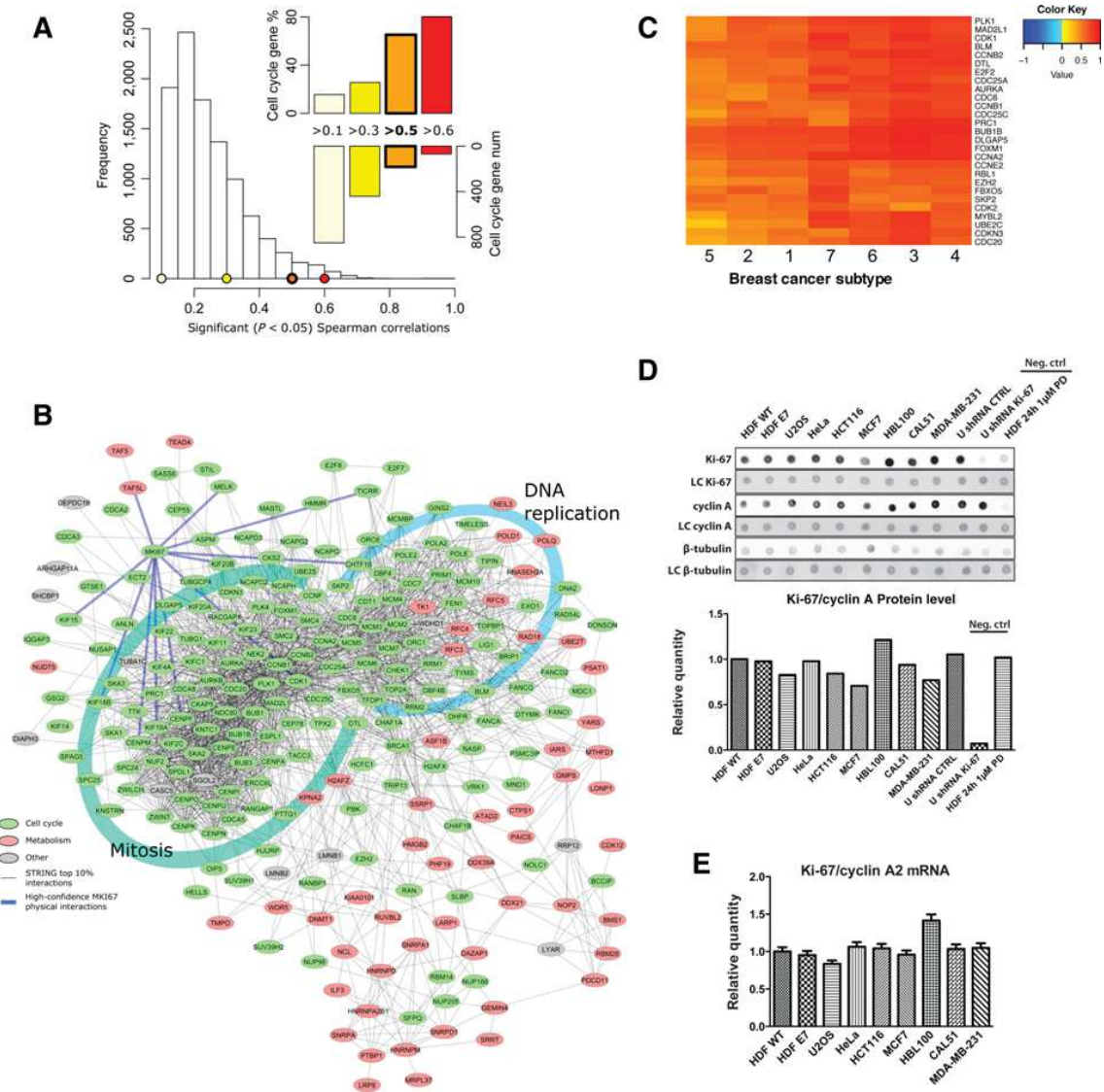
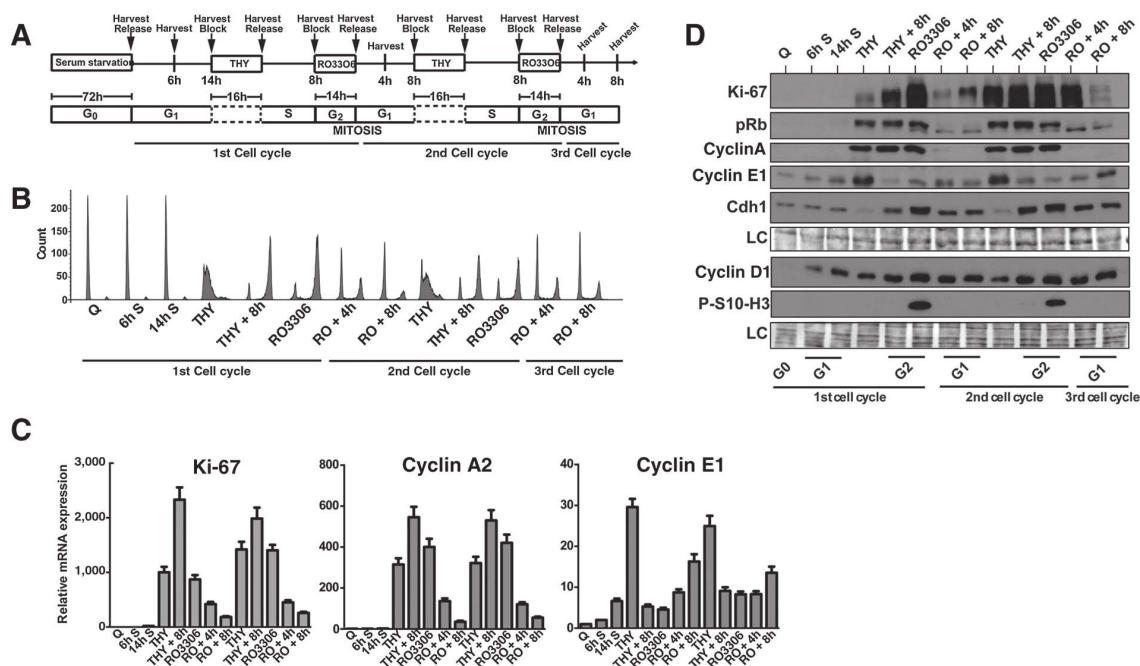


Figure 2. Ki-67 expression is determined by the cell-cycle stage. **A**, Histogram of the number of *MKI67* significantly correlated genes in colorectal tumors with respect to Spearman correlation values (all correlations adjusted $P < 0.05$). The upper right bar plots report the proportion and number of cell-cycle genes among genes above a given correlation coefficient. **B**, Ki-67 interactome obtained combining STRING database interactions and our own Ki-67 protein physical interactions for all genes with correlation > 0.5 in **A**. **C**, Comparison between *MKI67* and other genes in TCGA breast cancer transcriptomic data showing that mitotic genes are strongly correlated with Ki-67 expression in all cancer subtypes. For a full heatmap of correlated genes with a cancer annotation see Supplementary Fig. S2D. **D**, Ki-67 levels in cycling cells are comparable between primary human fibroblasts (HDF) and cancer cells. Immunoblot of Ki-67 and cyclin A2 proteins from asynchronous cell lysates from the indicated cell lines compared with total protein as loading control (LC) and β -tubulin. Controls include U2OS stably expressing shRNA control silencing or Ki-67 silencing vectors (where Ki-67 is absent but cyclin A2 remains) or HDF arrested by treatment with PD0332991 (both Ki-67 and cyclin A2 are absent). Bottom, quantitation of results by densitometry analysis. **E**, The ratio of Ki-67 to cyclin A2 mRNA is similar in all cell lines as quantified by qRT-PCR (experiment as in **A**).

mRNA and protein. Both Ki-67 loss and G_1 arrest were prevented by inactivating RB via expression of the HPV16 E7 oncogene (Fig. 4B–E). Ki-67 protein was degraded after release from the G_2 –M block (Fig. 4F), rather than throughout the cell cycle as reported for HL60 cells (6). Ki-67 degradation at the

mitosis/ G_1 transition suggested that it involves the ubiquitin–proteasome system, in agreement with our previous demonstration (13) that Ki-67 downregulation is dependent on FZR1 (also known as CDH1), which activates the Anaphase-Promoting Complex (APC/C). Indeed, inhibiting the proteasome with

**Figure 3.**

Ki-67 expression is dynamically controlled by a cell-cycle-regulatory network. **A**, Scheme. HDFs were sequentially synchronized over two cell cycles upon entry from quiescence. **B**, DNA content was analyzed by flow cytometry. **C**, qRT-PCR analysis of indicated mRNA. **D**, Western blotting of indicated proteins (Q, quiescence; S, serum stimulation; THY, thymidine block; THY +, time point after release from thymidine block; RO3306, RO3306 block; RO +, time point after release from RO3306 block). LC, loading control (amido black).

MG132 prevented loss of Ki-67 protein upon PD treatment (Fig. 4G). Thus, CDK4/CDK6 inhibition eliminated Ki-67 expression by G₁ arrest, where Ki-67 mRNA expression is abolished and ubiquitin-mediated protein degradation occurs.

Ki-67 expression is a late marker of cell-cycle entry and persists on cell-cycle exit

We next investigated how Ki-67 levels change in cells entering or leaving the cell cycle. First, HDFs were released from serum starvation, and DNA content and Ki-67 expression were determined over 30 hours (Fig. 5A). Very low levels of Ki-67 were detected in serum-starved cells, although cyclin A2 was absent and no cells were in S-phase. Whereas cyclin D1 levels rose rapidly, Ki-67 protein remained at a low level throughout the G₀-G₁ transition and rose upon entry into S-phase, when cyclin A2 became detectable. The major increase in Ki-67 expression occurred between S-phase and mitosis.

To verify whether persistent Ki-67 expression is a consistent feature of physiologically quiescent cells, we analyzed human umbilical cord T lymphocytes, which enter the cell cycle upon IL2 stimulation. Ki-67 was completely undetectable in non-stimulated T-lymphocytes. Again, Ki-67 appeared at a late stage, after 48-hour stimulation, coincident with cyclin A2 expression (Fig. 5B).

We reasoned that low level Ki-67 might persist in early stages of cell-cycle arrest and is gradually eliminated. To test this, we assessed Ki-67 expression by immunofluorescence in individual cells arrested using different approaches. We induced quiescence either by contact inhibition or serum starvation, or by DNA-

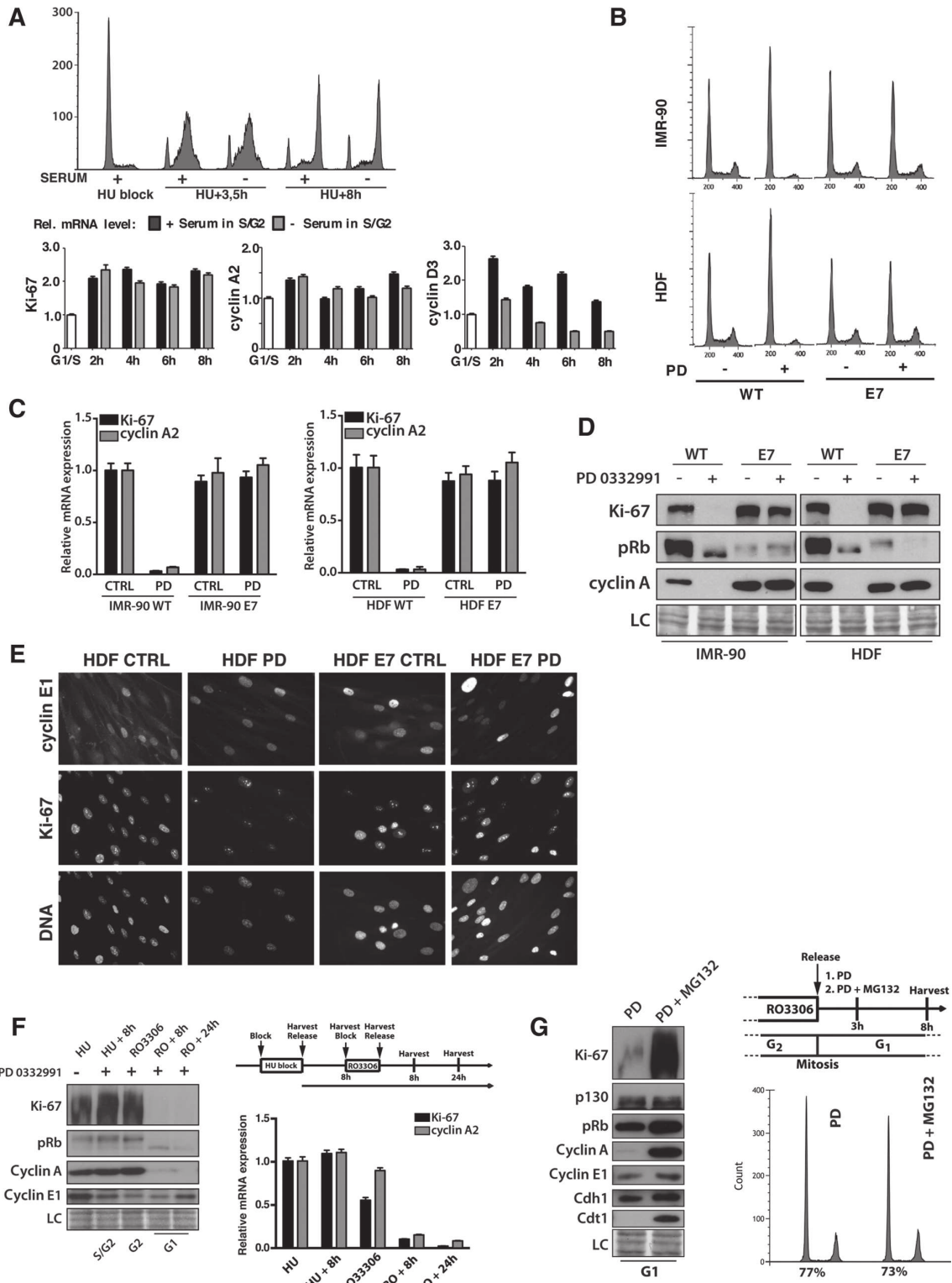
damaging agents, ICRF-193 or bleomycin (Supplementary Fig. S4; ref. 20). Residual nuclear Ki-67 staining could clearly be seen in quiescent cells and was higher in contact-inhibited cells, which more readily enter the cell cycle when released, than serum-starved cells (Fig. 5C and D). However, Ki-67 was similar to background staining in cells with DNA damage (Fig. 5E and F). In all cases, cyclin A2 disappearance confirmed cell-cycle exit. Background Ki-67 levels could be detected 1 day after bleomycin treatment (Fig. 5F), but were essentially undetectable after 3 days and 7 days, by which time (7 days) senescent cells were readily visualized by β -galactosidase activity staining (Supplementary Fig. S5).

Taken together, these results show that high Ki-67 expression is a late marker of cell-cycle entry and its highest levels occur in G₂ and M-phase. Quiescent cells and cells entering the cell cycle have low Ki-67, and Ki-67 is undetectable in deeply quiescent or senescent cells.

Ki-67 expression reveals responses to drugs that target cell proliferation

Our results suggest that Ki-67 expression could be useful for assessing cellular responses to CDK4/CDK6 inhibition. However, as neither CDK4/CDK6 nor Ki-67 are essential for cell proliferation in all cells, it was important to verify whether Ki-67 expression always recapitulates cell proliferation status upon CDK4/CDK6 inhibition. We tested this using a panel of cancer cell lines treated with a range of concentrations of PD for 24 hours, and then exposed to 5-ethynyl-2-deoxyuridine (EdU) for a further 24 hours, to assess DNA replication. Samples were taken to

Sobecki et al.



measure Ki-67 protein and mRNA. This revealed that the cell-cycle responses to PD strictly correlated with the effects on Ki-67 mRNA and protein levels (Fig. 6A). In RB-positive cells, this was further correlated with loss of RB phosphorylation. PD most effectively prevented S-phase onset and downregulated Ki-67 in RB-positive MDA-MB-231 and MCF7 cells. HCT-116 cells, which are RB-positive, responded poorly to PD, possibly because they are also mutated for *KRAS* and *PI3KCA* (35). PD had no effect on low-RB-expressing HeLa cells.

To confirm the robustness of Ki-67- and cyclin A2-correlated expression upon PD treatment, we interrogated the Cancer Cell Line Encyclopedia (36). We also compared expression of *Mki67* with mRNA encoding cyclins B1, D1, and D3. This showed an extremely tight correlation between *MKI67* and *CCNA2* (cyclin A2) in all cell lines at any concentration of PD, and a good, but slightly lower, correlation with *CCNB1* (cyclin B1; Fig. 6B). Ki-67 and D-type cyclin expression was not correlated. This data also shows that PD sensitivity (inversely related to IC_{50}) and Ki-67 levels were not correlated. Thus, there is no general value of Ki-67 expression in predicting sensitivity to PD. We then extended this question to all drugs analyzed in the CCLE. Considering all drugs together, *MKI67* expression showed no correlation with drug-sensitivity (IC_{50} ; Supplementary Fig. S6A). However, *MKI67* and *CCNA2* showed a weak correlation with sensitivity to topoisomerase inhibitors irinotecan and topotecan (Supplementary Fig. S6B).

Finally, we performed an experiment in mice to see whether effects of CDK4/CDK6 inhibition on cell proliferation and Ki-67 expression correlate in tumors *in vivo*. We compared PD-sensitive and resistant cell lines, MDA-MB-231 and MDA-MB-468, respectively (37). We engrafted these lines subcutaneously into nude mice and allowed tumors to grow to 200 mm³ before treating mice with vehicle or PD for 5 days by oral administration. As expected from *in vitro* experiments, PD treatment arrested tumor growth from MDA-MB-231, but not MDA-MB-468 (Fig. 7A). This was reflected by strongly decreased IHC staining for cyclin A2, PCNA, and Ki-67 in MDA-MB-231, but no change in these markers in MDA-MB-468 (Fig. 7B). The number of cells scored positive for Ki-67 and PCNA was most similar in untreated samples, and higher than cyclin A. This is because Ki-67 and PCNA, although variable, are present throughout the cell cycle, whereas cyclin A is only present from S-phase to G₂. However, responses to PD in MDA-MB-231 were more complete for Ki-67 and cyclin A than for PCNA, where low level staining remained in a minority of treated cells. This might reflect a difference in half-life of PCNA compared with cyclin A and Ki-67, both of which are degraded by the APC/C in mitosis and G₁. Analysis by qRT-PCR confirmed that

protein levels were recapitulated by mRNA levels, and also showed that cyclin D mRNA levels did not change (Fig. 7C). Thus, Ki-67 is a good marker for cell proliferation status in response to PD *in vivo*.

Discussion

In light of the variability of the Ki-67 index in cancer biopsies and lack of consistent correlation with responses to therapy, it is important to understand how Ki-67 expression is controlled. We find that cell-cycle regulation accounts for variability in Ki-67 expression in primary cells and cancer cell lines as well as in tumors and human cancers. Thus, low and high level Ki-67 should be scored as positive to determine the Ki-67 labeling index. However, extremely low Ki-67 levels can be detected in quiescent cells by IHC upon long exposure. Unlike the situation in senescent cells, which have no Ki-67, such low levels of Ki-67 staining persist in cells that have recently stopped proliferating and entered quiescence.

Ostensibly, this is incompatible with the idea of Ki-67 as a specific marker for proliferating cells, but is consistent with a previous report that Ki-67 could be detected at sites of ribosomal RNA synthesis in quiescent cells (38). We speculate that a basal level of Ki-67 might be a marker for the recently described primed state for cell-cycle reentry termed G(Alert) (39). This basal level of Ki-67 in arrested cells contributes to the variability in assessments of Ki-67 staining index in cancers as cells might be variably classed as Ki-67-positive or negative. Basal Ki-67 expression might itself be a useful marker to identify cells within tumors that proliferate slowly or are quiescent, and thus are more resistant to chemotherapy or radiotherapy than proliferating cells (40). Such populations appear to be responsible for relapse after chemotherapy in colorectal cancer patients (41). Furthermore, in breast cancer, cells with low proliferation rates, and therefore low Ki-67 index, can sustain the tumor niche for highly proliferative clones, with which they remain in equilibrium (42). Quiescent cells would likely be undetectable upon standard IHC analysis, but our data suggest that they could be identified and distinguished from proliferating or senescent cells by more sensitive IHC analysis. Cells with such low levels of Ki-67 should be scored separately from cells with higher Ki-67 levels, which are proliferating, as they may have implications for prognosis of relapse.

We find that Ki-67 cell-cycle regulation relies on two opposing mechanisms dependent on conserved cell-cycle regulators: CDK4/CDK6 phosphorylates RB, allowing Ki-67 mRNA expression in G₁, and this is opposed by protein degradation in late mitosis and early G₁ by the ubiquitin-proteasome system. This

Figure 4.

Ki-67 expression is restricted to proliferating cells by CDK4/CDK6 and proteasome-mediated degradation. **A**, Top, flow cytometry DNA content profiles of HDF released for the indicated time from a HU block in the absence or presence of serum. Bottom, qRT-PCR analysis of the indicated mRNAs during this time course. **B**, Flow cytometry DNA content profiles of WT (left) or HPV-E7-expressing (right) IMR-90 (top) or HDF (bottom) treated or not with PD0332991 (PD) for 24 hours. **C**, Analysis of cyclin A2 and Ki-67 mRNA levels by qRT-PCR in the experiment from **B**. **D**, Western blot analysis of Ki-67, cyclin A2, and total RB1 protein (pRb) in the experiment from **B**. LC, loading control (amido black). **E**, Immunofluorescence of Ki-67 and cyclin E1 in HDFs, with or without HPV16-E7 oncogene expression, treated or not with PD for 24 hours. **F**, HDFs were synchronized with HU, followed by RO3306 and released to G₁ with PD0332991 for indicated times. Top right, scheme of the experiment; left, Western blot analysis of indicated proteins. LC, loading control. Bottom right, qRT-PCR analysis of Ki-67 and cyclinA2 mRNA levels. (HU, hydroxyurea block; HU +, release from HU block; RO3306, RO3306 block; RO +, release from RO3306 block). **G**, HDFs were blocked in G₂ with RO3306, released in the presence of PD0332991 (PD), with or without MG132 (added 3 hours after release from RO3306 block). Cells were collected 8 hours after release from RO3306 block and the indicated proteins were analyzed by Western blotting (left). LC, loading control. Right, FACS analysis of cell cycle distribution indicates similar number of cells in G₁.

Sobecki et al.

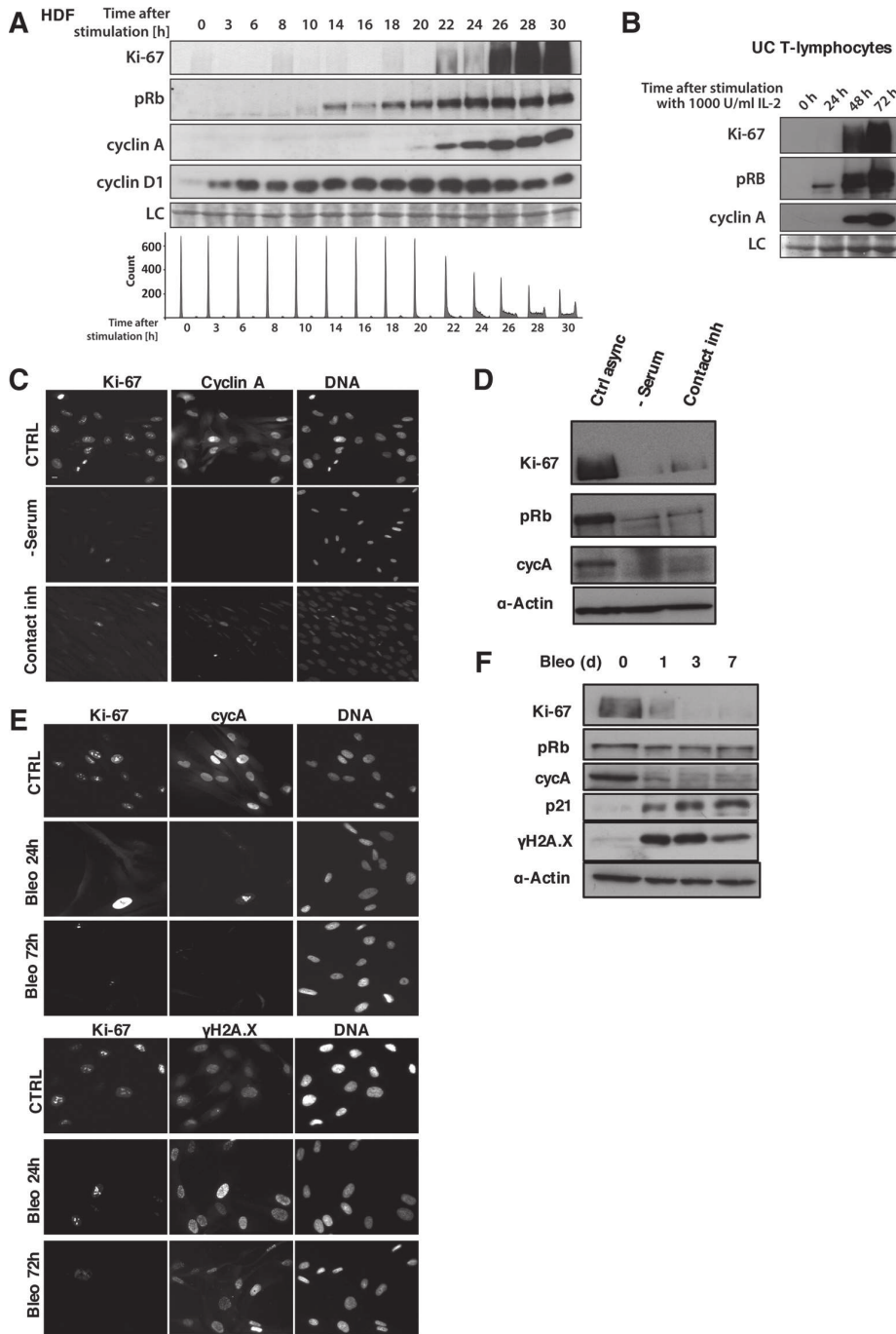


Figure 5.

Ki-67 is expressed at low levels in early cell-cycle arrest *in vitro*. **A**, Top, Western blot for indicated proteins in HDF upon cell-cycle entry and progression. LC, loading control. Bottom, DNA flow cytometry profiles. **B**, Western blot analysis of the indicated proteins in a time course of lymphocytes purified from umbilical cord blood and stimulated by the addition of IL2 to the media. LC, loading control (amido black). **C**, Ki-67 immunofluorescence in HDFs, control or growth arrested by serum starvation (-serum) or contact inhibition (contact inh), stained for Ki-67 or cyclin A2. Scale bar, 10 μm. **D**, Ki-67, total RB (pRb), and cyclin A2 Western blot analysis upon growth arrest by serum starvation or contact inhibition. **E**, Immunofluorescence for the indicated proteins in asynchronous HDFs (CTRL) or HDFs arrested by DNA damage by 24 or 72 hours treatment with bleomycin (Bleo). **F**, Time course (days) of Ki-67 protein expression upon bleomycin treatment. The indicated proteins were analyzed by immunoblotting.

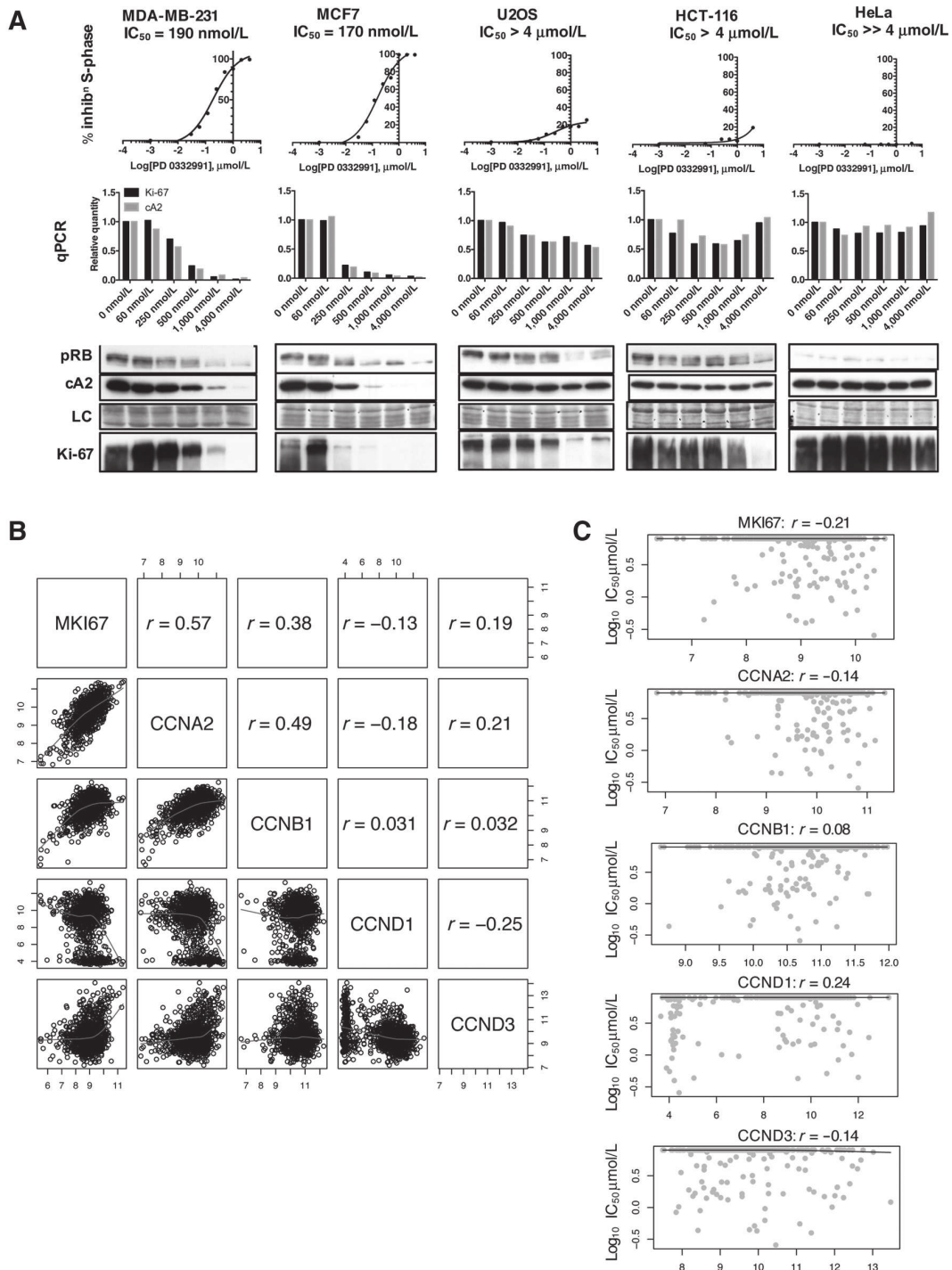


Figure 6.

Responses to CDK4/CDK6 inhibition of cancer cell lines correlate with effects on Ki-67 mRNA and protein. **A**, After treatment with the indicated dose of the PD0332991 for 24 hours, EdU was added and EdU-positive staining assessed after a further 24 hours by flow cytometry. Middle, qRT-PCR quantification of Ki-67 and cyclin A2 (cA2) mRNA. Bottom, Western blotting for total RB1 (pRb), Ki-67, and cyclin A2 (cA2), with loading controls (LC; amido black). **B**, Correlation (Spearman) between *MKI67* and *CCNA2*, *CCNB2*, *CCND1*, and *CCND3* across all CCLE cell line transcriptomes. **C**, Correlation between response to PD0332991 and *MKI67*, *CCNA2*, *CCNB2*, *CCND1*, and *CCND3* expression levels in CCLE cell lines.

Sobecki et al.

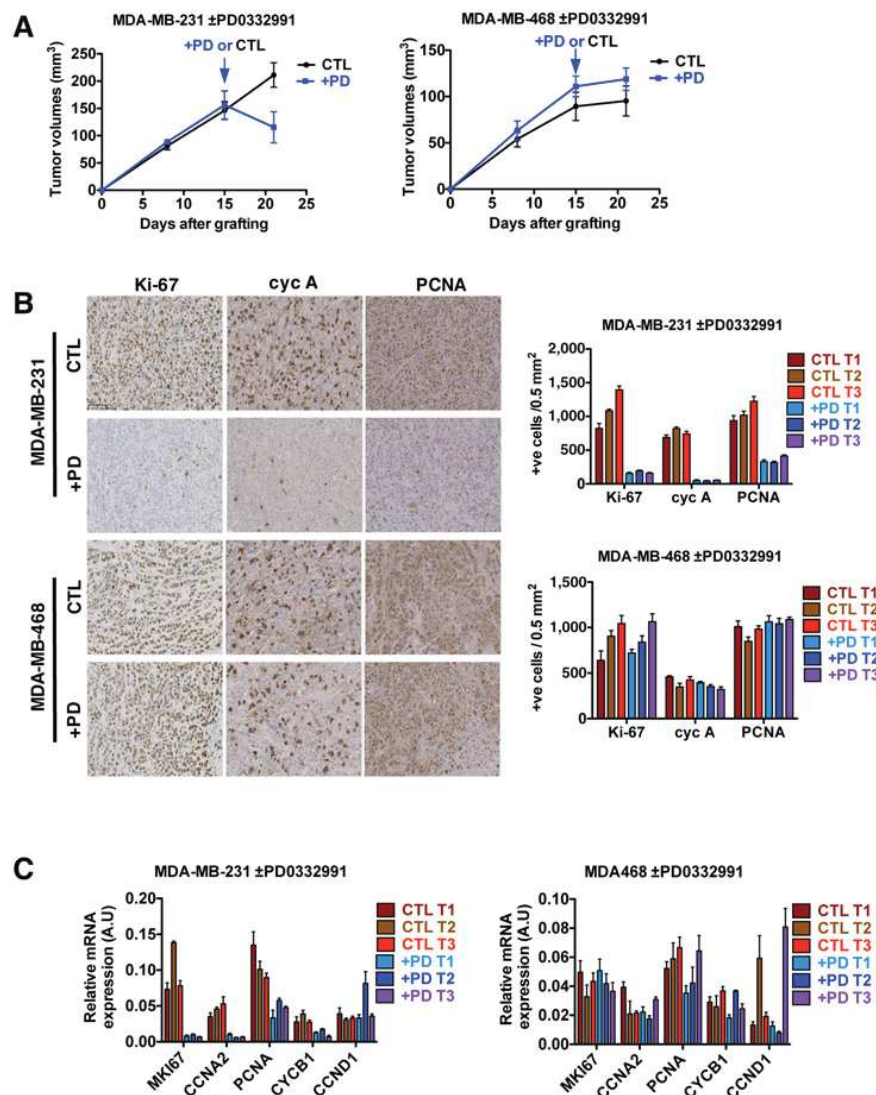


Figure 7.

Ki-67 is a good biomarker for responses to CDK4/CDK6 inhibition *in vivo*. **A**, Tumor growth in nude mice of xenografts of MDA-MB-231 cells (left) or MDA-MB-468 cells (right) treated for 5 days from day 15 with vehicle control (CTL) or PD0332991 (PD) by oral administration. Error bars, SEM ($n = 3-6$ mice). **B**, Left, IHC of tumors dissected after treatment and stained for the indicated proteins. Right, graphs showing scores of positive (+ve) cells per 0.5 mm² area for each marker; mean \pm SEM ($n = 3$) for each of three separate tumors from different mice per cell line and treatment (T1-T3). **C**, Graphs showing relative mRNA levels for the indicated genes in tumors after treatment, as determined by qRT-PCR. Means \pm SEM ($n = 3$), for each of three separate tumors from different mice per cell line and treatment (T1-T3).

corroborates our recent findings that Ki-67 protein expression is maintained in nonproliferating cells mutated for the *Fzr1* gene, which encodes the CDH1 activator of the mitotic/G1 ubiquitin ligase, APC/C. Eliminating both RB and APC/C-CDH1 bypasses CDK4/CDK6 inhibition in breast cancer cells, and their combined gene knockout in nematodes circumvents the requirement for CDK4 (43). Thus, CDK4/CDK6 inhibition might both prevent Ki-67 transcription and promote its degradation. The mechanisms regulating Ki-67 expression link it to the cell cycle, resulting in maximal Ki-67 levels in mitosis and minimal Ki-67 levels in late G₁. In cancer cells, inhibition of entry into S-phase strictly correlates with downregulation of Ki-67. Although tumor explants with inactivated RB, which do not respond to PD0332991, have a higher initial Ki-67 index (17), we find that in CCLE data, Ki-67 expression does not generally correlate with PD0332991 sensitivity. However, we confirmed *in vivo* that PD0332991 treatment abrogates Ki-67

expression only when it abolishes cell proliferation. This provides a rationale for using Ki-67 expression as a biomarker to measure responses to PD0332991 or other CDK4/CDK6 inhibitors currently under development. Indeed, recent phase II trials with one such inhibitor, abemaciclib, found that it significantly reduced Ki-67 expression in patients with untreated early-stage breast cancer (44). Our data confirm that this reliably indicates reduced cell proliferation.

It has long been assumed that Ki-67 is essential for cell proliferation, and several previous studies have supported this notion (45-50). However, using mice mutant for Ki-67, we recently demonstrated that, rather than controlling cell proliferation directly, Ki-67 is required to organise heterochromatin in proliferating cells (11). Nevertheless, Ki-67 downregulation using oncolytic viruses armed with Ki-67 shRNA decreased tumor growth in xenograft experiments in immunodeficient mice (50). Taken together, this suggests that even if Ki-67 is not

required for cell proliferation directly, it might promote tumorigenesis. Further analysis will be required to determine whether Ki-67 expression is required for tumorigenesis and its biochemical mechanisms of action.

Taken together, our results show that the average level of Ki-67 mRNA and protein in proliferating cells is similar and independent of cell type, and its levels in any one cell depend on the cell-cycle phase. In all circumstances examined, including CDK4/CDK6 inhibition, loss of Ki-67 reflected loss of cell proliferation. Thus, Ki-67 expression can be used as a biomarker for inhibition of cell proliferation by CDK4/CDK6 inhibitors, and probably any drug.

Disclosure of Potential Conflicts of Interest

No potential conflicts of interest were disclosed.

Authors' Contributions

Conception and design: M. Sobceki, K. Mrouj, L. Krasinska, V. Dulic, D. Fisher
Development of methodology: J. Colinge
Acquisition of data (provided animals, acquired and managed patients, provided facilities, etc.): M. Sobceki, F. Gerbe, P. Jay, V. Dulic, D. Fisher
Analysis and interpretation of data (e.g., statistical analysis, biostatistics, computational analysis): M. Sobceki, J. Colinge, F. Gerbe, P. Jay, V. Dulic, D. Fisher
Writing, review, and/or revision of the manuscript: J. Colinge, L. Krasinska, V. Dulic, D. Fisher

Administrative, technical, or material support (i.e., reporting or organizing data, constructing databases):
Study supervision:

Acknowledgments

The authors thank the members of the Fisher laboratory for helpful discussions, technical staff of MRI imaging facility and IGMM and IGF mouse facilities, IRCM Cell culture unit of Montpellier SIRIC (INCa-DGOS-Inserm 6045) for cell lines, Karim Chebli and Susan Prieto for help with xenograft experiments, and Benedicte Lemmers and Susana Prieto for help with immunohistochemistry.

Grant Support

This work was supported by grants from the GEFLUC LR, Agence Nationale de la Recherche (ANR-09-BLAN-0252) and the Ligue Nationale contre le Cancer (EL2010.LNCC/DF and EL2013.LNCC/DF; all to D. Fisher). Further funding was provided by Worldwide Cancer Research (16-0006 to D. Fisher). M. Sobceki was supported by the Ligue Nationale Contre le Cancer and by the Fondation pour la Recherche Médicale. K. Mrouj was supported by the Ligue Nationale contre le Cancer. J. Colinges was supported by the Fondation ARC pour la Recherche sur le Cancer (PJA 20141201975).

The costs of publication of this article were defrayed in part by the payment of page charges. This article must therefore be hereby marked *advertisement* in accordance with 18 U.S.C. Section 1734 solely to indicate this fact.

Received March 11, 2016; revised April 8, 2016; accepted March 2, 2017; published OnlineFirst March 10, 2017.

References

- Cuzick J, Dowsett M, Pineda S, Wale C, Salter J, Quinn E, et al. Prognostic value of a combined estrogen receptor, progesterone receptor, Ki-67, and human epidermal growth factor receptor 2 immunohistochemical score and comparison with the Genomic Health recurrence score in early breast cancer. *J Clin Oncol* 2011;29:4273-8.
- Dowsett M, Nielsen TO, A'Hern R, Bartlett J, Coombes RC, Cuzick J, et al. Assessment of Ki67 in breast cancer: recommendations from the International Ki67 in Breast Cancer working group. *J Natl Cancer Inst* 2011;103:1656-64.
- Hao S, He Z-X, Yu K-D, Yang W-T, Shao Z-M. New insights into the prognostic value of Ki-67 labeling index in patients with triple-negative breast cancer. *Oncotarget* 2016;7:24824-31.
- Wang W, Wu J, Zhang P, Fei X, Zong Y, Chen X, et al. Prognostic and predictive value of Ki-67 in triple-negative breast cancer. *Oncotarget* 2016;7:31079-87.
- Endl E, Gerdes J. The Ki-67 protein: fascinating forms and an unknown function. *Exp Cell Res* 2000;257:231-7.
- Bruno S, Darzynkiewicz Z. Cell cycle dependent expression and stability of the nuclear protein detected by Ki-67 antibody in HL-60 cells. *Cell Prolif* 1992;25:31-40.
- Pei DS, Qian GW, Tian H, Mou J, Li W, Zheng JN. Analysis of human Ki-67 gene promoter and identification of the Sp1 binding sites for Ki-67 transcription. *Tumour Biol* 2012;33:257-66.
- Tian H, Qian GW, Li W, Chen FF, Di JH, Zhang BF, et al. A critical role of Sp1 transcription factor in regulating the human Ki-67 gene expression. *Tumour Biol* 2011;32:273-83.
- Ren B, Cam H, Takahashi Y, Volkert T, Terragni J, Young RA, et al. E2F integrates cell cycle progression with DNA repair, replication, and G(2)/M checkpoints. *Genes Dev* 2002;16:245-56.
- Ishida S, Huang E, Zuzan H, Spang R, Leone G, West M, et al. Role for E2F in control of both DNA replication and mitotic functions as revealed from DNA microarray analysis. *Mol Cell Biol* 2001;21:4684-99.
- Sobceki M, Mrouj K, Camasses A, Parisi N, Nicolas E, Llères D, et al. The cell proliferation antigen Ki-67 organises heterochromatin. *eLife* 2016;5:e13722.
- Cuylen S, Blaukopf C, Politi AZ, Müller-Reichert T, Neumann B, Poser I, et al. Ki-67 acts as a biological surfactant to disperse mitotic chromosomes. *Nature* 2016;535:308-12.
- Cidado J, Wong HY, Rosen DM, Cimino-Mathews A, Garay JP, Fessler AG, et al. Ki-67 is required for maintenance of cancer stem cells but not cell proliferation. *Oncotarget* 2016;7:6281-93.
- Malumbres M, Sotillo R, Santamaria D, Galan J, Cerezo A, Ortega S, et al. Mammalian cells cycle without the D-Type cyclin-dependent kinases Cdk4 and Cdk6. *Cell* 2004;118:493-504.
- Choi YJ, Li X, Hydbring P, Sanda T, Stefano J, Christie AL, et al. The requirement for cyclin D function in tumor maintenance. *Cancer Cell* 2012;22:438-51.
- Finn RS, Crown JP, Lang I, Boer K, Bondarenko IM, Kulyk SO, et al. The cyclin-dependent kinase 4/6 inhibitor palbociclib in combination with letrozole versus letrozole alone as first-line treatment of oestrogen receptor-positive, HER2-negative, advanced breast cancer (PALOMA-1/TRIO-18): a randomised phase 2 study. *Lancet Oncol* 2015;16:25-35.
- Dean JL, McClendon AK, Hickey TE, Butler LM, Tilley WD, Witkiewicz AK, et al. Therapeutic response to CDK4/6 inhibition in breast cancer defined by ex vivo analyses of human tumors. *Cell Cycle* 2012;11:2756-61.
- Colnot S, Niwa-Kawakita M, Hamard G, Godard C, Le Plenier S, Houbiron C, et al. Colorectal cancers in a new mouse model of familial adenomatous polyposis: influence of genetic and environmental modifiers. *Lab Invest* 2004;84:1619-30.
- el Marjoui F, Janssen KP, Chang BH, Li M, Hindie V, Chan L, et al. Tissue-specific and inducible Cre-mediated recombination in the gut epithelium. *Genesis* 2004;39:186-93.
- Baus F, Gire V, Fisher D, Piette J, Dulic V. Permanent cell cycle exit in G2 phase after DNA damage in normal human fibroblasts. *EMBO J* 2003;22:3992-4002.
- Gerbe F, van Es JH, Makrini L, Brulin B, Mellitzer G, Robine S, et al. Distinct ATOH1 and Neurog3 requirements define tuft cells as a new secretory cell type in the intestinal epithelium. *J Cell Biol* 2011;192:767-80.
- Marisa L, de Reyniès A, Duval A, Selves J, Gaub MP, Vescovo L, et al. Gene expression classification of colon cancer into molecular subtypes: characterization, validation, and prognostic value. *PLoS Med* 2013;10:e1001453.
- Benjamini Y, Hochberg Y. Controlling the false discovery rate: a practical and powerful approach to multiple testing. *J R Stat Soc Ser B Methodol* 1995;57:289-300.

Sobecki et al.

24. Mellacheruvu D, Wright Z, Couzens AL, Lambert J-P, St-Denis NA, Li T, et al. The CRAPome: a contaminant repository for affinity purification-mass spectrometry data. *Nat Methods* 2013;10:730–6.
25. Szklarczyk D, Franceschini A, Wyder S, Forslund K, Heller D, Huerta-Cepas J, et al. STRING v10: protein-protein interaction networks, integrated over the tree of life. *Nucleic Acids Res* 2015;43:D447–452.
26. Okamura Y, Aoki Y, Obayashi T, Tadaka S, Ito S, Narise T, et al. COXPRESdb in 2015: coexpression database for animal species by DNA-microarray and RNAseq-based expression data with multiple quality assessment systems. *Nucleic Acids Res* 2015;43:D82–86.
27. Huang da W, Sherman BT, Lempicki RA. Systematic and integrative analysis of large gene lists using DAVID bioinformatics resources. *Nat Protoc* 2009;4:44–57.
28. The Cancer Genome Atlas Network. Comprehensive molecular portraits of human breast tumours. *Nature* 2012;490:61–70.
29. Fu Z, Malureanu L, Huang J, Wang W, Li H, van Deursen JM, et al. Plk1-dependent phosphorylation of FoxM1 regulates a transcriptional programme required for mitotic progression. *Nat Cell Biol* 2008;10:1076–82.
30. Wong J, Fang G. HURP controls spindle dynamics to promote proper interkinetochore tension and efficient kinetochore capture. *J Cell Biol* 2006;173:879–91.
31. Schmidt MHH, Broll R, Bruch H-P, Finniss S, Böglar O, Duchrow M. Proliferation marker pKi-67 occurs in different isoforms with various cellular effects. *J Cell Biochem* 2004;91:1280–92.
32. Leontieva OV, Blagosklonny MV. CDK4/6-inhibiting drug substitutes for p21 and p16 in senescence: duration of cell cycle arrest and MTOR activity determine geroconversion. *Cell Cycle* 2013;12:3063–9.
33. Vassilev LT. Cell cycle synchronization at the G2/M phase border by reversible inhibition of CDK1. *Cell Cycle* 2006;5:2555–6.
34. Ly T, Ahmad Y, Shlien A, Soroka D, Mills A, Emanuele MJ, et al. A proteomic chronology of gene expression through the cell cycle in human myeloid leukemia cells. *eLife* 2014;3:e01630.
35. Ahmed D, Eide PW, Eilertsen IA, Danielsen SA, Eknæs M, Hektoen M, et al. Epigenetic and genetic features of 24 colon cancer cell lines. *Oncogenesis* 2013;2:e71.
36. Barretina J, Caponigro G, Stransky N, Venkatesan K, Margolin AA, Kim S, et al. The cancer cell line encyclopedia enables predictive modelling of anticancer drug sensitivity. *Nature* 2012;483:603–7.
37. Finn RS, Dering J, Conklin D, Kalous O, Cohen DJ, Desai AJ, et al. PD 0332991, a selective cyclin D kinase 4/6 inhibitor, preferentially inhibits proliferation of luminal estrogen receptor-positive human breast cancer cell lines in vitro. *Breast Cancer Res* 2009;11:R77.
38. Bullwinkel J, Baron-Luhr B, Ludemann A, Wohlenberg C, Gerdes J, Scholzen T. Ki-67 protein is associated with ribosomal RNA transcription in quiescent and proliferating cells. *J Cell Physiol* 2006;206:624–35.
39. Rodgers JT, King KY, Brett JO, Cromie MJ, Charville GW, Maguire KK, et al. mTORC1 controls the adaptive transition of quiescent stem cells from G0 to G1(Alert). *Nature* 2014;510:393–6.
40. Lord CJ, Ashworth A. The DNA damage response and cancer therapy. *Nature* 2012;481:287–94.
41. Kreso A, O'Brien CA, van Galen P, Gan OI, Notta F, Brown AM, et al. Variable clonal repopulation dynamics influence chemotherapy response in colorectal cancer. *Science* 2013;339:543–8.
42. Marusyk A, Tabassum DP, Altmann PM, Almendro V, Michor F, Polyak K. Non-cell-autonomous driving of tumour growth supports sub-clonal heterogeneity. *Nature* 2014;514:54–8.
43. The I, Ruijtenberg S, Bouchet BP, Cristobal A, Prinsen MBW, van Mourik T, et al. Rb and FZR1/Cdh1 determine CDK4/6-cyclin D requirement in C. elegans and human cancer cells. *Nat Commun* 2015;6:5906.
44. Hurvitz S, Abad MF, Rostorfer R, Chan D, Egle D, Huang C-S, et al. Interim results from neoMONARCH: A neoadjuvant phase II study of abemaciclib in postmenopausal women with HR + /HER2- breast cancer (BC). *Ann Oncol* 2016;27: LBA13.
45. Schluter C, Duchrow M, Wohlenberg C, Becker MH, Key G, Flad HD, et al. The cell proliferation-associated antigen of antibody Ki-67: a very large, ubiquitous nuclear protein with numerous repeated elements, representing a new kind of cell cycle-maintaining proteins. *J Cell Biol* 1993;123:513–22.
46. Kausch I, Lingnau A, Endl E, Sellmann K, Deinert I, Ratliff TL, et al. Antisense treatment against Ki-67 mRNA inhibits proliferation and tumor growth in vitro and in vivo. *Int J Cancer* 2003;105:710–6.
47. Starborg M, Gell K, Brundell E, Hoog C. The murine Ki-67 cell proliferation antigen accumulates in the nucleolar and heterochromatic regions of interphase cells and at the periphery of the mitotic chromosomes in a process essential for cell cycle progression. *J Cell Sci* 1996;109:143–53.
48. Rahmzadeh R, Huttmann G, Gerdes J, Scholzen T. Chromophore-assisted light inactivation of pKi-67 leads to inhibition of ribosomal RNA synthesis. *Cell Prolif* 2007;40:422–30.
49. Zheng JN, Ma TX, Cao JY, Sun XQ, Chen JC, Li W, et al. Knockdown of Ki-67 by small interfering RNA leads to inhibition of proliferation and induction of apoptosis in human renal carcinoma cells. *Life Sci* 2006;78:724–9.
50. Zheng JN, Pei DS, Mao LJ, Liu XY, Mei DD, Zhang BF, et al. Inhibition of renal cancer cell growth in vitro and in vivo with oncolytic adenovirus armed short hairpin RNA targeting Ki-67 encoding mRNA. *Cancer Gene Ther* 2009;16:20–32.

Cancer Research

The Journal of Cancer Research (1916–1930) | The American Journal of Cancer (1931–1940)

Cell-Cycle Regulation Accounts for Variability in Ki-67 Expression Levels

Michal Sobacki, Karim Mrouj, Jacques Colinge, et al.

Cancer Res 2017;77:2722-2734. Published OnlineFirst March 10, 2017.

Updated version	Access the most recent version of this article at: doi: 10.1158/0008-5472.CAN-16-0707
Supplementary Material	Access the most recent supplemental material at: http://cancerres.aacrjournals.org/content/suppl/2017/03/10/0008-5472.CAN-16-0707.DC1

Cited articles	This article cites 50 articles, 10 of which you can access for free at: http://cancerres.aacrjournals.org/content/77/10/2722.full#ref-list-1
Citing articles	This article has been cited by 1 HighWire-hosted articles. Access the articles at: http://cancerres.aacrjournals.org/content/77/10/2722.full#related-urls

E-mail alerts	Sign up to receive free email-alerts related to this article or journal.
Reprints and Subscriptions	To order reprints of this article or to subscribe to the journal, contact the AACR Publications Department at pubs@aacr.org .
Permissions	To request permission to re-use all or part of this article, use this link http://cancerres.aacrjournals.org/content/77/10/2722 . Click on "Request Permissions" which will take you to the Copyright Clearance Center's (CCC) Rightslink site.

III. Ki-67: a new important player in cancerogenesis

1. The ablation of Ki-67 affects the transforming potential of Ras in mouse cells

Previous results from our team showed that Ki-67 knockdown strongly hindered growth of tumours from HeLa cells in nude mice. This suggested that although Ki-67 is not required for cell proliferation *in vitro* and Ki-67 mutant animals are healthy, Ki-67 might be specifically required in cancers. If so, Ki-67 would be a potential therapeutic target. We therefore wished to determine which stages of carcinogenesis might be affected by loss of Ki-67, *in vitro* and *in vivo*.

In 3T3 cells, Ras activation alone transforms cells, promoting proliferation, loss of contact inhibition and the acquisition of anchorage-independent growth that can be visualised as multi-layered foci ⁹⁶. We tested whether the absence of Ki-67 would affect the transforming potential of Ras using our Ki-67 TALEN-mutant 3T3 cells. For this, we used a mutant form of Ras (Ras G12V) that can be permanently active within the cell. 3T3 Wild-type (WT) and two Ki-67 TALEN-mutant clones were transduced with either empty control retroviruses or H-Ras-G12V expressing retroviruses. Following cell transduction, we first verified Ras G12V expression by western blot analysis using a specific anti-Ras antibody capable of recognizing this specific Ras G12V mutation. The results showed that Ras G12V was similarly expressed by 3T3 WT and Ki-67 TALEN-mutant clones (**fig.12A**). We then assessed cell transformation in response to Ras activation through the ability of transformed cells to grow in dense multi-layered foci that can be visualized by crystal violet staining.

In WT cells, overexpression of Ras led to the production of visible, well-defined colonies, as revealed by crystal violet staining. In contrast, colony number and size were strongly reduced in both Ki-67-mutant clones tested (**fig.12B**), indicating that the transforming potential of Ras in these mutants was strongly reduced. These results suggest that Ki-67 is required in order for Ras to transform immortalised cells. This preliminary result indicates that Ki-67 might be specifically required for tumour initiation and progression.

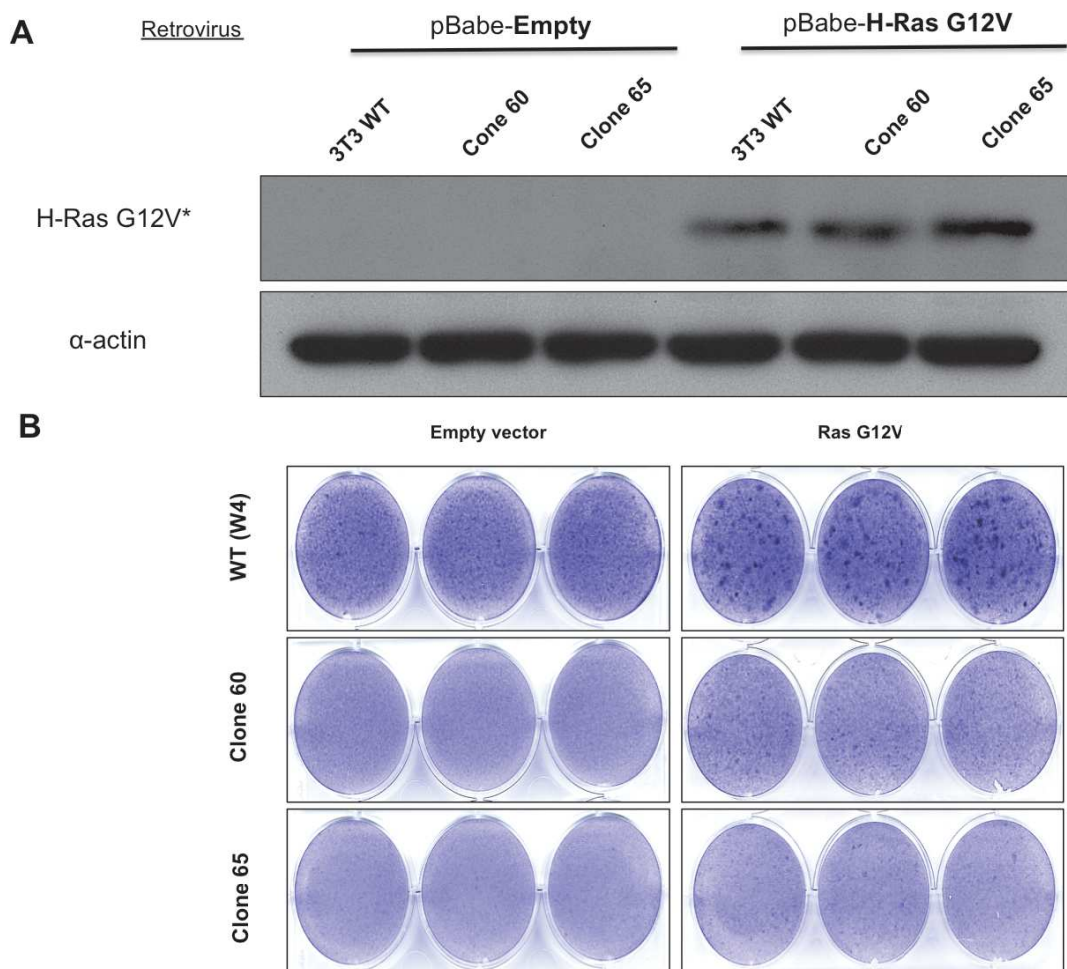


Figure 12: Ki-67 ablation affects the transforming capacity of oncogenic Ras.

(A) Western blot analysis of H-Ras G12V expression in 3T3 wild-type (WT) & Ki-67-TALEN mutant cells (clone 60 & 65) transduced with either an empty or H-Ras G12V expressing retroviruses using an anti-Ras G12V mutant specific antibody. Actin expression served as loading control. (B) 3T3 wild-type & Ki-67 mutant cells (clones 60 & 65) transduced with either an empty or H-Ras G12V expressing retroviruses were grown following cell transduction for 2 weeks and then were fixed and stained for focus formation (dark violet foci) by crystal violet.

2. Ki-67 depletion can protect mice from intestinal carcinogenesis

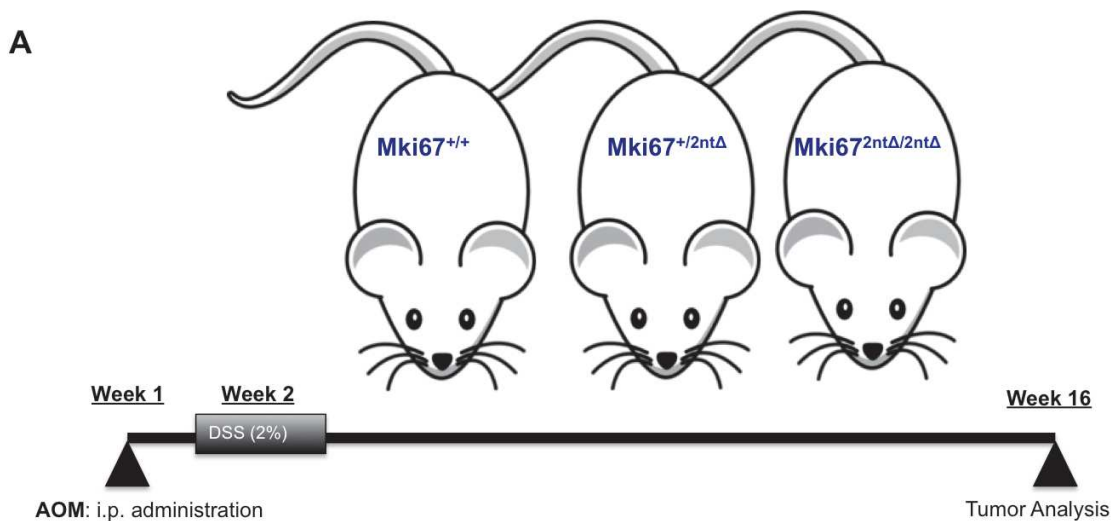
2.1. Ki-67 depletion inhibits the development of colonic neoplasms in AOM-DSS treated mice

Using our TALEN-mediated Ki-67 germline mutant mice ($Mki67^{2nt\Delta/2nt\Delta}$), we asked whether disruption of Ki-67 could protect mice against initiation and/or progression of tumours.

To answer this question we first used a chemically induced model of colorectal cancer (CRC), one of the most frequent and aggressive human malignancies. In this chemically induced CRC model, the combination of one single injection of the pro-

carcinogen azoxymethane (AOM) with the inflammatory agent dextran sodium sulphate (DSS) was shown to induce CRC in mice. Several studies have revealed that tumours induced in mice following AOM-DSS exposure share the same patterns as seen in humans, demonstrating the relevance of this model for investigating mechanisms that underlay human CRC^{97, 98}. Similarly to the human CRC, the canonical Wnt signalling pathway in tumours from the AOM-DSS model is altered, resulting in aberrant accumulation of β -catenin in colonic neoplasms as documented in immuno-histochemical (IHC) analysis of these tumours^{97, 98}. Nevertheless, AOM-DSS induced colon tumours do not display mucosal invasiveness or metastatic capacities^{97, 98}.

Using this CRC model, we subjected the different mouse groups ($Mki67^{+/+}$; $Mki67^{+/2nt\Delta}$ & $Mki67^{2nt\Delta/2nt\Delta}$) to a single injection of AOM (10mg/Kg) followed by a single cycle of 2% DSS in drinking water for one week. We recovered then the colons at week-16 post AOM injection from the different mouse groups (**fig.13A**) and compared tumour development using β -catenin IHC analysis (**fig.13B**). Quantification of total neoplastic lesions and tumorigenic area count showed a strong decrease of the colonic neoplasms seen in the $Mki67^{2nt\Delta/2nt\Delta}$ group compared to both $Mki67^{+/+}$ and $Mki67^{+/2nt\Delta}$ mouse groups (**fig.13C**). This important result indicates that Ki-67 depletion can protect mice from developing tumours following AOM-DSS treatment, suggesting a specific role of Ki-67 in tumour initiation and/or development.



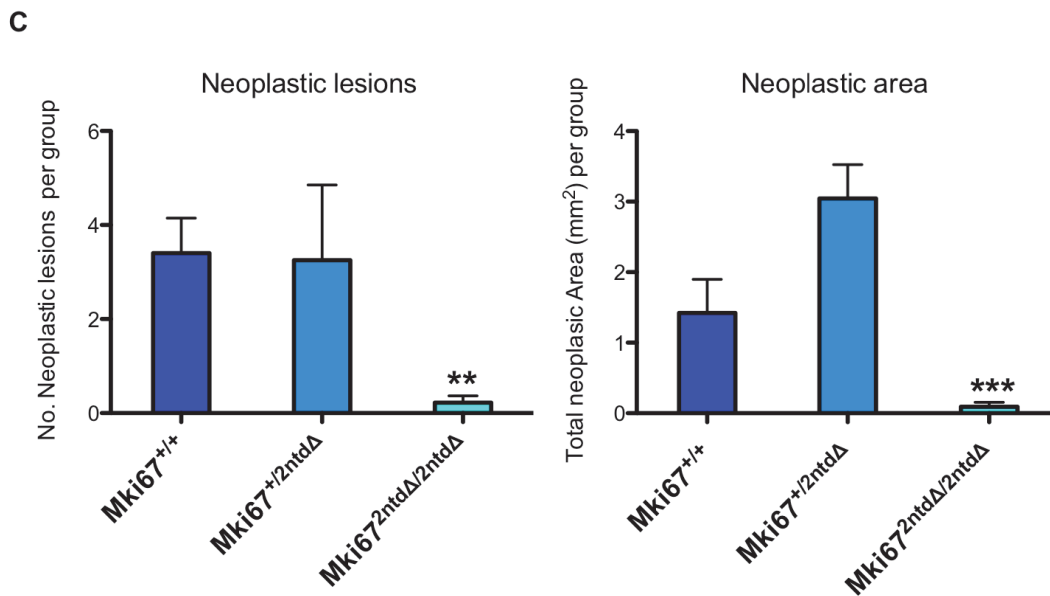
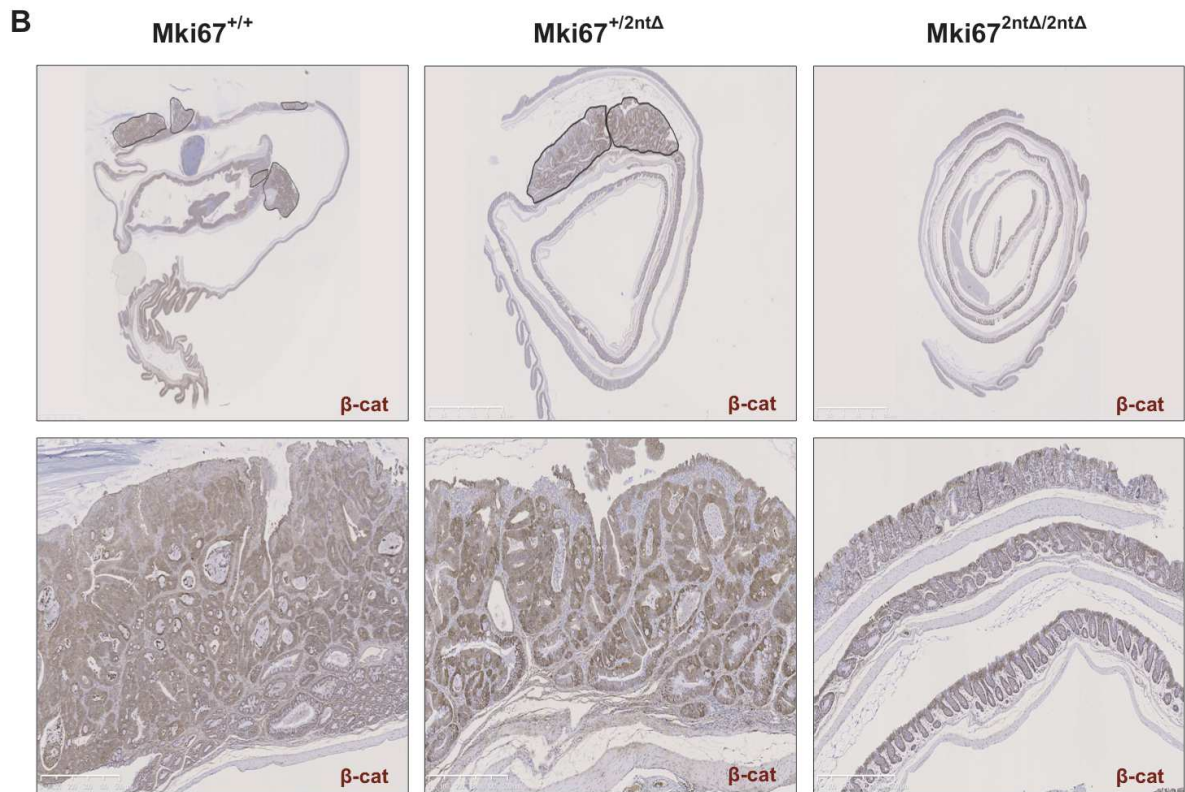


Figure 13: Ki-67 depletion inhibits the development of colonic neoplasms in AOM-DSS treated mice.

(A) scheme of AOM-DSS induced colorectal cancer (CRC) model. Mice (Mki67^{+/+}; Mki67^{+/2ntΔ} and Mki67^{2ntΔ/2ntΔ}) were first subjected to a single intraperitoneal (i.p) injection of AOM (10mg/Kg) followed by a single cycle of 2% DSS before recovering the colons at week-16 post treatment. (B) Representative IHC analysis of β -catenin (β -cat) expression in whole colons recovered from each group at week-16 post AOM-DSS treatment. The dark brown staining indicates the accumulation of B-cat in all neoplastic lesions (upper panels, scale bar; 2.5mm). High power field of one tumorigenic area showing the accumulation of β -cat at the nuclei (lower panels, scale bar; 500um). (C) Quantification of total neoplastic lesions (left) and tumorigenic area count (right) in each experimental group. Error bars indicate the standard error of the mean. **P=0.0055, ***P=0.0007 (ANOVA).

2.2. Ki-67 depletion affects the formation of intestinal neoplasms in the Apc^{d14} mouse model

Using this time a genetic model for intestinal carcinogenesis, we wanted to test whether Ki-67 depletion could affect tumour development in the adenomatous polyposis coli (*Apc*) mouse model. The APC tumour suppressor gene is crucial for intestinal homeostasis, and inactivation of this gene is considered as the initial event in human CRC development. In fact, loss of *Apc* in mice leads to a constitutive accumulation of β -catenin and aberrant Wnt signalling pathway resulting therefore in the malignant transformation of intestinal cells⁹⁹. Among the different *Apc* mutant mice, we used a model of germline *Apc* invalidation⁹⁹, where the exon 14 of one allele is deleted (Apc^{+d14}). To investigate whether Ki-67 could affect the development of intestinal carcinogenesis in this model, we crossed the Apc^{+d14} mice to either $Mki67^{+/2nt\Delta}$ or $Mki67^{2nt\Delta/2nt\Delta}$ mice in order to generate two groups ($Apc^{+d14}/Mki67^{+/2nt\Delta}$ and $Apc^{+d14}/Mki67^{2nt\Delta/2nt\Delta}$), both bearing the Apc^{d14} mutation, and differing only in Ki-67 expression. Indeed, the loss of the *Apc* wild-type allele in these mice will trigger intestinal carcinogenesis during their lifetime.

After 6-7 months from their birth, we compared tumour development throughout the intestine using IHC analysis of β -catenin (**fig.14A**). Although in both groups intestinal lesions were observed in the small and large intestines, quantification of neoplastic lesions and total neoplastic area per mouse showed a reduction of intestinal neoplasms in the $Apc^{+d14}/Mki67^{2nt\Delta/2nt\Delta}$ mice compared to $Apc^{+d14}/Mki67^{+/2nt\Delta}$ (**fig.14B**). This result suggests that depletion of Ki-67 in this Apc^{d14} model had affected the formation and development of intestinal tumours.

Together, findings in both the AOM-DSS and Apc^{d14} mouse models revealed that Ki-67 presence was required for efficient tumour initiation and development.

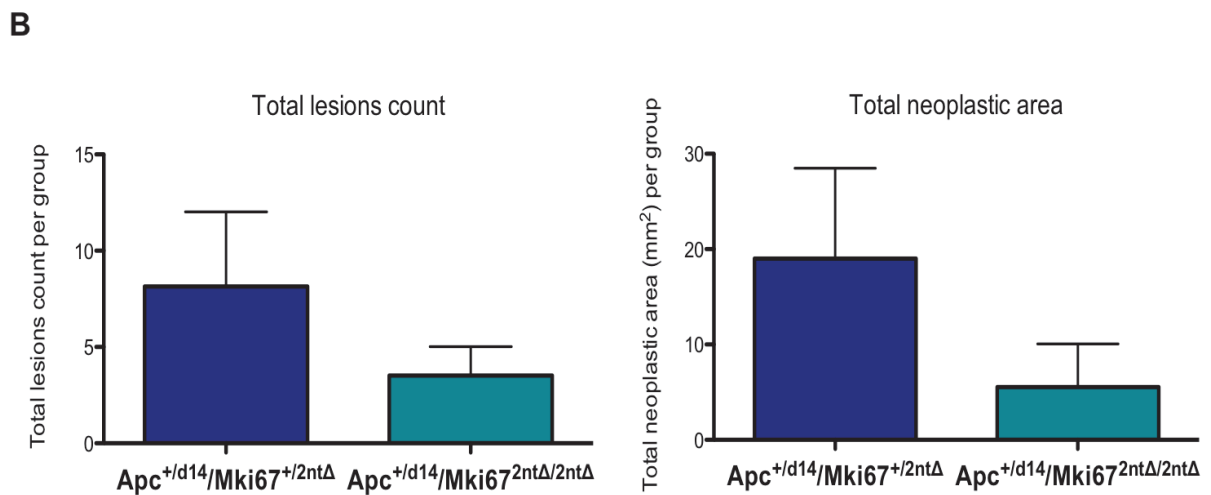
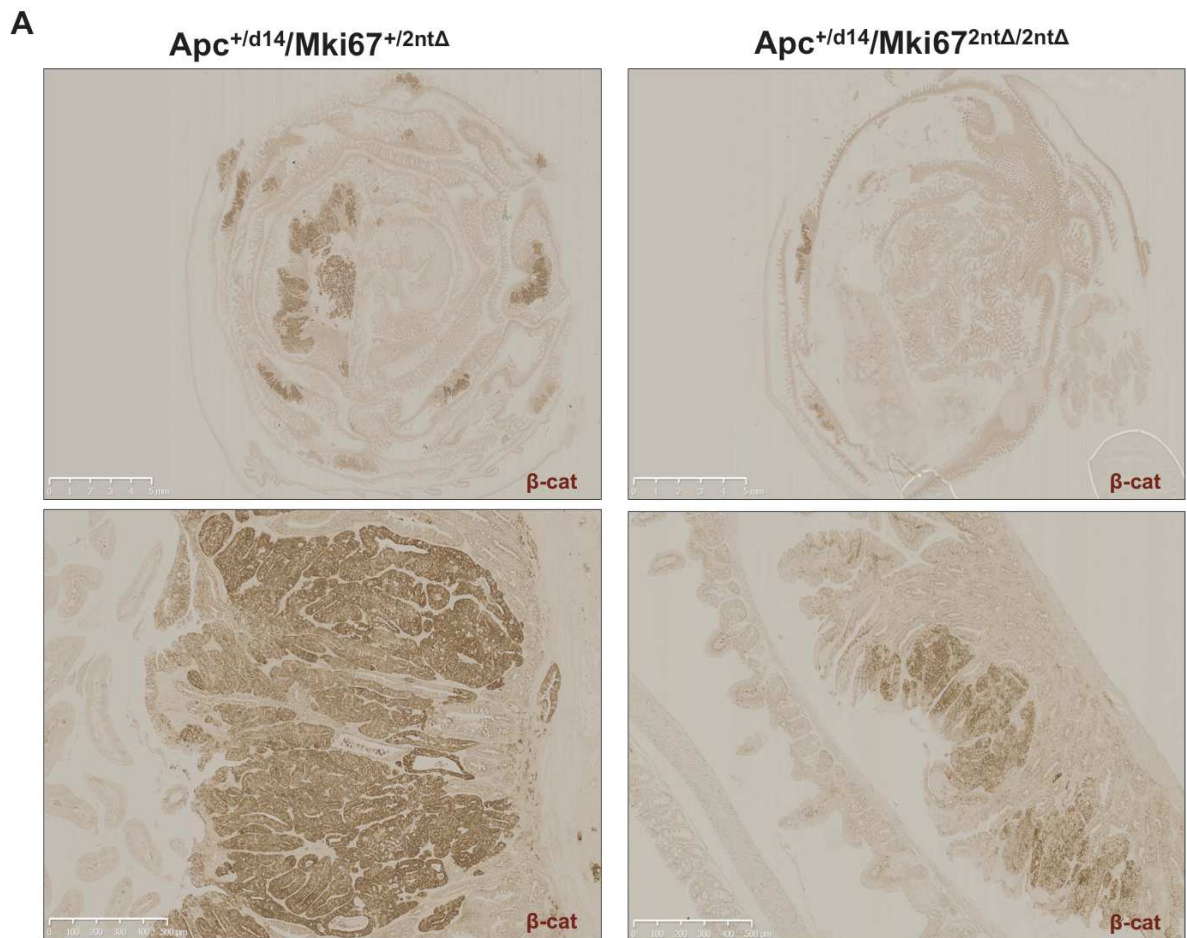


Figure 14: Ki-67 depletion affects the formation of intestinal neoplasms in the Apc^{d14} mouse model. **(A)** Representative IHC of B-catenin (β-cat) expression in whole intestine swiss-roll from 6-7 old-months Apc^{+d14}/Mki67^{+2ntΔ} and Apc^{+d14}/Mki67^{2ntΔ/2ntΔ} mice. The dark brown staining indicates the accumulation of β-cat in all neoplastic lesions (upper panels, scale bar; 5mm). High power field of one tumorigenic area showing the accumulation of β-cat at the nuclei (lower panels, scale bar; 500um). **(B)** Quantification of total neoplastic lesions (left) and tumorigenic area count (right) in each experimental group. Error bars indicate the standard error of the mean.

3. Ki-67 depletion does not affect the chemically acute induced intestinal inflammation in mice

During intestinal carcinogenesis, inflammation provides promoting stimuli and mediators, which in turn favour a more tumour prone microenvironment⁹⁸. Indeed, we asked whether the strong decrease in intestinal neoplasms seen in our models upon Ki-67 depletion was due to a defect in the inflammatory-associated response. To answer this question, we used a chemically induced intestinal inflammation, by subjecting either Mki67^{+/-2ntΔ} or Mki67^{2ntΔ/2ntΔ} to DSS via drinking water to trigger an inflammatory response. DSS exposure induces weight loss, but, most importantly, results in epithelial injury that compromises the barrier integrity. This subsequently exposes mucosal and submucosal immune cells to luminal antigens (e.g., bacterial antigens), resulting in a rapid and profound inflammatory immune response¹⁰⁰. To trigger this response, the mice were treated with DSS for 8 consecutive days followed by a 3-day rest period. Body weight of the mice was monitored during the treatment period before euthanasia (day-11) to assess the degree of intestinal inflammation. The results showed that DSS induced weight loss similarly in both mouse groups tested (**fig.15A**). More importantly, H&E-stained sections of the colons revealed histological alterations (i.e. colonic crypt loss) and disruption of the colonic mucosal barrier (i.e. immune cells infiltration) in both mouse groups (**fig.15B**), indicating an inflammatory-mediated response. These findings suggest that the refractory response to AOM-DSS treatment in Mki67^{2ntΔ/2ntΔ} mice or the reduction of intestinal neoplasms observed in Apc^{+/-d14}/Mki67^{2ntΔ/2ntΔ} mice was not caused by a defect in the inflammatory induction that is required for promoting tumour growth in these mouse tumour models.

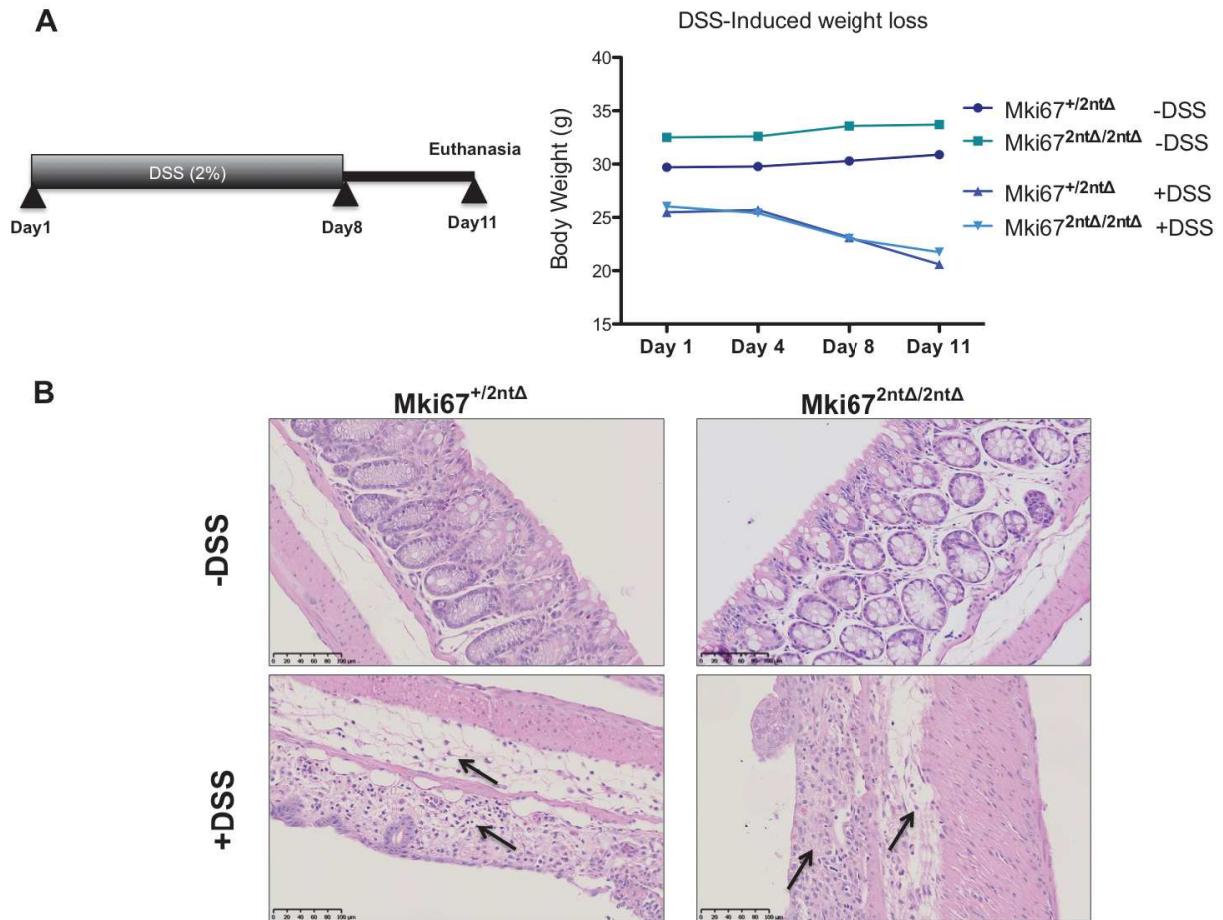


Figure 15: Ki-67 depletion does not affect the chemically acute induced intestinal inflammation in mice.

(A) To trigger an intestinal inflammation, Mki67^{+/2ntΔ} and Mki67^{2ntΔ/2ntΔ} mice were treated (+DSS) for 8 consecutive days followed by a 3-day rest period. Body weight of the mice was monitored during the treatment period before euthanasia (day11) to assess the degree of intestinal inflammation. A control without (-DSS) treatment was also included for each group. (B) Representative Haematoxylin & Eosin (H&E)-stained sections of the colonic mucosa showing histological alterations (i.e. colonic crypt loss, arrow) and disruption of the mucosal barrier (i.e. immune cells infiltration, arrow) in both groups following DSS-treatment (lower panels). Scale bar; 100um

4. Ki-67 is required for tumour development and establishment of metastasis

4.1. Ki-67 is dispensable for 4T1 cell proliferation

To further investigate the role of Ki-67 in cancer initiation and progression, we chose the mouse 4T1 breast cancer model. 4T1 is a transplantable mammary carcinoma cell line derived from Balb/c mice, that it is easily transplanted into the mammary gland. It is highly tumorigenic and as seen in the human disease, 4T1 tumours are able to spontaneously metastasize from the primary tumour in the mammary gland to

multiple distant sites including lymph nodes, blood, liver, lung, brain, and bone¹⁰¹.

To see if Ki-67 is required for 4T1 cells to establish tumours and/or metastasise in mice following tumour cell injection, we generated a 4T1 Ki-67 mutant cell line using a CRISPR/Cas9 mediated genome-editing approach. To do this, we engineered lentiviruses encoding sgRNA targeting specifically a sequence found in exon 3 of the murine Mki67 (**fig.16A**). We also engineered lentiviruses encoding a non-targeting sgRNA, which serves as a control for Ki-67 targeting. Following 4T1 transduction with these lentiviruses, we selected for CRISPR/Cas9 activity using puromycin. Resistant cells were then isolated and were seeded as a single cell clones in 96 well-plate. To test Mki67 targeting in 4T1 Cells, we screened clones for Ki-67 expression by immunofluorescence using automated high-content microscopy. 6 out of 100 clones tested showed a >95% decrease in Ki-67 staining compared to the control. We amplified 3 of these 6 clones and re-tested for Ki-67 expression by immunoblotting and qRT-PCR, confirming loss of Ki-67 expression (**fig.16B, D**). We sequenced the targeted genomic DNA (gDNA) region of these 3 clones (101, 117 & 119), which revealed a 5 nucleotides bi-allelic deletion in exon 3, that resulted in Mki67 knock out (**fig.16C**). We then tested whether Ki-67 depletion could affect the proliferative potential of 4T1 cells, by performing an EdU incorporation assay to directly measure active DNA synthesis in these engineered cells. As expected, there was no difference in EdU incorporation for 2h or 22h between 4T1 control (CTRL) and Ki-67-mutant clones (**fig.16E**), demonstrating that Ki-67 ablation does not affect proliferation of 4T1 cells as previously found.

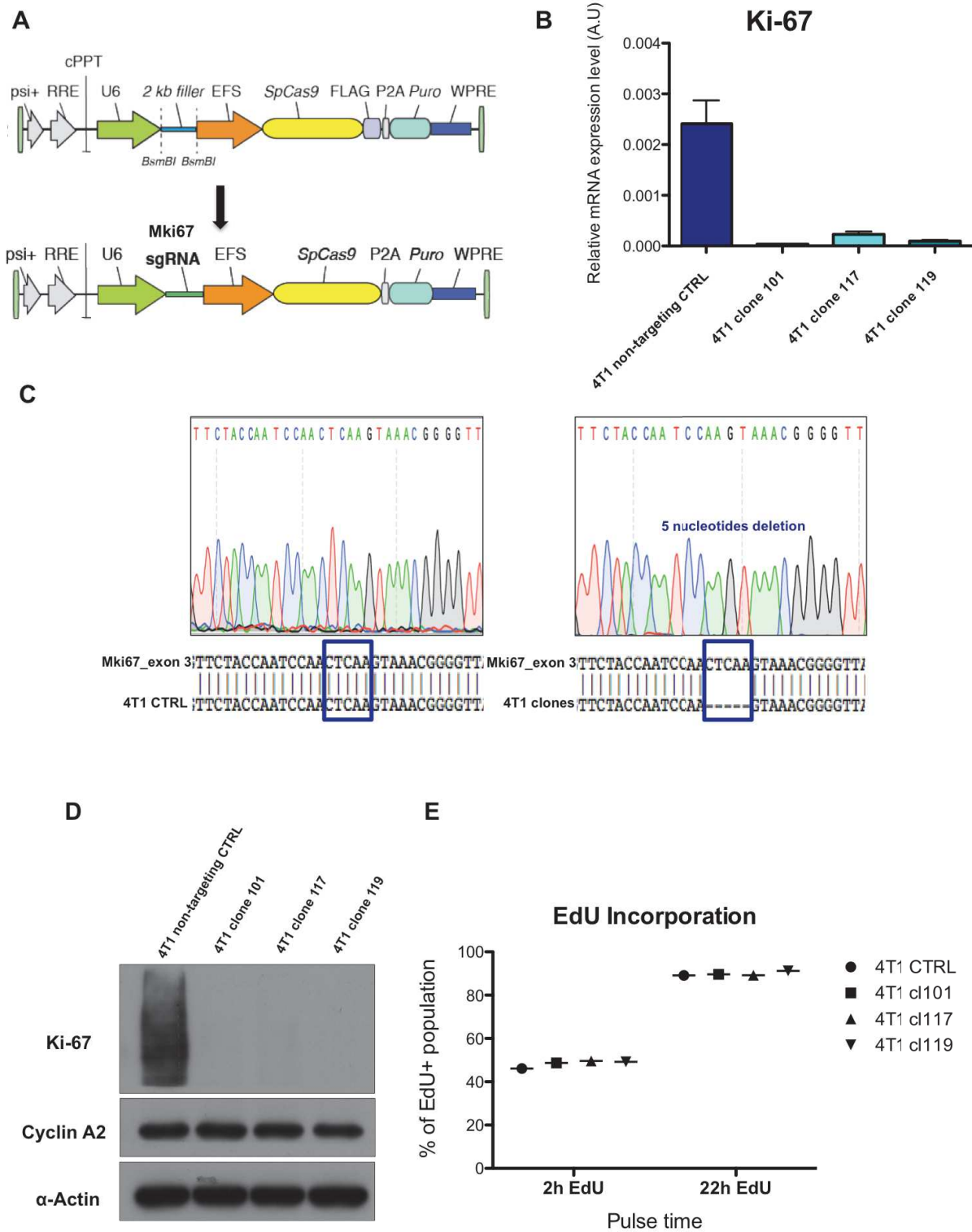


Figure 16: CRISPR/Cas9-mediated ablation of Ki-67 does not affect the proliferative capacity of 4T1 cells.

(A) Scheme of the engineered vector (LentiCRISPRv2, Addgene #52961) after cloning the sgRNA targeting a sequence found in exon 3 of the murine Mki67. (B) qRT-PCR analysis of Ki-67 mRNA expression in 4T1 control (non targeting CTRL) and selected Ki-67 mutant 4T1 clones (cl101, cl117 & cl119). (C) Sequencing results of the CRISPR/Cas9-mediated deletion at the targeted genomic region (Mki67) in Ki-67 mutant 4T1 clones indicating a 5 nucleotides bi-allelic deletion (right) at exon 3. (D) western blot analysis of Ki-67 and cyclin A2 expression in 4T1 CTRL and Ki-67 mutant 4T1 clones

(101, 117 & 119). Actin served as loading control. (E) Analysis of EdU incorporation (2h & 22h) in 4T1 CTRL and Ki-67-mutant 4T1 clones (cl101, cl117 & cl119).

4.2. Ki-67 is required for the maintenance of the stem-like properties of 4T1 cells

Next, we asked whether Ki-67 depletion could affect the cancer stem cells, which are characterized by their potential to self-renew and highest clonogenic ability to grow *in vivo* in animal tumour models⁷⁸. Many studies have shown that these cells are strongly involved in tumour initiation and development and that their presence is associated with tumour therapy resistance¹⁰². Indeed, the mammosphere assay constitutes a useful tool for the quantification of breast cancer stem cell activity and stem cell self-renewal¹⁰³.

In order to test whether the stem cell activity could be affected upon Ki-67 ablation, we used the mammosphere formation assay to quantify the formation of primary mammospheres derived from either 4T1 CTRL or Ki-67-depleted 4T1 cells.

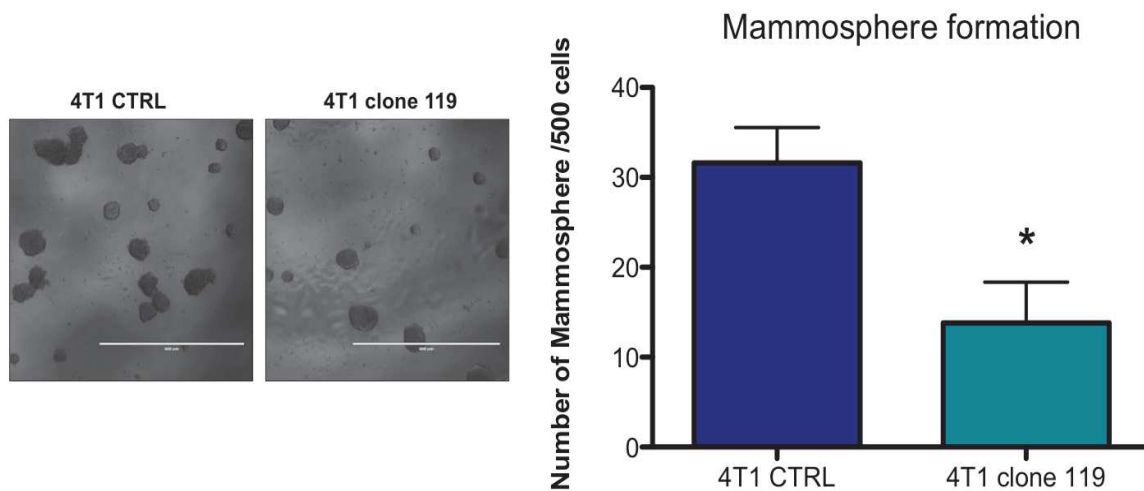
Quantification of the mammospheres formed after seven days showed a significant reduction in the number of primary mammospheres that are derived from Ki-67-depleted cells compared to CTRL cells (**fig.17A**), indicating that the stem cell activity was altered following Ki-67 depletion.

Previous studies that aimed to characterize cancer stem cells revealed that these cells exhibit a high aldehyde dehydrogenase 1 (ALDH1) activity. Furthermore ALDH1 was found to be a good marker of the stem cells of the human breast cancer and a predictor of poor clinical outcome¹⁰². Interestingly, assessment of ALDH1 activity using the 'ALDEFLUOR' test revealed that Ki-67-depleted cells displayed a marked reduction in this activity compared to CTRL cells (**fig.17B**).

These results suggest that the reduced cancer stem cell activity seen in the absence of Ki-67 could be due to a defect in stem cell self-renewal capacities. To test this, primary mammosphere derived from Ki-67-depleted 4T1 cells can be disaggregated and passaged on to determine whether continuous Ki-67 absence will result in further diminution of mammospheres during a secondary generation.

Together, these findings point toward a role of Ki-67 in promoting cancer stemness that may drive tumour growth *in vivo* through the modulation of the intrinsic features of CSCs or by supporting the niche components that host this cell population.

A



B

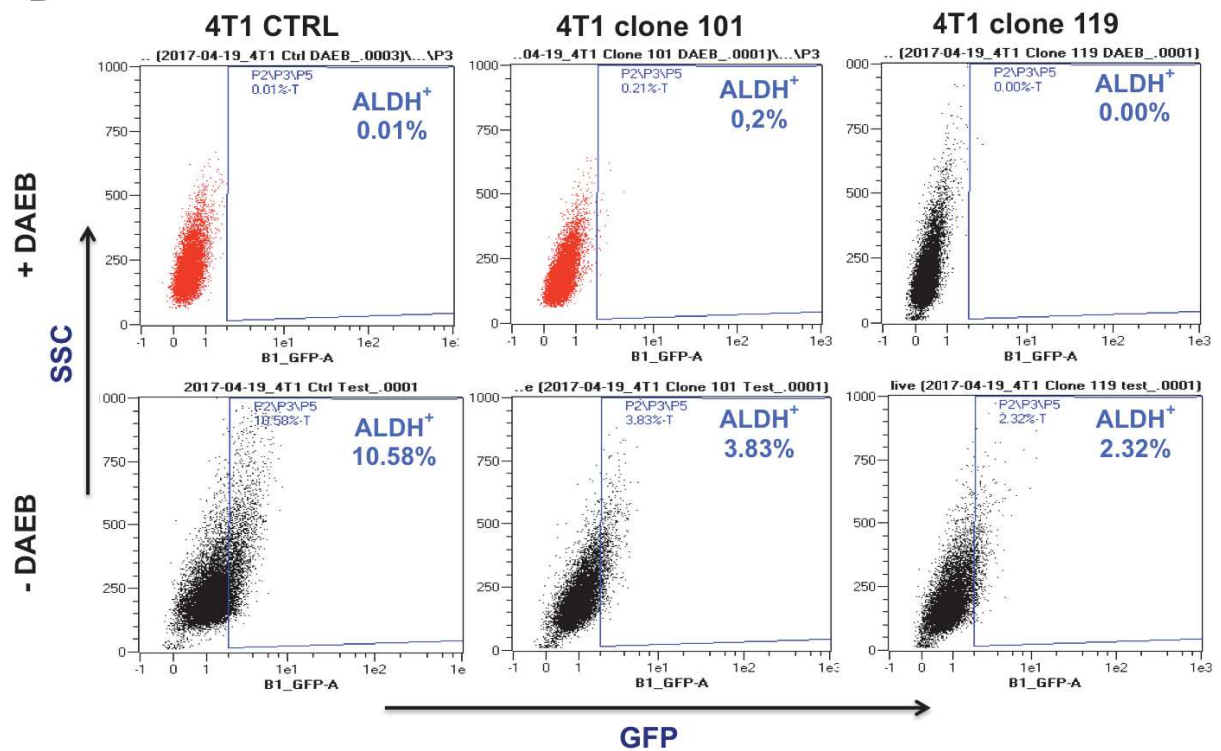


Figure 17: Ki-67 is required for the maintenance of the stem-like properties of 4T1 cells.

(A, left) Representative photographs of mammospheres from either 4T1 CTRL or Ki-67-depleted 4T1 cells (clone119) formed after 7 days of culture. (A, right) Quantification of the primary mammospheres formed after 7 days in both 4T1 CTRL or Ki-67-depleted 4T1 cells (clone 119). Error bars indicate the standard error of the mean. *P=0.0148 (Unpaired t-test). (B) ALDH1 expression was measured through flow-cytometry in 4T1 CTRL and Ki-67-depleted 4T1 clones (101 & 119) using the 'ALDEFLUOR' assay. Values mentioned along with the dot plots indicate percentage (%) of ALDH1+ population. DAEB, an inhibitor of ALDH was used as a negative control (+DAEB).

4.3. Ki-67 depletion strongly affects 4T1 tumour growth and formation of lung metastases in athymic nude mice

As mentioned earlier, the CSCs are characterized by their high ability to sustain tumour growth *in vivo* and most importantly their involvement in establishing metastasis at distant sites. Since Ki-67 depletion had affected the cancer stem population of 4T1 cells, we sought to determine whether Ki-67 might be required for tumour development and establishment of distant metastases. To test this, we transplanted orthotopically either 4T1 CTRL or Ki-67 depleted cells into the mammary fat pads of 6-8 weeks-old female athymic nude mice. Following cell transplantation, we monitored tumour growth for four weeks and lung metastases formed in these mice at the end of the experiment. Although Ki-67 absence did not impede the initial tumour establishment at the primary site following cells injection, the growth rate of these tumours was significantly impacted compared to their CTRL counterparts. Indeed, toward the end of the experiment the size of Ki-67-depleted tumours was nearly twice smaller compared to the 4T1 CTRL tumours (**fig.18A**). More importantly, assessment of formed metastasis in the lungs revealed a strong reduction in the occurrence of metastasis in the Ki-67-depleted group. Indeed, quantification of macroscopic metastasis nodules in the lungs showed that Ki-67 absence significantly impeded the formation of metastasis at this distant site (**fig.18B**). These results suggest that Ki-67 presence is required for efficient tumour development and, more importantly, for metastatic colonization of distant sites.

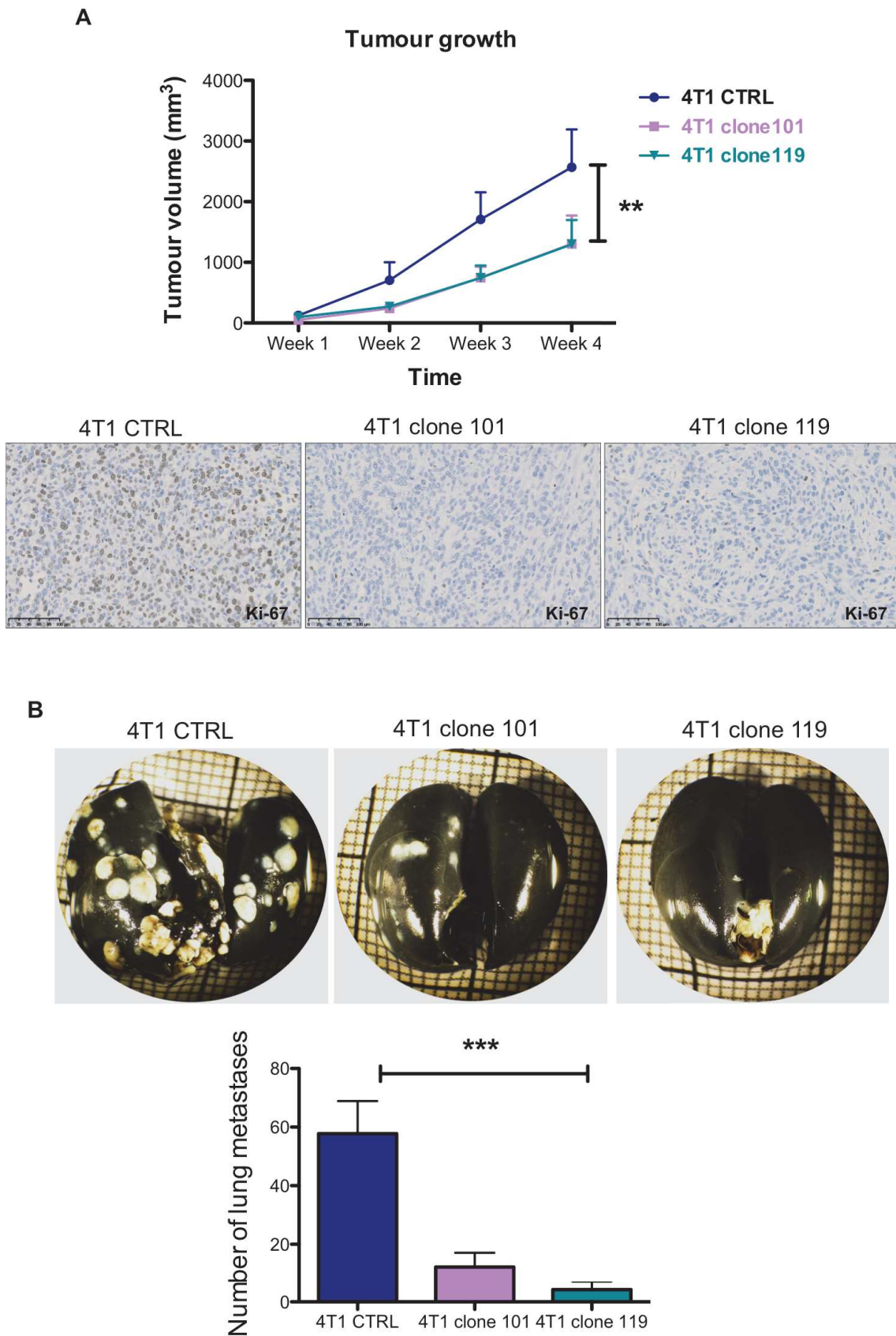


Figure 18: Ki-67 depletion strongly affects 4T1 tumour growth and formation of lung metastases in athymic nude mice.

(A) 4T1 CTRL or Ki-67 depleted cells (clones 101 & 119) were transplanted orthotopically (1.10^6 cells/mouse) into the mammary fat pad of 6-8 weeks-old female nude mice ($n=8$ in each group). (A,

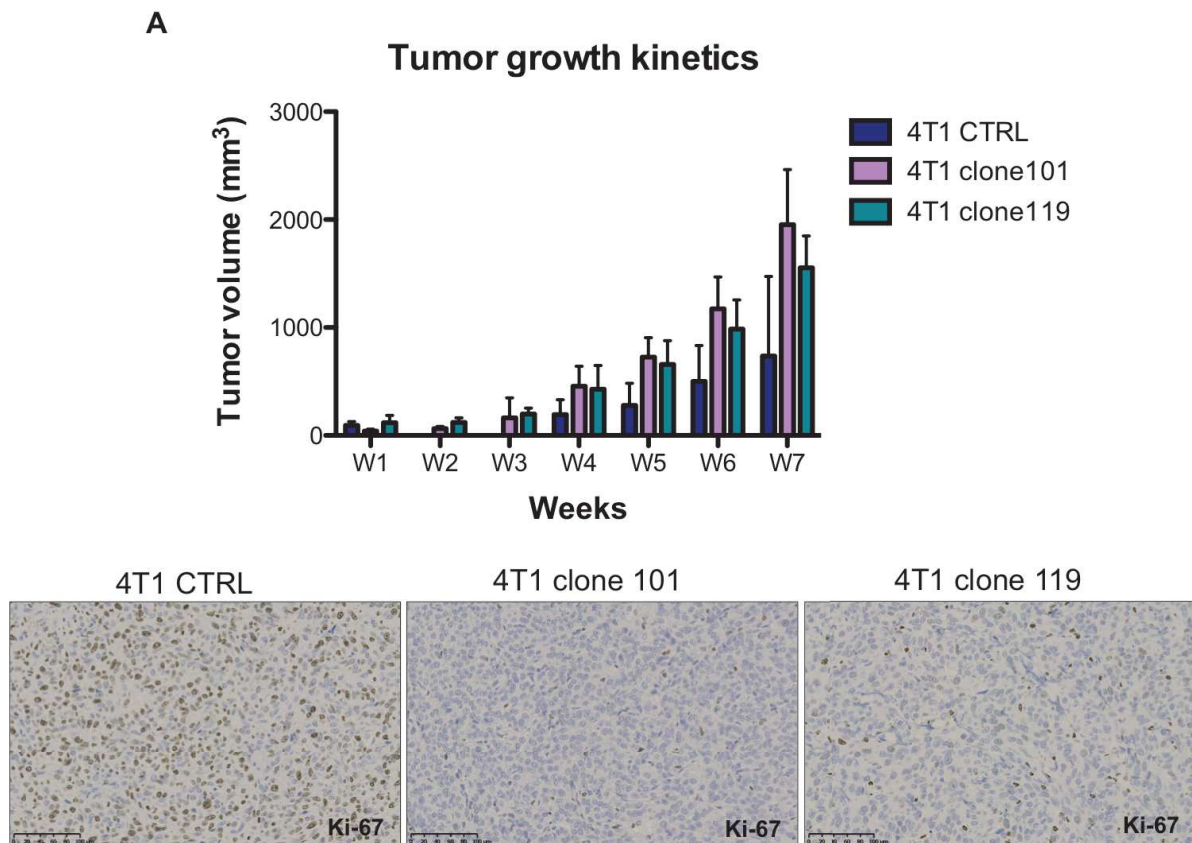
upper) Tumour growth (volume) was monitored every week over a period of 4 weeks. Error bars indicate the standard error of the mean. ****P=0.0024** (ANOVA). **(A, lower)** Representative tissue sections from each group (at week-4) analysed by IHC using an antibody against Ki-67. Scale bar; 100µm. **(B)** Lung metastasis formed at week-4 following 4T1 CTRL or Ki-67 depleted cells (clones 101 & 119) injection. **(B, upper)** Representative images of lungs stained with India ink and photographed using a digital camera. Lung metastases correspond to the white nodules on the black stained lung. Scale bar; 10mm. **(B, lower)** Quantification of lung metastases formed in each experimental group at week-4. *****P=0.0001** (ANOVA).

4.4. Ki-67 absence prevents 4T1 tumour immune-mediated response and affects lung metastasis formation in immuno-competent mice

Given that athymic nude mice previously used are known for their deficit in immune-mediated response to tumours, we wondered whether Ki-67 depletion would affect tumour growth in immuno-competent mice. Since 4T1 cells were originally derived from Balb/c mice, we transplanted orthotopically either 4T1 CTRL or Ki-67 depleted cells into the mammary fat pads of 6-8 weeks female Balb/c mice. Following cell transplantation, we monitored tumour growth for 7 weeks in addition to the metastasis nodules formed in the lungs at the end-point (i.e. Week 7). Both 4T1 CTRL and Ki-67-depleted cells displayed a rapid growth at the primary site during the first week. Similar to the previously described growth pattern¹⁰⁴, 4T1 CTRL tumours were completely cleared between week 2 and 3, before starting to grow again through week 4 to week 7, indicating that 4T1 tumour growth triggered an immune-mediated response. Surprisingly, this biphasic tumour growth pattern did not occur in Ki-67-depleted tumours. In fact, these tumours were not cleared and did grow continuously from week 1 to week 7 (**fig.19A**).

Although, in their second growth phase 4T1 CTRL tumours did not reach the size of Ki-67-depleted tumours, they displayed higher numbers of lung metastasis compared to their Ki-67-depleted counterparts at the end of the experiment (**fig.19B**). These results suggest that Ki-67 absence prevented tumour immune-mediated response in Balb/c mice. In fact, previous studies that aimed to characterize the immune landscape within 4T1 tumours showed the prevalence of highly immune suppressive sub-population (GR1⁺/CD11b⁺) of myeloid-derived suppressor cells (MDSCs) that inhibit anti-tumour immunity by suppressing T cell and NK functions^{105, 106}. This suggests that the absence of Ki-67 may allow an increasing infiltration of MDSCs in the microenvironment at least between week 2 and 3, which in turn impairs tumour

immunity, thereby preventing their clearance. Whereas in CTRL tumours this tumour-induced expansion of MDSCs did probably occur afterwards at week 4. Nevertheless, despite the differences observed regarding tumour immunity, Ki-67 ablation affected the capacity of formed primary tumours to metastasize efficiently as previously observed in immune-deficient nude mice. Indeed, analysis of lung metastases following tail vein injection of either 4T1 CTRL or Ki-67-depleted (clone 119) cells in 6-8 weeks female Balb/c mice showed a strong reduction of pulmonary metastasis burden in mice injected with Ki-67-depleted cells compared to the CTRL group (fig.19C).



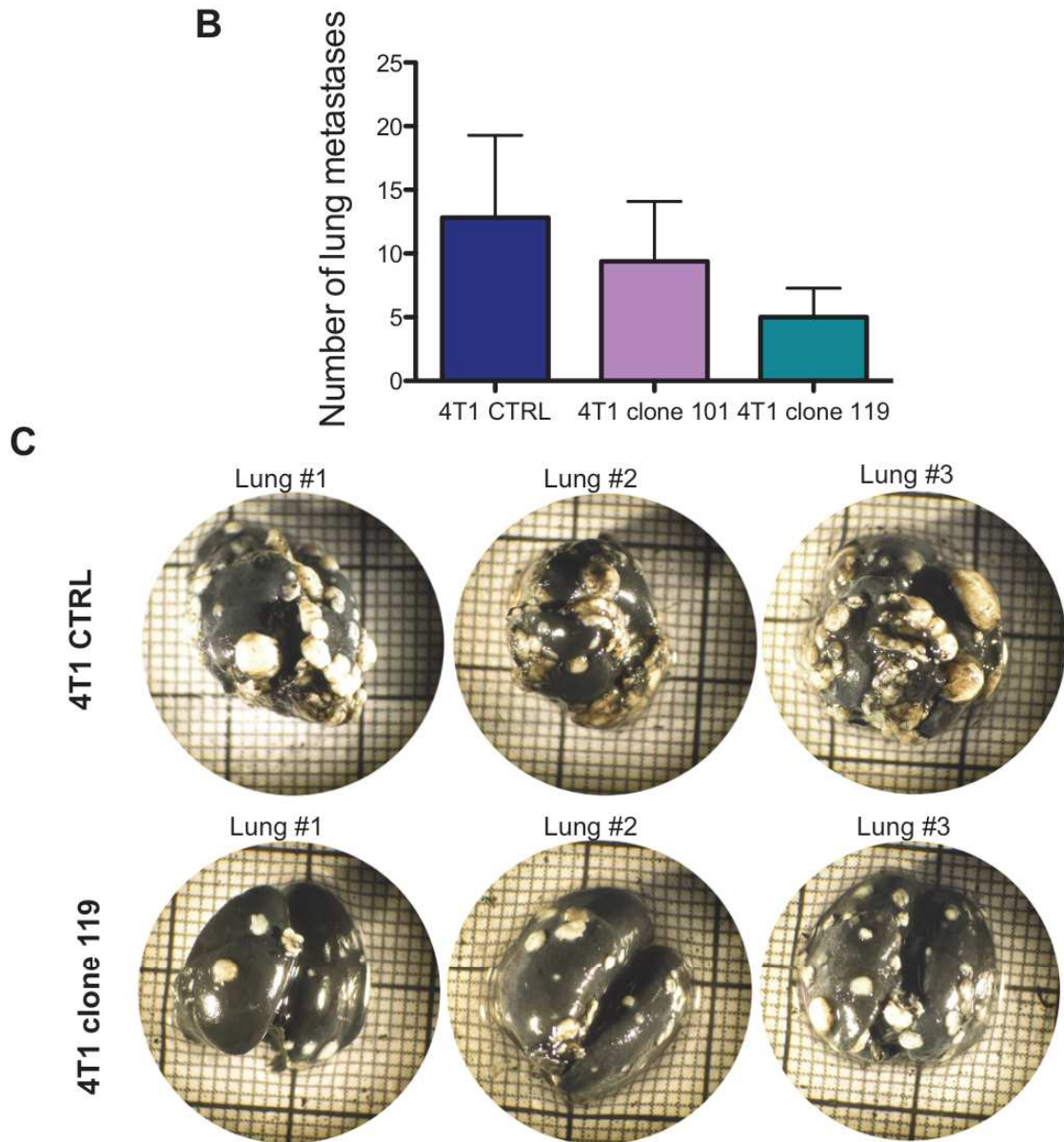


Figure 19: Ki-67 absence prevents 4T1 tumour immune-mediated response and affects lung metastasis formation in Balb/c mice.

4T1 CTRL or Ki-67 depleted cells (clones 101 & 119) were transplanted orthotopically (1.10^6 cells/mouse) into the mammary fat pad of 6-8 weeks-old female Balb/c mice ($n=8$ in each group). **(A, upper)** The growth of tumours (volume) was monitored every week over a period of 7 weeks. Contrary to CTRL tumour (dark blue), Ki-67 depleted tumours were not cleared between weeks 2 & 3. Error bars indicate the standard error of the mean. **(A, lower)** Representative tissue sections from each experimental group at week-7 analysed by IHC using an antibody against Ki-67. Scale bar; 100 μ m. **(B)** Quantification of lung metastases formed in each experimental group at week-7 following 4T1 CTRL or Ki-67 depleted cells (clones 101 & 119) injection at the mammary fat pad. **(C)** Evaluation of lung metastasis burden. A total of 1.10^6 cells of either 4T1 CTRL or Ki-67 depleted cells (clone 119) were injected intravenously (tail) into 6-8 weeks-old female Balb/c mice ($n=7$ in each group). Representative images of 3 different lungs from each experimental group after euthanasia (at day-25 post cells injection) stained with India ink and photographed using a digital camera. Lung metastases correspond to the white nodules on the black stained lung. Scale bar; 10mm.

5. Ki-67 ablation sensitize cells to DNA methyltransferases

inhibition

DNA methylation of cytosine is an essential epigenetic modification, required for different cellular processes. This function is carried out by a family of DNA methyltransferases (DNMTs), DNMT1, DNMT3A and DNMT3B. As mentioned earlier, many studies have revealed a deregulated DNA methylation pattern in cancer cells. Indeed, targeting the methylation machinery in tumour cells using nucleoside analogues of cytosine, such as 5-aza-2-deoxycytidine (5-aza-dC), which inhibits DNMTs, holds a great promise for treating some specific malignancies. In fact, DNA methylation inhibitor 5-aza-dC induces reversible genome-wide DNA damage resulting in growth inhibition of tumour cells ¹⁰⁷.

Since interactors of methylated chromatin and proteins involved in histone methylation complexes were among Ki-67 interacting partners, we asked whether Ki-67 absence would sensitize cells to DNA methyltransferase inhibition. To do this, we subjected either 4T1 CTRL or Ki-67-depleted (clone 101) cells to increasing concentrations of 5-aza-dC for 48h, and assessed the clonogenic survival of these cells at day-6 post-treatment. As expected, 5-aza-dC treatments resulted in decrease clonogenic survival in both cell lines tested, in a dose-dependent manner. However, this effect was much stronger in Ki-67 depleted cells as mirrored by the low number of colonies formed compared to CTRL cells (**fig.20**). This indicates that in the absence of Ki-67, cancer cells might display a higher sensitivity toward DNMTs inhibition, suggesting a potential cooperation between Ki-67 and DNA methylation that can promote tumour growth *in vivo*.

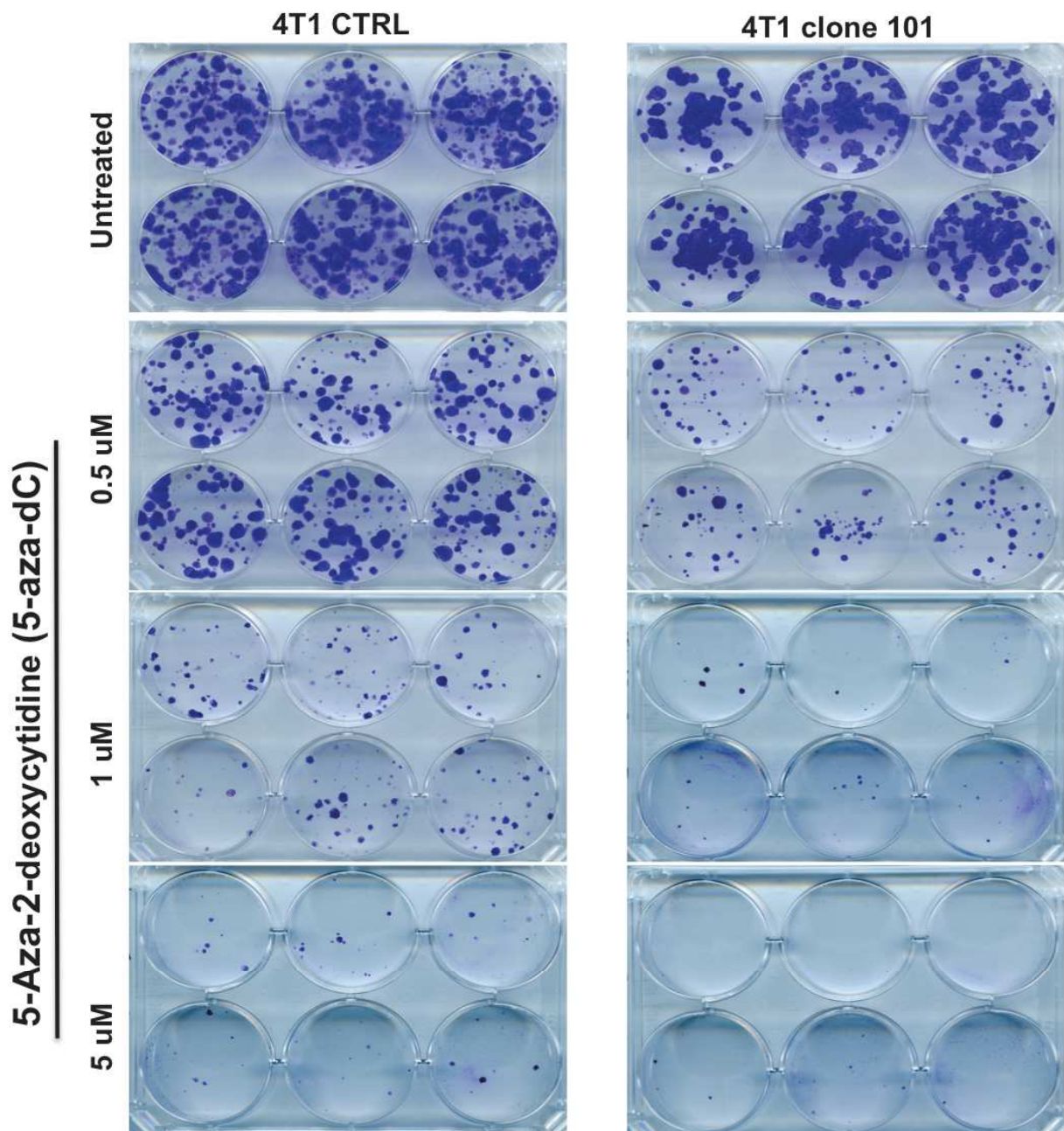


Figure 20: Ki-67 ablation sensitizes cells to DNA methyltransferases inhibition.

Clonogenic assay of 4T1 CTRL and Ki-67 depleted cells (clone 101) treated with increasing concentrations of 5-aza-dC. Cells were seeded into 6 well plates (2000 cells/well) and treated with 5-aza-dC (0,5, 1 & 10uM) for 48h. Cultures were then fixed and stained with crystal violet for colonies formation at day-6 post treatment with 5-aza-dC.

6. Ki-67 absence strongly impaired the development of MDA-MB-231 tumours in vivo

Given the results obtained in these different tumorigenesis mouse models, we wanted to test if Ki-67 is also required for efficient development of human tumours. For this, we used the TNBC-derived cell line, MDA-MB-231 as a model for investigating whether Ki-67 depletion could affect tumour development of MDA-MB-231 xenografts in nude mice. Using CRISPR/Cas9 mediated genome-editing approach; we first generated MDA-MB-231 Ki-67 mutant cells by specifically targeting a sequence found in exon 6 of the human MKI67. This gene targeting resulted in Ki-67 loss of expression as revealed by qRT-PCR analysis in selected MDA-MB-231 Ki-67 mutant clones (**fig.21A**). Indeed, gDNA sequencing identified insertion and deletion events introduced by CRISPR/Cas9 in exon 6 in 3 clones tested: A7 (1-nt insertion), B10 (7-nt deletion) and E8 (2-nt deletion), confirming the disruption of Ki-67 encoding gene. As shown in **fig.21B**, Ki-67 depletion did not affect the proliferative potential of MDA-MB-231 cells as mirrored by comparable Cyclin A2 and PCNA levels between MDA-MB-231 Ki-67 mutant clones and CTRL cells. This was confirmed by EdU incorporation assay, as no defect in active DNA synthesis was found following Ki-67 depletion (**fig.21C**). Together, these results confirmed that Ki-67 expression is dispensable for cell proliferation *in vitro*.

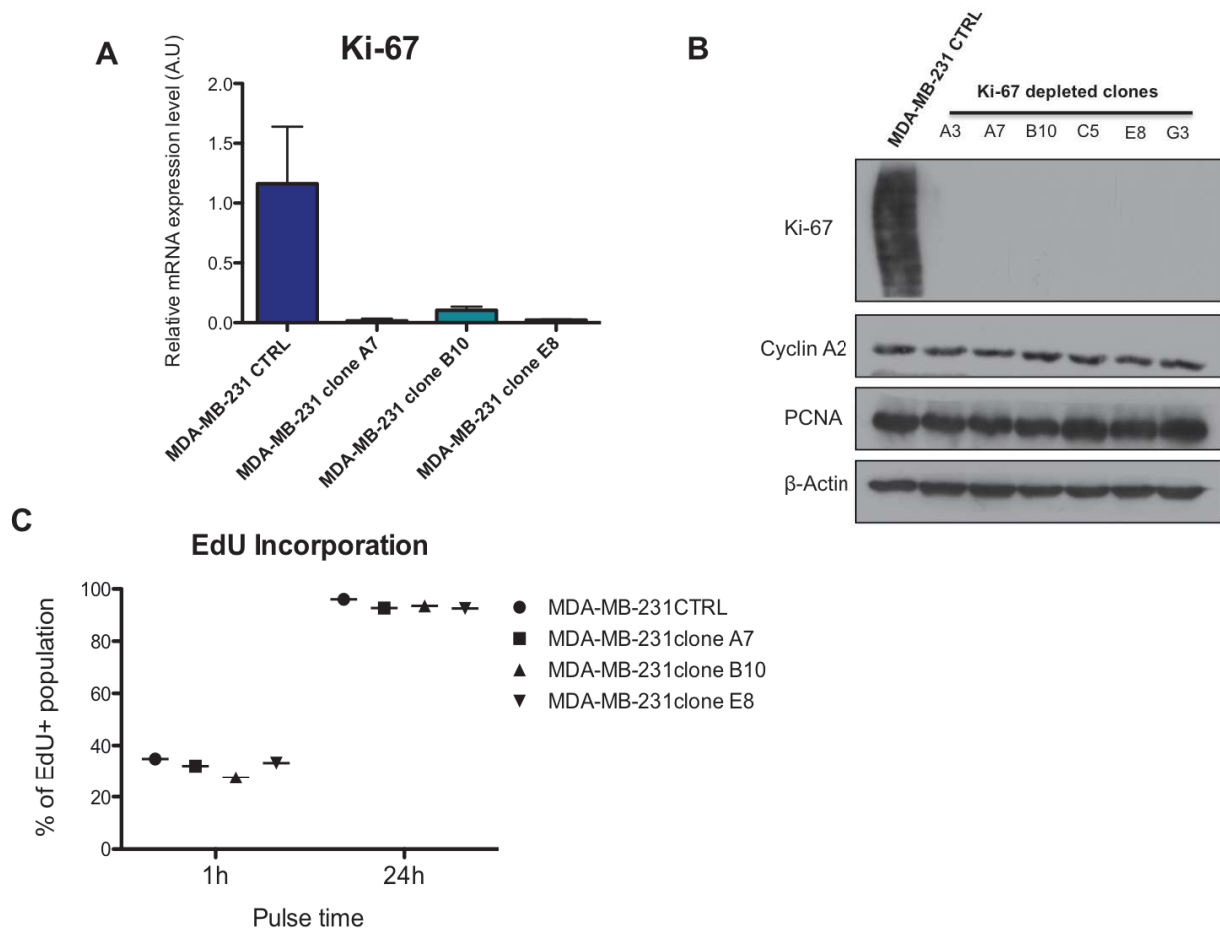


Figure 21: CRISPR/Cas9-mediated ablation of Ki-67 does not affect the proliferative capacity of the TNBC-derived cell line, MDA-MB-231.

(A) qRT-PCR analysis of Ki-67 mRNA expression in MDA-MB-231 CTRL and selected Ki-67 depleted clones (A7, B10 & E8) generated by CRISPR/Cas9 targeting of a sequence found in exon 6 of the human MKI67. (B) Western blot analysis of Ki-67, Cyclin A2 and PCNA expression in MDA-MB-231 CTRL and Ki-67 depleted clones (A3, A7, B10, C5, E8 & G3). Actin served as loading control. (C) Analysis of EdU incorporation (1h & 24h) in MDA-MB-231 CTRL and Ki-67 depleted clones (A7, B10 & E8).

To determine whether Ki-67 might be required for tumour development and establishment of distant metastasis. We transplanted orthotopically either an MDA-MB-231 Ki-67-depleted cell line (clone E8) or CTRL cells into the mammary fat pads of 6-8 weeks female athymic nude mice. Following cell transplantation, we monitored tumour development to determine the effect of Ki-67 absence on tumour growth. Although, Ki-67 absence did not impede the initial tumour establishment at the mammary fat pad, tumour development was strongly impaired in the absence of Ki-67 compared to the CTRL group (**fig.22**). This was mirrored by the 4-fold decrease in tumour size of tumours derived from Ki-67-depleted cells at week 6 compared to their CTRL counterparts. These results suggest that Ki-67 presence is strongly involved in

sustaining and promoting the growth of MDA-MB-231 tumours *in vivo*.

While no macroscopic colonization at distant organs (e.g. lungs) was found in both groups after euthanasia, only mice transplanted with CTRL cells displayed a significant enlargement of the axillary lymph nodes draining the mammary gland (data not shown), probably due to the presence of cancer disseminated cells from the primary site. This may suggest that the invasive capacities of MDA-MB-231 are also strongly hampered upon Ki-67 depletion, similar to the previous findings in 4T1 model.

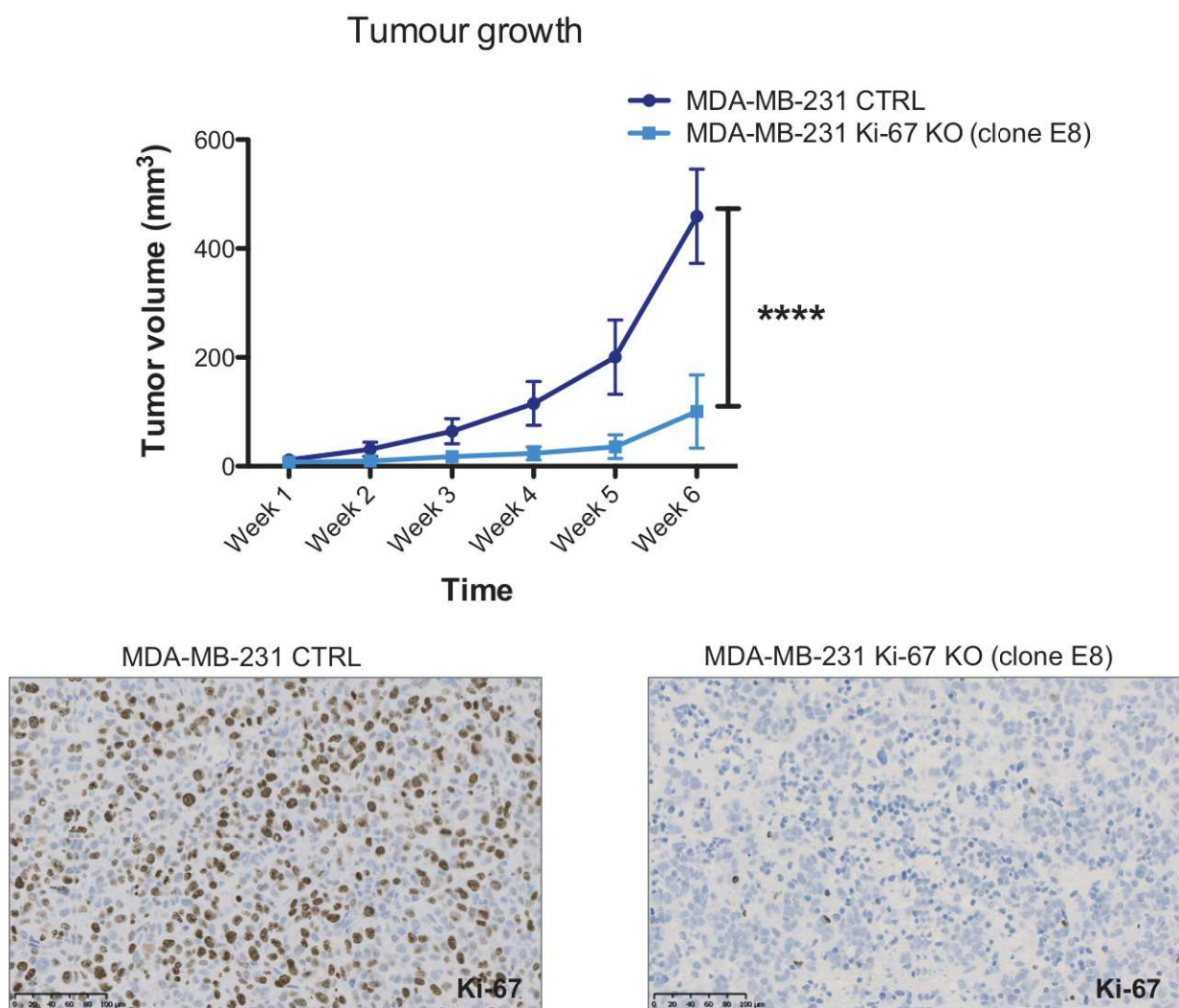


Figure 22: Ki-67 absence strongly impaired the development of MDA-MB-231 tumours *in vivo*. MDA-MB-231 CTRL or Ki-67 depleted cells (clone E8) were transplanted ($3 \cdot 10^6$ cells/mouse) into the mammary fat pad of 6-8 weeks-old female nude mice (n=8 in each group). (**Upper panel**) The growth of tumours (volume) was monitored every week over a period of 6 weeks. Error bars indicate the standard error of the mean. ****P=0.0003 (ANOVA). (**Lower panel**) Representative tumour tissue sections from each experimental group (week-6) analysed by IHC using an antibody against Ki-67. Scale bar; 100µm.

7. Ki-67 depletion does not affect MDA-MB-231 migration ability in vitro

Cancer migration and invasion represent important steps of the cancer-invasion metastasis cascade. Indeed, we sought to determine whether the impaired cancer dissemination of Ki-67-depleted tumours was caused by impaired migration capacities. Using the wound closure assay, we asked if Ki-67 depletion via siRNA-mediated knockdown could affect *in vitro* the collective migration ability of MDA-MB-231 cells. Cells were either transfected with an siRNA targeting Ki-67 or a control siRNA (**fig.23A**), and were then seeded in a 2-well silicone insert with a defined cell-free gap. When cells reached a confluence state, the insert was removed to create a wound and the rate of the gap (wound) closure was subsequently monitored (cell migration) over time using time-lapse microscopy (**fig.23B**). Based on the wound area (μm^2) closed due to cell movement, the rate ($\mu\text{m}^2/\text{h}$) of cell migration was calculated at different time points (0 to 14h). The results revealed that the rate of wound closure of Ki-67 knockdown cells was almost similar to the one of control cells (**fig.23C**). This indicates that Ki-67 depletion does not affect the collective migration ability of MDA-MB-231 cells, which may imply that the impaired invasive ability observed following Ki-67 depletion could result for example from a defect in lymphogenesis or angiogenesis induction or other defects related to their intrinsic properties.

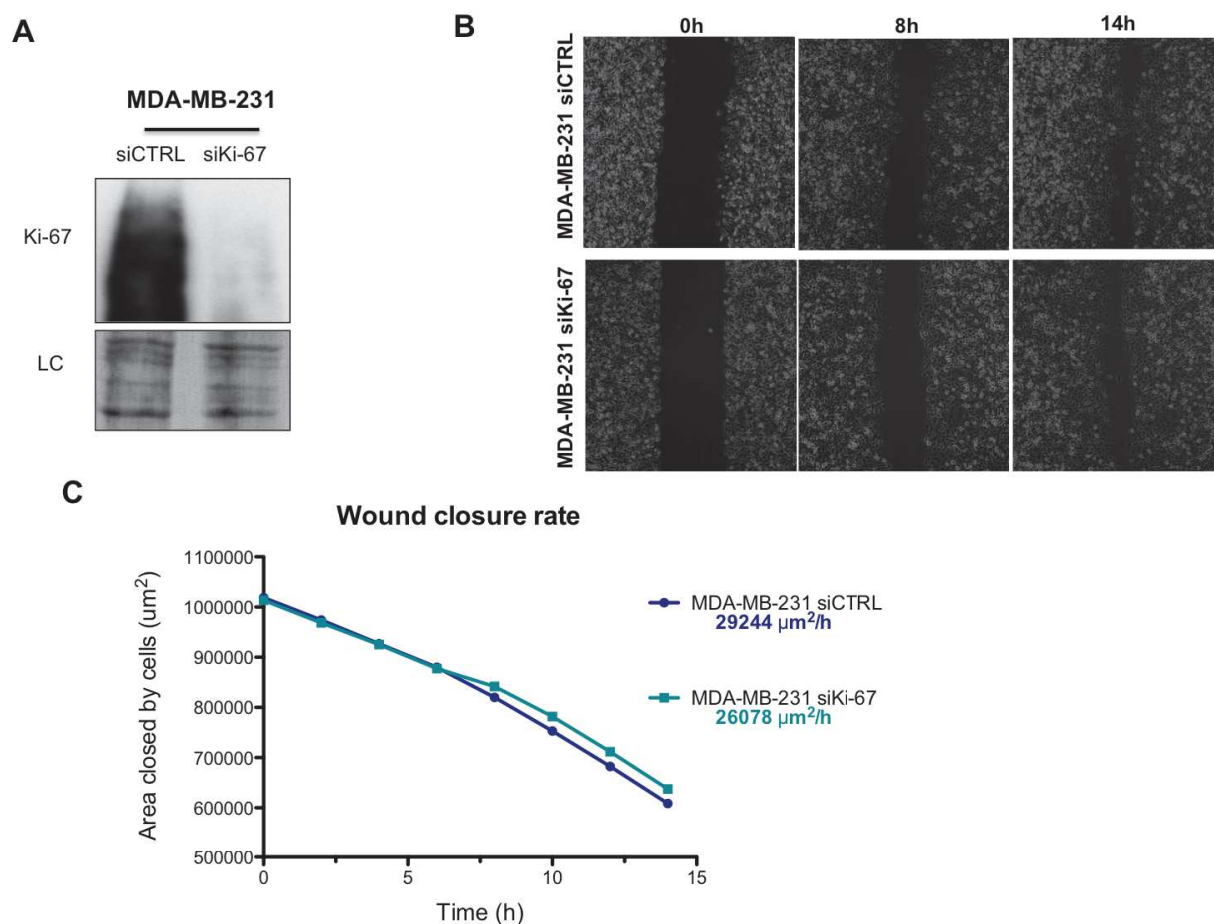


Figure 23: Ki-67 depletion does not affect MDA-MB-231 migration ability *in vitro*.

(A) MDA-MB-231 were transfected with control (siCTRL) or Ki-67 siRNA (siKi-67). At 72h post transfection, lysates were analysed by western blot with an antibody against Ki-67. LC; Loading control (Amido-black staining). (B) Phase contrast photographs (magnification 20X) of siCTRL and siKi-67 MDA-MB-231 cultures taken at 0h (immediately after the wound) and at the indicated time intervals (8h & 14h) highlighting the extent of wound closure by cells. (C) The wound area (μm^2) closed by cells was monitored every 2h over a period of 14h using time-lapse microscopy. The rate of cell migration ($\mu\text{m}^2/\text{h}$) was then calculated using the slope.

8. Ki-67 depletion generates widespread transcriptomic changes in

4T1 cancer cells

To better understand the mechanisms by which Ki-67 influences cancerogenesis, we compared Ki-67-dependent alterations in gene expression in 4T1 cancer cells by RNA sequencing (RNA-seq), using wild-type and genome-editing Ki-67 mutant lines of each. RNAs depleted of rRNA were first converted into a library of cDNA fragments after RNA fragmentation. Sequencing adaptors were added and the libraries were sequenced, then the aligned reads for each transcript between WT control and Ki-67 mutant cell lines were compared. Comparison of differentially expressed genes

between wild-type and Ki-67 mutant cell lines revealed widespread transcriptome changes following Ki-67 depletion (**fig.24A**). In Ki-67-depleted 4T1 cells the analysis has revealed 154 up- and 616 down-regulated genes compared to the control conditions (3 fold, FDR <0.05). In fact, many of these genes are known to be involved in tumour growth and cancer progression. For example, genes encoding proteins known for their contribution in angiogenesis (e.g. VEGF family, Angiopoitin family), cancer inflammation (e.g. interferon regulatory factor-1 (IRF-1)), remodelling of extracellular matrix (e.g. Matrix metalloproteinases (MMPs) family) and EMT (e.g. Vimentin) were among those deregulated genes.

Interestingly, Gene Set Enrichment Analysis (GSEA) of an a priori defined set of genes (**fig.24B**) shows that genes defining epithelial-mesenchymal transition (EMT) were significantly down-regulated in 4T1 Ki-67-depleted cells. In addition, genes encoding proteins involved in interferon α and γ responses were also strongly down-regulated. This suggests that through its ability to influence the chromatin organization and interact with chromatin-modifying proteins, Ki-67 may participate in the implementation of gene expression programs (e.g. EMT program) involved in tumour growth and cancer cells dissemination.

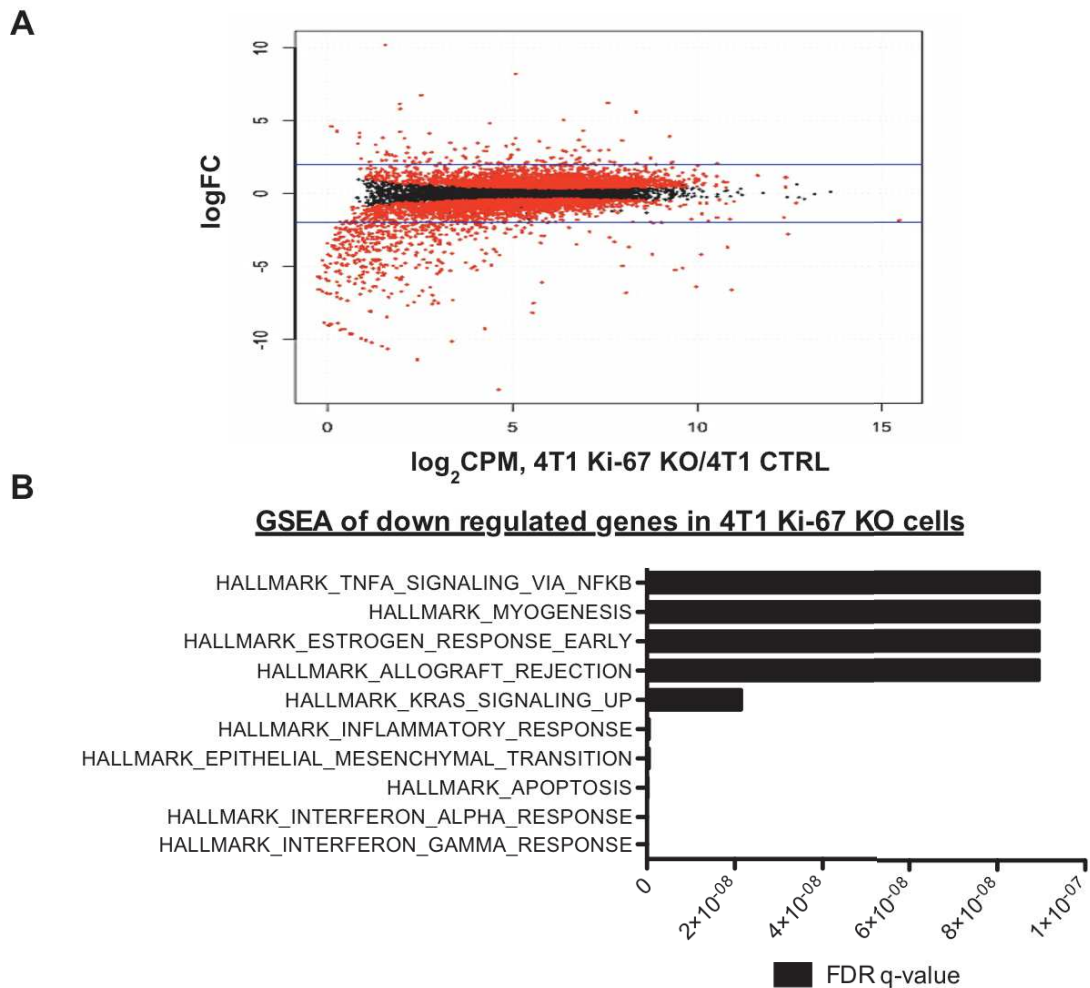


Figure 24: Widespread transcriptomic changes in Ki-67 depleted 4T1 cells.

(A) Dot plot analysis of differentially expressed genes (DEGs) in 4T1 Ki-67 KO compared to 4T1 CTRL cells. Each dot corresponds to a transcript; Y-axis indicates log fold-changes (FC) in gene expression level in Ki-67 depleted cells relative to CTRL cells. The genes represented with red dot are DEGs under conditions of $\log_2FC > 1$ and $P\text{-value} < 0.01$. (B) Gene sets enrichment was performed using GSEA computational method on two highly differential transcript clusters between 4T1 CTRL and Ki-67 KO cells. Results are obtained from the statistically significant (FDR q-value) hallmark gene sets. FC; fold change. GSEA; Gene Set Enrichment Analysis. FDR; false discovery rate.

Discussion & perspectives

Since the discovery of Ki-67, the use of this protein in cancer histopathology has helped assess tumour growth in cancer patients. Although, Ki-67 represents a valuable tool in the clinic, its functional role remains largely unknown. Studies investigating the cellular functions of Ki-67 have suggested that its presence is essential for cell proliferation^{7, 21, 74, 43, 42}. In fact, experiments using complementary oligonucleotides to Ki-67 mRNA resulted in an inhibition of DNA synthesis⁷. Similarly, microinjection of antibodies against murine Ki-67 caused a significant reduction in the proportion of dividing cells²¹. In addition, some anti-proliferative effects of Ki-67 antisense oligonucleotides were also reported in mouse renal carcinoma monolayer cell culture⁷⁴. A potential role of Ki-67 in the early steps of rRNA synthesis and ribosome biogenesis in response to mitogenic signals was also suggested^{42, 43}. However, due to the incomplete nature of the techniques used to target Ki-67, potential off-target effects could lead to inaccurate conclusions regarding the involvement of Ki-67 in cell proliferation. In addition, these previous studies did not use gene knockout approaches to address the consequence of the loss of Ki-67 encoding gene on cell proliferation.

Using genome editing (i.e. TALEN & CRISPR-Cas9) and knockdown approaches, we tested whether Ki-67 depletion could affect cell growth, in both mouse and human cell lines. Contrary to the previous assumptions, Ki-67 depletion did not affect cell proliferation and had no significant effect on pre-rRNA processing in the four cancer cell lines tested. More importantly, Ki-67 mutant mice did develop and age normally and were fertile, indicating that Ki-67 is dispensable for cell growth and tissue development. Our findings are corroborated by recent studies in which cell lines lacking Ki-67 expression were able to proliferate efficiently^{20, 41, 79, 64}.

Although Ki-67 silencing had no effect on cell proliferation, Ki-67 was required for promoting heterochromatin compaction and long-range genomic interactions in proliferating cells. Indeed, depletion of Ki-67 altered gene expression profiles and resulted for example in deregulation of genes that are physically associated with perinucleolar chromatin⁵⁹. In addition, during mitosis Ki-67 was required for the

formation of the perichromosomal layer of mitotic chromosomes, as documented by other studies^{20, 41, 65, 63}. Moreover, recent studies reported a chromosome-separation function of Ki-67 during mitosis that was attributed to its phase separation (surfactant-like) properties⁶⁴.

Interestingly, emerging evidence revealed that the formation of heterochromatin is driven by phase separation^{108, 109}. In fact, both human and drosophila HP1 α were able to form phase-separated droplets, which allowed the physical sequestration of compacted chromatin and the recruitment of repressive factors characteristic of heterochromatin domains^{108, 109}. Similar to HP1 α , Ki-67 may promote heterochromatin compaction during interphase through its phase-separation properties. In fact, Ki-67 may participate in the phase separation of heterochromatin and euchromatin and ensure the targeting of its partners involved in heterochromatin maintenance to their genomic sites in order to promote heterochromatin formation.

As discussed above, previous studies have shown a physical interaction between HP1 α and Ki-67²², which raises the possibility that both proteins might cooperate to modulate the recruitment of target effectors (e.g. DNA methyltransferase) to silenced heterochromatic regions commonly associated with HP1 α presence such as pericentromeric heterochromatin. Alternatively, Ki-67 presence may regulate the dynamic of HP1 α association or its chromatin retention within these heterochromatic regions. This can lead to the modulation of repressive chromatin marks controlling DNA methyltransferases (DNMTs) expression or recruitment of DNMTs to chromatin, which might influence the access of the gene regulation machinery to compact chromatin. Hence, Ki-67 depletion might affect the exposure of some DNA internal sites or of some specific chromatin modification state (e.g. DNA methylation, histone methylation), which might explain the altered gene expression seen in Ki-67 mutant cell lines.

In fact, different approaches can be used to test whether Ki-67 may regulate gene expression through an effect on chromatin state, for example by controlling DNA methylation. Among these techniques, reduced representation bisulfite sequencing (RRBS) represents an efficient high-throughput method to analyse the methylation landscapes at single CpG level of different genomic regions including promoters, CpG islands and repeated sequences¹¹⁰. The resulting data will allow a comparative

analysis of the differentially methylated regions between Ki-67 mutant cells and their control counterparts. This in turn will enable characterization of epigenetic states upon Ki-67 depletion.

Live cell imaging using the recently developed genetically encoded fluorescent dynamic sensors of DNA methylation (DYNAMETs), that selectively report CG and CHH methylation ¹¹¹ can be complementary to the sequencing approach. By analysing microscopically the fluorescence intensity and dynamics of this sensor, DNA methylation changes in real time can be monitored during cell cycle progression upon Ki-67 depletion.

As discussed above, many of Ki-67 physical interactors are involved, or required, for the maintenance of DNA or histone methylation (e.g.; UHRF1, SUZ12...). Using large-scale imaging-based screening, the sub-cellular localization and level of expression of these interactors can be monitored upon Ki-67 depletion. When the localization and expression level of these interactors are significantly affected, combining this screening with genetic perturbation (e.g. CRISPR-Cas9) can unravel how Ki-67 may participate in the modulation of DNA methylation and thus in heterochromatin maintenance at the molecular level.

Recently, new technologies were developed to resolve with high precision the biophysical state and conformation of the genome. Among these technologies, soft X-ray tomography allows imaging of intact eukaryotic cells and represents an ideal mean to quantify changes in 3D chromatin organization and compartmentalization ¹¹². Using this imaging technology, the quantitative effects on the density and 3D organization of chromatin can be investigated in our engineered Ki-67 mutant cell lines. This can provide more insights on how Ki-67 modulates the molecular organization of chromatin and how it may affect its compaction. Furthermore, by using this technique to map the relative spatial distribution of heterochromatin, the effect of Ki-67 on the dynamic re-organization of chromatin, that takes place for example during cell cycle progression, can be addressed. This should provide valuable functional insights on how Ki-67 expression may participate in the spatial regulation of heterochromatin organization in proliferating cells.

Although, Ki-67 is dispensable for cellular differentiation (which is not impaired in Ki-67 mutant animals), Ki-67 might be required for the reverse process, i.e.

reprogramming somatic cells into induced pluripotent stem (iPS) cells. Ki-67 might participate in this process by modulating for example the establishment and maintenance of DNA methylation or other histone modifications (e.g. acetylation). This would suggest that Ki-67 is required for the cellular plasticity that involves the *de novo* acquisition of developmental programs that are required for cellular reprogramming.

To investigate genetically the requirements for Ki-67 in cellular plasticity, we can take advantage of the considerable plasticity that distinguishes the intestinal epithelium from other tissues. In fact, recent studies have shown that not only enterocyte precursors, but also differentiated enteroendocrine and goblet cells, are able to revert rapidly into intestinal stem cells and regenerate paneth cells and proliferative stem cells at the crypt base in response to the ablation of native Lgr5+ cells. In fact, the de-differentiation process of these specialized cells was accompanied by the reorganization of chromatin, reflecting differential chromatin access between Lgr5+ intestinal stem cells and their secretory-lineage daughters^{113, 114}. Using our mutant Ki-67 mice, the efficient conversion of lineage-specified crypt cells into intestinal stem cells in response to the ablation (i.e. radiation-induced) of native Lgr5+ cells can be tested *in vivo*. This will reveal whether Ki-67 absence can affect the dynamic reorganization of chromatin that takes place during the de-differentiation process, which is required to restore intestinal stem cell function and thus intestinal homeostasis.

In vitro cellular reprogramming also offers an effective system for investigating the epigenetic requirement of Ki-67 in cellular plasticity. By inducing, for example, the ectopic expression of the 'Yamanaka' factors (Oct4, Sox2, c-Myc and Klf4) in our mutant Ki-67 MEFs (Mki67^{2ntΔ/2ntΔ}), the efficiency of reprogramming of these mutant MEFs to iPSs can be compared with their control counterparts. This will reveal whether the absence of Ki-67 can reduce the efficiency of cellular reprogramming, by affecting the remodelling of chromatin or epigenetic states that are required for this process.

If Ki-67 loss does affect the efficiency of reprogramming, subsequent characterization of the resulting cells can be conducted using RNA-seq to determine how Ki-67 may influence the establishment of gene expression programs or the acquisition of

specific epigenetic traits that are required for cellular reprogramming to pluripotency.

Analogous to cellular reprogramming, oncogenic transformation often involves the acquisition of epigenetic traits that yields cells with self-renewal potential, a characteristic also found in iPS ¹¹⁵. This suggests that epigenetic rewiring required for cellular reprogramming may also be implemented during cellular transformation. Furthermore, some studies have suggested that this “oncogenic reprogramming” may act within the established tumour to rewire differentiated cancer cells into stem-like cells ¹¹⁵. These epigenetic changes can confer survival advantages to the CSC sub-population, thus contributing to their enhanced tumour initiation and progression capabilities. The importance of the epigenetic regulations (e.g. DNA methylation) of CSC was documented in leukemia stem cells, where the abrogation of DNA methyltransferase Dnmt1 expression blocked the leukemia development. In line with this observation, haploinsufficiency of Dnmt1 impaired CSC self-renewal and resulted in delayed leukemogenesis ¹¹⁶. In addition to DNMTs, increasing evidence indicates the importance of core components EZH2 and SUZ12 of the PRC2 in maintaining CSC properties and promoting CSC metastasis in various tumour types. In fact, Gonzalez et al. (2014), showed that EZH2 knockdown in both tumours isolated from patients with triple-negative (TN) invasive breast carcinoma and from breast cancer cell lines led to a significant reduction of the proportion of CD44⁺/CD24⁻ and ALDH1⁺ cells. Furthermore, the tumorigenic capacity of ALDH1⁺ cells was strongly hindered upon reduced EZH2 expression ¹¹⁷. Similar to EZH2, SUZ12 expression in breast cancer was shown to be required for CSC formation and maintenance. Indeed, depletion of SUZ12 strongly affected the formation and maintenance of mammosphere growth. Conversely, ectopic SUZ12 expression in transformed cells was sufficient to generate CSCs ¹¹⁸.

Interestingly, we found proteins involved in the PRC2 complex, such as SUZ12, among Ki-67 physical interactors. Together, these findings suggest that Ki-67 may cooperate with components of PRC2 (e.g. SUZ12) or DNMTs to promote CSC maintenance and activity, which enable their enhanced tumour initiation capabilities. Indeed, during cellular transformation, by modulating epigenetic changes through its ability to interact with chromatin-modifying enzymes, Ki-67 might be required for the

implementation of gene expression programs involved in the cellular plasticity and acquisition of stem cell-like characteristics needed for efficient tumour initiation and progression. This would connect the cellular mechanisms of Ki-67 action to its apparent promoting effect during tumourigenesis.

We found that Ki-67 germline mutation protects mice against chemically induced (AOM-DSS) colon carcinogenesis, and that intestinal neoplasia was reduced in $Apc^{+/d14}$ -Ki-67 mutant mice. These findings are reminiscent of the effects of reduced DNA methylation on Apc^{Min} -induced intestinal neoplasia in mice. In fact, a reduction in the DNA methyltransferase activity through treatment with 5-aza-dC or through introduction of a mutant allele of the DNA methyltransferase gene reduced the average number of intestinal adenomas⁸⁴. Interestingly, hypomorphic alleles of $Dnmt1$ resulted in the complete suppression of intestinal polyp formation in $Apc^{Min/+}$ mice. This was accompanied by a reduction in the frequency of CpG island methylation in the normal mucosa and intestinal polyps¹¹⁹. Furthermore, the loss of *de novo* methyltransferase $Dnmt3b$ in $Apc^{Min/+}$ mice caused a significant decrease in the formation of macroscopic colonic adenomas¹²⁰. This suggests that sufficient DNA methyltransferase activity is necessary for efficient intestinal adenomas formation. Moreover, many studies (see above) have highlighted the cross talk between DNMTs and PcG proteins for *de novo* hypermethylation of key gene promoters that is required for colorectal cancer development.

Indeed, the strong decrease of intestinal neoplasia seen in both AOM-DSS and Apc^{d14} models following Ki-67 depletion could be explained by impaired maintenance of methylation marks (e.g. H3K27me3) that are acquired during tumourigenesis, or by an impairment of the *de novo* methylation that mediates the silencing of tumour suppressor genes necessary for promoting intestinal tumourigenesis. This suggests that the presence of Ki-67 might be required for DNA methyltransferases (e.g. DNMT1/3b) recruitment or PcG proteins targeting needed to induce transcriptional silencing by CpG methylation associated with intestinal adenomas development.

Indeed, the DNA methylation status of genomic regions involved in the AOM-DSS-induced colon carcinogenesis can be assessed in Ki-67 mutant mice by combining for example chromatin immunoprecipitation (ChIP) with bisulfite methylation

sequencing assays. This can reveal how Ki-67 absence influences the interactions between histone modifications (e.g. H3K27me3) and DNA methylation during colorectal carcinogenesis.

In addition to the prominent role of DNMTs and PcG proteins, aberrant transcriptional repression involving histone deacetylases (HDACs) was also linked to intestinal tumorigenesis. In fact, HDAC2 was found to be overexpressed in the majority of human colon cancer explants, and its expression was strongly induced in intestinal mucosa and polyps of APC-deficient mice. Moreover, targeting HDAC2 expression by valproic acid caused a severe diminution in adenomas formation in *Apc*^{Min/+} mice, indicating that HDAC2 represents a critical target of APC¹²¹. Interestingly, given the fact that HDAC2 was found to be among the physical partners of Ki-67, its absence may interfere with the aberrant HDAC2-dependent transcriptional repression machinery induced upon loss of APC. Indeed, the impaired tumour development seen in our mouse intestinal models following Ki-67 depletion could be the result of a faulty recruitment of HDAC2 or HDAC2-containing complexes needed for the down-regulation of critical target genes needed for tumour development. This can be tested for example by assessing the consequence of Ki-67 absence on HDAC2 expression, and on the associated repressed genes in intestinal mucosa and polyps of *Apc*^{d14} mice or following AOM-DSS treatment.

Although the role of aberrant methylation and inappropriate histone deacetylation in CRC initiation and development is well documented, driver pathway mutations (e.g. WNT, TGF- β) are strongly involved in colorectal carcinogenesis. Interestingly, using organoids derived from normal human intestinal epithelium, two recent studies have shown that organoids engineered to express the most commonly mutated colorectal cancer genes (APC, P53, KRAS and SMAD4) grew independently of all stem-cell niche factors and formed invasive carcinoma after implantation in mice^{122, 123}. Given our results from AOM-DSS model, it would be interesting to test whether Ki-67 depletion may impair the growth of these human gut stem cell mutant organoids in the absence of stem-cell niche factors. More importantly, it would be worth testing whether the ability of these engineered mutant organoids to form tumours *in vivo* with invasive carcinoma features might be impaired upon Ki-67 depletion. If the ability to form adenomas is affected or delayed, detailed histological

examination combined with gene profiling analysis could help uncover how Ki-67 may be integrated in driver pathway mutations that are essential for efficient intestinal carcinogenesis.

While AOM-DSS and *Apc*^{d14} mouse models constitute a valuable tool for studying intestinal carcinogenesis, these models do not display mucosal invasiveness or metastatic capacities. To further investigate the role of Ki-67 in tumour development and metastasis formation, we used the mouse 4T1 breast cancer model that possesses high metastatic capacities. We engineered 4T1 cells lacking Ki-67 expression using CRISPR-Cas9 genome editing, in order to compare their ability to form primary tumours and colonize distant sites such as the lungs.

As expected, Ki-67 was dispensable for 4T1 proliferation; however, Ki-67 absence strongly affected the subset of 4T1 CSC population, as mirrored by the reduced ALDH1 activity and mammosphere formation. This indicates that Ki-67 was required for the maintenance of the 4T1 CSC population. Similarly, a recent study has shown a strong decrease of CSC frequency and markers (i.e. CD44 and CD133) upon genetic disruption of Ki-67 in the human colon cancer derived-cell line DLD-1⁷⁹. Although, the exact mechanism of how Ki-67 regulates CSC properties was not elucidated in our study, Ki-67 could be involved in the intrinsic epigenetics mechanisms (e.g. DNA methylation, histone modifications) that are needed to sustain and maintain CSC functions, as discussed above. Nevertheless, extrinsic factors that originate from the niches where CSCs reside (that are part of the tumour microenvironment) are also essential to maintain CSCs properties. In fact, cells that constitute the CSC niche produce factors (e.g. chemokines, cytokines...) that are needed to stimulate CSC self-renewal, preserve their phenotypic plasticity, and recruit immune and other stromal cells, which facilitate their metastatic potential¹²⁴. Given the importance of the cancer stem cell niche, Ki-67 might be involved in the cross talk between CSCs and their niches, participating therefore in the regulation of the stemness of tumour cells, which in turn can promote their potential to colonize distant sites.

Nevertheless, more experiments will be required to determine how Ki-67 may regulate *in vivo* the properties of CSC, and whether or not it involves modulation of

their epigenetic states in cooperation with already known chromatin-modifying enzymes. Moreover, it would be interesting to determine how Ki-67 may influence the *in vivo* growth dynamics of CSC, following for example the administration of conventional drugs (e.g. Chemotherapy) or targeted drugs (e.g. epigenetic therapy). In addition to its effect on CSCs *in vitro*, Ki-67 depletion strongly affected tumour growth and metastasis formation in distant sites following orthopic transplantation into the mammary fat pads of athymic nude mice. Although development of Ki-67-depleted tumours in Balb/c mice could not be compared to their control counterparts due to the delayed growth of 4T1 control tumours caused by the immune response, the absence of Ki-67 affected the capacity of tumour cells to metastasize efficiently. Similar to the 4T1 model, the absence of Ki-67 strongly impaired tumour growth of MDA-MB-231-derived xenografts.

Together, both mouse intestinal carcinogenesis model and breast cancer model point to an apparent role of Ki-67 in promoting and sustaining tumour growth. Moreover, Ki-67 could play a prominent role in the dissemination of carcinoma cells to distant sites, thus participating in efficient metastatic colonization.

The EMT program is a central regulator of cancer progression and a driver of cancer cell dissemination in many carcinoma types (breast, colon, lung...).

Interestingly, analysis of our RNA-seq data using Gene Set Enrichment Analysis (GSEA) of an a priori defined set of genes shows that genes defining epithelial-mesenchymal transition (EMT) were significantly down-regulated in 4T1 Ki-67-depleted cells, suggesting a potential role of Ki-67 in this process. As mentioned above, many physical interactors of Ki-67 were chromatin regulators that are involved in chromatin methylation and heterochromatin maintenance. Interestingly, among these chromatin regulators, we found a number of polycomb group proteins (e.g. SUZ12) and proteins that bind methylated DNA and tri-methylated H3K9 (e.g. UHRF1) or regulate histone deacetylation, such as HDAC2. Given the importance of the epigenetic regulatory mechanisms that govern the EMT (see above), Ki-67 may participate in the modulation of the chromatin configuration required to activate the EMT program in response to appropriate inductive signals. For example, through its ability to modulate chromatin organization, Ki-67 may participate in the initial

recruitment of the EMT-TFs that cooperate with chromatin-modifying enzymes to confer various degrees of repression of key epithelial genes (e.g. CDH1, E-cadherin encoding gene) following EMT activation. Alternatively, since the EMT-TFs are initially recruited to key target loci, Ki-67 may ensure the continuous presence of chromatin-modifying enzymes to maintain the gene expression patterns required for the execution of the EMT program.

Although studies that addressed the epigenetic regulation underlying the EMT program have focused only on a small number of genes, recent studies have highlighted the 'long-range' epigenetic silencing (i.e. gain of repressive histone modifications) across domains that may contain genes involved in the regulation of the epithelial state, or tumour-suppressor genes⁹². Since our previous results suggest that Ki-67 may mediate interaction between different regions that are normally packaged into heterochromatin, Ki-67 could be involved in the genome-wide epigenetic remodelling that maintain the silencing of genes associated with an epithelial phenotype. Nevertheless, emerging evidences support the idea that carcinoma cells can reside in various phenotypic stages along the EMT-spectrum, in which they can retain some epithelial traits together with the newly acquired mesenchymal markers. This underlies the remarkable ability of carcinomas cells to adapt and survive which subsequently promote their dissemination to distant anatomical sites^{91, 90}. In fact, by modulating the activity of its chromatin partners, Ki-67 may participate in the epigenetic plasticity that enables dynamic transcriptional changes or specific chromatin configuration, which in turn results in different phenotypic states along the EMT-spectrum. This would raise the possibility that Ki-67 may be involved in epithelial–mesenchymal plasticity, which allows carcinoma cells to shift between the mesenchymal CSC state and more rapidly proliferating epithelial (i.e. differentiated) state⁹¹, contributing therefore to intratumoral heterogeneity.

Indeed, using an experimental setting for EMT (e.g. TGF- β -induced EMT), Ki-67 requirement for modulation of chromatin configuration and levels of histone modifications that occur at several key epithelial genomic loci during EMT can be addressed.

In addition to the epigenetic changes, alterations in their metabolism confer to cancer

cells traits that are required for adjusting to the changing availability in oxygen and nutrients in the tumour microenvironment. Recent evidence suggests bidirectional regulatory mechanisms between metabolic remodelling and the epigenome. In fact, many chromatin-modifying enzymes (e.g. DNMTs, HDACs...) rely on the metabolic activity to produce substrates for chromatin modification, such as methylation and acetylation ¹²⁵. Although in this study we didn't address the role of Ki-67 in cancer metabolism, it would be interesting to test whether Ki-67 absence can hinder this metabolic rewiring that affects the epigenome, which in turn can impede tumour development and/or progression. This would suggest that Ki-67 might participate in bidirectional regulatory mechanisms between metabolic remodelling and the epigenome (i.e. methylation, acetylation) of cancer cells. In fact, one model of coordination between metabolism and the epigenome suggested a localized metabolite production and chromatin regulation ¹²⁵. Indeed, given its physicochemical properties, Ki-67 can eventually act for example as a platform facilitating the direct recruitment of metabolic enzymes to specific sites on chromatin, where they locally produce substrates (e.g. S-adenosylmethionine) that are required for histone modification (e.g. Methylation).

To ensure an adequate supply of oxygen and nutrients and the elimination of waste products resulting from their metabolic activity, cancer tissues rely on the formation of new blood (i.e. angiogenesis) and lymphatic (i.e. lymphangiogenesis) vessels. Previous studies have highlighted the importance of these processes, which are triggered by several angiogenic and lymphangiogenic factors for sustaining tumour growth but also for subsequent metastatic spread ¹²⁶. Among the angiogenic factors, the vascular endothelial growth factor (VEGF) represents an important angiogenic agent in neoplastic tissues ¹²⁶. Using a mouse model of skin tumours, a study showed that VEGF has a dual role in tumour initiation by sustaining angiogenesis and creating a perivascular niche for CSCs that promote cancer stemness and renewal ¹²⁷. Interestingly, several members of the VEGF family (e.g. VEGFc, VEGFd), in addition to other angiogenic regulators (e.g. Angpt1; encoding the angiopoietin 1 protein) were found to be significantly down-regulated following analysis of the RNA-seq from Ki-67-depleted 4T1 cells. This suggests that the absence of Ki-67 may result in an impaired formation of vascular network that can in

turn affect tumour growth. Although more experiments are needed to test this potential involvement of Ki-67 in the angiogenesis process, Ki-67 may participate in the establishment of the perivascular niche that increases the stemness and renewal potential of CSCs.

In order to disseminate from the primary tumour and seed subsequent new tumour colonies in distant anatomical sites, cancer cells go through a sequence of events known as the invasion-metastasis cascade ¹²⁸. As discussed above, the EMT program constitutes an important driver in the metastatic colonization, since the activation of this program increases the frequency of CSCs with enhanced metastatic capacities. In fact, the metastatic potential of carcinoma cells appears to be correlated with the possession of tumour-initiating CSC population as argued earlier, and the capacity to engage adaptive programs that enable their robust proliferation in the new colonized secondary site. In addition to these two prerequisites, the development of a supportive microenvironmental niche is required for successful metastatic colonization ¹²⁸. Furthermore, sequencing of tumour samples in combination with other approaches revealed that successful metastatic colonization relies on epigenetic alterations (e.g. aberrant DNA methylation) or amplification, which promote subsequent cell-survival and self-renewal mechanisms ¹²⁹. Nevertheless, upon their arrival to the metastatic site, the majority of carcinomas cells are eliminated or enter a state of dormancy as single disseminated cells or as small micrometastatic clusters that are unable to outgrow into macrometastatic lesions ¹²⁸. Indeed, to survive in this foreign environment, disseminated cancer cells must establish a permissive microenvironment, for instance by up-regulating cell survival and anti-apoptotic pathways that will subsequently contribute to efficient metastatic colonization ¹²⁹.

Given the strong reduction of macrometastatic lesions observed in the lungs following the injection of Ki-67-depleted 4T1 cells, Ki-67 presence might participate in the creation of a permissive niche that support the survival and the expansion of disseminated cancer cells. Moreover, probably through its capacity to modulate the epigenetic states, Ki-67 may participate in the epigenetic reprogramming that may confer disseminated cells some adaptive traits that enable their survival and self-

renewal at the secondary sites. Ki-67 may therefore participate in the reactivation of cell growth in response to activating niche signals (e.g. Wnt, Notch...) or to escaping inhibitory niche signals, thus contributing to exiting the dormancy state, which in turn will give rise to overt metastatic colonies.

In order to decipher the potential role that Ki-67 might play during the metastatic colonization, it would be interesting to isolate for example Ki-67-depleted 4T1 cells from colonized lungs and tumour circulating cells following orthopic transplantation or tail vein injection in recipient mice. Isolation of these mutant cells from the lungs or the circulation would be technically challenging, given the strong reduction in lung metastasis compared to their control counterparts. However, successful isolation and culturing of disseminated tumour cells from the lungs would allow us to uncover the mechanisms by which Ki-67 may influence the metastatic colonization. For example, analysis of chromatin-state plasticity and epigenetic states (e.g. DNA methylation, histone modifications) in these mutant cells may reveal the precise regulatory mechanisms that underlay the impaired metastatic capacities of tumour cells lacking Ki-67 expression.

As mentioned earlier, Ki-67 forms a shell around the nucleoli and is co-localized with perinucleolar chromatin at the periphery of the nucleolus ⁵⁶. While the functional relevance of the perinucleolar compartment (PNC) presence in carcinoma cells is still unclear, PNC prevalence was correlated with metastatic capacities in different types of solid tumours such as breast and colon cancers ⁵⁸. Our results showed that upon Ki-67 knockdown, the prevalence of PNC in two tested cancer lines was strongly reduced, indicating a specific role of Ki-67 in the organization of PNC. This may suggest that Ki-67 enables a metastatic behaviour of carcinoma cells through its ability to control the organization of PNC. Further experiments will be necessary to clarify the mechanisms underlying the association between Ki-67 and PNC prevalence, which in turn allows carcinomas cells to seed distant metastasis.

Our results have demonstrated the importance of Ki-67 presence for sustaining tumour growth and formation of distant metastasis. Although the exact molecular mechanisms underlying this involvement is still elusive and requires more detailed investigations, Ki-67 may offer an interesting therapeutic window for targeting

carcinomas cells (e.g. TNBC, CRC).

As mentioned above, faulty expression of many epigenetic-modifying enzymes (e.g. DNA methylation enzymes, histone modification enzymes...) is frequently observed in various types of human cancer. For this reason, several therapeutic strategies are now emerging to target cancers with aberrant expression of these epigenetic proteins using specific chemical inhibitors. For instance, strategies using DNMT, HDAC or EZH2 inhibitors in combination with immune checkpoint blockade therapies (anti-PD1, PDL1 or CTLA4) have led to a remarkable tumour regression in syngeneic mouse models ¹³⁰.

Interestingly, Ki-67 depletion in 4T1 cells increased the sensitivity of these cells to DNMT inhibitor 5'-aza-dC *in vitro*. This may suggest that the combination of Ki-67 targeting with epigenetic inhibitors can improve the efficacy of epigenetic therapies. Indeed, it will be interesting to test *in vivo* whether treatment with DNMT or HDAC inhibitors can lead to a more pronounced regression of Ki-67-depleted tumours and/or to the abolition of their metastatic capacities. Alternatively, given the importance of epigenetic mechanisms in tumour immunity, combination of Ki-67 depletion with immune checkpoint blockade therapies can also be tested in syngeneic mice *in vivo* to determine whether Ki-67 absence may enhance the potency of these immune therapies.

Finally, in order to fully exploit the therapeutic window that Ki-67 may offer, it's important to first identify Ki-67 synthetic lethality interactions using for example CRISPR/Cas9 library screening. Indeed, a negative selection can be carried out to determine which gene perturbation will result in the loss of viability in cancer cells lacking Ki-67 expression.

References

1. Gerdes, J., Schwab, U., Lemke, H. & Stein, H. Production of a mouse monoclonal antibody reactive with a human nuclear antigen associated with cell proliferation. *Int. J. cancer* **31**, 13–20 (1983).
2. Gerdes, J. *et al.* Cell cycle analysis of a cell proliferation-associated human nuclear antigen defined by the monoclonal antibody Ki-67. *J. Immunol.* **133**, 1710–5 (1984).
3. Lelle, R. J., Heidenreich, W., Stauch, G. & Gerdes, J. The correlation of growth fractions with histologic grading and lymph node status in human mammary carcinoma. *Cancer* **59**, 83–88 (1987).
4. Sasaki, K., Murakami, T., Kawasaki, M. & Takahashi, M. The cell cycle associated change of the Ki-67 reactive nuclear antigen expression. *J. Cell. Physiol.* **133**, 579–584 (1987).
5. Gerdes, J. *et al.* Immunobiochemical and molecular biologic characterization of the cell proliferation-associated nuclear antigen that is defined by monoclonal antibody Ki-67. *Am. J. Pathol.* **138**, 867–873 (1991).
6. Ross, W. & Hall, P. A. Ki67 : from antibody to molecule understanding? *J. Clin. Pathol.* **48**, M113–M117 (1995).
7. Carsten Schluter, Michael Duchrow, Claudia Wohlenberg, Michael H. G. Becker, Gs. K. & Hans-D. Flad, and J. G. The Cell Proliferation-associated Antigen of Antibody Ki-67: A Very Large, Ubiquitous Nuclear Protein with Numerous Repeated Elements, Representing a New Kind of Cell Cycle-maintaining Proteins. *J. Cell Biol.* **123**, 513–522 (1993).
8. Duchrow, M., Gerdes, J. & Schliiter, C. The proliferation-associated Ki-67 protein : definition in molecular terms. *Cell Prolif.* **27**, 235–242 (1994).
9. Duchrow, M., Schlüter, C., Wohlenberg, C., Flad, H. D. & Gerdes, J. Molecular characterization of the gene locus of the human cell proliferation-associated nuclear protein defined by monoclonal antibody Ki-67. *Cell Prolif.* **29**, 1–12 (1996).
10. Pei, D., Qian, G., Tian, H. & Mou, J. Analysis of human Ki-67 gene promoter and identification of the Sp1 binding sites for Ki-67 transcription. *Tumor Biol.* **33**, 257–266 (2012).
11. Ishida, S. *et al.* Role for E2F in Control of Both DNA Replication and Mitotic Functions as Revealed from DNA Microarray Analysis. *Mol. Cell. Biol.* **21**, 4684–4699 (2001).
12. Kel, A. E. *et al.* Computer-assisted identification of cell cycle-related genes: new targets for E2F transcription factors. *J. Mol. Biol.* **309**, 99–120 (2001).
13. Ntzeros, K. *et al.* MKI67 (marker of proliferation Ki-67). *Atlas Genet. Cytogenet. Oncol. Haematol.* **3**, 105–116 (2015).

14. Durocher, D. & Jackson, S. P. The FHA domain. *FEBS Lett.* **513**, 58–66 (2002).
15. Takagi, M., Sueishi, M., Saiwaki, T., Kametaka, A. & Yoneda, Y. A Novel Nucleolar Protein, NIFK, Interacts with the Forkhead Associated Domain of Ki-67 Antigen in Mitosis. *J. Biol. Chem.* **276**, 25386–25391 (2001).
16. Li, H., Byeon, I. L., Ju, Y. & Tsai, M. Structure of Human Ki67 FHA Domain and its Binding to a Phosphoprotein Fragment from hNIFK Reveal Unique Recognition Sites and New Views to the Structural Basis of FHA Domain Functions. 371–381 (2004). doi:10.1016/j.jmb.2003.10.032
17. Byeon, I. J. L., Li, H., Song, H., Gronenborn, A. M. & Tsai, M. D. Sequential phosphorylation and multisite interactions characterize specific target recognition by the FHA domain of Ki67. *Nat. Struct. Mol. Biol.* **12**, 987–993 (2005).
18. Sueishi, M., Takagi, M. & Yoneda, Y. The forkhead-associated domain of Ki-67 antigen interacts with the novel kinesin-like protein Hklp2. *J. Biol. Chem.* **275**, 28888–28892 (2000).
19. Takagi, M., Nishiyama, Y., Taguchi, A. & Imamoto, N. Ki67 antigen contributes to the timely accumulation of protein phosphatase 1 γ on anaphase chromosomes. *J. Biol. Chem.* **289**, 22877–22887 (2014).
20. Booth, D. G. *et al.* Ki-67 is a PP1-interacting protein that organises the mitotic chromosome periphery. *Elife* **3**, 1–22 (2014).
21. Starborg, M., Gell, K., Brundell, E. & Höög, C. The murine Ki-67 cell proliferation antigen accumulates in the nucleolar and heterochromatic regions of interphase cells and at the periphery of the mitotic chromosomes in a process essential for cell cycle progression. *J. Cell Sci.* **109** (Pt 1, 143–53 (1996).
22. Scholzen, T. *et al.* The Ki-67 protein interacts with members of the heterochromatin protein 1 (HP1) family: a potential role in the regulation of higher-order chromatin structure. *J. Pathol.* **196**, 135–144 (2002).
23. Takagi, M., Matsuoka, Y., Kurihara, T. & Yoneda, Y. Chmadrin: a novel Ki-67 antigen-related perichromosomal protein possibly implicated in higher order chromatin structure. *J. Cell Sci.* **112**, 2463–2472 (1999).
24. Rechsteiner, M. & Rogers, S. W. PEST sequences and regulation by proteolysis. *Trends Biochem. Sci.* **21**, 267–271 (1996).
25. Schmidt, M. H. H. *et al.* Proliferation marker pKi-67 occurs in different isoforms with various cellular effects. *J. Cell. Biochem.* **91**, 1280–1292 (2004).
26. Sobecki, M. *et al.* The cell proliferation antigen Ki-67 organises heterochromatin. *Elife* **5**, 1–33 (2016).
27. Lopez, F. *et al.* Modalities of Synthesis of Ki67 Antigen During the Stimulation of Lymphocytes '. *Cytometry* **12**, 42–49 (1991).
28. Stanislas du Manoir, Philippe Guillaud, Emmanuel Camus, Seigneurin, D. *et al.* Ki-67 Labeling in Postmitotic Cells Defines Different Ki-67 Pathways Within the

- 2c Compartment'. *Cytometry* **12**, 455–463 (1991).
29. Scholzen, T. & Gerdes, J. The Ki-67 protein: from the known and the unknown. *J. Cell. Physiol.* **182**, 311–322 (2000).
 30. Malumbres, M. & Barbacid, M. TO CYCLE OR NOT TO CYCLE: A CRITICAL DECISION IN CANCER. *Nat. Rev. Cancer* **1**, (2001).
 31. Knudsen, E. S. & Witkiewicz, A. K. The Strange Case of CDK4/6 Inhibitors: Mechanisms, Resistance, and Combination Strategies. *TRENDS in CANCER* **3**, 39–55 (2017).
 32. Ren, B. *et al.* E2F integrates cell cycle progression with DNA repair, replication, and G₂/M checkpoints. *Genes Dev.* **16**, 245–256 (2002).
 33. Li, M. & Zhang, P. The function of APC/C Cdh1 in cell cycle and beyond. *Cell Div.* **4**, 1–7 (2009).
 34. Littlepage, L. E. & Ruderman, J. V. Identification of a new APC/C recognition domain, the A box, which is required for the Cdh1-dependent destruction of the kinase Aurora-A during mitotic exit. *Genes Dev.* **16**, 2274–2285 (2002).
 35. García-higuera, I. *et al.* Genomic stability and tumour suppression by the APC/C cofactor Cdh1. *Nat. Cell Biol.* **10**, (2008).
 36. Bridger, J. M., Kill, I. R. & Lichter, P. Association of pKi-67 with satellite DNA of the human genome in early G₁ cells. *Chromosom. Res.* **6**, 13–24 (1998).
 37. Boisvert, F., Koningsbruggen, S. Van, Navascués, J. & Lamond, A. I. The multifunctional nucleolus. *Nat. Rev. Mol. Cell Biol.* **8**, 574–585 (2007).
 38. Kill, I. R. Localisation of the Ki-67 antigen within the nucleolus. Evidence for a fibrillar-deficient region of the dense fibrillar component. *J. Cell Sci.* **109** (Pt 6), 1253–1263 (1996).
 39. Maccallum, D. E. & Hall, P. A. The biochemical characterization of the DNA binding activity of pKi67. *J. Pathol.* **191**, 286–298 (2000).
 40. Maccallum, D. E. & Hall, P. A. Biochemical Characterization of pKi67 with the Identification of a Mitotic-Specific Form Associated with Hyperphosphorylation and Altered DNA Binding. *Exp. Cell Res.* **252**, 186–198 (1999).
 41. Booth, D. G. *et al.* 3D-CLEM Reveals that a Major Portion of Mitotic Chromosomes Is Not Chromatin. *Mol. Cell* **64**, 790–802 (2016).
 42. Bullwinkel, R. N., Baron-lu, B., Lu, A., Gerdes, J. & Scholzen, T. Ki-67 Protein Is Associated With Ribosomal RNA Transcription in Quiescent and Proliferating Cells. *J. Cell. Physiol.* **206**, 624–635 (2006).
 43. Rahmzadeh, R., Hüttmann, G., Gerdes, J. & Scholzen, T. Chromophore-assisted light inactivation of pKi-67 leads to inhibition of ribosomal RNA synthesis. *Cell Prolif.* **40**, 422–430 (2007).
 44. Winking, H., Gerdes, J. & Trauta, W. Expression of the proliferation marker Ki-67 during early mouse development. *Cytogenet. Genome Res.* **105**, 251–256 (2004).
 45. Wang, J., Jia, S. T. & Jia, S. New Insights into the Regulation of Heterochromatin. *Trends Genet.* **32**, 284–294 (2016).

46. Déjardin, J. Switching between Epigenetic States at Pericentromeric Heterochromatin. *Trends Genet.* **31**, 661–672 (2015).
47. Guenatri, M., Bailly, D., Maison, C. & Almouzni, G. Mouse centric and pericentric satellite repeats form distinct functional heterochromatin. *J. Cell Biol.* **166**, 493–505 (2004).
48. Jin, B., Li, Y. & Robertson, K. D. DNA Methylation: Superior or Subordinate in the Epigenetic Hierarchy? *Genes Cancer* **2**, 607–617 (2011).
49. Saksouk, N., Simboeck, E. & Déjardin, J. Constitutive heterochromatin formation and transcription in mammals. *Epigenetics Chromatin* **8**, 1–17 (2015).
50. Wiles, E. T. & Selker, E. U. H3K27 methylation: a promiscuous repressive chromatin mark. *Curr. Opin. Genet. Dev.* **43**, 31–37 (2017).
51. Sharma, S., Kelly, T. K. & Jones, P. A. Epigenetics in cancer. *Carcinogenesis* **31**, 27–36 (2010).
52. F.Lopez, F.Belloc, F.Lacombe, P.Dumain, J.Reiffers, P.Bernard, M. R. B. The Labeling of Proliferating Cells by Ki67 and MIB-1 Antibodies Depends on the Binding of a Nuclear Protein to the DNA. *Exp. Cell Res.* **210**, 145–153 (1994).
53. Kreitz, S., Fackelmayer, F. O., Gerdes, J. & Knippers, R. The proliferation-specific human Ki-67 protein is a constituent of compact chromatin. *Exp. Cell Res.* **261**, 284–292 (2000).
54. Canzio, D., Larson, A. & Narlikar, G. J. Mechanisms of functional promiscuity by HP1 proteins. *Trends Cell Biol.* **24**, 377–386 (2014).
55. Kametaka, A. *et al.* Interaction of the chromatin compaction-inducing domain (LR domain) of Ki-67 antigen with HP1 proteins. *Genes to Cells* **7**, 1231–1242 (2002).
56. Cheutin, T. *et al.* Three-dimensional Organization of pKi-67: A Comparative Fluorescence and Electron Tomography Study Using Fluoronanogold. *J. Histochem. Cytochem.* **51**, 1411–1423 (2003).
57. Pollock, C. & Huang, S. The Perinucleolar Compartment. *Cold Spring Harb. Perspect. Biol.* **2**, 1–10 (2010).
58. Norton, J. T., Pollock, C. B., Wang, C., Schink, J. C. & Kim, J. J. Perinucleolar Compartment Prevalence Is a Phenotypic Pancancer Marker of Malignancy. *Cancer* **113**, 861–869 (2008).
59. Attila Németh, Ana Conesa, Javier Santoyo-Lopez, Ignacio Medina, David Montaner, Bálint Péterfia, Irina Solovei, Thomas Cremer, Joaquin Dopazo, G. L. Initial Genomics of the Human Nucleolus. *PLoS Genet.* **6**, (2010).
60. Matheson, T. D. & Kaufman, P. D. The p150N domain of chromatin assembly factor-1 regulates Ki-67 accumulation on the mitotic perichromosomal layer. *Mol. Biol. Cell* **28**, 21–29 (2017).
61. Traut, W. *et al.* Chromatin preferences of the perichromosomal layer constituent pKi-67. *Chromosom. Res.* **10**, 685–694 (2002).
62. Booth, D. G. & Earnshaw, W. C. Ki-67 and the Chromosome Periphery

- Compartment in Mitosis. *Trends Cell Biol.* **27**, 906–916 (2017).
63. Hayashi, Y., Kato, K. & Kimura, K. The hierarchical structure of the perichromosomal layer comprises Ki67 , ribosomal RNAs , and nucleolar proteins. *Biochem. Biophys. Res. Commun.* **493**, 1043–1049 (2017).
 64. Cuylen, S. *et al.* Ki-67 acts as a biological surfactant to disperse mitotic chromosomes. *Nature* **535**, 308–312 (2016).
 65. Takagi, M., Natsume, T., Kanemaki, M. T. & Imamoto, N. Perichromosomal protein Ki67 supports mitotic chromosome architecture. *Genes to Cells* **21**, 1113–1124 (2016).
 66. Miroslava Juríkováa, L'udovít Danihelb, Stefan Poláka, I. V. Ki67 , PCNA , and MCM proteins : Markers of proliferation in the diagnosis of breast cancer. *Acta Histochem.* **118**, 544–552 (2016).
 67. Dowsett, M. *et al.* Assessment of Ki67 in Breast Cancer: Recommendations from the international Ki67 in breast cancer working Group. *J. Natl. Cancer Inst.* **103**, 1656–1664 (2011).
 68. Inwald, E. C. *et al.* Ki-67 is a prognostic parameter in breast cancer patients: Results of a large population-based cohort of a cancer registry. *Breast Cancer Res. Treat.* **139**, 539–552 (2013).
 69. Cuzick, J. *et al.* Prognostic Value of a Combined Estrogen Receptor , Progesterone Receptor , Ki-67 , and Human Epidermal Growth Factor Receptor 2 Immunohistochemical Score and Comparison With the Genomic Health Recurrence Score in Early Breast Cancer. *J. Clin. Oncol.* **29**, 4273–4278 (2011).
 70. Polley, M. Y. C. *et al.* An international ki67 reproducibility study. *J. Natl. Cancer Inst.* **105**, 1897–1906 (2013).
 71. Yerushalmi, R., Woods, R., Ravdin, P. M., Hayes, M. M. & Gelmon, K. A. Ki67 in breast cancer : prognostic and predictive potential. *Lancet Oncol.* **11**, 174–183 (2010).
 72. Fry, D. W. *et al.* Specific inhibition of cyclin-dependent kinase 4 / 6 by PD 0332991 and associated antitumor activity in human tumor xenografts. *Mol. Cancer Ther.* **3**, 1427–1438 (2004).
 73. Finn, R. S. *et al.* The cyclin-dependent kinase 4 / 6 inhibitor palbociclib in combination with letrozole versus letrozole alone as first-line treatment of oestrogen receptor-positive , HER2-negative , advanced breast cancer (PALOMA-1 / TRIO-18) : a randomised phase 2 stud. *Lancet Oncol.* **16**, 25–35 (2015).
 74. Kausch, I. *et al.* Ki-67-directed antisense therapy in an orthotopic renal cell carcinoma model. *Eur. Urol.* **46**, 118–125 (2004).
 75. Kausch, I. *et al.* Inhibition of Ki-67 in a renal cell carcinoma severe combined immunodeficiency disease mouse model is associated with induction of apoptosis and tumour growth inhibition. *BJU Int.* **95**, 416–420 (2005).
 76. Zheng, J. *et al.* Inhibition of renal cancer cell growth in vitro and in vivo with

- oncolytic adenovirus armed short hairpin RNA targeting Ki-67 encoding mRNA. *Cancer Gene Ther.* **16**, 20–32 (2009).
77. Rahmanzadeh, R., Rai, P., Celli, J. P. & Rizvi, I. Ki-67 as a Molecular Target for Therapy in an In vitro Three-Dimensional Model for Ovarian Cancer. *Cancer Res.* **70**, 9234–9243 (2010).
 78. Al-hajj, M., Wicha, M. S., Benito-hernandez, A., Morrison, S. J. & Clarke, M. F. Prospective identification of tumorigenic breast cancer cells. *PNAS* **100**, 3983–3988 (2003).
 79. Cidado, J. *et al.* Ki-67 is required for maintenance of cancer stem cells but not cell proliferation. *Oncotarget* **7**, 6281–6293 (2016).
 80. Lin, T. *et al.* The nucleolar protein NIFK promotes cancer progression via CK1 α / β -catenin in metastasis and Ki-67-dependent cell proliferation. *Elife* **5**, 1–21 (2016).
 81. Biswas, S. & Rao, C. M. Epigenetics in cancer: Fundamentals and Beyond. *Pharmacol. Ther.* **173**, 118–134 (2017).
 82. Ting, D. T. *et al.* Aberrant Overexpression of Satellite Repeats in Pancreatic and Other Epithelial Cancers. *Science (80-.)*. **331**, 593–597 (2011).
 83. Klutstein, M., Nejman, D., Green, R. & Cedar, H. DNA Methylation in Cancer and Aging. *Cancer Res.* **76**, 3446–3451 (2016).
 84. Laird, P. W. *et al.* Suppression of Intestinal Neoplasia by DNA Hypomethylation. *Cell* **81**, 197–205 (1995).
 85. Jin, B. *et al.* DNMT1 and DNMT3B Modulate Distinct Polycomb-Mediated Histone Modifications in Colon Cancer. *Cancer Res.* **69**, 7412–7422 (2009).
 86. Schlesinger, Y. *et al.* Polycomb-mediated methylation on Lys27 of histone H3 pre-marks genes for de novo methylation in cancer. *Nat. Genet.* **39**, 232–236 (2007).
 87. Widschwendter, M. *et al.* Epigenetic stem cell signature in cancer. *Nat. Genet.* **39**, 2006–2008 (2007).
 88. Wainwright, E. N. & Scaffidi, P. Epigenetics and Cancer Stem Cells: Unleashing , Hijacking , and Restricting Cellular Plasticity. *TRENDS in CANCER* **3**, 372–386 (2017).
 89. Funato, K., Major, T., Lewis, P. W., Allis, C. D. & Tabar, V. Use of human embryonic stem cells to model pediatric gliomas with H3.3K27M histone mutation. *Science (80-.)*. **346**, 1529–1534 (2014).
 90. Chaffer, C. L., Juan, B. P. S., Lim, E. & Weinberg, R. A. EMT , cell plasticity and metastasis. *Cancer Metastasis Rev.* **35**, 645–654 (2016).
 91. Ye, X. & Weinberg, R. A. Epithelial – Mesenchymal Plasticity: A Central Regulator of Cancer Progression. *Trends Cell Biol.* **25**, 675–686 (2015).
 92. Tam, W. L. & Weinberg, R. A. The epigenetics of epithelial-mesenchymal plasticity in cancer. *Nat. Genet.* **19**, 1438–1450 (2013).
 93. Ophir Shalem, Neville E. Sanjana, Ella Hartenian, Xi Shi, David A. Scott, Tarjei S. Mikkelsen, Dirk Heckl, Benjamin L. Ebert, David E. Root, John G. Doench,

- F. Z. Genome-Scale CRISPR-Cas9 Knockout in human cells. *Science* (80-.). **343**, 84–87 (2014).
94. Neville E Sanjana, O. S. & F. Z. Improved vectors and genome-wide libraries for CRISPR screening. *Nat. Methods* **11**, 783–785 (2014).
 95. Sobecki, M. *et al.* Cell-cycle regulation accounts for variability in Ki-67 expression levels. *Cancer Res.* **77**, (2017).
 96. Alvarez, A., Barisone, G. A. & Diaz, E. Focus Formation: A Cell-based Assay to Determine the Oncogenic Potential of a Gene. *J. Vis. Exp.* **94**, 1–6 (2014).
 97. Rosenberg, D. W., Giardina, C. and T. & Tanaka. Mouse models for the study of colon carcinogenesis. *Carcinogenesis* **30**, 183–196 (2009).
 98. Robertis, M. De, Massi, E., Poeta, M. L., Carotti, S. & Morini, S. The AOM / DSS murine model for the study of colon carcinogenesis: From pathways to diagnosis and therapy studies. *J. Carcinog.* **10**, 1–32 (2011).
 99. Colnot, S. *et al.* Colorectal cancers in a new mouse model of familial adenomatous polyposis: influence of genetic and environmental modifiers. *Lab. Investig.* **84**, 1619–1630 (2004).
 100. Wirtz, S. *et al.* Chemically induced mouse models of acute and chronic intestinal inflammation. *Nat. Protoc.* **12**, 1295–1309 (2017).
 101. Aslakson, C. J. & Miller, F. R. Selective Events in the Metastatic Process Defined by Analysis of the Sequential Dissemination of Subpopulations of a Mouse Mammary Tumor1. *Cancer Res.* **52**, 1399–1405 (1992).
 102. Ginestier, C. *et al.* Article ALDH1 Is a Marker of Normal and Malignant Human Mammary Stem Cells and a Predictor of Poor Clinical Outcome. *Cell Stem Cell* **1**, 555–567 (2007).
 103. Shaw, F. L. *et al.* A Detailed Mammosphere Assay Protocol for the Quantification of Breast Stem Cell Activity. *J. Mammary Gland Neoplasia* **17**, 111–117 (2012).
 104. Tao, K., Fang, M., Alroy, J. & Sahagian, G. G. Imagable 4T1 model for the study of late stage breast cancer. *BMC Cancer* **8**, 1–20 (2008).
 105. Simpson, K. D. *et al.* Macrophage Migration Inhibitory Factor Promotes Tumor Growth and Metastasis by Inducing Myeloid-Derived Suppressor Cells in the Tumor Microenvironment. *J. Immunol.* **189**, 5533–5540 (2012).
 106. Kim, K. *et al.* Eradication of metastatic mouse cancers resistant to immune checkpoint blockade by suppression of myeloid-derived cells. *PNAS* **111**, 1–6 (2014).
 107. Palii, S. S., Emburgh, B. O. Van, Sankpal, U. T., Brown, K. D. & Robertson, K. D. DNA Methylation Inhibitor 5-Aza-2 J -Deoxycytidine Induces Reversible Genome-Wide DNA Damage That Is Distinctly Influenced by DNA Methyltransferases 1 and 3B □. *Mol. Cell. Biol.* **28**, 752–771 (2008).
 108. Larson, A. G. *et al.* Liquid droplet formation by HP1α suggests a role for phase separation in heterochromatin. *Nature* **547**, 236–240 (2017).
 109. Amy R. Strom, Alexander V. Emelyanov, Mustafa Mir, Dmitry V. Fyodorov, X.

- D. and G. H. K. Phase separation drives heterochromatin domain formation. *Nature* **547**, 241–245 (2017).
110. Boyle, P. *et al.* Gel-free multiplexed reduced representation bisulfite sequencing for large-scale DNA methylation profiling. *Genome Biol.* **13**, R92 (2012).
 111. Ingouff, M. *et al.* Live-cell analysis of DNA methylation during sexual reproduction in *Arabidopsis* reveals context and sex-specific dynamics controlled by noncanonical RdDM. *Genes Dev.* **31**, 72–83 (2017).
 112. Mark A LeGros *et al.* Soft X-Ray Tomography Reveals Gradual Chromatin Compaction and Reorganization during Resource Soft X-Ray Tomography Reveals Gradual Chromatin Compaction and Reorganization during Neurogenesis In Vivo. *CellReports* **17**, 2125–2136 (2016).
 113. Tetteh, P. W. *et al.* Replacement of Lost Lgr5- Positive Stem Cells through Plasticity of Their Enterocyte-Lineage Article Replacement of Lost Lgr5- Positive Stem Cells through Plasticity of Their Enterocyte-Lineage Daughters. *Cell Stem Cell* **18**, 203–213 (2016).
 114. Jadhav, U. *et al.* Dynamic Reorganization of Chromatin Accessibility Signatures during Dedifferentiation of Secretory Precursors into Lgr5 + Intestinal Stem Cells Article Dynamic Reorganization of Chromatin Accessibility Signatures during Dedifferentiation of Secretory Prec. *Cell Stem Cell* **21**, 65–77.e5 (2017).
 115. Suvà, M. L., Riggi, N. & Bernstein, B. E. Epigenetic Reprogramming in Cancer. *Science (80-.)*. **339**, 1567–1570 (2013).
 116. Purificacion Munoz, Maria S. Alioua, M. E. Epigenetic alterations involved in cancer stem cell reprogramming. *Mol. Oncol.* **6**, 620–636 (2012).
 117. Gonzalez, M. E. *et al.* EZH2 expands breast stem cells through activation of NOTCH1 signaling. *PNAS* **111**, 3098–3103 (2014).
 118. Iliopoulos, D., Lindahl-allen, M., Polytaichou, C., Hirsch, H. A. & Tschlis, P. N. Loss of miR-200 Inhibition of Suz12 Leads to Polycomb-Mediated Repression Required for the Formation and Maintenance of Cancer Stem Cells. *Mol. Cell* **39**, 761–772 (2010).
 119. Eads, C. A., Nickel, A. E. & Laird, P. W. Complete Genetic Suppression of Polyp Formation and Reduction of CpG-Island Hypermethylation in *Apc*(Min/+) *Dnmt1*-Hypomorphic Mice. *Cancer Res.* **62**, 1296–1299 (2002).
 120. Lin, H. *et al.* Suppression of Intestinal Neoplasia by Deletion of *Dnmt3b*. *Mol. Cell. Biol.* **26**, 2976–2983 (2006).
 121. Zhu, P., Martin, E., Schlag, P. & Janssen, K. Induction of HDAC2 expression upon loss of APC in colorectal tumorigenesis. *Cancer Cell* **5**, 455–463 (2004).
 122. Matano, M. *et al.* Modeling colorectal cancer using CRISPR-Cas9 – mediated engineering of human intestinal organoids. *Nat. Med.* **21**, 256–262 (2015).
 123. Drost, J. *et al.* Sequential cancer mutations in cultured human intestinal stem cells. *Nature* **521**, 43–47 (2015).

124. Plaks, V., Kong, N. & Werb, Z. Perspective The Cancer Stem Cell Niche : How Essential Is the Niche in Regulating Stemness of Tumor Cells? *Cell Stem Cell* **16**, 225–238 (2015).
125. Kinnaird, A., Zhao, S., Wellen, K. E. & Michelakis, E. D. Metabolic control of epigenetics in cancer. *Nat. Rev. Cancer* **16**, 694–707 (2016).
126. Naoyo Nishida, Hirohisa Yano, Takashi Nishida, Toshiharu Kamura, and M. K. Angiogenesis in cancer. *Vasc. Health Risk Manag.* **2**, 213–219 (2006).
127. Benjamin Beck, Gregory Driessens, Steven Goossens, Khalil Kass Youssef, Anna Kuchnio, Amélie Caauwe, Panagiota A. Sotiropoulou, Sonja Loges, Gaëlle Lapouge, Aurélie Candi, Guilhem Mascre, Benjamin Drogat, Sophie Dekoninck, Jody J. Haigh, P. C. and C. B. A vascular niche and a VEGF-Nrp1 loop regulate the initiation and stemness of skin tumours. *Nature* **478**, 399–403 (2011).
128. Lambert, A. W., Pattabiraman, D. R. & Weinberg, R. A. Emerging Biological Principles of Metastasis. *Cell* **168**, 670–691 (2016).
129. Thordur Oskarsson, Eduard Batlle, and J. M. Metastatic Stem Cells : Sources , Niches , and Vital Pathways. *Cell Stem Cell* **14**, 306–321 (2014).
130. Pfister, S. X. & Ashworth, A. Marked for death: targeting epigenetic changes in cancer. *Nat. Rev. Drug Discov.* **16**, 241–263 (2017).

Résumé

Initialement identifié par Gerdes et ses collègues en 1983, l'antigène de prolifération Ki-67 a été caractérisé grâce à un anticorps monoclonal obtenu par injection sur souris, de noyaux de cellules dérivées du lymphome Hodgkinien. L'anticorps obtenu était capable de reconnaître un antigène nucléaire (i.e. protéine Ki-67) présent uniquement dans les cellules proliférantes (e.g. spermatogonies indifférenciées ...). Par la suite, la caractérisation du profil d'expression de Ki-67 a montré une présence continue de cette protéine dans toutes les phases du cycle cellulaire avec un niveau d'expression très élevé durant la phase G2/M. Cependant, Ki-67 était absent dans les cellules quiescentes et les cellules différenciées. En raison de sa présence dans toutes les phases du cycle cellulaire, les techniques d'immuno-marquage de Ki-67 sont devenues un outil précieux d'évaluation de la proportion de cellules en prolifération dans les coupes de tissus de divers néoplasmes humains.

Bien que des progrès considérables aient été réalisés afin de caractériser la structure moléculaire de la protéine Ki-67, sa fonction biologique reste peu connue.

Les premières études visant à déchiffrer le rôle fonctionnel de Ki-67 dans les cellules proliférantes ont suggéré que cette protéine est nécessaire à la prolifération cellulaire ainsi que dans la progression du cycle cellulaire. Cependant, en plus des limitations techniques des méthodes employées, les auteurs de ces études n'ont pas utilisé d'approches génétiques de perte de fonction (i.e. mutation nulle) permettant l'étude du rôle de Ki-67 dans la prolifération cellulaire. Plus important encore, il a été montré que Ki-67 est exprimé dans les noyaux embryonnaires au cours du développement de la souris. Il est donc essentiel de déterminer in vivo si la présence de Ki-67 est requise pour le développement (e.g. organogenèse) et la différenciation des tissus.

Des progrès ont récemment été réalisés dans la compréhension de l'importance biologique du Ki-67, et des études ont suggéré son un rôle potentiel dans la promotion de la compaction de la chromatine. En outre, des études récentes ont montré l'implication de Ki-67 dans l'organisation de la couche périchromosomale pendant la mitose.

Malgré l'utilisation très répandue de Ki-67 en clinique, la variabilité substantielle des méthodologies d'évaluation de l'expression de Ki-67 dans les laboratoires cliniques, en l'absence de seuils définis, a empêché ses utilisations potentielles, pour exemple,

dans le pronostic et l'efficacité des options thérapeutiques chez les patientes atteintes d'un cancer du sein. De plus, une hétérogénéité du niveau d'expression de Ki-67 est souvent observée à travers les échantillons analysés, ce qui affecte l'interprétation biologique des résultats.

Toutes ces observations indiquent la nécessité d'une meilleure caractérisation de la variabilité de l'expression de Ki67 et des mécanismes qui régulent son expression afin d'exploiter de manière optimale cette protéine pour une meilleure en charge clinique des patients.

Bien que l'utilité de Ki-67 en tant que marqueur de prolifération soit abondamment documentée, son rôle fonctionnel dans le développement des tumeurs et la formation des métastases au niveau de sites distants n'est pas encore connu. Il est donc essentiel de déterminer, dans des modèles de cancérogenèse déjà établis, si l'expression de Ki-67 souvent associé aux tumeurs, pourrait influencer la croissance de ces dernières ainsi que la dissémination des cellules cancéreuses.

Objectif du projet

Ki-67 exprimé de manière constitutive dans les cellules proliférentes de mammifères, est largement utilisé en histopathologie du cancer, comme marqueur de prolifération pour grader les tumeurs. Malgré tout, ses fonctions sont mal comprises. Ainsi, le but de ce projet est d'améliorer la compréhension des fonctions biologiques de Ki-67 et les mécanismes qui régulent son expression ainsi que de déterminer son implication dans l'initiation et la progression du cancer.

Ki-67 n'est pas requis pour la prolifération cellulaire mais nécessaire pour l'organisation d'hétérochromatine.

Bien que la découverte initiale de Ki-67 remonte à plus de 30 ans, les fonctions biologiques assurées par cette protéine demeurent largement inconnues. Généralement associé à des états prolifératifs, il a été suggéré que Ki-67 pourrait s'avérer indispensable à la prolifération cellulaire.

Des travaux antérieurs à ce projet, menés par notre équipe, ont permis de générer avec succès des souris mutantes Ki-67 en utilisant l'approche d'édition génomique TALEN. Des souris ayant des mutations perturbant la séquence codante du gène (*Mki67*) codant pour Ki-67 ont été obtenues. Afin d'étudier les conséquences biologiques potentielles de la perturbation de *Mki67*, deux lignées de souris mutantes ont été sélectionnées, l'une montrant une délétion de 2 nucléotides (*Mki67^{2ntΔ/2ntΔ}*) au niveau de la séquence codante et l'autre une délétion de 21 nucléotides (*Mki67^{21ntΔ/21ntΔ}*) pour une analyse plus approfondie.

Ces lignées mutantes ne présentaient aucune anomalie de développement, fertiles et vieillissant bien. Comme on a pu le voir, Ki-67 est fortement exprimée dans les cellules proliférantes telles que celles situées à la base des cryptes de la muqueuse intestinale chez la souris. Ces cellules migrent à la surface des villosités, où elles se différencient par exemple en cellules caliciformes. Un marquage de Ki-67 dans ces cryptes en utilisant des approches d'IHC/IF et d'immunoblotting a montré une forte réduction de son expression (>90%) chez ces souris mutantes (*Mki67^{2ntΔ/2ntΔ}*). De plus, l'analyse de la réplication active d'ADN *in vivo* a révélé que la vitesse de prolifération cellulaire au niveau de ces mêmes cryptes n'est pas affectée chez les souris *Mki67^{21ntΔ/21ntΔ}*. En outre, dans l'épithélium intestinal de ces souris mutantes, l'analyse de la signalisation Wnt et de la différenciation des cellules caliciformes et des cellules "tuft" a été comparable à celle des souris sauvages. Ces résultats suggèrent que la présence de Ki-67 n'est pas nécessaire au développement de la souris et à la différenciation tissulaire *in vivo*.

Afin d'étudier les conséquences physiologiques de la déplétion de Ki-67, nous avons ensuite isolé et mis en culture des fibroblastes embryonnaires (MEFs) à partir d'embryons issus de ces souris mutantes à 13 jours de gestation. L'analyse a montré que les MEFs *Mki67^{2ntΔ/2ntΔ}* présentaient une réduction importante (90%) de

l'expression de Ki-67 par rapport aux MEFs Mki67^{+/+} et Mki67^{+/2ntΔ}. En outre, la croissance *in vitro* de ces MEFs déplétés en Ki-67 n'a pas été affectée, démontrant ainsi que Ki-67 n'est pas requis pour la prolifération cellulaire.

Comme mentionné ci-dessus, la perturbation du gène Mki67 codant pour Ki-67 médiée par TALEN n'a pas entraîné une ablation complète de ce gène. Ainsi, une lignée cellulaire NIH 3T3 Ki-67-nulle a été préalablement générée en utilisant deux paires de TALEN, l'une en amont de l'ATG d'initiation et l'autre en aval du codon stop de la séquence codante. L'analyse par qRT-PCR, immunofluorescence et Western blot a montré que l'expression de Ki-67 a été complètement éliminée dans ces lignées cellulaires. Comme observé dans les MEFs mutantes Ki-67, ces cellules Ki-67-nulles 3T3 prolifèrent normalement et peuvent entrer et sortir du cycle cellulaire avec des cinétiques similaires à celles des cellules sauvages. Ceci confirme que l'absence de Ki-67 n'affecte pas la prolifération cellulaire.

Bien que Ki-67 ait été découplé de la prolifération cellulaire, il s'est révélé nécessaire pour l'organisation de l'hétérochromatine dans les cellules proliférantes. Ki-67 est requis pour le maintien d'un haut niveau de compactage typique de l'hétérochromatine, et des interactions à longue distance entre les différentes régions du génome caractéristiques de l'hétérochromatine. En effet, l'analyse protéomique des interacteurs de Ki-67 a révélé que les partenaires de Ki-67 sont impliqués dans la formation et le maintien de l'hétérochromatine.

Ces résultats suggèrent que Ki-67 pourrait participer au ciblage de ces protéines vers leurs sites génomiques afin de favoriser le compactage de la chromatine. Ainsi, la déplétion de Ki-67 a conduit à une réorganisation à l'intérieur du noyau des marques d'histones H3K9me3 et H3K20me3 typiquement associées à l'hétérochromatine. En outre, la surexpression de Ki-67 a induit la formation de foyers hétérochromatiques ectopiques hautement enrichis en ces marques, en plus des protéines HP1 également associées à l'hétérochromatine.

Comme discuté ci-dessus, plusieurs études ont révélé le rôle important joué par Ki-67 dans l'organisation de la couche périchromosomale mitotique (PR) et donc le partage fidèle des protéines nucléolaires entre les cellules filles. Conformément à ces études, Ki-67 a été identifié comme l'un des premiers facteurs impliqués dans la

formation de PR et dans la distribution des composants nucléolaires dans les cellules filles, nécessaire pour une nucléogénèse appropriée.

Ces résultats indiquent un rôle important de Ki-67 dans l'organisation de l'hétérochromatine. Ces données ont été publiées dans la revue scientifique eLife (Sobecki et al., 2016).

La variabilité des niveaux de Ki-67 est expliquée par la régulation de son expression par le cycle cellulaire

La prolifération incontrôlée représente l'une des principales caractéristiques des tumeurs. Dans le cancer du sein par exemple, l'analyse immuno-histochimique du pourcentage de cellules cancéreuses positives pour Ki-67 est la méthode la plus utilisée pour mesurer et surveiller la prolifération tumorale. Bien que Ki-67 constitue un outil précieux dans le diagnostic des tumeurs, une variabilité importante de son expression est souvent observée en clinique.

En effet, cette variabilité des niveaux d'expression peut contribuer à des incohérences empêchant ainsi toute utilisation pour classer les patients pour la thérapie, par exemple dans le cancer du sein triple négatif (TNBC). Définir ce qui constitue l'expression positive de Ki-67 et les mécanismes qui gouvernent sa régulation est donc essentiel pour comprendre la signification clinique des différences d'expression observées de cette protéine.

Des travaux antérieurs de notre équipe ont suggéré que Ki-67 est régulé par la machinerie du cycle cellulaire dans les cellules humaines non transformées ou cancéreuses. Nous avons donc cherché à déterminer si cette régulation pouvait expliquer toute la variabilité des niveaux d'expression de Ki-67. Nous avons trouvé que, de façon similaire à la protéine PCNA, l'expression de Ki-67 est variable dans l'intestin de souris sauvages et dans les adénomes intestinaux selon le stade du cycle cellulaire.

Ces résultats ont indiqué que les niveaux de Ki-67 sont liés au cycle cellulaire chez la souris. Pour déterminer si cette corrélation est aussi valable chez l'humain, nous avons évalué la proportion de gènes du cycle cellulaire dont l'expression est corrélée à celle de Ki-67 dans un grand ensemble de données de cancer colorectaux. A un coefficient de corrélation très élevé ($> 0,6$), environ 80% des gènes ont une

annotation du cycle cellulaire. En outre, l'interactome de Ki-67, obtenu en combinant les interactions de base de données STRING pour tous les gènes (avec une corrélation > 0.5) et les partenaires physiques identifiés de Ki-67, a révélé que de nombreuses protéines codées par ces gènes interagissent dans un réseau de cycle cellulaire. De plus, cette corrélation de Ki-67 avec les gènes du cycle cellulaire a été maintenue dans les sous-types de cancers colorectaux, ainsi que dans les données du TCGA sur le cancer du sein.

Nous avons ensuite testé expérimentalement si le couplage de l'expression de Ki-67 avec la prolifération cellulaire se maintient lors de traitements médicamenteux, *in vivo*. Ainsi, suite à l'inhibition de CDK4/6 (i.e. régulateur de l'expression de Ki-67), nous avons cherché à déterminer si Ki-67 continue d'identifier les cellules proliférantes, et par conséquent, constitue un bio-marqueur utile pour la réponse au *palbociclib*, un inhibiteur de CDK4/6 récemment approuvé dans le traitement de certains cancers du sein. Pour cela nous avons testé chez les souris la réponse de deux lignées de cancer du sein triple négatif, MDA-MB-231 (sensible) et MDA-MB-468 (résistante) au *palbociclib*. Les résultats ont montré que l'inhibition de CDK4/CDK6 provoque l'arrêt du cycle cellulaire et conduit à l'élimination de Ki-67 ainsi que les protéines analysées (PCNA, cycline A2) dans les tumeurs MDA-MB-231 mais n'a aucun effet sur les tumeurs MDA-MB-468, qui continuent à proliférer et à exprimer Ki-67.

En outre, cette régulation du cycle cellulaire de l'expression de Ki-67 a également été trouvée dans d'autres situations analysées *in vitro*, y compris des cellules humaines non transformées et des lignées cellulaires cancéreuses humaines avec ou sans traitements médicamenteux.

Ces résultats indiquent que la régulation du cycle cellulaire explique la variabilité du Ki-67 et que Ki-67 constitue un bon biomarqueur de la réponse au *palbociclib in vivo*. L'article décrivant ces résultats a été publié dans la revue scientifique *Cancer Research* en 2017 (Sobecki, Mrouj et al., 2017).

Ki-67: un nouvel acteur important dans la cancérogenèse

Les résultats antérieurs de notre équipe ont montré que la déplétion de Ki-67 a fortement entravé la croissance des xénogreffes de cellules HeLa chez des souris immuno-déficientes. Ce résultat suggère que Ki-67 pourrait être spécifiquement requis dans le développement et la progression des cancers.

Nous avons testé si l'absence de Ki-67 affectait le potentiel de transformation de Ras (Ras G12V, forme active de Ras) dans nos cellules 3T3 Ki-67-nulle *in vitro*. Dans les cellules 3T3 sauvages, la surexpression de Ras G12V a conduit à la production de colonies visibles et bien définies. Cependant, le nombre et la taille des colonies ont été fortement réduits dans les deux clones 3T3 Ki-67-nulle testés, indiquant que le potentiel de transformation de Ras a été fortement réduit en absence de Ki-67. Ces résultats suggèrent que Ki-67 est nécessaire pour que Ras transforme les cellules immortalisées. Ainsi, ce résultat préliminaire indique que le Ki-67 pourrait être spécifiquement requis pour l'initiation et la progression des tumeurs.

En utilisant nos souris mutantes Ki-67 ($Mki67^{2nt\Delta/2nt\Delta}$), nous avons testé si la perturbation de l'expression de Ki-67 est capable de protéger les souris contre l'initiation et/ou la progression des tumeurs.

Pour répondre à cette question, nous avons utilisé un modèle d'induction chimique du cancer colorectal (CRC). Dans ce modèle, la combinaison d'une seule injection de l'azoxyméthane (AOM), un pro-cancérigène avec l'agent inflammatoire sulfate de sodium dextran (DSS) a été utilisé pour induire le CRC chez les souris.

En utilisant ce modèle de CRC, nous avons traité les différents groupes de souris ($Mki67^{+/+}$, $Mki67^{+/2nt\Delta}$ et $Mki67^{2nt\Delta/2nt\Delta}$) avec une seule injection d'AOM (10 mg/kg) suivie d'un cycle unique de DSS 2% pour une semaine. Nous avons ensuite récupéré les côlons (semaine-16) post-traitement et comparé le développement des tumeurs chez les souris testées. La quantification des lésions néoplasiques totales et du nombre de zones tumorigéniques a montré une forte diminution des néoplasmes coliques observés dans le groupe $Mki67^{2nt\Delta/2nt\Delta}$ par rapport aux groupes de souris $Mki67^{+/+}$ et $Mki67^{+/2nt\Delta}$. Ce résultat important indique que la déplétion de Ki-67 peut protéger les souris contre le développement de tumeurs suite au traitement AOM-DSS, suggérant un rôle spécifique de Ki-67 dans l'initiation et/ou le développement des tumeurs.

En utilisant un modèle génétique pour la carcinogenèse intestinale, nous avons voulu tester si la déplétion de Ki-67 pouvait affecter le développement des tumeurs dans le modèle de souris “*adenomatous polyposis coli*” (Apc). Pour cela, nous avons croisé les souris $Apc^{+/d14}$ aux souris $Mki67^{+/2nt\Delta}$ ou $Mki67^{2nt\Delta/2nt\Delta}$ afin de générer deux groupes ($Apc^{+/d14} / Mki67^{+/2nt\Delta}$ et $Apc^{+/d14} / Mki67^{2nt\Delta/2nt\Delta}$), portant tous les deux la mutation Apc^{d14} , et ne différant que par l'expression de Ki-67. Dans les deux groupes de souris, des lésions dans l'intestin grêle et le côlon ont été observées, mais la quantification et la surface néoplasique totale ont montré une réduction des néoplasies intestinales chez les souris $Apc^{+/d14} / Mki67^{2nt\Delta/2nt\Delta}$ comparées à $Apc^{+/d14} / Mki67^{+/2nt\Delta}$.

Ces résultats suggèrent que la déplétion de Ki-67 affecte la formation et le développement des tumeurs. Néanmoins, les tumeurs issues de ces modèles de carcinogenèse intestinale ne présentent pas de capacités métastatiques. Afin d'étudier cela, nous avons choisi d'utiliser le modèle murin de cancer du sein 4T1 de haute capacité métastatique. Ainsi, nous avons généré une lignée cellulaire 4T1 Ki-67-nulle en utilisant l'approche d'édition génomique CRISPR/Cas9. De fait, l'ablation de Ki-67 n'affecte pas la prolifération des cellules 4T1 comme il a été précédemment montré. Par contre, l'analyse de la conséquence de cette ablation de Ki-67 a révélé que Ki-67 est requis pour le maintien des propriétés souches de ces cellules cancéreuses 4T1 *in vitro*. Nous avons donc cherché à déterminer si la présence de Ki-67 est nécessaire pour le développement de tumeurs et la formation de métastases au niveau des sites distants. Afin de tester cette hypothèse, nous avons transplanté orthotopiquement les cellules 4T1 contrôles ou déplétées en Ki-67 au niveau de la glande mammaire de souris femelles athymiques âgées de 6-8 semaines.

Bien que l'absence de Ki-67 n'ait pas empêché l'établissement de la tumeur au site primaire d'injection, le taux de croissance des tumeurs dérivées a été significativement affecté par rapport à leurs homologues contrôles. En effet, à la fin de l'expérience, la taille des tumeurs déplétées en Ki-67 a été réduite d'un facteur 2 par rapport à celle des tumeurs du groupe contrôle. Plus important, l'évaluation des métastases formées dans les poumons a révélé que l'absence de Ki-67 induit une forte réduction de celles-ci.

En poursuivant, nous avons testé si l'ablation de Ki-67 affecterait la croissance des tumeurs 4T1 chez des souris immunocompétentes (Balb/c). Après transplantation des cellules, nous avons surveillé la croissance tumorale pendant 7 semaines ainsi que les métastases formées dans les poumons à la fin de cette période. Les tumeurs 4T1 contrôles et Ki-67-nulle ont montré une croissance rapide au niveau du site primaire au cours de la première semaine. Comme décrit précédemment, les tumeurs 4T1 contrôles ont été complètement éliminées entre les semaines 2 et 3, avant de recommencer à croître de la semaine 4 à la semaine 7, indiquant que la croissance tumorale a déclenché une réponse immunitaire. De façon surprenante, cette croissance tumorale bi-phasique ne s'est pas produite dans les tumeurs déplétées en Ki-67. En effet, ces tumeurs n'ont pas été éliminées et se sont développées de façon continue de la semaine 1 à la semaine 7. Bien que, dans leur seconde phase de croissance, les tumeurs 4T1 contrôles n'aient pu atteindre la taille des tumeurs déplétées en Ki-67, elles ont formé davantage de métastases pulmonaires à la fin de l'expérience. Ces résultats suggèrent que l'absence de Ki-67 empêcherait l'induction d'une réponse immunitaire tumorale chez les souris Balb/c. Néanmoins, malgré les différences observées concernant l'immunité tumorale, l'ablation de Ki-67 a affecté la capacité des tumeurs primaires formées à se métastaser efficacement.

Compte tenu des résultats obtenus dans ces différents modèles murins de tumorigenèse, nous avons voulu tester si Ki-67 est également nécessaire au développement efficace des tumeurs humaines. La lignée cellulaire MDA-MB-231a été retenue.

Ainsi, nous avons généré une lignée cellulaire MDA-MB-231 Ki-67-nulle en utilisant l'approche d'édition génomique CRISPR/Cas9. Pour déterminer les conséquences de l'absence de Ki-67 sur le développement des xénogreffes MDA-MB-231. Nous avons transplanté orthotopiquement soit une lignée cellulaire MDA-MB-231 Ki-67-nulle, soit des cellules MDA-MB-231 contrôles au niveau de la glande mammaire de souris femelles immuno-déficientes âgées de 6-8 semaines. Ensuite, nous avons surveillé le développement de ces xénogreffes pour une durée de 6 semaines afin de déterminer l'effet de l'absence de Ki-67 sur la croissance tumorale. Bien que l'absence de Ki-67 n'ait pas empêché l'établissement initial de la tumeur au niveau

du site primaire, leur développement a été fortement altéré en l'absence de Ki-67. En effet, une diminution très significative de la taille des tumeurs dérivées de cellules déplétées en Ki-67 par rapport à celle des tumeurs contrôles a été observée à la fin de l'expérience. Ces résultats suggèrent que Ki-67 est fortement impliqué dans le maintien et la promotion de la croissance des tumeurs MDA-MB-231 *in vivo*.

Il est important de noter qu'aucune colonisation macroscopique d'organes distants (e.g. poumons) n'a été retrouvée dans les deux groupes après sacrifice des animaux. Néanmoins, les souris transplantées avec des cellules contrôles présentaient un gonflement important des ganglions lymphatiques axillaires drainant la glande mammaire, probablement en raison de la présence de cellules cancéreuses disséminées. Cela suggère que les capacités invasives de MDA-MB-231 sont également fortement entravées suite à la déplétion de Ki-67, comme observé précédemment dans le modèle 4T1.

Afin de mieux comprendre les mécanismes par lesquels Ki-67 influence le processus de cancérogenèse, nous avons analysé par séquençage de l'ARN (RNA-seq) les altérations au niveau de l'expression génique dans les cellules cancéreuses 4T1 suite à la déplétion de Ki-67.

La comparaison des gènes différentiellement exprimés a révélé que l'ablation de Ki-67 a causé des changements importants dans le transcriptome des cellules 4T1. En effet, parmi ces gènes dérégulés, nombreux sont connus pour être impliqués dans la croissance tumorale et la progression du cancer. Par exemple, les gènes codant pour des protéines connues pour leur rôle dans l'angiogenèse (e.g. VEGF, Angiopoïtin), l'inflammation tumorale (e.g. IRF), le remodelage de la matrice extracellulaire (e.g. MMP) et la transition épithélio-mésenchymateuse (e.g. Vimentine). En outre, en utilisant l'approche GSEA (Gene Set Enrichment Analysis), l'analyse d'un ensemble de gènes définis 'à priori' a montré que l'expression des gènes définissant la transition épithéliale-mésenchymateuse a été significativement diminuée dans les cellules 4T1 déplétées en Ki-67.

Ainsi ces résultats suggèrent que Ki-67 peut participer à la mise en œuvre de programmes d'expression génique (e.g. transition épithéliale-mésenchymateuse) qui sont fortement impliqués dans la croissance tumorale et la dissémination des cellules cancéreuses.